EFFECTS OF COPPER AND NICKEL ON THE STRUCTURE AND PROPERTIES OF HEAT TREATED Al-6Si-0.5Mg ALLOY

by

Abul Hossain

Student No: 1009114002P

A thesis submitted in partial fulfillment of the requirements for the degree of

DOCTOR OF PHILOSOPHY

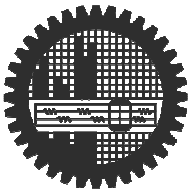

Department of Materials and Metallurgical Engineering

BANGLADESH UNIVERSITY OF ENGINEERING AND TECHNOLOGY

2014

The thesis titled “EFFECTS OF COPPER AND NICKEL ON THE STRUCTURE AND PROPERTIES OF HEAT TREATED Al-6Si-0.5Mg ALLOY”, submitted by Abul Hossain, Roll No: 1009114002P, Session: October 2009, has been accepted as satisfactory in partial fulfillment of the requirement for the degree of Doctor of Philosophy in Materials and Metallurgical Engineering on 31 May 2014.

BOARD OF EXAMINERS

CANDIDATE'S DECLARATION

It is hereby declared that this thesis or any part of it has not been submitted elsewhere for the award of any degree or diploma.

Signature of the Candidate

Abul Hossain

Name of the Candidate

Table of Contents

List of Tables

Chapter 2 Literature Review

Chapter 3 Experimental Procedure

Chapter 4 Results and Discussion

List of Figures

Chapter 2 Literature Review

Chapter 3 Experimental Procedure

Chapter 4 Results and Discussion

List of Abbreviations of Technical Symbols and Terms

AA	Aluminum Association
ASTM	American Society for Testing and Materials
A.Q	As-Quench
B.I	Before Isothermal
CCT	Continuous Cooling Transformation
CF	Conventional Furnace
DC	Direct Chill
DTA	Differential Thermal Analysis
DSC	Differential Scanning Calorimetry
E	Elongation
EDS	Energy Dispersive Spectroscopy
EIS	Electrochemical Impedance Spectroscopy
E_{corr}	Corrosion Potential
E_{pit}	Pitting Corrosion Potential
F	Faraday constant 96485 C/ (mole of electrons)
GP	Guinier-Preston
HIP	Hot Isostatic Pressing
HRC	Rockwell Hardness (C scale)
HRF	Rockwell Hardness (F scale)
IACS	International Annealed Copper Standard
IADS	International Alloy Designation System
IMP	Intermetallic Phase
I_{corr}	Corrosion Current

OCP	Open Circuit Potential
OLM	Optical Light Microscopy
P.A.	Pre-Ageing
ppm	Parts Per Millions
R	Universal Gas Constant, 8.314 $Jmol^{-1}K^{-1}$
SCE	Saturated Calomel Electrode
SSSS	Super-Saturated Solid Solution
SDAS	Secondary Dendrite Arm Spacing
SEM	Scanning Electron Microscopic
TEM	Transmission Electron Microscopic
UTS	Ultimate Tensile Strength
Vp	Volume of Precipitate
XRD	X-Ray Diffraction
YS	Yield Strength
ρ	Resistivity
σ	Stress
η	Over-Potential

Acknowledgements

I would like to express my sincere thanks and gratitude to my honorable supervisor, Professor ASW Kurny, Department of Materials and Metallurgical Engineering, Bangladesh University of Engineering and Technology, Dhaka for his guidance, constant advice, support, cordial encouragement, patience, helpful suggestions and excellent supervision throughout this work, and also for setting a high standard for my future with his professionalism.

I would like to thank all my teachers in the Department of Materials and Metallurgical Engineering. I am particularly indebted to Dr. Fahmida Gulshan, Dr. Ahmed Sharif, Prof. A. K. M Bazlur Rashid and Prof. Md. Mohar Ali for their useful suggestions.

I express my thanks and gratitude to Dr. M. A. Gafur and Engr. Md. Rakibul Qadir (PP &PDC, BCSIR, Dhaka), Engr. M. Ismail Hossain (QC and Product Development, Linde Bangladesh Limited), Engr. M. A. Mamun (Materials Division, BAEC, Dhaka) for their continuous help, suggestions and also for allowing access to their laboratories facilities.

Special thanks are due to Professor Jayati Datta and Dr. Atanu Jana of Bengal Engineering and Science University, Shibpur (BESUS) West Bengal, India, for their invaluable help in the corrosion experiments.

I wish to record my sincere thanks to Sylhet Gas Fields Limited (A company of Petrobangla-Bangladesh Oil, Gas Mineral Corporation), Energy and Mineral Resource Division under the Ministry of Power, Energy and Mineral Resources) for permitting me to undertake this study and to the honorable Manager Operation Engr. Mohammed Sultanul Bahar (MSTE), Deputy General Manager, Engr. Md. Abdul Jalil Pramanik (HGF) and General Manager Engr. Md. Haronur Rashid Mullah (LPM and PD of KTL-7 Oil Well) for their encouragement and support.

Finally, I would like to express my hanks and gratitude to all members of my family, especially to my mother Mrs. Anawara Begum and wife Farjana Ferdous Nitu, for their understanding and constant encouragement throughout the period of my study.

Department of Materials and Metallurgical Engineering
BUET, Dhaka.

Abstract

The purpose of this research was to investigate the influence of copper and nickel on Al-6Si-0.5Mg alloy. Copper in the range of 0.5 - 4 wt%, individual nickel 2wt% and combined 2wt%Cu and 2wt% Ni have been added to Al-6Si-0.5Mg alloy by melt processing technique. The cast alloys were subjected to homogenization at 500^{o}C for 24 hours. The homogenised alloys were solution treated for 2 hours at 540^{o}C and quenched in ice-salt-water solution.

The evolution of microstructure and mechanical properties during heat treatment was studied. The temperature ranges of interest were; solution treatment at 540°C, natural ageing at room temperature, and artificial ageing at 100-400°C. The changes in dendritic composition and eutectic morphology due to solution treatment were quantified by optical and scanning electron microscopic analysis. For the ageing investigations, characterisation of mechanical properties was done by hardness, resistivity and tensile testing.

Artificial and isochronal ageing was conducted in an electric furnace. Isochronal ageing was conducted at 100, 150, 175, 200, 225, 250, 300, 350 and 400^{o}C for 1 hour. For all alloys, the hardness increase was remarkable in the temperature range of 200-250^{o}C and maximum hardness was found at ~225^{o}C. The electrical resistivity of the alloys was found to decrease significantly at 225^{o}C. The isothermal ageing was carried out at 150, 200, 225, 250 and 300^{o}C for time ranging from 15 minutes to 360 minutes. For all alloys under investigation, significant improvement of hardness was achieved by ageing for ~60 minutes at 225^{o}C.

Optical Microscopes (OM) and Scanning Electron Microscopes (SEM) were used for the microstructural investigation. The morphology of the intermetallic phases were observed in the as-cast and the heat treated samples. The Cu and Mg-rich intermetallics completely dissolved but the Ni-rich intermetallics did not dissolve completely during solutionising. The eutectic Al-Si phases were modified after homogenization and solution treatment.

The aged samples were tested for tensile properties. Tensile tests were performed at a constant strain rate of $10^{-3}s^{-1}$ for all ageing conditions. In addition, the peakaged samples (1hr at 225^{o}C) were tested at three different strain rates of $10^{-2}s^{-1}$, 10^{-3} s^{-1} and $10^{-4}s^{-1}$. Tensile strength was found to increase with ageing temperature, the maximum being attained at peak aged condition (1 hr at 225^{o}C). The additions of Cu and/or Ni resulted in an increase in tensile strength and maximum strength was found for 2 wt% Cu addition. The strain rates affected the tensile properties

significantly. At higher strain rates, higher strengths were obtained but these samples showed poor ductility.

The effects of ageing temperature on the impact strength (absorbed energy) of the alloys were studied. The impact strength was found to decrease with ageing temperature, the minimum being found at peakaged condition. Further increase in ageing temperature beyond 225^{o}C slightly increased the absorbed energy.

A peak of mechanical properties was obtained with about 2wt% Cu. The increment of copper seems to have a remarkable impact on the mechanical properties and especially after the ageing process showing a significant increase on the ultimate tensile strength and yield strength.

The corrosion behaviour of the alloys in 0.1M NaCl solution was investigated using potentiodynamic polarization and electrochemical impedance spectroscopy (EIS) techniques. The potentiodynamic polarization curves reveal that 2wt% Cu and 4 wt%Cu containing alloys are more prone to corrosion than the other alloys under investigation. But the EIS test results showed that charge transfer resistance (Rct) increases with increasing Cu content. Maximum charge transfer resistance (Rct) was reported with the individual addition of 2 wt% Cu and combined addition of 2wt% Cu and 2wt% Ni.

A pin-on-disc test apparatus was used to explore the dry sliding wear characteristics of the alloys. No detailed study was attempted. Addition Cu and/or Ni into Al-6Si-0.5Mg alloy seem to increase the wear resistance. The wear resistance was found to increase with ageing temperature, the maximum being found at ~ 200^{o}C - 225^{o}C. The individual addition of 2wt% Cu gives the maximum wear resistance after ageing at 225^{o}C for 1 hr. The combined addition of 2wt% Cu and 2wt% Ni also showed the maximum wear resistance also gave the maximum wear resistance. Overageing resulted in an increase in wear loss of the alloys.

Chapter 1
Introduction

Cast aluminum-silicon alloys, especially hypoeutectic alloys, are widely used in the aerospace and automotive industries due to light weight and superior mechanical properties. For many years, one of the largest potential markets for aluminum alloys has been the transportation sector, primarily due to their increasing use in automotive applications as a way of light weighting cars. The major driving forces for this increase have been the implementation of graduated government standards for vehicle fuel efficiency and recyclability, as well as the effects of higher fuel costs to the consumer. As a consequence, automotive manufacturers have a strong incentive to reduce fuel consumption while maintaining product performance and cost levels. One of the most cost effective ways of addressing these challenges has been to substitute lightweight materials such as aluminum alloys in existing automotive designs. High goals has been put up for the car manufacturers regarding fuel consumption in vehicles; during a short period of time the discharge of CO_2 shall have to be reduced from 158.7 g/km year in 2007 to 95 g/km in year 2020. Under the Cars Regulation, the fleet average to be achieved by all new cars is 130 g/km by 2015 – with the target phased in from 2012 - and 95 g/km by 2020. The 2015 and 2020 targets represent reductions of 18% and 40% respectively compared with the 2007 fleet average of 158.7g/km.

Lightweight materials, particularly Al-Si alloys, have been developed for use in engine applications as a way to meet the automotive industry's continuous demand for better fuel efficiency and cleaner exhaust. The Al-Si alloys used in engine blocks can be divided into three categories, based on their silicon percentages: hypoeutectic (5-10 wt% Si, as in 356, 380), eutectic and hypereutectic alloys (14-20 wt% Si, as in 390 series). The binary eutectic Al-Si alloy contains 12.6 wt% Si. When cylinder blocks cast of hypoeutectic alloys like AA319 or AA 356 are used, cylinder liners made of cast iron or, in some cases, metal matrix composite must be inserted.

Al-Si-Mg based alloys are widely used for the casting of high strength components in automotive, aerospace and military applications, because they offer a combination of high achievable strength, castability and corrosion resistance in both the sand cast and permanent mould condition. However these alloys are rarely used in the as-cast condition, without any pre-

treatment, because it exhibits relatively poor mechanical properties due to the presence of eutectic silicon in the form of coarse acicular plates which act as internal stress raiser under an applied load.

Cast components account for over 80% of aluminum alloy use in vehicles [1]. These castings have replaced their steel counterparts on a part-by-part basis over a number of years, and include relatively large items such as engine blocks, transmission cases and wheels. Often these aluminum cast components are given a heat treatment after casting to improve their mechanical properties. An important aspect of the research efforts aiming to meet the demand for highly reliable cast automotive components is that an improved understanding of alloy behaviour during multi-stage heat treatment can allow the optimization of the process from the standpoint of the material, resulting in lower variability in the properties of the heat treated component. In addition there is a need to understand the heat treatment process from a metallurgical standpoint so that efficient heat treatments can be developed.

Chemical treatment and heat treatment are the two main processes used to improve the properties of the Al-Si-Mg alloys. The chemical treatment, also known as modification, is a liquid state process that is achieved by the addition of small amounts of Na or Sr to the melt. It results in a change of morphology of the eutectic silicon phase from coarse acicular to fibrous resulting in an improvement of the mechanical properties. Heat treatment processes are used to obtain a desired combination of mechanical properties. The most common is the T6, which consists of a solution treatment, water quenching and artificial ageing. The solution treatment generally carried out at a temperature slightly under the eutectic temperature. This treatment dissolves the hardening elements (Si, Mg, Cu, Ni etc.) in the Al matrix, homogenizes the casting and spheroidizes the eutectic Si. After the solution treatment, casting must be quenched to avoid the precipitation of dissolved elements and to create a supersaturated solid solution at room temperature, an essential condition for further ageing. Natural ageing takes place at room temperature after quenching and artificial ageing (carried out at elevated temperature) is the step where hardening elements are precipitated in order to improve the strength of the Al matrix [2].

Although the benefit of heat treatment is undisputed, there exist several challenges for heat treatment operators, including market expectations of higher performance and reliability, lower production costs and energy use, as well as concern over environmental impacts. Standard heat treatment practices were established many years ago, and require re-examination as they remain

unchanged despite product and process improvements occurring in the interim. Developments in casting process technologies have led to changes in the scale of the as-cast microstructure, while current furnace designs produce higher heating rates and lower thermal variation within the charged components during heat treatment. Consequently, there is scope for the optimization of heat treatment processes by reducing the times and temperatures of each stage.

The aim of the present work was to study the effects of Cu and/or Ni on Al-6Si-0.5Mg alloy. The particular objectives of this study can be listed as:

- To study the effect of age hardenable elements (Mg, Cu and Ni) on the ageing behavior of the Al-6Si-0.5Mg alloys.
- To study the effect of heat treatment on the structures of Al-6Si-0.5Mg alloys in the as-cast, as-solutionized, underaged, peakaged and overaged conditions.
- Evaluating the tensile properties of Cu and/or Ni containing heat treated Al-6Si-0.5Mg alloys at various strain rates.
- Evaluating the effects of Cu and/or Ni content on the impact properties of heat treated Al-6Si-0.5Mg alloys.
- To study the mode of deformation and fracture during uniaxial tensile and impact testing of the Cu and/or Ni containing heat treated Al-6Si-0.5Mg alloys.
- Some of the thermal treated (peakaged) samples were subjected to electrochemical measurements to assess the corrosion behaviour of the alloys.
- Dry sliding wear tests were performed using as pin-on-disc type set up. The investigations were exploratory in nature.

Chapter 2
Literature Review

2.1 Introduction

Al-Si-Mg alloy finds widespread applications in automotive, aerospace and general engineering industries due to its excellent combination of properties such as good fluidity, low coefficient of thermal expansion, high strength-to-weight ratio and good corrosion resistance. These foundry alloys possess excellent tensile and fatigue properties and good corrosion resistance [3]. Heat treatable aluminium alloys can be strengthened considerably by appropriate heat treatments. The most common heat treatment is known as artificial ageing and the resulting condition is designated the T6 temper. A modified heat treatment has been developed recently, wherein artificial ageing is interrupted by holding the alloy at a reduced temperature for a prolonged period of time [4]. The T4, T5, T6 and T7 treatment changes the properties of Al-Si alloys. Artificial ageing has been found to the improvement of properties, in a wide range of aluminium alloys. The improvement in mechanical properties has been ascribed to the formation of more finely dispersed precipitates in the final microstructure.

2.1.1 Solubility of Alloying Elements in Aluminium

Hypoeutectic alloys in the Al-Si-Mg system containing nominally 5 to 7% Si and about 0.25 to 0.7% Mg have widespread applications especially in the aerospace and automotive industries. Properties of Al are usually enhanced by the addition of major alloying elements such as Cu, Si, Mg, Mn, Zn, Li, Ni, and then subjecting the alloys to various thermal, mechanical and thermomechanical treatments. The alloying elements are divided into two classes depending on their contribution into Al. Major alloying elements (introduce certain specific properties) and Minor alloying elements (usually low solid solubility). Solid solution strengthening, strain hardening, precipitation or age hardening and ease of casting are the main characteristics of major alloying elements. Minor alloying elements usually form coarse and fine intermetallic phases and indirectly affect properties, e.g. by grain refining during casting or heat treatments.

Most alloying elements have limited solubility in solid Al. Beyond the limit demarcated by the solvus on the phase diagram (Figure 2.1.1), further amounts lead to formation of intermetallic phases. Table 2.1.1 shows that different alloying elements have different solubilities in solid Al [5].

Table 2.1.1: Solubility of alloying elements in Al

Element	Temperature ^{o}C	Maximum solubility		Atom size (d, nm)
		Wt%	At%	
Al	-	-	-	0.29
Si	577	1.65	1.59	0.23
Mg	450	17.4	18.5	0.32
Cu	548	5.65	2.40	0.26
Ni	640	0.04	0.02	0.25
Fe	655	0.05	0.025	0.25
Mn	658	1.82	0.90	0.25
Zn	443	82.8	66.4	0.28

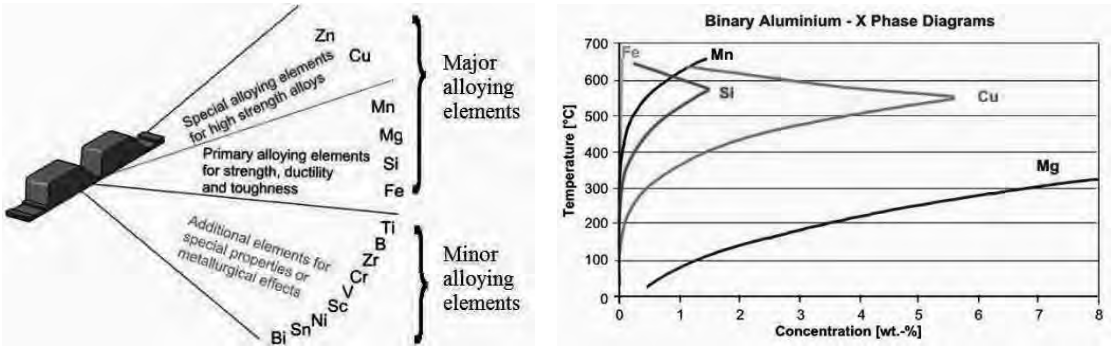

Figure 2.1.1: Alloying elements and their binary phase diagrams showing differing solute solubility in Aluminium

2.1.2 Al-Si Foundry Alloys

Aluminum with silicon as a major alloying element is the most common of the aluminum casting alloys due to the impact of fluidity. Aluminum-silicon alloys supplies a good combination of mechanical properties and castability and for those reasons, they are widely used in the automotive and aerospace industry [6]. Silicon increases the fluidity in aluminum casting alloys and reduces the solidification interval and hot tears tendencies. Mechanical properties depend more on the way silicon are distributed than the amount of it in the alloy. In alloys where silicon particles are small, round and evenly distributed are usually displaying high ductility. Silicon are inexpensive and one of the few elements that can be added without increasing

weight. Porosity slightly decreases with increasing the silicon content [7-8]. Aluminum-silicon alloys are divided into three groups.

- Hypoeutectic containing 5-10% silicon
- Eutectic containing 10-13% silicon
- Hypereutectic containing 13-25% silicon

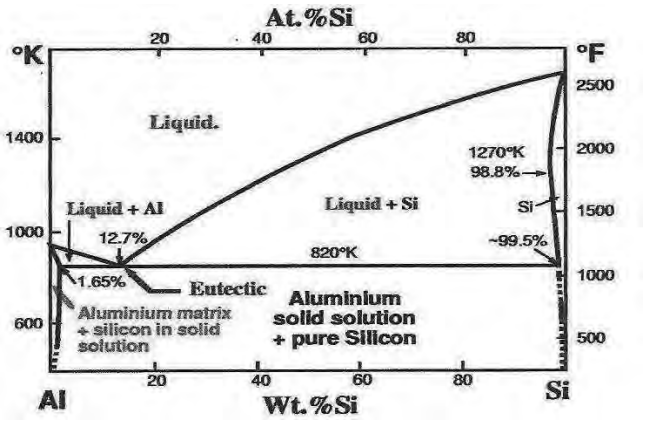

Figure 2.1.2: Illustration of the aluminum-silicon phase diagram

2.1.3 Effects of Alloying Elements on the Properties of Al-Si Cast Alloys

There are many ways of changing properties of aluminium cast alloys. One of them is of course change in composition of the alloy. Although the influence of elements that are noticeable in the alloy is mainly considered, elements which are known as impurities cannot be omitted, and its effect are not always negative. Influence of all alloying elements as well as impurities which can be found in aluminium alloys are as following [9].

Effect of Cu

Copper as an alloying element increase the strength, hardness, fatigue, creep resistance and machinability in an aluminum-silicon alloy. Strength and ductility are depending on how copper is distributed in the alloy. Copper is found dissolved in the dendrite matrix or as aluminum-copper rich phases. Alloys with dissolved copper in the matrix shows the most increase of strength and retains ductility. Continues network of copper at the grain boundaries increases the strength to appreciable levels but the ductility decreases [10]. By increasing the content of copper in the alloy a higher hardness is achieved and porosity formation increases. Aluminum-

silicon alloys that contains 1.5 % copper has the optimal mechanical properties comparing to alloys having lower or higher content of copper. Alloys in which copper can be found in the form of evenly distributed sphereodised particles show biggest increase in strength without negative effects on ductility, while alloys with copper present as continuous network at grain boundaries appear to be less ductile without noticeable increase in strength. Addition of copper will also reduce corrosion resistance of the alloy. It happens because copper disperses the oxide film which appears on the metal surface and it this way it prevents alloy to be electrically neutral. It leads to the fact that Al-Cu alloys can corrode not only by contacting another materials but also another Al-Cu alloy.

Effect of Mg

The role of magnesium in aluminium-silicon alloys is to precipitate β" phase (Mg_2Si) [10]. The coefficient of thermal expansion and its electrical resistively increases a little. Aluminum-magnesium alloys have high strength, good ductility and excellent corrosion resistance. Aluminum-magnesium alloys respond well to heat treatment and a higher ultimate tensile strength and yield strength is achieved. The purpose of magnesium in aluminum-silicon alloys are to precipitate Mg_2Si particles but a disadvantage is that big intermetallic compounds, that reduce the ductility, can appear. In alloys that have an amount of magnesium between 0.05 wt% to 0.3 wt% seems to decrease the amount of porosity [11].

Effect of Fe

Iron added to aluminium alloys negatively influence its corrosion resistance, Fe improves strength of the alloy and at the same time reduces its ductility. Iron improves also resistance to hot tearing during solidification. Formations of beta iron needles have detrimental effect on mechanical properties of aluminum alloy. It happens because needle-shape like iron phases act as stress risers and crack propagation can start in these points.

Effect of Ni

Nickel slightly improves both strength and ductility of the alloys at both room and elevated temperatures. What is more, when adding nickel together with iron, corrosion resistance against hot water is improved [62-64].

2.1.4 Classification of Aluminum Alloys

Classification of aluminum alloys is established by the International Alloy Designation System (IADS), based on the classification developed by Aluminum Association of the United States. This classification is accepted by most countries.

- Classification of wrought aluminum alloys
- Classification of cast aluminum alloys

2.1.4.1 Classification of Wrought Aluminum Alloys

The majority of aluminium used in engineering applications is in the wrought form; that is, as rolled plate, sheet and foil, extrusions, tube, bar and wire. The number of alloys available to the engineer is large, but can be divided into two main groups; non-heat treatable alloys and heat treatable alloys. Before looking at the characteristics of these two classes of wrought alloy, let us first define the modern method of designation of wrought alloys and their processing.

Table 2.1.2: Wrought Al alloy designations according to American system [12]

Wrought AA Designation	Major Alloying Elements	Heat Treatable	Tensile Strength, MPa	Major Applications	Representative Alloys
1XX.X	None	No	69-186	Electrical & chemical	1100 &1350
2XX.X	Cu	Yes	186-427	Aircraft & transportation	2014,2017,2024, 2219, 2195
3XX.X	Mn	No	110-283	Heat transfer, packaging, roofing & siding	3003,3004,3005
4XX.X	Si	No	172-379	Pistons, complex-shaped forgings	4032 and filler alloy 4043
5XX.X	Mg	No	124-351	Building & construction, automotive, cryogenic, marine	5052,5083,5754
6XX.X	Mg+Si	Yes	124-400	Building & construction, highway, automotive, marine	6061,6063, 6111
7XX.X	Zn	Yes	220-607	Aerospace, automotive	7005,7075,7475, 7150
8XX.X	Others	Yes	117-241	Electrical, aerospace, bearing	8017,8176,8081, 8280, 8090

2.1.4.2 Classification of Cast Aluminum Alloys

The Aluminum Association (AA) has adopted a nomenclature similar to that of wrought alloys. British Standard and DIN have different designations. In the AA system, the second two digits reveal the minimum percentage of aluminium, e.g. 150.x corresponds to a minimum of 99.50% aluminium. The digit after the decimal point takes a value of 0 or 1, denoting casting and ingot respectively. The main alloying elements in the AA system are as follows:

Table 2.1.3: Cast Al alloy designations according to American system [12]

Cast AA Designation	Major Alloying Elements	Heat Treatable	Tensile Strength, MPa	Major Applications	Representative Alloys
1XX.X	None	No	Not specified	Not specified	Not specified
2XX.X	Cu	Yes	131-448	Aircraft, automotive applications as engines	201.0,203.0
3XX.X	Si + Mg/Cu	Yes	131-275	Automotive, pistons, pumps, electrical	356.0, A356.0, A360.0, 319.0, 380.0
4XX.X	Si	No	117-172	Typewriter frames, dental equipment, marine, architectural	413.0, 443.0
5XX.X	Mg	No	117-172	Cooking utensils, food handling, aircraft, highway fittings	512.0,514.0, 518.0, 535
6XX.X	Not assign	N/A	N/A	N/A	N/A
7XX.X	Zn	Yes	207-379	Furniture, garden tools, office machines, farm, mining equipment	705.0, 712.0
8XX.X	Sn	Yes	103-207	Bearings and bushings of all types	850.0, 851.0
9XX.X	Reserve	Yes	Not specified	Not specified	Not specified

Each aluminum alloy is designated by a four digit number. The first digit indicates the alloy group according to the major alloying element. The second digit indicates modification of the alloy or impurity limits. Original (basic) alloy is designated by “0” as the second digit. Numbers 1…9 indicate various alloy modifications with slight differences in the compositions. In the

alloys of the 1xxx series the second digit indicates modifications in impurity limits: 0 means natural impurity limit, 1…9 indicate special control of one or more impurities or alloying element. The last two digits identify aluminum alloy or indicate the alloy purity. In the alloys of the 1xxx series the last two digits indicate the level of purity of the alloy: 1070 or 1170 mean minimum 99.70% of aluminum in the alloys, 1050 or 1250 mean 99.50% of aluminum in the alloys, 1100 or 1200 mean minimum 99.00% of aluminum in the alloys.

2.2 Overview of Al-Si-Mg Cast Alloys

2.2.1 Al-Si-Mg Cast Alloy

Hypoeutectic Al-Si-Mg alloys are common non-ferrous foundry alloys due to their excellent castability, fluidity and corrosion resistance. A large portion of aluminum development focuses on the alteration of the Al-7Si-0.3Mg (356) alloy. Al-Si-Mg alloy is a ternary system. Most engineering Al-Si-Mg alloys are based on the pseudo-binary composition Al-x% Mg_2Si (Figure 2.2.1). The equilibrium precipitate in the Al-Si-Mg is Mg_2Si, and the so-called balanced compositions contain magnesium and silicon in same atomic ratio of 2:1 as the equilibrium precipitate.

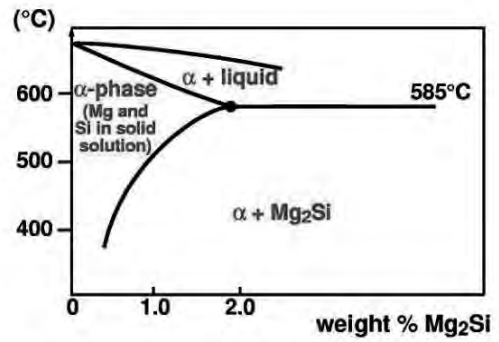

Figure 2.2.1: Pseudo-binary diagram of Al- Mg_2Si

2.2.2 Al-Si-Mg Cast Alloy Background

Typical applications of the A356 cast alloy is automotive transmission casings, aircraft pump parts, water cooled cylinder blocks, aircraft structures, nuclear energy installations, etc. Figure 2.2.2 shows commercial products manufactured used A356 cast alloy, engine cylinder head, water pump, alternator motor cases and vehicle manual transmission casing.

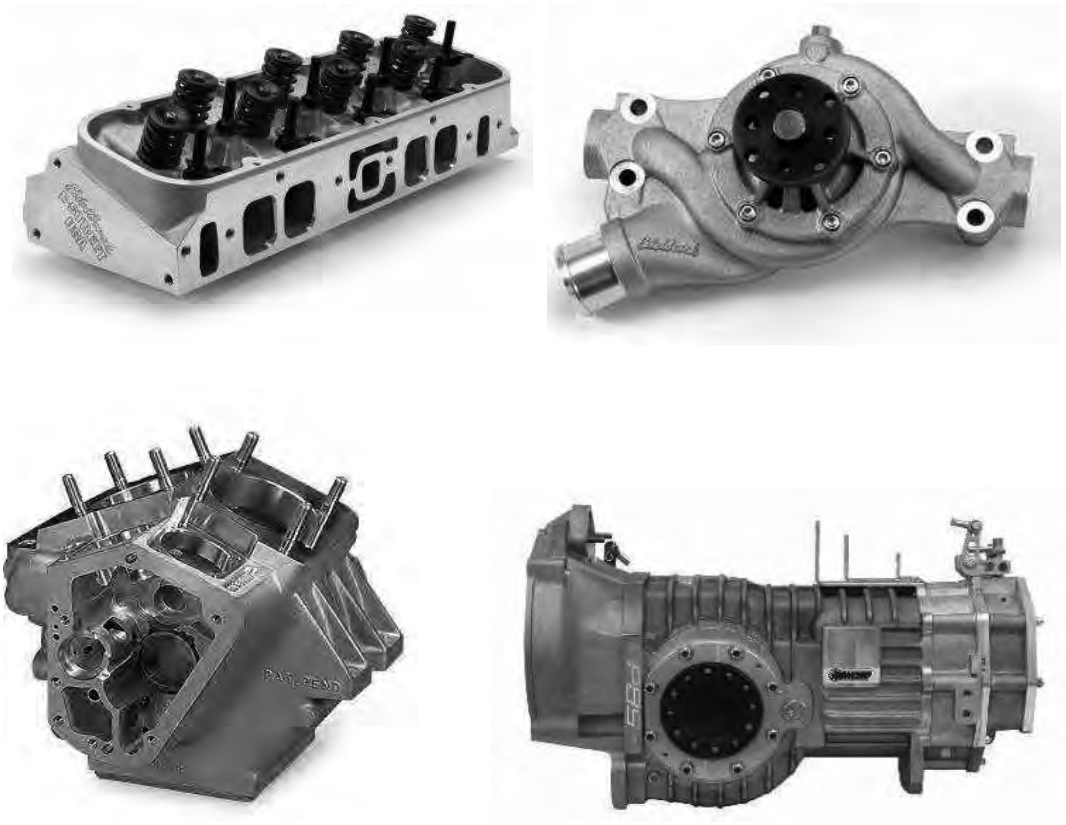

Figure 2.2.2: Typical A356 aluminum cast alloy commercial products and applications [14-16]

As mentioned earlier, alloy A356 is from the Al-Si-Mg family. The alloy typically consists of aluminum rich dendritic cells (α-aluminium), silicon particles in the inter-dendritic regions, porosity and minor intermetallic phases [17]. Table 2.2.1 shows the typical wt% range of different alloying elements that are typically used for the alloy.

Table 2.2.1: Composition of A356 aluminum casting alloys according Aluminum Association designation [18-21]

Si	Fe	Cu	Mn	Mg	Zn	Ti	Al
6.5-7.5	0.0-0.2	0.1-0.2	0.05-0.1	0.25-0.45	0.05-0.10	0.0-0.20	Bal.

Table 2.2.2: Typical mechanical properties of cast A356-T6 aluminum alloys [25]

Ultimate tensile strength (MPa)	0.2% offset yield strength(MPa)	Elongation in 50 mm, %
262	193	5

2.2.3 Al-Si-Mg Alloy Cast Microstructure

A typical microstructure of an Al-7Si-0.3Mg alloy (Figure 2.2.3) consists mainly of the primary aluminum dendrites (α-Aluminum) and the eutectic mixture composed of aluminum, silicon and other eutectic phases. Mg reacts with Si to form Mg_2Si which has Chinese script morphology in the eutectic region. The amount of this phase is usually low and it is difficult to observe in the as-cast condition. Based on the composition (usually/Mn) other coarse eutectic phases can also be found in the eutectic region. The cast microstructure of Al-Si-Mg alloys strongly depends on the alloy chemistry and the casting process. The rapid cooling in permanent mold casting gives a fine dendritic structure surrounded by fine eutectic phases and small grains whereas the slower cooling rate in sand casting causes larger dendrites and coarser eutectic phases. A fine microstructure is always desired in applications requiring high strength. Refinement of the phases can also be achieved through chemical modification without changing the casting process.

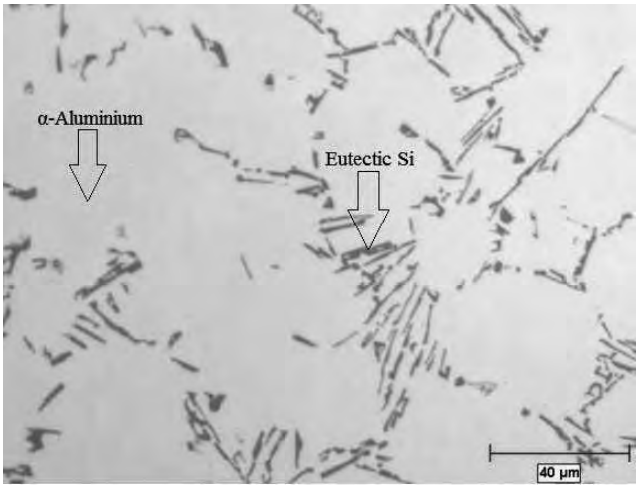

Figure 2.2.3: A typical permanent mould as-cast microstructure of an Al-7Si-0.3Mg [22]

2.2.4 Al-Si-Mg Alloy Treatments

2.2.4.1 The Eutectic Si Modification

The morphology of eutectic silicon is the predominant factor determining the mechanical properties. The silicon particles in the aluminium rich matrix generally grow in the form of coarse platelets and act as crack initiation sites because of their stress concentration effect resulting in poor mechanical properties [25]. The modification of the eutectic Si can be achieved

through rapid rates of solidification and by the addition of modifying agents (modifiers) to the melt. Full modification is difficult to achieve by only increasing the solidification cooling rate. It is therefore essential to modify the eutectic structure by introducing modifying agents [26-28].

2.2.4.2 Chemical Modification

The chemical modification of the eutectic Si is discussed extensively in the literature and the mechanisms behind it are well understood [29]. Several elements such as Na, Sr, Ce, Ca, Ba, La, Yb, Cd, Sb, As, Se, Y are known to cause modification. Basically, these impurity atoms poison the silicon crystal growth during solidification and cause the enhanced twinning of the growing Si phase. Depending on the amount and type of element, different modified structures can be obtained, from an acicular shape to a lamellar shape, and then to a fine fibrous microstructure.-In the case of the A356 alloy a level of 0.02% of strontium is sufficient to achieve a fully modified fibrous microstructure, (Figure 2.2.4). When the modifier is extensively added, another phenomenon, over-modification can occur, which will cause the advantages to regress back toward the premodified state which will lessen gains.

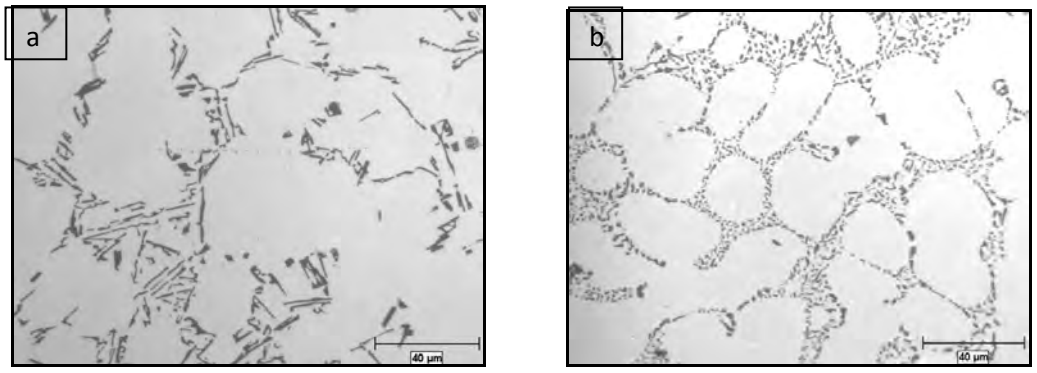

Figure 2.2.4: Optical micrograph of (a) an unmodified permanent mould A356, (b) a modified permanent mould A356 with 200 ppm Sr [30]

With modification, a finer and rounded Si is obtained in the microstructure that contributes to somewhat higher ultimate tensile strengths (UTS) and ductility. The effect of the modification on UTS is negligible in heat-treated alloys although a significant difference can still be found in ductility (Table 2.2.3). Similar to ductility, the impact toughness is also significantly improved by the modification by about 150% in 150 ppm Sr treated A356 alloy [31]. This is due to the decreased size of the brittle phases and better dispersion of those in the more ductile aluminum matrix.

Table 2.2.3: Room Temperature Tensile Properties of A356 Alloy Treated with Different Modifiers [30]

Modifier	Eutectic Si Structure	As-Cast		Heat Treated*	
		UTS, MPa	%E	UTS, MPa	% E
None	acicular	180	6.8	304	11.8
Na	fibrous	195	16.4	292	15.1
Sr	fibrous	196	15.9	301	14.4

* Solution treated at 540°C for ten hours, quenched and then aged at 160°C for 6 hours.

2.2.4.3 Thermal Modification

A fibrous eutectic structure can be obtained, by rapid solidification in the growth rate range 400 to 1000µm per second. Quenched modified structures appear optically identical to impurity modified material. However electron microscopy has reveal that Si is similar to the unmodified form in that it contains no, or very low, levels of twining. This structure is simply an exceedingly fine form of the unmodified eutectic occasioned by very rapid solidification. In practical terms it is of little consequence, as commercial casting process, with the possible exception of die casting, does not operate at solidification rates sufficient to cause quench modification. It is well known that chemical modifiers are more effective at higher freezing rates. For example, it is much easier to modify a chill casting than a heavy section sand casting .This is to be regarded as fundamentally different from quench modification. In the presence of a chemical modifier, both the twining frequency and the angle of branching increase with freezing rate. Both of these promote modification and lead to finer structure [33].

2.2.4.4 Grain Refinement

Two reviews on grain refinement of Al and its alloys published in 2002 and 2003 by Murthy et al. [34] and Greer et al. [35] respectively are available for reference. McCartney [36] has defined grain refinement as the deliberate suppression of columnar grain growth in ingots and castings and formation of fine equiaxed solidification structure throughout the material. An equiaxed grain structure ensures uniform mechanical properties, reduced hot tearing, improved feeding to eliminate shrinkage porosity, even distribution of second phases and microporosity on a fine scale as well as improved machinability in castings. Among the various methods to refine the grain, treating the melt with Al-Ti and AI-Ti-B master alloys providing large quantities of boride and aluminide nuclei into the molten metal is known to be effective.

Grain refinement exerts a positive influence on several properties of cast alloys; notably, hot tearing tendency and porosity shrinkage distribution. Properties such as tensile strength, ductility and impact properties are usually improved by grain refinement. In Al-Si alloys, this is mainly due to improvements in porosity distribution rather than to any decrease in grain size [33].

2.3 Processes of Heat Treatment of Aluminium Alloys

2.3.1 Requirements of the Aluminium Alloy to be Heat Treated

The main requirement for an alloy system to respond to heat treatment is a significant decrease in solid solubility of one or more of the alloying elements with decreasing temperature [37]. Alloys which are cast using high-pressure die-casting method are not suitable for heat treatment. During high pressure die casting gas bubbles are trapped inside the casting and create so called porosity. During heat treatment process these gas pores expand and distort the casting which makes component unusable.

2.3.2 Heat Treatment of Aluminium Alloys

The main heat treatment procedures are homogenization, annealing, and precipitation hardening involving solution heat treatment, quenching, and ageing. A heat treatment and temper designation system has been developed by the Aluminum Association to describe the processing of wrought and cast aluminum alloys.

2.3.2.1 Sequences of Heat Treatment

There are many different sequences of heat treatment which improves properties of aluminium alloys. Most common sequences of heat treatment of aluminium alloys are T5 and T6. To specify heat treatment more precisely one or more digits could be added to T1-T9. For exampleT351 means that the parts were solution heat treated, then stress were relieved by controlled amount of stretching. Aluminium receives no further straightening after stretching. This process can be applied to plate, rolled or cold finished rods and bars [37]. The T6 heat treatment for Al-Si-Cu alloy and the evolution of the microstructure are illustrated; as atoms in solid solution at the solution treatment temperature, through a supersaturated solid solution at room temperature after quench, to precipitates formed at the artificial ageing temperature. Figure 2.3.1 is the T6 (except natural ageing) heat treatment process [38].

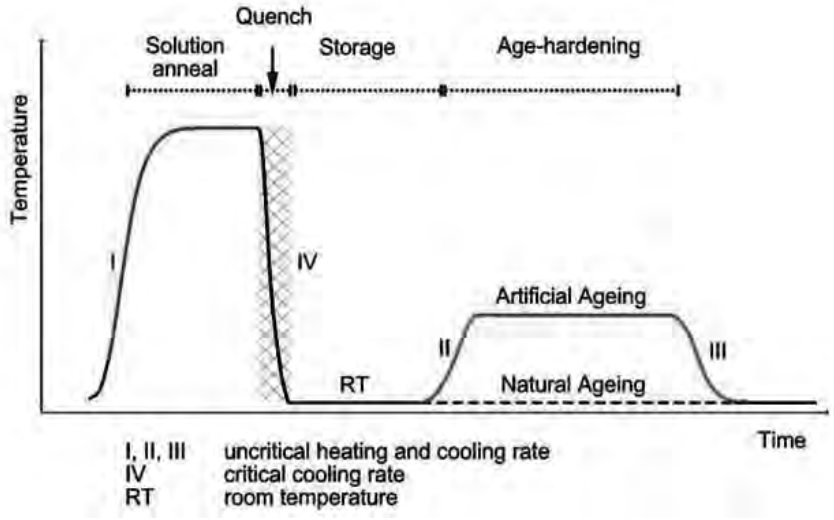

Figure 2.3.1: Diagram showing the three steps for precipitation hardening

Table 2.3.1: Common aluminum heat treatment designations

Treatment	Solution	Quench	Aging
T4	Yes	Yes	Room Temperature only
T5	No	No	Elevated Temperatures
T6	Yes	Yes	Elevated (to yield increased strength)
T7	Yes	Yes	Elevated (to yield dimensional stability)

2.3.2.2 Homogenization of the Cast Alloys

Homogenizing is a separate heat treatment step that requires many hours at elevated temperature and furnace cooling to allow for diffusion of alloying elements, and formation of grains from the as-cast dendritic structure. The as-cast microstructure of direct chill (DC) cast ingots normally displays significant segregation and supersaturation. Micro-segregation in the cast ingots, i.e., segregation on a microstructural scale, is manifested by coring in the dendrites and also non-equilibrium eutectics and intermetallic phases at the grain boundaries. The main aim of homogenization is to improve workability and mechanical properties by dissolving the non-equilibrium brittle inter dendritic constituents and by providing a more homogeneous structure throughout the ingot. Homogenization carried out at temperatures between the solvus and the solidus, ~450-600 °C, for extended periods of time, 2-10 h.

2.3.2.3 Solution Heat Treatment

Aluminum-silicon casting alloys, in which the eutectic silicon is modified by the addition of elements such as strontium, sodium, or antimony, undergo rapid spheroidization of the silicon particles, while complete spheroidization is never achieved in unmodified alloys. Solution heat treatment is normally performed in air, but molten salt baths or fluidized beds can be used to obtain more rapid heating.

Solution heat treatment process requires high enough temperature (not higher then liquidus temperature) and sufficiently long time (enough for phases containing copper and/or magnesium to dissolve completely to achieve nearly homogenous solid solution. Solution Heat Treatment is changing Silicon structure from needle to spherical shape which is supporting coarsening of particles - decreasing interfacial energy caused by instability between phases [39-43]. Mostly alloy composition and melting point of intermetallic phases gives information in which temperature and what time solution heat treatment should be conducted. For example Al-Si with 1 wt% Copper should be limited to 535ºC and for more than 2 wt% Copper 500ºC, to avoid grain boundary melting [44].

2.3.2.4 Quenching

Generally the highest attainable strength levels, the best combination of strength and toughness, and best corrosion resistance and resistance to stress corrosion cracking are associated with the most rapid quenching rates. The sensitivity of alloys to quench rate and the allowable delay between solution heat treatment and quenching is determined from quench factor analysis which is based on avoiding the tip of the nose of the Continuous Cooling Transformation (CCT) diagram (Figure 2.3.2).

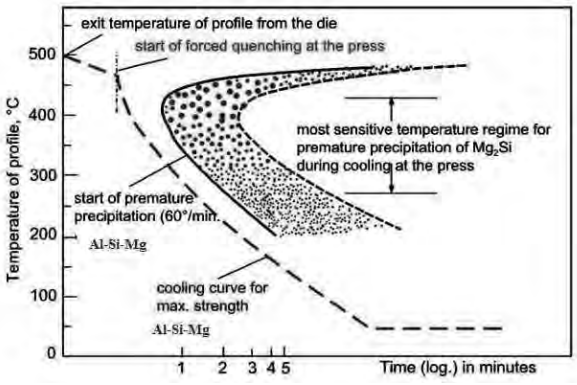

Figure 2.3.2: Continuous Cooling Transformation (CCT) diagram for Al-Si-Mg alloys

Precipitation kinetics is a compromise between degrees of supersaturation and diffusion rate which depend on temperature in opposite ways, resulting in maximum nucleation and growth occurring over a critical temperature range which is between 290°C and 400°C for most alloys. Quench sensitivity is generally higher for higher solute levels and in alloys containing dispersoids which can act as nucleants for coarse precipitates.

Quenching is done after solution heat treatment. At low rate of quenching, vacancies in some degree group with the α-Al or transfer to surface near silicon crystals. Result of this behavior is lower hardness. For example experiments concerning A356 alloy showed that most important and crucial range influencing strength is between 450 ^{o}C and 200 ^{o}C. It was revealed that for that range, when temperature decreases in less than 45s the highest strength is obtained [39, 42].

2.3.2.5 Solution Treatment of Al-Si-Mg Alloy

Studies by Closset et al [45] and Shivkumar et al [46] to examine the solution treatment behaviour of A356 alloys found that dissolution of Mg_2Si particles and homogenization of solute were complete after 30 minutes at 550°C, and other researchers report faster rates during solution treatment of permanent mould castings [47]. Typically, small amounts of magnesium and silicon are also present in the as-cast alloy as components of Fe-rich phases that are slow to dissolve, such as π-Al8Si6Mg3Fe; Gustafsson et al. [48] found these particles dissolve after 4 hours at 520°C.

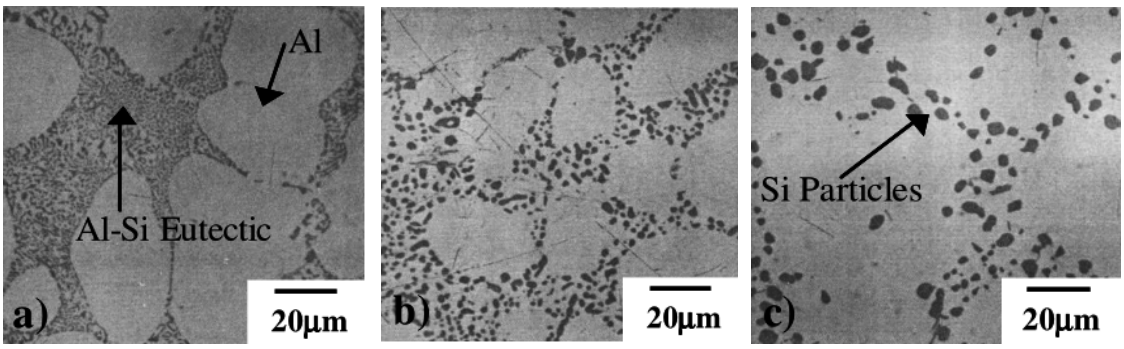

Figure 2.3.3: Morphological evolution of eutectic silicon in A356 aluminum alloy during solution treatment at 540°C; (a) as-cast, (b) 2 hours, (c) 8 hours [49]

Another important metallurgical process during solution treatment is the change in shape of insoluble second phase particles. In the case of Al-Si-Mg alloys this involves a change in the eutectic silicon phase from the as-cast structure to spheroidal globules. The spheroidization

process is illustrated in Figure 2.3.3, which shows (a) the as-cast eutectic silicon network, (b) its fragmentation, and (c) coarsening of fragmented particles during solution treatment.

The use of fluidized beds for rapid heat transfer during solution treatment of Al-Si-Mg casting alloys has been studied in recent years. Chaudhury et al. [50] found that the increased heating rate due to the fluidized bed resulted in faster spheroidisation times than conventional furnaces. This has been attributed to brittle fracture of eutectic silicon particles due to strains induced by the thermal expansion mismatch between the silicon and aluminum phases during heat up.

2.3.2.6 Solution Treatment of Al-Si-Mg-Cu Cast Alloys

Based on conventional solution treatment rule, the restrictive solution temperature to avoid local melting is 550^{o}C in Al-Si-Mg alloys without Cu, but solution temperature of Al-Si-Mg-Cu alloys with high Cu content, such as 319 alloy, are generally restricted below 495^{o}C [51-53, 57]. Solution treatment at low temperature cannot take copper-rich intermetallic compounds in solution into Al matrix fully. Crowell et al. [52] suggests that there are a little of $CuAl_2$ undissolved even after 64 h while solution treating at 500 ^{o}C for Al-Si-Mg-Cu (3.32 wt.% Cu, 0.29 wt.% Mg) cast alloy. In order to further improve the mechanical properties of high Cu containing alloys, many investigators have tried to utilize a higher solution temperature than normal in order to fully, or at least substantially, dissolve the copper containing intermetallic compounds, which has met with varying degrees of success due to incipient melting of intermetallic phases [54-55]. Sokolowski et al. [56-57] have studied a two-stage solution treatment.

Cast Al-Si-Mg alloys can be solution treated at 540-550 °C [58], while alloys containing Cu must be solution treated at a lower temperature due to the risk of local melting of Cu-containing phases. According to Samuel [59] Cu-containing phases start to melt at 519 °C in an A319 alloy with low Mg concentration, while melting starts at 505°C in an A319 alloy with 0.5 wt.% Mg, due to the presence of the Q phase. A two step solution treatment can be used for Cu-containing alloys to increase strength and ductility. The alloy is first solution treated at a low temperature to dissolve Cu-rich phases and then at a higher temperature to increase the speed of homogenisation and spheroidization. Not all phases will dissolve during a solution treatment. The Q phase is reported to be stable or to dissolve very slowly having a high Cu concentration (3.5-4.4wt %) and various Mg concentrations when solution treated at 500°C [60-61].

2.3.2.7 Solution Treatment of Al-Si-Mg-Cu-Ni Cast Alloys

When Ni is added to the Al-Si system, the eutectic transformation is characterized by a simultaneous formation of eutectic Si and Al_3Ni and consequently, eutectic Si and Al_3Ni form a geometrically entangled system. During the course of a solution treatment eutectic Al_3Ni does not significantly change its shape, as can be metallographically observed [59]. Furthermore, in the presence of Ni-aluminides the loss of interconnectivity of eutectic Si is significantly reduced [61-62].

Casting eutectic and near-eutectic Al-Si alloys usually contain some major alloying components such as nickel, copper and magnesium and so on, which are known to form several intermetallic phases (IMPs) with very complex morphologies. Generally, the IMPs include Mg_2Si, Al_2Cu, $Al_5Cu_2Mg_8Si_6$, Al_3Ni, Al_3CuNi and Al_7Cu_4Ni phases and so on [67-68]. The complex microstructural characters lead to excellent properties, such as good abrasion and corrosion resistance, low coefficient of thermal expansion, and high strength-to-weight ratio [69-70]. These alloys are therefore widely used in the automotive industry such as alloy wheel [71-72] and piston applications [73]. Obviously, the mechanical properties of Al-Si multi-component piston alloys depend on the chemical composition, morphology features and evolutions of IMPs [74-75]. In fact, the addition of transition alloying elements such as copper and nickel is the most effective and practical method to improve the mechanical properties, especially for the high temperature performance of piston alloys [76].

In recent years, the precipitation hardening process of Al-Si alloys have been investigated by additional Cu or Mg [78]. The sample was produced by the non-modification and rapid solidification in the steel mold. As cast Al-Si-Cu-Ni alloys consisted of the eutectic Si, Al_3Ni (gray), Mg_2Si (black) and Fe-rich intermetallic phases in α-Al matrix. The eutectic Si phase was flake-like and acicular.

It has been well known that casting product has very low mechanical properties due to micro-segregation in solid solution state. Therefore, a homogenization heat treatment processes becomes necessary. It was found that after 0.5 and 1 h of solution treatment at 520^{o}C, the flake-like and acicular eutectic silicon appear to be fragmented compared to the as cast sample.

After 2 h of solution treatment, the eutectic silicon was clearly fragmented and more spherical. After 4 h of solution treatment, the silicon particle become coarser and the inter particle spacing

was increased. After 10 h of solution treatment, size of eutectic silicon was substantially coarser while the inter particle spacing was longer distance. However, the uniform distribution of particles can be clearly observed in prolonged solution treated samples. Moreover, it was found that the NiAl3 phase was also dissolved by prolonged solution treatment time [77-79].

In Al-Si-Cu-Mg-Ni-Cr alloy the complex eutectic mixture experienced fragmentation in the early stage of solution treatment, and a large number of individual particles were formed. The θ phase dissolved completely after solution treatment for 2 h at 500^{o}C, whereas the γ phase was substituted by the Al_3CuNi (δ) phase, which can still be detected after solution treatment for 24 h at 520^{o}C [80]. On the other hand, the Q phase underwent spheroidization during solution treatment at temperature below 520^{o}C. Other researchers reported that the Q phase has a low solubility in solid solution [81], being insoluble at solution temperature as high as 530^{o}C [82]. In addition, the $Al_{15}(Cr, Fe, Ni, Cu)_4Si_2$ phase retained its blocky morphology, being insoluble at all the experimental solution temperatures.

The major phases observed in the as cast alloy are α-aluminum dendrite, primary Si particle, eutectic Si, Al_7Cu_4Ni, $Al_5Cu_2Mg_8Si_6$, $Al_{15}(Cr, Fe, Ni, Cu)_4Si_2$ and Al_2Cu. The Al_2Cu phase dissolves completely after being solution treated for 2 h at 500^{o}C, while the eutectic Si, $Al_5Cu_2Mg_8Si_6$ and $Al_{15}(Cr, Fe, Ni, Cu)_4Si_2$ phases are insoluble. In addition, the Al_7Cu_4Ni phase is substituted by the Al_3CuNi phase. The α-aluminum dendrite network disappears when the solution temperature is increased to 530^{o}C. Incipient melting of the Al_2Cu-rich eutectic mixture occurs at 520^{o}C, and melting of the $Al_5Cu_2Mg_8Si_6$ and Al_3CuNi phases is observed at a solution temperature of 530^{o}C. The void formation of the structure and deterioration of the mechanical properties are found in samples solution treated at 530^{o}C [80].

2.3.2.8 Ageing Processes

In Al-Si-Mg casting alloys, natural ageing prior to artificial ageing is generally considered detrimental because the clustering of solute atoms during natural ageing reduces the driving force for precipitation and increases the time needed to reach the peak aged condition during artificial ageing. Despite this, a period of natural ageing is included in the ASTM standard, mainly because it is difficult to avoid at least a short delay between quenching and artificial ageing during industrial processing.

2.3.2.8.1 Natural Ageing

Natural ageing is practiced industrially with alloys that display the most significant changes in microstructure and properties over a period of a few days (< 4 days), while the subsequent changes are minor. Other alloys can continue to naturally age for many years. During natural ageing the high level of supersaturation and the high vacancy concentration causes rapid formation of clusters or coherent stable Guinier-Preston (GP) zones.

Natural ageing is inevitable before artificial ageing and has harmful effect on hardness [83]. During natural ageing clusters are formed. This effect can negatively affect properties of the alloy because when clusters are not stable and critical radius is not attained; fewer coarse precipitates are formed [84]. Nevertheless natural ageing cannot be omitted during production process and that is why it is generally taken into consideration while performing research in the field of heat treatment of aluminium alloys.

2.3.2.8.2 Artificial Ageing

Temperature control during artificial ageing is important while there are often large tolerances on treatment time. The T6 temper normally yields the highest practical strength combined with useful engineering performance with respect to other specific requirements. Castings have the highest combination of strength, ductility, and toughness in the T6 temper. The T5 and T7 (overageing) treatments are more commonly used for castings than for wrought products. Overageing often involves heat treating at higher temperatures to carry the alloy beyond the maximum strength level. It results in lower strength and hardness than the T6 temper but yields improved dimensional stability during elevated temperature service. The level of residual stress is reduced during artificial ageing, ranging from 10% to 35% for T6, while T7 provides even more substantial reductions.

Artificial ageing process is based on phase separation which happens in supersaturated solid solution in room temperature or in slightly elevated temperature. The ageing must be accomplished not only below the equilibrium solvus temperature, but below a metastable miscibility gap called the Guinier-Preston (GP) zone solvus line. [85-87]

In Al-Si-Mg alloys separate clusters of Mg and Si atoms form initially, which develop into co-clusters. GP zones form from the co-clusters, which elongate and transform into the β"-Mg_5Si_6

phase, which is the phase having the greatest strength contribution. Overageing transforms some of β" phase into the rod-like β" phase. The Mg: Si ratio increases through the precipitation sequence [88], which makes the supersaturation of Si an important parameter as it influences the fraction of precipitates formed during initial ageing.

The precipitation sequence for Al-Si-Cu-Mg alloys is similar, but more complex, as the Q" phase and the θ" phase also may form. Cu can increase the fraction of the β" phase formed, but it can also form the Q" phase [89-90], which has a lower strength contribution than the β" phase. The β" phase is therefore preferred, rather than the Q" phase. It is however not clearly stated when the Q'' phase forms at the expense of the β" phase in cast alloys. For wrought alloys it has been shown that the fraction of the Q" phase increases with natural ageing and artificial ageing time and temperature [91].

2.4 Evolution of Microstructure during Heat Treatment

Metallurgical processes occurring during solution treatment include: i) the dissolution of soluble second phase particles, ii) the homogenization of solute and iii) the morphological change of insoluble second phase particles. Quenching involves rapid cooling to form a supersaturated solid solution although some precipitation is expected to occur at slower cooling rates. The supersaturated solution decomposes during artificial ageing as the precipitation of a fine dispersion of second phase particles takes place. Each process is discussed separately in the following sections.

2.4.1 Dissolution of Soluble Second Phase Particles

A number of theoretical approaches have been applied to describe the diffusion-controlled dissolution of a second phase particle in an infinite matrix [92]. While these analyses consider a single particle in an infinite matrix, the presence of other particles cause overlapping of the diffusion fields and this has been taken into account by using a finite diffusion field approach [93-95]. This approach is commonly known as the "cell concept" [95], and assumes the particles are equidistant and of uniform size. Reasonable descriptions of dissolution processes have resulted from the application of the cell concept to a number of alloy systems containing non-equilibrium particles [96-97].

In recent years numerical models have been developed to describe the dissolution kinetics of second phase particles [98-100]. Rometsch et al. [101] presented a model simulating dissolution of the Mg_2Si phase and homogenization of magnesium in Al-Si-Mg alloys during solution treatment, and predicted complete dissolution and homogenization after 15 minutes, consistent with the experimental findings for the A356 alloy [102]. Subsequently, a numerical model based on a mass balance was developed to predict co-dissolution of Mg_2Si and π-Al8Si6Mg3Fe in A356 [103]. They predicted that Mg_2Si dissolves completely within 4 minutes at 540°C, whereas most π-Al8Si6Mg3Fe particles dissolve within 30 minutes and complete dissolution occurs within 12 hours.

2.4.2 Morphological Change of Insoluble Second Phases

In Al-Si-Mg casting alloys, the eutectic silicon phase evolves during solution treatment from the as-cast morphology to spheroidal particles. Many authors [104-106] have analyzed this spheroidization process using the eutectic particle size, spacing and aspect ratio, and found that modified eutectic particles spheroidize faster than unmodified particles [107-109] due to the refined structure's larger interfacial area and driving force for morphological change. The spheroidization and coarsening of eutectic silicon particles is driven by the reduction of the surface energy associated with the Al/Si interface [111-113]. At high temperature, the size and frequency of surface perturbations at the Al/Si interface increase, causing the breakdown of the eutectic into a series of near-spherical particles that subsequently coarsen to further reduce the interfacial area [112-116].

2.5 Precipitation Hardening in Aluminum Alloys

2.5.1 Introduction

Precipitation occurs as a result of a diffusional transformation in which thermally activated atomic movements control the nucleation, growth and coarsening of second phase particles forming within a supersaturated solid solution. The precipitation reaction is expressed as follows; $\alpha' \rightarrow \alpha + \beta$, where α' is the initial supersaturated solid solution, β is a stable or metastable precipitate, and α is a more stable solid solution with an equilibrium composition [120]. As the precipitate has a different composition to the matrix, long-range diffusion of solute is required, and the precipitation rate is temperature dependent.

Typically, a series of metastable phases precipitate during ageing prior to the equilibrium phase. Despite having a lower driving force for their precipitation, these transition phases have a lower activation energy barrier for nucleation and therefore the free energy of the system can be reduced more quickly through their formation in preference to the direct formation of the equilibrium phase.

2.5.2 Precipitation from Supersaturated Solid Solution

2.5.2.1 Precipitation in Al-Si-Mg Alloys

Al-Si-Mg alloys are heat treated, most commonly to a T6 condition which consists of a solution heat treatment, quenching and artificial aging. During solutionizing, the following might take place:

- Dissolution of Mg, Si and other elements into the α-Al,
- Homogenization of the casting (elimination of microsegregation, coring and metastable phases),
- Spheroidization, coarsening and fragmentation of the eutectic phases those are not soluble in α-Al.

Solutionizing is followed by quenching. Quenching results in the supersaturation of alloying elements and quenched-in vacancies which are retained in the aluminum matrix (Alssss). Fast quenching results in higher amount of those in the matrix which gives better age-hardening response, but causes thermal stresses and distortion. Therefore, an optimum quenching rate is necessary. Precipitation goes through a series of precipitation beginning with the formation of needlelike Guinier-Preston (G.P) zones, continuing with metastable phases (β", β') and ending with the formation of the β-Mg_2Si phase [122-124]: α-Al_{ssss} → Vacancy rich G.P zones → Needlelike β" → Rod-like β' → β plates.

In the precipitation sequence, coherent G.P zones (2.5-30 nm) start to elongate in the [100] matrix direction and reach a needle shape forming the metastable semi-coherent β" phase (46-70nm). These needles grow with time to rods (β') and eventually to the equilibrium β phase. The strengthening obtained though precipitation depends on the volume fraction and the size of the precipitates. Usually the peak strength is achieved between the β" and the β' phase.

Artificial aging temperatures may vary, but in general to obtain the maximum strength, a temperature between 155 - 175°C for 3-5 hours is used. The increase in artificial aging temperature may enhance the room temperature tensile strength, however, the elongation is sacrificed, (Table 2.5.1). It should be noted this relationship is affected by the casting process for a given alloy composition.

The temperatures above the artificial aging range such as 200-240°C increase the ductility and again there is a loss of strength due to the fact that the peak-strength phases (β'' and β') start to disappear and the equilibrium phase is reached. This situation is called over-aging and the over-aging heat treatment is known as the T7 treatment. Hernandez et al. [124] stated that the average length of the precipitates in the A356 alloy changes from 22.1 nm (β'') to 203.2 nm (β) by increasing the aging temperature from 170°C to 236°C for 6 hours. The effect of aging time and temperature on the yield strength and hardness of Al-Si-Mg alloys is given in Table 2.5.1. It can be seen that aging at 180°C for 16 hours is equivalent to aging at 200°C for 4 hours. Therefore, it can be concluded that the diffusion process is extremely temperature dependent but less time dependant. Other than the β phase, the excess Si can precipitate in 356 alloys [125]. These Si clusters are observed when the artificial temperature is above 200°C [124,126].

Table 2.5.1: Effect of aging temperature on room temperature tensile properties of permanent mold 356 Alloy [127]

Ageing temperature oC/time(h)	Y.S, MPa	UTS, MPa	%E
155/3	207	303	14.6
165/3	241	327	11.8
175/3	262	331	10.6

The precipitation of metastable Mg-rich phases depends on the Mg-to-Si ratio. The excess of Si in solid solution can significantly alter the kinetics of precipitation and the phase composition. In other words, equilibrium phases are enriched in Mg and metastable phases are enriched in Si. Silicon precipitates are observed if stable phases are formed [130].

2.5.2.2 Precipitation in Al-Si-Cu Alloys

The precipitation sequence for an Al-Si-Cu alloy, such as 319, is based upon the formation of Al_2Cu-based precipitates. The Al_2Cu precipitation sequence is generally described as follows: $\alpha_{ssss} \rightarrow$ GP Zones $\rightarrow \theta'' \rightarrow \theta' \rightarrow \theta$ (Al_2Cu) [131-133].

The sequence begins with the decomposition of the solid solution and the clustering of Cu atoms; the clustering then leads to the formation of coherent, disk-shaped GP zones. At room temperature aging conditions, GP zones arise homogeneously; these zones manifest as two-dimensional, copper-rich disks with diameters of approximately 3-5 nm. As time increases, these GP zones increase in number while remaining approximately constant in size. With regard to the Al-Cu alloys, as the aging temperature is increased above 100 ^{o}C, the GP zones dissolve and are replaced by the θ'' precipitate. This precipitate is a three dimensional disk-shaped plate having an ordered tetragonal arrangement of Al and Cu atoms; θ'' also appears to nucleate uniformly in the matrix, and is coherent with the matrix in binary Al-Cu alloys. The high degree of coherency causes extensive coherency strain fields to arise [134]; giving peak strength to the material at this time.

Increases in Cu were found mainly to reduce ductility and change the morphology of the Cu-containing phases [135]. Increasing the solution temperature during the heat treatment of an automotive 319 alloy has the greatest influence in the dimensional change of samples due to dissolution of the Al_2Cu (θ) eutectic phase [136]. By increasing the aging temperatures, however, expansion is produced as a result of the transformation of the metastable phases into equilibrium phases.

2.5.2.3 Precipitation in Al-Si-Mg-Cu Alloys

Aging causes precipitation of one or more of the phase(s) Mg_2Si, $Al_5Cu_2Mg_8Si_6$, or Al_2Cu in the Al-Si-Cu-Mg alloys depending upon the chemical composition [137-140]. These precipitates cause strengthening of the alloy. Heat-treatment characteristics of Al-Si-Cu-Mg alloys have been investigated [137,139]. The precipitation strengthening response in these alloys is due to the decomposition of metastable supersaturated solid solution obtained by solution heat treatment and quenching. Phases that have been reported to precipitate during aging of Al-Si-

Cu-Mg alloys (depending upon the chemical composition) are Al_2Cu (θ), Mg_2Si (β), $Al_5Cu_2Mg_8Si_6$, and Al_2CuMg (S) phases [137-140].

Kang et al.[140]reported that the θ' phase has a preferential tendency to precipitate on dislocations around Si particles, while the $Al_5Cu_2Mg_8Si_6$ phase homogeneously precipitates in the α-Al matrix. Zafar et al. [139] suggested that the $Al_5Cu_2Mg_8Si_6$ phase contributes significantly to the age hardening behavior of these alloys, since it is uniformly distributed in the Al matrix. Li et al. [137] have reported that the precipitation sequence in Al-Si-Cu-Mg alloys is supersaturated solid solution → formation of Guinier-Preston (GP) zones → dissolution of GP zones → formation of metastable phase → formation of equilibrium phase. The aging sequence for these alloys is quite complicated and often two aging peaks are observed. The first peak of the age hardening curve is probably due to the high density of GP zones, while the formation of the metastable phase contributes to the second peak. Between the two peaks, the alloy has low strength [137].This is because, at the intermediate stage of aging (i.e., during the transition of GP zones to metastable phases), the density of GP zones is significantly low owing to their dissolution, while the semi- coherent metastable precipitates are too small to offer any resistance to dislocation motion.

Therefore, the age hardening curve shows a dip (low hardness) at this intermediate stage. Oullet et al. [141] studied the effect of Mg content and Sr modification on the heat treating characteristics of Al-Si-Cu-Mg alloys and observed that tensile strength improved significantly with Mg additions up to 0.45 wt pct, while the addition of Sr increased porosity and thereby reduced tensile strength. In addition, Sr-modified Al-Si-Cu-Mg alloys show severe segregation of Cu-rich intermetallics in areas away from the growing Si regions. However, Beumleret al. [142] observed that the addition of Mg in sand-cast Al-Si-Cu alloys has a negligible effect on tensile strength. In general, for Al-Si-Cu-Mg alloys, the duration of a T6 heat treatment cycle using a conventional electrical furnace (CF) is about 12 to 20 hours [143].

2.5.3 Evaluation of Resistivity during Nucleation of Clustering

The electrical resistivity in an alloy is mainly caused by the thermal vibration of atoms, solute atoms and precipitates. Osamura et al. [144] investigated the changes of the electrical resistivity of Al alloys as: $\rho = \rho_o + \rho_m + \rho_p$, where ρ_o, ρ_m and ρ_p represent resistivity by the lattice vibration in the pure Al, solute atoms in the matrix and precipitates, respectively. Meanwhile, ρ_o is not

changed during isothermal aging for the electrical resistivity measurement and ρ_m does not depend on the temperature, but concentration of the solute atoms. Among them, ρ_p strongly affects the changes of electrical resistivity through the formation of precipitates with different size, number density and size distribution. Besides, ρ_p can be expressed as- $\rho_p = N_p \times G_p(r)$**,** where, N_p and $G_p(r)$ represent the number density of precipitates per unit volume and resistivity from one precipitate with radius r. Furthermore, Vp, volume of the precipitate, is represented as: $Vp= N \times 4\pi r^3/3$, Namely, the number density of precipitates is substantially decreased with increase of the radius of a precipitate. From this basis, the maximum of the electrical resistivity is drawn during isothermal aging. The electrical resistivity change during isothermal aging is simply expressed using a dotted line in Figure 2.5.1 regarding the size and number density changes with aging time.

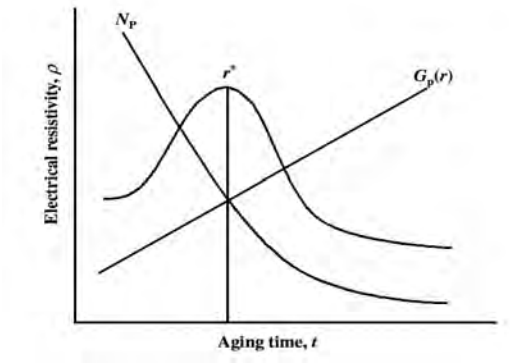

Figure 2.5.1: Schematic diagram of the electrical resistivity change regarding the radius and number density change of precipitates during isothermal aging [155]

It has been shown that electrical conductivity or resistivity [145-146] can be employed as a non-destructive method to monitor the microstructure, modification process and heat treatment in Al-Si-Mg alloys in which the eutectic Si undergoes change in form and size. Moreover electrical conductivity measurements have been successfully used in the evaluation of natural and artificial ageing during heat treatment. In the case of solution heat treatment, electrical conductivity measurements can be related to the changes in Si morphology as shown by Mulazimoglu [147]. He also found that precipitation of Mg_2Si during artificial ageing results in higher electrical conductivity. This can be explained by the precipitation of Mg_2Si and the consequent improvement of the electron flow in the Al matrix.

Figure 2.5.2 shows the changes of electrical resistivity during aging at 100^{o}C in the both Cu-free and Cu-added Al-Si-Mg alloys. It is confirmed that the Cu-added alloy shows higher number

density of cluster than the Cu-free alloy. As confirmed by the electrical resistivity, the Cu-added alloy represents the higher hardness than the Cu-free alloy. The reason why Cu enhances the formation of Cluster is discussed in the next section.

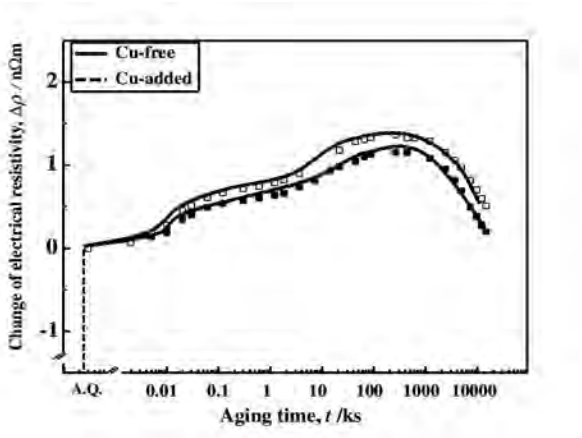

Figure 2.5.2: Changes of the electrical resistivity during aging at 100°C in the both Cu-free and Cu-added alloys

Figure 2.5.3 shows the changes of the electrical resistivity during isothermal aging at 170°C in the both Cu-free and Cu-added Al-Si-Mg alloys. Some more details of the age-hardening behaviors are confirmed due to the advantages of the experiment for the electrical resistivity such as the possible measurement of the initial stage of aging without interruption of the natural aging during the preparation of the specimens.

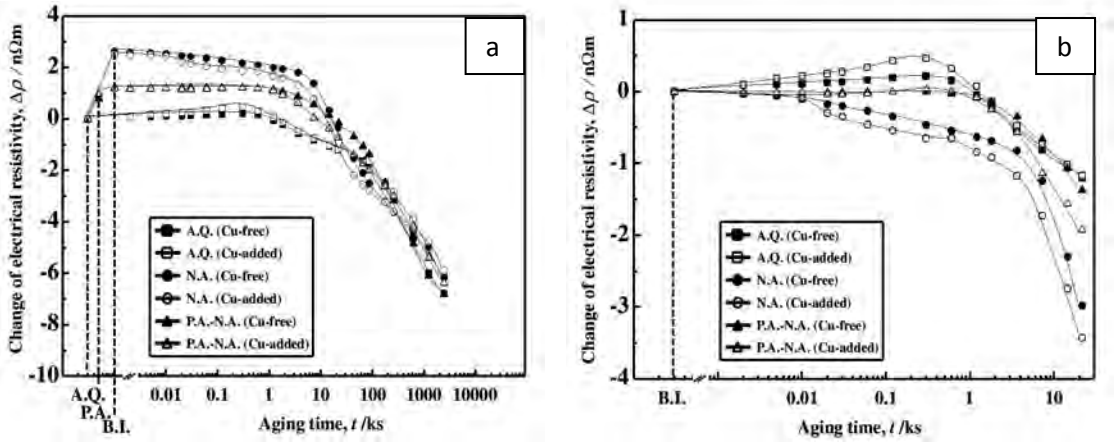

Figure 2.5.3: Changes of electrical resistivity aged at 170°C with different heat treatment conditions in the Cu-free and Cu-added alloys: (a) changes from A.Q. and (b) early stage changes from A.Q. at 170°C

Figure 2.5.3 shows that the electrical resistivity is increased due to the formation of nanoclusters during natural ageing (N.A.) and pre-ageing (P.A.) - natural ageing(N.A.) in the both Cu-free and Cu-added alloys. In order to understand the complicated behavior of nanoclusters before isothermal aging at 170^{o}C with the multi-step heat treatment, electrical resistivity is normalized by the electrical resistivity before isothermal aging (B.I.) regardless of the prior heat- treatment histories in Figure 2.5.3b. The Cu-added alloy shows the higher increase of the electrical resistivity than the Cu-free alloy for the as-quenched condition at the initial stage of the isothermal aging at 170^{o}C. It is noted that the Cu-added alloy produces higher number density precipitates than the Cu-free alloy at the early stage of aging at 170^{o}C.

On the other hand, the electrical resistivity for the N.A. specimens is slightly decreased in both Cu-free and Cu-added alloys. It is plausible that thermally unstable nanoclusters are dissolved. On the other hand, P.A. specimens keep a constant value of the electrical resistivity in the both Cu-free and Cu-added alloys at the early stage of aging at 170^{o}C. The substantial decrease of the electrical resistivity is caused by the decrease of number density with increase of the volume fraction of the precipitates. The decrease of the electrical resistivity is in order of as-quenched (A.Q.), P.A.-N.A. and N.A. specimens [148].

It is well known that the presence of alloying elements or impurities in solid solution increases the electrical resistivity of aluminum alloys [149-150]. Moreover, the presence of small particles in the structure, such as precipitates or dispersoids, causes significant scattering of conduction electrons and, hence, increases the electrical resistivity of an alloy [149-150].The size and distribution of small particles affect the electrical resistivity of the alloy [151,152-154]. The contribution of precipitates and dispersoid particles could be neglected if the precipitate spacing is greater than the mean free path of the electron, i.e., particle spacings larger than 100 nm in aluminum alloys [150].

2.6 Developments in Alloying of Al-Si Alloys

Some automakers have developed new casting alloys by alloying the commercial alloys, mostly the 356, 319 and the 390 with new elements based on statistical casting experiments [156-158, 159]. It is difficult to compare the properties of these new alloys based on what is reported in the literature due to the widely varying heat treatments and mechanical testing conditions that were used. Furthermore, there is limited data on the microstructures of the alloys since much research

focuses on mechanical tests under service conditions. In this section, the new alloys will be discussed as classified according to their compositions.

2.6.1 Effect Cu Additions to Al-Si-Mg Alloy

As in wrought alloys, Cu and Mg together might enhance the precipitation behavior of the cast Al-Si alloys under the right heat-treated condition. Feikus et al. [158] studied two Cu versions (0.5 and 1%) of the commercial A356, where Cu addition improves the mechanical properties for the critical temperature range between 150 and 200°C. Since both versions have similar properties, the lower-Cu alloy has been investigated extensively. This alloy has started to get a big market share in Europe and is currently being used in diesel cylinder heads [157]. The microstructure, precipitation behavior and mechanical properties of this alloy are discussed in some detail here.

2.6.1.1 Effect of Cu on as-Cast Microstructure of Al-Si-Mg Alloy

The increased amount of copper in 356 results in the formation of two copper-enriched phases, Q-$Al_5Mg_8Cu_2Si_6$ and θ-$CuAl_2$, shown in Figure 2.6.1. The Q phase has a fine Chinese-script morphology in the eutectic solidification region, whereas the blocky θ phase either nucleates independently or exists with other phases such as the β-Al_5FeSi platelet. The eutectic Si, β-Mg_2Si, as well as other Fe-rich intermetallic phases (depending on the Fe/Mn ratio and cooling rate) are the other second phases in the Cu alloyed 356.

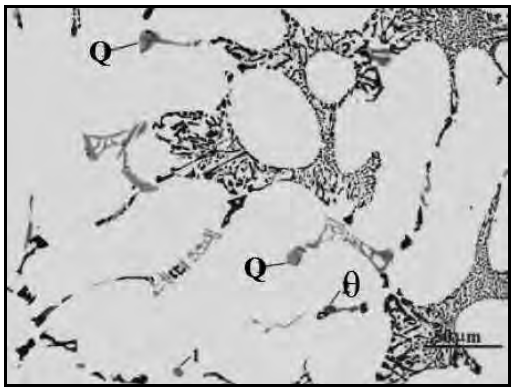

Figure 2.6.1: (1) Q-$Al_5Mg_8Cu_2Si_6$ and (2) θ-$CuAl_2$ phases formed in an Al-Si-Mg alloy with 0.22% Cu [160]

Cu additions tend to increase the amount of micro shrinkage and/or micro porosity in the as-cast 356 microstructure, which is an effect similar to that of Fe and Sr additions. Cho et al. [161]

state that the 356 alloy with 0.50% Cu has twice the amount of shrinkage porosity of the Cu-free alloy. Further increase in the Cu content (1%) results in higher amounts (up to six times) of total porosity [160]. This is explained by a reduction in the solidification temperature which gives longer freezing time and an extended eutectic mushy-zone. The Cu-enrichment of inter dendritic liquid causes the formation of certain solid phases that solidify at lower temperatures than the Al-Si eutectic. These solid phases physically block the liquid decreasing the feeding characteristics of the solidification. The resulting micro porosity is often associated with the poor ductility of the Cu-containing alloys.

2.6.1.2 Effect of Cu on Precipitation of Al-Si-Mg Alloy

Mg and Cu containing phases dissolve in the aluminum matrix during the solutionizing treatment followed by quenching and it is usually assumed that the peak strength and hardness achieved with artificial aging in Cu containing alloys are due to the precipitation of β" (Mg_2Si) and θ' (Al_2Cu) phases. However, Li et al [162] have stated that after the artificial aging, the Q' ($Al_5Mg_8Cu_2Si_6$) phase having a lath-shaped morphology and the β" (Mg_2Si) phase coexist in the 356 alloy with 1% Cu. Only with higher Cu contents such as 3%, the θ' (Al_2Cu) has been additionally observed, (Figure 2.6.2). This contradicts the work of Eskin [130] where no Q phase or its precursors were reported after the aging treatment of an Al-Mg-Si-Cu alloy. The λ' ($Al_5Cu_2Mg_8Si_5$) or L phase has also been observed by some other authors [157, 163, 164] which can be the precursor of the Q phase and responsible for peak strengthening.

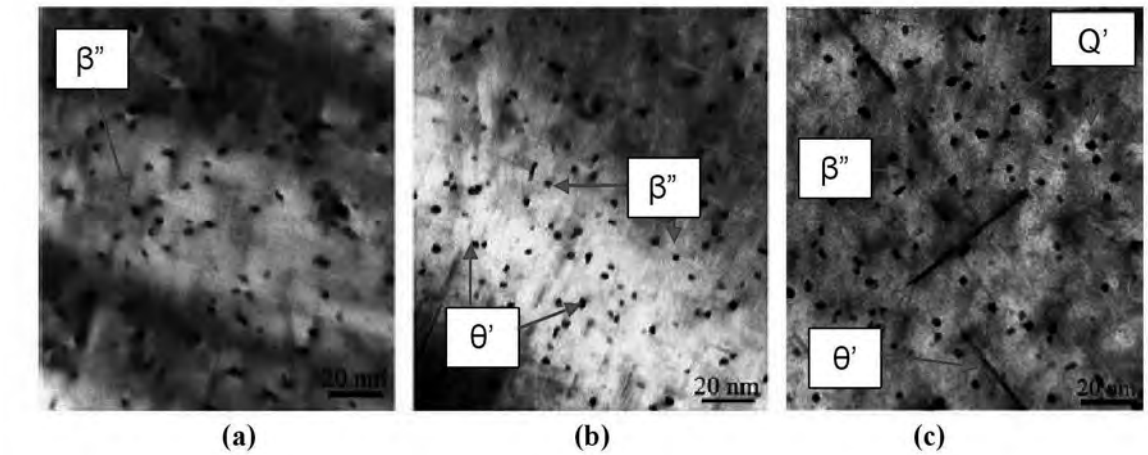

Figure 2.6.2: TEM micrographs of the 356 alloy with (a) 0% Cu (b) 1% Cu (c) 3% Cu [162]

2.6.1.3 Effect of Cu on Tensile Properties of Al-Si-Mg Alloy

Some of the tensile data are summarized in Table 2.6.1 and Table 2.6.2. It can be seen that at room temperature, Cu additions decrease the yield strength and slightly increase the ultimate tensile strength. At 250°C, a significant improvement is noted not only in the tensile but the ultimate strength of the Cu-containing alloys.

Table 2.6.1: Tensile properties of A356 Alloys at 25°C

%Cu content	Ageing temperature ^{o}C/time(h)	YS, MPa	UTS, MPa	%E	References
0.0	165/4	214	294	9.5	[158]
0.5	165/4	190	280	8.0	[158]
0.0	190/3	233	306	12.8	[258]
0.5	165/3	219	319	11.8	[258]
0.0	175/6	310	375	12.2	[162]
1.0	175/6	288	380	11.0	[162]
0.0	200/5*	257	299	9.9	[126]
0.5	200/5*	275	327	9.8	[126]

**HIP* treated (2 hours at 485^{o}C, 100MPa)

Table 2.6.2: Tensile properties of A356 Alloys at 250°C

%Cu content	Ageing temperature ^{o}C/time(h)	YS, MPa	UTS, MPa	%E	References
0.0	165/4	45	61	45.5	[158]
0.5	165/4	63	83	20.0	[158]
1.0	165/4	62	83	23.6	[158]
0.0	200/5*	55	61	34.5	[126]
0.5	200/5*	66	73	34.5	[126]

**HIP* treated (2 hours at 485^{o}C, 100MPa)

The addition of 0.5% Cu has nearly the same effect on tensile properties as the addition of 1% Cu. The elongation values of the 356 alloy at both temperatures are lowered due to the increased

microporosity when Cu is added [160, 162]. This negative effect can be overcome with a hot isostatic pressing (HIP) treatment, where a great portion of the internal porosity is healed. Hence, the HIP treated alloys might have better tensile properties while displaying the same ductility.

2.6.1.4 Effect of Artificial Ageing on the Strength of Al-Si-Mg-Cu Alloy

The age hardening response of the Al-Si-Mg alloy is high and fast, compared to the Al-Si-Cu alloy which has a low and slow age hardening response (Table 2.6.3). When both Mg and Cu are present the highest age hardening response is obtained. In Al-Si-Cu-Mg alloys either the β" phase or the Q" phase may form, or a combination of them [162, 36]. The Q" phase is reported to the position of the peak yield strength towards longer ageing times [36,165]. In this investigation the time to peak yield strength of the Al-Si-Cu-Mg alloy is longer than for the Al-Si-Mg alloy, indicating the presence of the Q" phase. The formation of the Q" phase may be a consequence of the use of natural ageing prior to artificial ageing [165]. A further difference between the Al-Si-Mg alloy and the Al-Si-Cu-Mg alloy is that the peak yield strength of the Al-Si-Mg alloy is less sensitive to the ageing temperature. It can be seen in Table 2.6.3 that the difference in age hardening response between the Al-Si-Cu-Mg alloy and the Al-Si-Mg alloy is smaller for ageing at 210°C than at 170°C.

The coarseness of the microstructure did not have a large influence on the yield strength when the solution treatment time was chosen to be long enough to achieve complete dissolution and homogenisation. For the Al-Si-Mg alloy aged at 170°C the difference in peak yield strength between the coarsest and the finest microstructure was 7MPa.The solution treatment time for the coarsest microstructures of the Cu containing alloys was not long enough, resulting in a lower concentration of Cu in solid solution and a lower yield strength after artificial ageing.

Table 2.6.3: Age hardening response and peak properties for the three alloys

	Time to peak t_{peak}[h]		Age hardening response, YS [MPa]		Peak properties for SDAS 25µm YS [MPa] / Elongation (%)	
	170°C	210°C	170°C	210°C	170°C	210°C
Al-Si-Mg	10	0.3	139	123	213/11	213/12
Al-Si-Cu	>170	12	76	44	206/4	175/6
Al-Si-Mg-Cu	20	2	168	138	375/1	348/1

2.6.1.5 Effect of Artificial Ageing on the Ductility of Al-Si-Mg-Cu Alloy

An increase in yield strength generally leads to a decrease in ductility for a material that exhibits necking [166]. All samples of the Al-Si-Mg alloy having the finest microstructure reached necking, except the ones naturally aged or artificially aged 20 min. at 170°C. The elongation to fracture of the Al-Si-Mg alloy decreases when the yield strength increases during under ageing. The elongation to fracture however does not increase directly when the yield strength starts to decrease after the yield strength plateau, but remains low during initial overageing. For longer overageing of 5 h at 210°C, the elongation to fracture increases slightly. The values deviating from a continuous decrease in elongation to fracture for the intermediate microstructure, in correspond to samples which fractured without reaching necking, which all the other samples did. The trend with the overaged condition giving a lower elongation to fracture for a certain yield strength compared to the underaged condition is clear in the investigation. The formation of small Si particles in the matrix during initial overageing [167-168] can be hypothesized to be the cause of the continued decrease in elongation to fracture during initial overageing.

Samples of the Al-Si-Cu-Mg alloy having the finest microstructure reach or are close to reaching necking, while samples of the coarser microstructures fracture before necking. The elongation to fracture for the finest microstructure of the Al-Si-Cu-Mg alloy shows the expected behaviour and increases directly after the peak aged condition when the yield strength decreases. The two coarser microstructures of the Al-Si-Cu-Mg alloy have a low elongation to fracture, around 1%, for ageing times between 10 h and 100 h at 170°C. These ageing times correspond to the highest yield strength. The high yield strength in combination with larger brittle phases and defects in the coarser microstructures, compared to in the finest microstructure, is thought to cause the low elongation to fracture. An increase in elongation to fracture for the coarser microstructures is obtained when the yield strength has decreased significantly. The Al-Si-Mg alloy in the underaged condition has a better combination of yield strength and elongation to fracture compared to the Al-Si-Cu-Mg alloy. Al-Si-Mg alloys are therefore preferable to Al-Si-Cu-Mg alloys as long as the Al-Si-Mg alloys can reach the required strength [169].

2.6.2 Effect of Ni Additions to Al-Si-Mg (-Cu) Alloy

The effect of Ni on the high-temperature strength of Al-Si foundry alloys was discussed in detail elsewhere [174-175]. It was shown that the whole microstructure of Al-Si alloys can be considered as a coarse two-phase system, with the phases 'primary Al solid solution (α_{prim})' and 'eutectic (E)' [174-175]. When comparing the hardness or strength of these phases qualitatively, one can assume E to be the stronger/harder phase. In coarse two-phase systems the stronger phase will contribute significantly to the overall strength only if it is subjected to load transfer. Load transfer, however, requires a continuous network of the respective phase. Such continuity of the harder phase E undoubtedly exists for the microstructures of the alloys investigated [170,174-175].

We now have to consider the microstructural features within the eutectic. In Ni-containing alloys the eutectic phase E consists of more or less soft 'eutectic Al (αE)' and hard 'eutectic Si and Al_3Ni'. The eutectic phase E can therefore also be treated as a composite, with the same requirements as discussed above for the α_{prim} + E-compound. In order to form a strong/hard E-phase the hard 'eutectic Si and Al_3Ni' needs to be connected 3- dimensionally [173].

In Ni-free alloys the Si contiguity is completely lost after a solution treatment at 540°C for 24 h and an AlSi12 alloy e.g. changes from a 'fibre-reinforced' to a 'particle-reinforced' type of material, with the same strength as an AlSi1 alloy [173, 175]. When Ni is added to the Al-Si system, the eutectic transformation is characterized by a simultaneous formation of eutectic Si and Al3Ni and consequently, eutectic Si and Al_3Ni form a geometrically entangled system. During the course of a solution treatment eutectic Al_3Ni does not significantly change its shape, as can be metallographically observed. Furthermore, in the presence of Ni-aluminides the loss of interconnectivity of eutectic Si is significantly reduced [174-175].

The Ni-phase in combination with eutectic Si forms a strongly interconnected 3D-structure, whose contiguity is highly preserved even after a solution treatment for 24 h [173]. However, depending on the amount of eutectic phase, more or less Ni is required to restore the connectivity of the 'eutectic Si + Al_3Ni' network. For Mg-containing eutectic alloys the authors determined 2% Ni to be sufficient to sustain the contiguity of solution-treated samples, and an increase in the Ni concentration has no further positive effect on strength [174-175].

For this reason the high-temperature strength of the Mg- containing alloys 1-4 increases with increasing Ni concentration up to 2%, whereas the positive effect of Ni is much more considerable for the solution-treated alloys, especially with respect to the yield strength. While for Ni-containing alloys the contiguity of the 'eutectic Si and Al_3Ni' is more or less preserved due to the presence of Ni-aluminides, the spheroidization of the eutectic Si in the Ni-free alloy 1 ($AlSi_{12}$(Mg)) results in its reduced contiguity and thus reduced strength values[171, 173,175]

2.6.3 Impact Behaviour of Al-Si-Mg Alloys

Both Flinn [176] and Sicha [177] affirm in their works that, due to their excellent castability and good compromise between mechanical properties and lightness, aluminium-silicon alloys are the most important and widely used casting alloys in order to cast components with complex shapes. A consolidated example of aluminium alloy employment regards the production of wheels, which, together with an improved aesthetic appearance, guarantees an improvement of driving, like directed consequence of the inertia reduction of the wheels. These components are somewhat unique as they must meet, or exceed, a combination of requirements, from high quality surface finish, as wheels are one of the prominent cosmetic features of cars, to impact and fatigue performance, because wheels are critical safety components.

Li et al. [178] analysed the effect of various alloying elements and different heat treatments in A319-type alloys by means of instrumented impact test. Analysing the impact properties of Al-Si foundry alloys, Paray et al. [179] evaluated the total absorbed energy of the samples subjected to impact test like the sum of the energy required for crack nucleation and the energy required for crack propagation, in order to describe the dynamic toughness of the material. Srivastava et al [180] demonstrated that in the case of cast aluminium alloys the presence of a notch can decrease the impact values even further, by up 80%, when compared to un-notched specimens; even a shallow scratch of 0.1 mm reduces the energy absorption by 30%. If a notch is present, the absorbed energy can be dependent on the notch geometry than on the microstructure.

Murali et al. [181] evaluated the influence of magnesium content in the $AlSi_7Mg_{0.3}$ alloy with low iron level: the absorbed energy drops significantly by about 50% with increasing magnesium content from 0.32 wt.% to 0.65 wt.%. Similar behaviour is observed increasing the iron content from 0.2 wt. % to 0.8 wt.%, at 0.32 wt.% Mg, due to an increased precipitation of β-Al5FeSi platelets.

Shivkumar et al. [182] analysing Charpy specimens in A356 T6 machined from plate and cylindrical castings, demonstrated that the strontium modification, as well as an increase of solidification rate, improves the impact properties of sand and permanent mould castings, even if the effect is more pronounced at low magnesium and iron content.

As specified by Zhang et al. [183] the T6 heat treatment provides beneficial effects to cast aluminium components: it increases the yield strength, through the precipitation of a large number of fine β'-Mg_2Si particles, and improves the ductility, through spheroidisation of the eutectic silicon particles.

Earlier Càceres et al. [184] and later Wang and Càceres [185] observed that the inter-particle spacing plays a dominant role in determining cracks' nucleation and propagation and that the fracture path considerably depends on the dendrite cell size. The nucleation of the cracks usually starts with cracking of brittle particles. Once a large number of particles are cracked, cracks grow by linking microvoids formed by the cracking of these particles. With a smaller inter-particle spacing, the microvoids link and grow easily.

Li et al. [178] demonstrated that oxides, such as phosphorous oxides, which act as nucleation sites for Al_2Cu precipitates in A319-T6 alloy, can accelerate the cracking process reducing the impact properties.

While the benefit effect of T6 heat treatment is recognized, the additional cost and required time are substantial. Zhang et al. [183] showed that shortening the total time of the T6 heat treatment cycle there exist a region where the impact energy decreases to a minimum before increasing. The cause of this region seems due to a conflict between the negative effect of solution treatment on ductility and impact strength, associated with a rapid increase in the yield strength and the more slowly developing positive effect associated with the spheroidization and coarsening of silicon particles.

Microstructural features, such as dendrite arm spacing (SDAS) and eutectic silicon particles have been correlated to impact properties: absorbed energy, maximum load, crack nucleation and propagation energy. In addition to metallographic with Optical Light and Scanning Electron Microscopic inspections, fractography has been presented to underline the effect of micro constituents on crack nucleation and propagation.

2.7 Strengthening Mechanisms in Al-Si-Mg Alloys

In this section, the strengthening mechanisms arising from the presence of precipitates as well as larger second phase particles are discussed, as these are both relevant to Al-Si-Mg casting alloys that contain strengthening precipitates and eutectic particles.

2.7.1 Precipitation Strengthening Mechanisms

In the early stages of ageing, the precipitates are small and coherent or semi-coherent with the matrix and thus are shearable by dislocations, as illustrated in Figure 2.7.1.

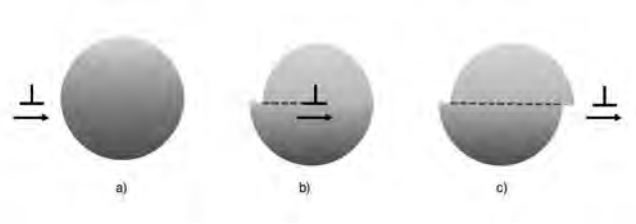

Figure 2.7.1: Schematic view of three stages of the dislocation cutting mechanism

The following strengthening mechanisms are considered to arise in the presence of coherent/semi-coherent particles and the dislocation cutting mechanism [186-188];

- Coherency Strengthening - Coherent/semi-coherent particles increase the free energy of the system due to the elastic misfit between the particle and matrix.
- Modulus Strengthening - If the particle has a higher elastic modulus than the matrix, a larger stress is required for the dislocation to continue moving forward.
- Chemical Strengthening - There is an increase in interfacial energy when the particle is cut by the dislocation.
- Atomic Order Strengthening - If an ordered particle is cut by a dislocation, the free energy increases due to creation of an anti-phase boundary.
- Stacking Fault Strengthening - This arises from differences between the stacking fault energy of the matrix and precipitate.

As ageing continues the precipitate grows and becomes incoherent with respect to the matrix. In this case, the dislocation bows between precipitates and forms loops in order to move forward,

as shown in Figure 2.7.2. Strengthening arises from bowing of the dislocation which is opposed by its line tension, as well as the formation of dislocation loops (Orowan loops) around precipitates.

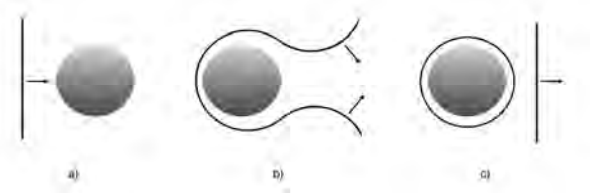

Figure 2.7.2: Schematic view of three stages of the Orowan looping mechanism

2.7.2 Optimal Strengthening

The relationship between particle size and yield stress is given in Figure 2.7.3. At the commencement of ageing, both the size and the mean spacing between the precipitates are small and the stress required for a dislocation to cut through these precipitates is lower than the stress required for the dislocation to bow around the particles.

As the size of the precipitates increases, the yield strength of the alloy continues to increase, provided that the number of precipitates remains unchanged (curve A in Figure 2.7.3). However, this does not occur since as the ageing process proceeds, small precipitates dissolve and coarser precipitates form at their expense. This leads to a decrease in the number of precipitates and thus an increase in their mean spacing. The stress required for a dislocation to bow around the particles is now smaller than the stress required for the dislocation to cut through them. As the size of the particles increases, the distance between them becomes progressively greater and the looping process becomes even easier, which then causes the yield strength to decrease with increasing ageing time (curve B in Figure 2.7.3).

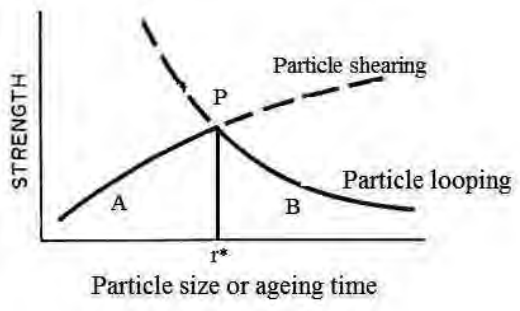

Figure 2.7.3: Variation of yield strength with particle size and ageing time [189,193]

A microstructure which yields by a combination of particle shearing and particle looping processes exhibits the maximum strength. This corresponds to a critical dispersion of precipitates of size r = r* (Figure 2.7.3). This condition is satisfied by a combination of fine coherent and semi-coherent particles, which is generally the case in age-hardenable alloys. The magnitude of the maximum strength achieved is proportional to the volume fraction of the precipitates.

The existence of an interrelationship between the morphology, orientation and distribution of the strengthening precipitates and the yield strength has long been recognized and this has been the subject of a number of studies [190-192]. Generally, plate shaped precipitates contribute to an increase in critical resolved shear stress more effectively than rod-shaped precipitates. In the case of Al-Mg-Si (-Cu) alloys the strengthening precipitates appear as both spherical precipitates and needle- or rod-shaped precipitates along <100> matrix directions. Nie et al. have shown that the rod-shaped precipitates are far more effective in strengthening than the spherical precipitates [190, 193].

2.7.3 Strengthening due to Second Phase Particles

Casting alloys based on the Al-Si system may be considered to be two-phase materials composed of hard silicon particles contained in the softer aluminum matrix. The presence of a distribution of hard particles embedded in a metal matrix is known to result in an overall strengthening of the material, and there has been large interest in this area of research concerning metal matrix composites (MMC's) [194]. Typically, reinforcing particles are present in volume fractions between 5% and 20%, and are usually 10µm to 30µm in diameter, although they can range between 5µm and 250µm. In Al-Si-Mg casting alloys, the silicon phase is present up to a volume fraction of 11%; however the particles are usually smaller than 5µm in diameter except after prolonged solution treatment.

The strengthening effect of eutectic silicon particles in an Al-Si-Mg alloy can be explained by the transfer of load from the ductile aluminum matrix to the brittle silicon particle via the development of shear stresses at the particle-matrix interface. In general, if the second phase particles are strongly bonded to the matrix, and both particle and matrix behave elastically, a simple rule of mixtures equation can be used to predict the overall strength: $\sigma_{tot}=V_{f.particle} \times \sigma_{particle} + (1-V_{f.particle}) \times \sigma_{matrix}$. where $V_{f.particle}$ is the volume fraction of the strengthening particle, and σ_{tot},

$\sigma_{particle}$ and σ_{matrix} are the total stress acting on the material, the stress acting on the particle and the stress acting on the matrix respectively. If the material is allowed to deform plastically, then equation is modified as follows; $\sigma_{tot}=V_{f.particle} \times \sigma_{particle} + (1-V_{f.particle}) \times \sigma'_{matrix}$. Where; σ'_{matrix} is the stress acting on the matrix at the particle fracture strain [195].

2.8 Corrosion Behaviour of Aluminium Alloys

2.8.1 Introduction

To characterize the susceptibility of metallic materials to electrochemical degradation modern research techniques increasingly use the relationship between voltage and current intensity occurring in corrosive systems. Such studies rely on computerized measuring system, in which suitable electrical stimulation is generated numerically while the system simultaneously analyzes the response. The results are presented in the form of graphs showing the current - voltage relationships [201].

2.8.2 Corrosion Behavior of Al-Si-Mg Alloys

In recent years, there has been considerable research on the corrosion and corrosion protection of AA2024, AA6061 and AA7075 because they are widely used in critical structural applications. However, cast alloys like AA356 and AA380 can be more corrosion prone and more difficult to protect than 2024 due to the presence of high concentration of alloying elements and intermetallic particles. Comparatively, little studies have been carried out to understand the corrosion behavior of these alloys [208-210]. Cast alloys generally contain a high concentration of intermetallic compound particles, whose electrochemical behavior has not been completely characterized.

2.8.3 Electrochemistry of Intermetallics Phases

Differences in the electrochemical properties of solute enriched α-Al matrix, solute depleted zones, and precipitate phases are important factors affecting localized corrosion susceptibility (pitting corrosion) of Al base alloy systems [211]. The electrochemistry of intermetallic compound (IMC) particles plays an important role in governing localized corrosion and environmentally assisted cracking of many engineering aluminum alloys [212]. The role of IMC particles are often described in the context of their galvanic relationship with their surrounding

matrix phase, solute depleted zone, or other IMC particles. As we have discussed in previous sections, intermetallics generally found in cast alloys are: Al_2Cu, Mg_2Si and Al_2CuMg etc.

Copper is mainly added to increase the strength; at low temperature by heat treatment, at higher temperature through the formation of compounds with iron, manganese, nickel etc [213]. As with wrought alloys, copper is the alloying element most deleterious to general corrosion of cast alloys [214-216]. Alloys such as 356.0, 513.0 and 514.0 that do not have copper as an alloying element have a high resistance to general corrosion comparable to that of non-heat treatable wrought alloys [215]. In other alloys, resistance becomes progressively less the greater the copper content [217]. Copper-bearing alloys tend to pit severely in the annealed condition and when age hardened may be susceptible to intergranular or stress corrosion [213]. Cu increases the electrochemical potential, and decreases corrosion resistance [213]. Corrosion is greatly increased, although copper in solid solution has less effect than copper as Al_2Cu, provided that the aging does not progress to the point where the alloys become susceptible to intergranular or stress corrosion [213]. Particularly poor is the corrosion resistance of cast alloys with cored dendrites and Al_2Cu particles in the interdendritic spaces [213, 217].

Cu also shifts the open-circuit potential in the positive or noble direction [218], the upward shift does not imply that the alloy is less susceptible to corrosion. The shift in the noble direction occurred as a result of addition of elements more noble than Al. The presence of noble elements, especially if present as precipitated constituents, actually leads to an increase in the corrosion susceptibility of the alloy as a result of formation of localized galvanic couple [212, 219].

A considerable amount of research has been carried out to characterize the electrochemical behavior of Al_2Cu. Authors have found that intergranular attack of Cu containing alloys is not due to difference in corrosion potential between grain boundary and grain bodies, but due to a difference in the breakdown potential of these phases [220]. Electrochemical behavior of intermetallic particles revealed that OCPs of Cu and Al_2Cu observed was $\geq$0.75 V more positive than Al over the pH range of 2-12 [211, 221, 222]. The relationship between Epit and Cl^- concentration for pure Al is: Epit ($V_{Hg/Hg2SO4}$) = -1.120-0.121 log(Cl^-). Using this equation, it was concluded that the OCPs of Al_2Cu in solutions of near neutral pH were more positive than or equal to the Epit for pure Al over a broad range of Cl concentrations [211, 221]. This suggests that galvanic coupling of the intermetallic phase to the α-Al matrix will promote pitting and deposition corrosion [211, 221, 222].

Deposition corrosion appears to stem from dealloying of IMC particles as well as from solid solutions [212]. Deposition corrosion involves dissolution of copper by corrosion and replating of copper elsewhere in the alloy surface [221, 223]. Replated copper is a far more efficient catalyst for hydrogen and oxygen reduction than an oxide covered surface on aluminum, and this increased cathodic efficiency stimulates further alloy corrosion. The gap in understanding deposition corrosion in aluminum alloys has been in how copper is oxidized from the alloy during a corrosion process that occurs hundreds of millivolts negative of the oxidation potential of the oxidation potential of copper [212, 221, 223].

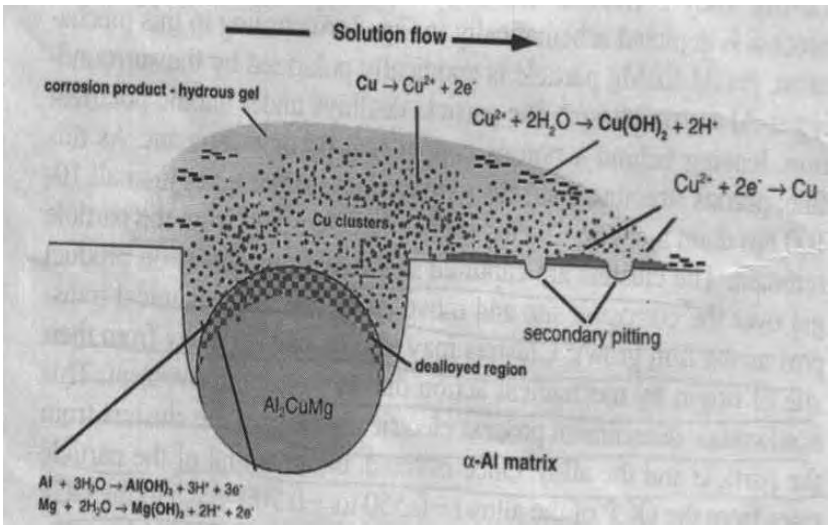

Figure 2.8.1: Distribution mechanism of Cu by dissolution of Cu-rich intermetallic in Al alloys [223]

Under aerated chloride solutions, Al_2Cu phase particles are usually noble, and are therefore polarized cathodically [219]. Under these conditions, the particle is a local cathode and supports net reduction, while the copper depleted zones around the intermetallic particles undergo net oxidation [224]. However, the active component, Al in this case is still oxidized, resulting in dealloying [221]. Dealloying is found to occur independent of whether the phase is polarized anodically or cathodically, and results in the formation and emission of nanometer-diameter Cu clusters [221]. The dealloyed particles coarsen with time. During coarsening, clusters of Cu become detached and are emitted from the particle remnant into the corrosion product or surface film over the particles [219], resulting in a rise in potential of the particles. After being detached, the clusters are captured in the hydrous corrosion product over the corrosion site and move away

due to mechanical transport as the film grows [225]. Clusters may also be carried away from their site of origin by mechanical action due to solution movement [223]. The detachment is confirmed by XPS analysis, which showed the presence of elemental copper in Al_2O_3 and enhanced cathodic electron transfer reaction on these detached copper clusters [211, 217]. This non-faradic detachment process electrically isolates the clusters from the particles and the alloy.Once isolated, the potential of the particles rises from the OCP of the alloy to the OCP of Cu (-0.050 to –0.700 V_{sce} in 0.1M NaCl solution). Schematic illustration of copper redistribution and copper ion generation is shown in Figure 2.8.1[223].

Another intermetallic of equal importance in this category is S phase (Al_2CuMg) because of its abundance in many wrought aluminum alloys. Like θ (Al_2Cu), some alloy systems have Cu depleted zones around S phase [226] while some do not [227]. Unlike θ, which is noble to the matrix, S phase is active to α-Al in chloride solutions. It exhibits an open-circuit potential (OCP) of -0.920 to –0.930 Vsce, which is 0.300 to 0.400V negative to the OCP of the matrix [228]. However, morphological studies by many authors show that pitting can occur in the matrix phase at the periphery of these particles suggesting that the phase is electrochemically noble [221, 227, 229]. Polarization curves collected for S phase reveal that oxidation and reduction kinetics are very rapid in chloride solutions indicating that they can function as potent local cathodes, or suffer intense dissolution as dictated by their galvanic relationship with the surrounding matrix [229]. Corrosion experiments clearly show that even when the passivity of the aluminum surface is broken (uniform dissolution of grain interiors), dissolution along grain boundaries progresses faster than the dissolution of grain interiors, due to the presence of segregated intermetallic particles at the grain boundaries [219].

In aerated chloride solutions, Si particles are electrochemically active with respect to the matrix phase and are polarized anodically by the surrounding matrix [222, 226]. Under these conditions the active components (aluminum and magnesium) are oxidized leaving behind a porous dealloyed structure of Cu, which can then behave as noble sites for pitting in matrix at periphery of the particle[221, 226]. Eventually, porous remnant structure of copper is mechanically detached resulting in rise in its potential and possible direct oxidation [223]. The copper depleted dispersoid-free zones at the periphery of the intermetallics are anodic both to dealloyed S phase and the matrix, resulting in dissolution of the matrix around S phase particles at potentials lower than pitting potential of S phase [226, 229]. On further increase in potential, up

to the pitting potential of S phase, dissolution and dealloying of the intermetallic results in rapid increase in current density [220, 226].

The electrolytic potential of aluminum is made more positive by silicon in solution but this change is of the order of few hundredths of a volt and is not very significant [213, 228].Magnesium in solution on the other hand makes corrosion potential of aluminum more negative. Thus, the change produced by these additions together is within the error of measurement. Overall, Mg_2Si does not affect the potential of aluminum appreciably and alloys have very good corrosion resistance in all tempers, but an excess of silicon may result in a depleted zone at the grain boundary [213]. This depleted zone, which is created due to diffusion of silicon to the grain boundary to form Si precipitates, becomes anodic to the matrix making the alloy susceptible to intergranular corrosion [213, 230]. From the studies [230] carried out on Al-Mg-Si alloys where silicon content was around 1.0%, it was found that in the early state of aging, Mg_2Si is produced as the initial grain boundary precipitate where small amounts of Mg_2Si usually behaves as anodic site and results in lined up pits along the grain boundary giving rise to intergranular corrosion[230]. Other authors have also observed corrosion potential of Mg_2Si particles to be very similar to that of pure magnesium and preferential dissolution of magnesium from the particle occurs [231, 232]. In silicon rich alloys, the aluminum-silicon couple is the main factor controlling corrosion and small amount of Mg_2Si has a negligible effect. The potential of aluminum alloy itself does not change appreciably by solution or precipitation of Mg_2Si [213]. Thus, overall the corrosion resistance of aluminum-magnesium-silicon alloys with the correct proportion of magnesium and silicon is very good [213, 230].

2.9 Wear Behaviour of Aluminum Alloys

2.9.1 Wear Behavior of Al-Si Alloys

The literature survey is carried out to study and evaluate the wear properties of Al-Si alloys used in automotive applications. The various parameters such as Silicon content, applied load, sliding distance, effect of microstructure, etc have been studied. The work of researchers in this respect is been considered. Their conclusions are as follows:

Tuti Y. Alias and M.M Haque [235] have studied the wear behaviour of as-cast and heat treated Al-Si eutectic alloys. Wear tests on the alloys were performed on a pin on disk type wear testing apparatus and parameters were size and shape of the pin, load, speed and the material pairs.

Increase in the rotational speed of the disk leads to the increase in the mass loss of the as-cast and heat treated alloys. The wear rate is higher for as-cast samples. High speed leads to reduction in wear rate. The reduction is pronounced in heat treated samples. This is because during sliding, heat is developed and the material becomes softer and weaker. This heat might not affect the hardness of heat treated alloys due to their inherent characteristics.

Increase in the applied load leads to a high wear rate for both as-cast and heat treated alloys. But at higher loads, strain-hardening of the materials in contact increases, resulting in increase in the resistance to abrade or erode. At higher load, real surface area in contact is more which increases the gripping action and due to which wear rate slows down.

At longer sliding distances, volumetric wear rate and specific wear rate are low. This was attributed to the fact that during sliding, heat develops due to friction which makes some of the adhered materials soften and loosen. As sliding goes on, these loosened particles are thrown away showing higher loss in weight. Heat treated alloys are not much affected due to their inherent characteristics due to heat treatment cycles whereas as cast alloys show higher weight loss.

S.A. Kori and T.M. Chandrashekharaiah [236] have studied the effect of grain refiner and or modifier on the wear behaviour of hypoeutectic (Al-0.2, 2, 3, 4, 5 and 7Si) and eutectic (Al-12Si) alloys using a Pin-On-Disc machine under dry sliding conditions. It is important that Al-Si alloys solidify with fine equiaxed α-Al in hypoeutectic/fine primary Si particles in hypereutectic and fine eutectic Si.

Addition of grain refiner and modifier to Al-Si alloys resulted in less specific wear rate for these samples. An increase in sliding speed led to the decrease of specific wear rate both in the case of grain refined/modified and grain unrefined/unmodified alloys. This may be due to the fact that, at low sliding speeds, more time is available for the formation and growth of micro welds, which leads to increase in the force required to shear off the micro welds to maintain the relative motion, resulting in an increase in specific wear rate. Less specific wear rate was observed in grain refined/modified alloys under these conditions. Addition of grain refiner and modifier led to decrease in wear rate at longer sliding distances. Grain refinement and modification led to increase in toughness and strength of the alloy. Increase in Silicon content leads to solid solution strengthening and precipitation hardening and a subsequent increase in the strength of the alloy. Addition of grain refiner and modifier leads to better mechanical properties [238].

H. Torabian, J.B Pathak and S.N Tiwari [237] have studied the effects of alloy composition, sliding distance, sliding speed and load on the wear rate of Al-Si alloys. The wear rate is strongly dependent on the applied load. It increases linearly with load in three distinct regions in all the alloys. Mild wear, Intermediate wear and Severe wear. Mild wear takes a longer duration and takes place under low loads. The intermediate wear and severe wear regions are distinguished from the mild region by higher rates of increase in the wear rate per unit weight.

2.9.2 Wear behavior of Al-Si-Mg Alloys

Tribological properties of forged A356 alloy mainly depend on the shape and size of the α-Al dendrites and the eutectic silicon morphology. The coarse silicon plates/needles of the unmodified acicular silicon structure act as internal stress raisers in the microstructure and provide easy paths for the fracture. From the literature it is observed that, addition of grain refiners (Al-Ti and Al-B) to A356 alloy converts predominantly columnar dendritic structure into fine equiaxed dendritic structure and addition of modifier (Sr) changes plate like eutectic Si into fine particles which leads to the improvements in tensile properties and wear behavior of the product. The wear behavior of Al-Si alloys depends on a number of mechanical properties (hardness, ductility and toughness) and microstructure (such as eutectic silicon morphology, dendrite arm spacing (DAS), grain size, composition, distribution of micro-constituents in addition to load, speed, temperature and counter face [238-240].

2.9.2.1 Effect of Microstructure on the Wear

There have been many attempts to study the effect that silicon content has on the wear behaviour of the Al-Si alloys, with a variety of conclusions particularly regarding to the effect of silicon content on the dry sliding wear of Al-Si alloys as obtained in past studies [243]. Shivanath et al [241] studied the wear of Al-Si binary alloys containing 4, 8, 11, 16, and 20% silicon under dry sliding condition, and concluded that the mild wear rate (oxidative wear rate) was independent of the silicon content, silicon particle size and applied load as well. Only the transition from mild wear to severe wear increased when the silicon content increased. Antoniou et al [242] also found that increasing in the silicon content from 8.6 to 14.2% extended the load range, in which fine equiaxed particles were produced.

Silicon particles play an important role in an Al-Si alloy the wear resistance. The general mechanism responsible for an increase in the wear resistance of an Al-Si alloy is that silicon can

increase the overall hardness of the alloy, making it more resistant to wear. This does not always mean, however, that the higher the fraction of silicon in the alloy, the greater the alloy‘s wear resistance. Due to its high brittleness, impact load can break silicon and thus may increase the overall wear of the alloy, so the optimal fraction and morphology of silicon in an Al-Si alloy is a vital key to improving its wear performance.

2.9.2.2 Effect of Cu and other Elements on Wear

Copper increases the strength and wear resistance of aluminum alloys through a mechanism of precipitation hardening. The wear and seizure resistance of Al-Cu alloys were found to increase up to Cu contents of about 4%, after which it levels off [241]. The highest wear resistance is obtained with the peak aged precipitates [244]. The addition of magnesium up to 1 % is also useful in reducing wear. It is added to provide strengthening through precipitation of Mg_2Si in the matrix [245]. However, large amounts of magnesium degrade the mechanical properties of aluminum alloys [245, 244]. When elements such as manganese, chromium, cobalt and molybdenum are present, iron combines with them to form intermetallic compounds which are less harmful. Other elements usually added to aluminum include nickel, titanium and zirconium (grain refiners), sodium and strontium (eutectic silicon modifiers) and phosphorus (primary silicon refiner) [244, 245].

Chapter 3

Experimental Procedure

3.1 Introduction

This work was undertaken to study the effects of Cu and/or Ni addition on the microstructure and properties of heat treated Al-6Si-0.5Mg alloys. This chapter outlines materials, thermal treatment and experimental methods used to characterize the evolution of precipitation hardening, microstructures and properties in the alloys during heat treatment.

3.2 Materials

3.2.1 Reference Alloy

Industrial A356 aluminum alloy used in this investigation was provided by WALTON Hi-Tech industry Ltd. (A sister concern of R.B group of industries, Chandra, Gazipur, Bangladesh) in the form of bar (each bar weighing 6kg) as-cast condition. The chemical composition of this material is given in Table 3.2.1, and photograph of an as-cast bar provided by WALTON is shown in Figure 3.2.1.

Figure 3.2.1: Photograph of an A356 ingot bar collected from WALTON with pieces prepared for further processing

Table 3.2.1: Chemical compositions (wt %) of the WALTON supplied A356 alloy

	Alloy Compositions (wt %)										
Alloy	**Si**	**Mg**	**Cu**	**Ni**	**Fe**	**Zn**	**Mn**	**Sb**	**Ti**	**Sn**	**Al**
A356	7.094	0.346	0.007	0.006	0.122	0.004	0.002	0.052	0.105	0.008	Bal.

The as-cast microstructure of the A356 alloy was found to consist of dendrites of primary α-Al, with an interdendritic Al-Si eutectic phase containing Mg-rich and Fe-rich intermetallic particles. Figure 3.2.2 shows an image of the as-cast microstructure. The dendritic structure can be clearly seen as the lighter phase with the darker eutectic phase in the interdendritic regions.

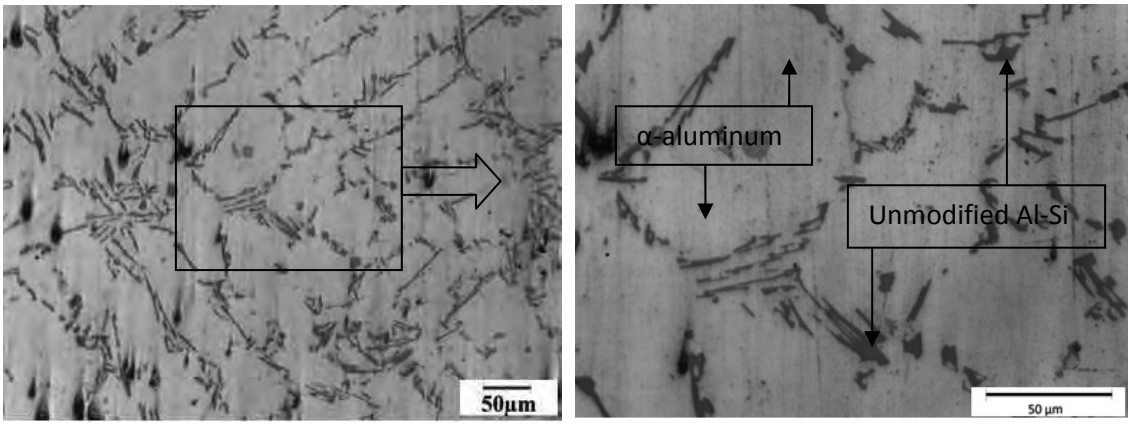

Figure 3.2.2: Micrograph the as-cast microstructure of the A356 alloy

3.3 Alloy Design

The experimental alloys were prepared by adding two elements (Cu and Ni) into A356 melt. A number of different additions and combinations were investigated. Among the seven alloys studied, the Al-6Si-0.5Mg alloy was chosen as the reference alloy (Alloy-1). Four new alloys were synthesized by varying the Cu content in the range 0.5 – 4.0 %. One alloy containing 2wt% Ni and another alloy containing 2 wt% Cu and 2wt% Ni were also synthesized. The alloy codes and target compositions of the reference and developed alloys are given in Table 3.3.1. All compositions given in this thesis are in weight percent.

Table 3.3.1: Alloy codes and target compositions

Alloy Code	Target Alloy Compositions (wt %)
Alloy-1	Al-6Si-0.5Mg
Alloy-2	Al-6Si-0.5Mg-0.5Cu
Alloy-3	Al-6Si-0.5Mg-1Cu
Alloy-4	Al-6Si-0.5Mg-2Cu
Alloy-5	Al-6Si-0.5Mg-4Cu
Alloy-6	Al-6Si-0.5Mg-2Ni
Alloy-7	Al-6Si-0.5Mg-2Cu-2Ni

3.4 Experimental Method

The overall experimental method is shown in Figure 3.4.1.

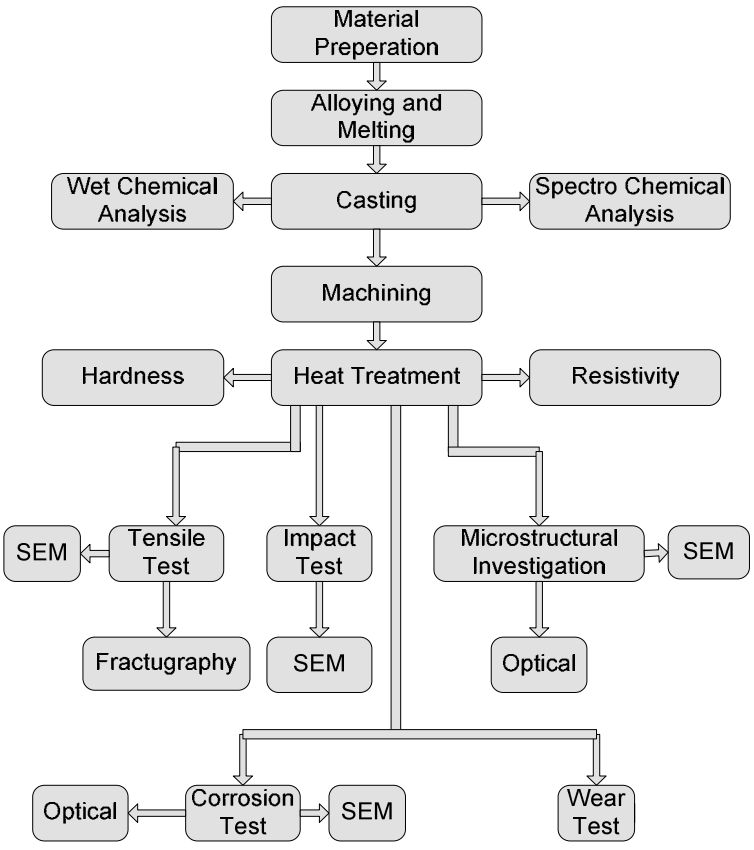

Figure 3.4.1: Summary of experimental methods

3.4.1 Alloy Making and Melting

For each casting experiment, approximately 1.70 kg of A356 alloy and 0.3kg pure Aluminum were melted in a clay-graphite crucible furnace fired by natural gas. The melt temperature was monitored with a chromel-alumel (type K) thermocouple. Once molten, the liquid was kept at 750^{o}C to limit the absorption of hydrogen. The oxide layer of the melt was skimmed off before any alloying elements were added, and this was made to get as pure melt as possible. Mg was added to the melt duly packed in an Al foil. The melt was stirred for 20s with an alumina rod. After Mg addition the melt was degassed with solid hexachloroethane (C_2Cl_6). For each composition, a specific casting procedure was developed until the dissolution of the master alloys was completed. The master alloys with high liquidus temperatures were added initially and held for longer times when necessary. Sufficient additions (Cu sheet or Ni chips or Cu sheet and Ni chips) were ensured for the targeted alloy compositions.

3.4.2 Casting

The melts (correct combination of requirements) were poured at 720^{o}C into a metal mould to produce a casting plate (300mm x 150mm x 15mm) in the Foundry shop, MME department, BUET. The metal moulds were preheated at ~200^{o}C before tapping the molten metal into the mould to avoid solidification during casting. The castings were removed from the mould 10 minutes after pouring. Figure 3.4.2 shows the casting plates which were used for further testing.

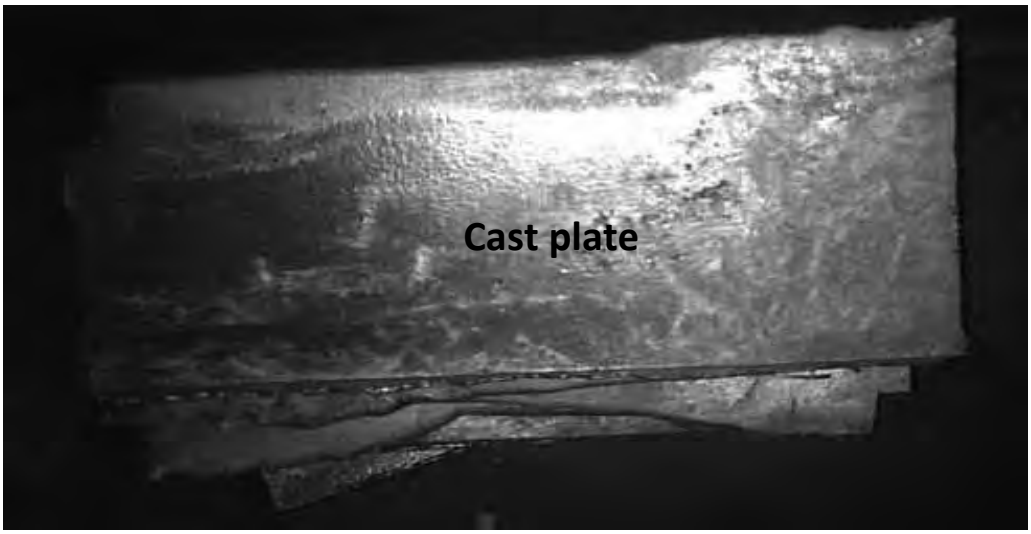

Figure 3.4.2: Picture of the cast plates

3.4.3 Chemical Analysis - Optical Emission Spectroscopy

A small piece was cut from one corner of each casting plate. The oxide layer that formed on the surface was removed by emery paper. The chemical compositions of the cast alloys were evaluated using an optical emission spectrometer (FOUNDRY MASTER PRO, Germany).

3.5 Heat Treatment

Homogenization, solutionization, T4, T6 and T7 heat treatment were applied to all alloys under investigation. The details of the above heat treatment are shown in Table 3.5.1.

Table 3.5.1: The designations of heat treatments used

Treatment	Solutionizing	Quenching	Ageing
T4	Yes	Yes	Room Temperature only
T6	Yes	Yes	Elevated (to yield increased strength)
T7	Yes	Yes	Elevated (to yield dimensional stability)

3.5.1 Homogenization Treatment

The cast alloys were homogenization using an electrical heating furnace (Lenton, Model: AWF 13/42). The cast plates were directly charged into the furnace. Homogenization treatment applied for the alloys is shown in Figure 3.5.1.

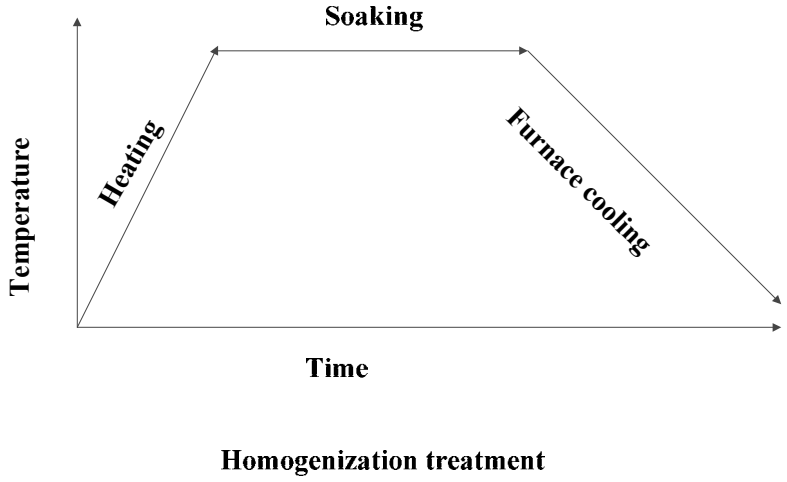

Figure 3.5.1: Homogenization treatment applied for the cast plates

In this study homogenizing was carried out at 500^0C for 24 hours. The furnace heating rate was 15^0C per minute and furnace cooling was ensured to allow for diffusion of alloying elements, and formation of grains from the as-cast dendritic structure.

3.5.2 Sample Preparation for Ageing Studies

Flat rectangular samples (slices) for hardness and resistivity measurement (30mm x 15mm x 8mm) were prepared from the homogenized alloys. All the slices were cut from the homogenized castings with a hand hacksaw, water being poured to keep the slices cool during cutting. The pieces were finally mechanically polished to produce a flat surface. Both sides were made to be smooth parallel surface, free of coatings, scale and gross components.

3.5.3 Solution Treatment

Solution treatment was conducted in an electrical furnace (Lenton: AWF 13/42). The heating rate was 15^oC per minute. The solution treatment temperature was 540°C and soaking time was 2 hours. The samples were rapidly quenched from the furnace in ice-salt-water solution. Figure 3.5.2 shows the applied solution treatment for the alloys under investigation.

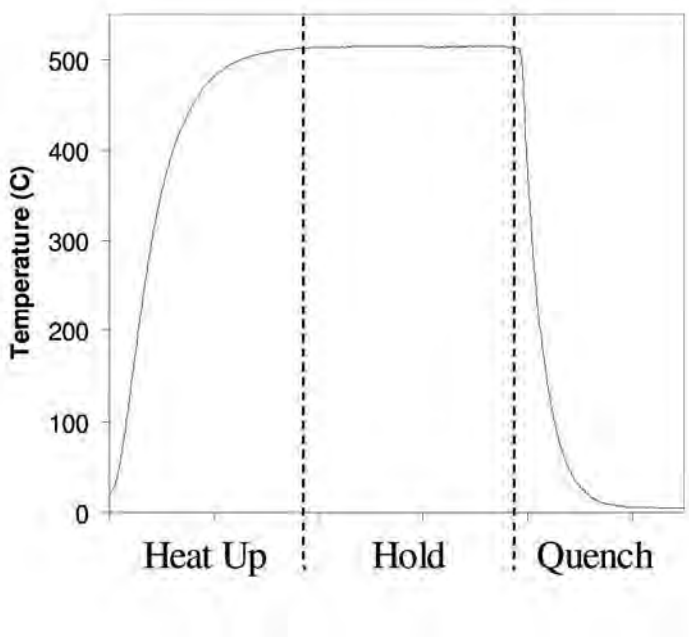

Figure 3.5.2: Temperature-time profile during solution treatment

3.5.4 Natural Ageing

Rectangular (30mm x 15mm x 8mm) slices from the homogenized alloys were cut for solutionizing. The slices were subjected to solution treatment at 540^{o}C for 2hr and rapidly quenched. The hardness of the as quenched samples was measured immediately since hardening process starts at room temperature after quenching. The hardness of the as quenched samples was measured successively after 1, 2, 3, 4, 5, 7, 10, 15, 20, 35, 50, 60, 75 and 90 days at room temperature. The T4 heat treatment schematic representation is shown in Figure 3.5.3.

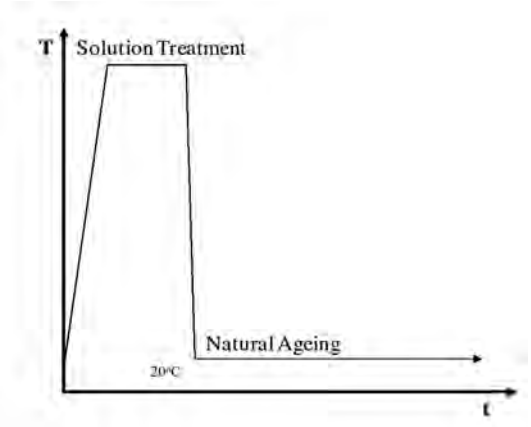

Figure 3.5.3: Schematic representation of natural ageing (T4) at room temperature after solution treatment

3.5.5 Artificial Ageing

Slices were cut from each of the homogenized alloys. The slices were subjected to solution treatment at 540^{o}C for 2hr and rapidly quenched in ice salt water solution. The solutionized and quenched samples were used for the artificial ageing (isochronal and isothermal tests) and metallography studies.

3.5.5.1 Isochronal Ageing

For isochronal test, the solutionized samples were aged at room temperature for 1 day prior to artificial ageing. Artificial ageing was conducted in an electrical furnace (Lenton: AWF 13/42). The slices of the seven alloys were aged at 100, 150, 175, 200, 225, 250, 350 and 400^{0}C. The time needed for heating the samples to the artificial ageing temperature was 1 hour. The samples were taken out of the furnace and cooled in still air. Subsequently the hardness of each slice was measured.

3.5.5.2 Isothermal Ageing

The solutionized and quenched samples were artificially aged in the electrical furnace (Lenton: AWF 13/42). After loading, the samples in the furnace were tempered at 100, 150,175, 200, 225, 250 and 300^{o}C. The tempered samples for each alloy were successively removed after 15, 30, 60, 90, 120, 240 and 360 minutes at each of the above mentioned temperatures and cooled in still air. Finally the hardness of each slice was measured. Artificial ageing treatment applied to the alloys is shown in Figure 3.5.4.

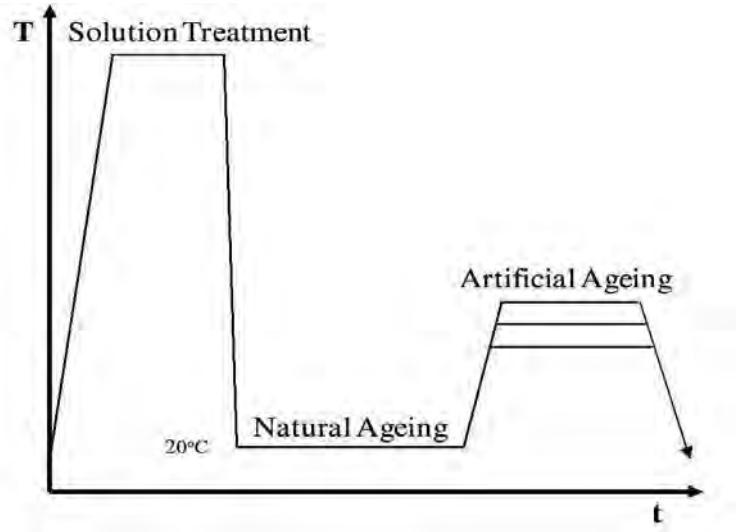

Figure 3.5.4: Schematic representations of the artificial ageing processes

3.6 Evaluation of Hardness and Resistivity

3.6.1 Hardness Test

The macrohardness of all the naturally and artificially aged samples were measured using a Rockwell hardness testing machine (FR-IE, Future Tech. Corporation, Tokyo, Japan). All hardness measurements were performed on blocks of > 5 mm thickness using F scale. The blocks for hardness measurement were ground using 600 µm SiC paper prior to hardness measurements. A 1/16 inch steel ball indenter was used, 60 kg load was applied for a period of 15 s. The hardness number was displayed on the LCD screen. An average of seven consistent readings was accepted as the representative hardness value of an alloy.

3.6.2 Resistivity Measurement

The resistivity of all the artificially aged (isochronal and isothermal) samples was measured by using a conductivity meter type 979 testing machine (Figure 3.6.1). All conductivity measurements were performed on blocks used for hardness measurement. The blocks were ground using 600 µm SiC paper prior to conductivity measurements. Conductivity Meter Type 979 works on the principle of eddy currents. A probe induces eddy currents at a fixed frequency in the test part. These current affect the electrical impedance of the test probe. The change in impedance is proportional to the electrical conductivity of the test part. Thus, conductivity measurement is possible by measuring the corresponding change in probe impedance. The change in probe impedance is sensed and processed and the conductivity of the test sample is expressed as % I.A.C.S (International Annealed Copper Standard) on digital display. The probe was 12 mm in diameter and can be used on any reasonably flat accessible surface of at least 15 mm dia. Minimum thickness (for error free reading) is in the range of 0.8 mm (for metals having conductivity around 100% I.A.C.S.) to 2.00 mm (for material having 13% I.A.C.S. conductivity). The resistivity was calculated according the following relationship:

172.41 / resistivity = % IACS

Figure 3.6.1: Picture of conductivity meter type 979

3.7 Tensile Testing

The tensile samples were prepared from the homogenized plates as per ASTM B-557M-06 standard (subsize, E8 M–04) and the specimen geometry and dimensions are shown in Figure 3.7.1 and Table 3.7.1[256].

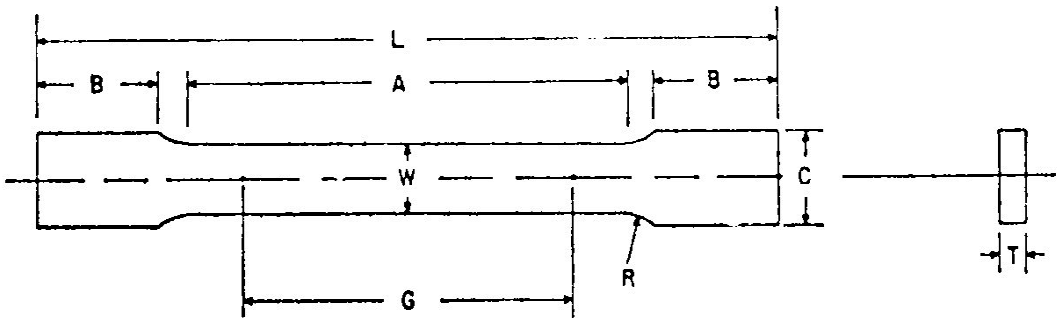

Figure 3.7.1: ASTM B 557M-06 subsize (E8M–04) standard rectangular tension test specimen

Table 3.7.1: Dimensions of the ASTM B 557M-06 subsize (E8M–04) standard

	Dimensions		
	Standard Specimens		Subsize Specimen
	Plate-Type, 32mm, Wide	Sheet -Type, 12.5mm,Wide	6mm, Wide
	mm	mm	mm
G - Gage length	200.0±0.2	50.0±0.1	25.0±0.1
W - Width	40.0±0.2	12.5±0.2	6.0±0.1
T - Thickness	Thickness of material		
R - Radius of fillet, min	25	12.5	6
L - Over-all length	450	200	100
A - Length of reduced section, min	225	57	32
B -Length of grip section	75	50	30
C -Width of grip section, approximate	50	20	10

The samples were polished with emery paper to reduce the sharpness of edges of the plate-like samples. The samples were solution treated at 540^{o}C for 2hr and quenched in ice-salt-water solution. The ageing conditions of the samples are given in Table 3.7.2. The measured values of stress are expressed to the nearest whole number.

Table 3.7.2: Ageing conditions of the six tempers sample for which the tensile properties were determined

Group	Temper Designation	Treatment Condition	Ageing
1	T4	Quenched	Room temperature only
2	T6	Underaged	Ageing at 150^{o}C for 1 hr
3	T6	Underaged	Ageing at 200^{o}C for 1 hr
4	T6	Peakaged	Ageing at 225^{o}C for 1 hr
5	T7	Overaged	Ageing at 250^{o}C for 1 hr
6	T7	Overaged	Ageing at 300^{o}C for 1 hr

Tensile properties of the alloys were determined by using INSTRON 3369 computer controlled system. Tensile tests were carried out with different crosshead speeds of 15, 1.5 and 0.15 mm/min, which corresponds to nominal strain rate of 10^{-2}, 10^{-3} and 10^{-4} s^{-1} respectively. All the thermal treated samples were tested in a common strain rate 10^{-3} s^{-1} but only the peakaged alloys were subjected to three different strain rates of 10^{-2}, 10^{-3} and 10^{-4} s^{-1}. During the tests, the load - elongation data was captured by software and was used for further analysis. The specimen dimension was measured and recorded (diameter and gauge length) for the calculation of the engineering stress and engineering strain. In each case at least 3 samples were tested and then average values are given as the results. Three parameters were extracted from the recorded curves: the ultimate tensile strength (UTS), the yield strength (YS) and the elongation. The UTS was recorded as the peak strength on the stress-strain curve whereas the YS was determined as the stress corresponding to the intersection of the curve with a line parallel to the elastic part of the curve offset by a strain of 0.2%. The elongation was determined by taking measurements of before and after gage length as follows:

$$e_{f=} (L_f - L_0)/L_0$$

Where e_f is the % elongation, L_f is the final gage length and L_0 is the initial gage length.

3.8 Impact Testing

Charpy impact testing was performed following the procedure given in ASTM E23 standard. The toughness behaviour was tested for the same aged conditions as used for tensile testing (Table 3.7.2). Impact tests were performed using impact testing machine (Model: JB-500B, Time group INC, The people's Republic of China). The Charpy test sample (10mm x 10mm x 55mm in dimensions, a 45^{o}V notch of 2 mm depth and a 0.25 mm root radius) was hit by a pendulum at the opposite end of the notch. The absorbed energy required to produce two fresh fracture surfaces were recorded in the unit of Joule.

3.9 Wear Testing

Wear testing was performed on an exploratory manner. The procedure given in ASTM G99 standard was followed to conduct the tests. The testing was performed on three specimens for each alloy in six tempers as for the tensile tests. Dry sliding wear tests were performed using a pin-on-disk type machine (Figure 3.9.1).

Figure 3.9.1: Pin-on-Disk type friction and wear test machine

The rotating disc, 45 mm in diameter, was made of carbon steel and the hardness of the disc was 30 HRC. The experimental samples were held stationary and a required normal load was applied through a lever mechanism. Wear tests were carried out under dry sliding conditions under a

normal load of 5.4N, 11.28N at a constant sliding speed of 900 rpm and the sliding distance per second is (900 x 2 x 3.14 x 0.0225 m)/60 s =2.12 m/s. The wear loss was measured directly as the weight loss of the specimen. The tests were carried out by applied load (5.4N for 10 min. and 11.28N for 5 min.) varying sliding distance and keeping sliding speed constants. All the thermal treated samples were tested at a constant applied load 5.4N, sliding speed and sliding distance but only the peakaged alloys were subjected for varying applied load and sliding distance at a constant sliding speed.

No lubricant was used during the test. Care has been taken that the specimens under test are continuously cleaned with woollen cloth to avoid the entrapment of wear debris and to achieve uniformity in experimental procedure. Optical light microscopy was used to analyze the morphology of the worn surfaces of sample.

3.10 Electrochemical Measurements

3.10.1 Preparation of Samples

Fourteen rectangular samples (two for each alloy) measuring 50mm x 10mm x 5mm were prepared from the homogenized plates. The samples were solutionized at 540^{o}C for 2 hours and quenched in ice-salt-water solution. The quenched samples were subjected to artificial ageing at 225^{o}C for 1 hour. After heat treatment the 10 mm x 5 mm surface of the rectangular samples were polished metallographically. The polished surface was washed with distilled water, degreased with acetone, washed again with distilled water and dried. Optical Light Microscopic (OLM) and scanning Electron Microscopic (SEM) observation were performed before and after corrosion test.

3.10.2 Test Solutions

The test solutions were produced by dissolving analytical reagent grade sodium chloride (NaCl) in deionized water and stirring for 20 minutes to ensure complete dissolution. The solutions were filtered to remove the remaining undissolved elements. Saturated KCl solution was prepared for use in reference electrode.

3.10.3 Potentiodynamic Polarization Principle

Potentiodynamic polarization method was used to characterize the current-potential relationship in corrosion systems under investigation. The corrosion current density and potential of tested metallic materials were determined by extrapolation of tangents to the curves of the cathodic and anodic polarization zones of the Butler-Volmer equation given below

$$j_{reaction} = j_o\{\exp(-\beta(nF/RT)\eta_{reaction}) - \exp((1-\beta)(nF/RT)\eta_{reaction})\}$$

where, $j_{reaction}$ is the anodic or cathodic current, β is the charge transfer barrier for the anodic or cathodic reaction, R is the universal gas constant (8.314 $Jmol^{-1}K^{-1}$), T is temperature in absolute scale and F is Faraday constant 96485 C/ (mole of electrons). When $\eta_{reaction}$ is cathodic, i.e. negative, the second term in the Butler-Volmer equation becomes negligible and equation can be written as:

$$J_{reaction} = j_{cath} = j_0 \exp(-\beta nF\, \eta_{reaction} / RT) \text{ and}$$
$$\eta_{reaction} = \eta_{cath} = b_c \log_{10}(j_{cath.} / j_o),$$

Where b_c is the cathodic Tafel coefficient and b_c = -2.303 RT / βnF. That can be obtained from the slope of a plot of η against log current density, with the intercept yielding a value for j_o as shown in the following Figure 3.10.1.

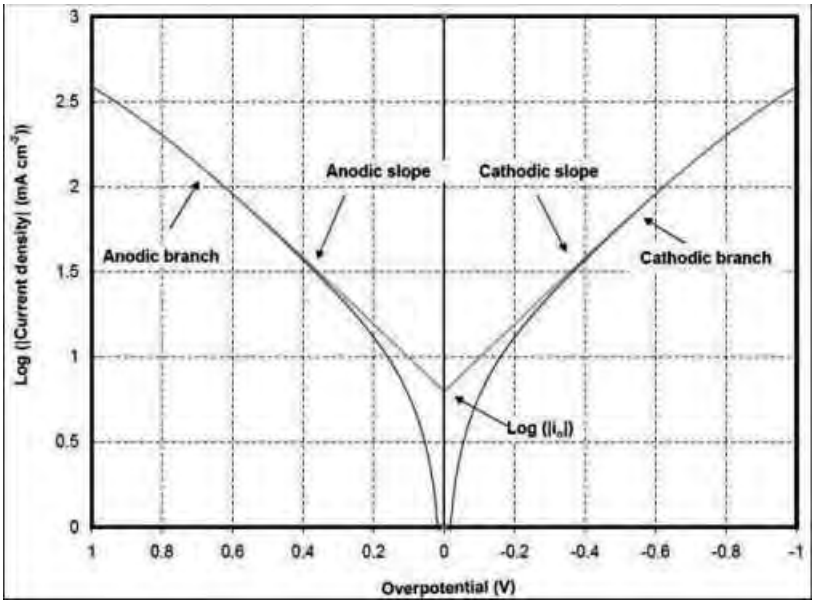

Figure 3.10.1: Plot of overpotential (η) vs. log current density

The disruption of the steady state corrosion by the electrical signal and the measurement of its response to the stimulation allow determining a set of electrical quantities that provide valuable information about electrochemical processes occurring in the system under study. The most common approaches for the electrochemical characterization of corrosion processes are non-stationary methods, which are easy to automate and computer-control.

3.10.4 Potentiodynamic Polarization Measurements

A computer-controlled Gamry Framework TM Series G 300™ and Series G 750™ Potentiostat/ Galvanostat/ZRA (Figure 3.10.2) was used for the electrochemical measurements. The Potentiodynamic polarization studies were configured in cells (Figure 3.10.5), using three-electrode assembly with a saturated calomel reference electrode, a platinum counter electrode and the sample as working electrode in the form of coupons of exposed area of 0.50 cm^2 or 10mm x 5mm. Only one 10mm x 5mm surface area was exposed to the test solution and the other surfaces were covered with Teflon tape and allowed to establish a steady-state open circuit potential (OCP). The potential range selected was -1 to +1V and measurements were made at a scan rate of 0.50 mV/s. The corrosion current (I_{corr}), corrosion potential (E_{corr}), pitting corrosion potential (E_{pit}) and corrosion rate (mpy) were calculated from Tafel curve. The tests were carried out at room temperature in solutions containing 0.1M of NaCl at a fixed and neutral pH value. The corroded samples were cleaned in distilled water and examined by optical light microscope (OLM) and scanning electron microscope (SEM).

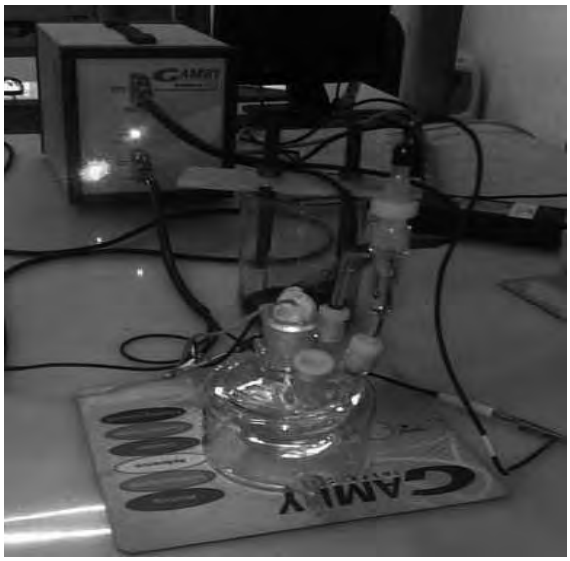

Figure 3.10.2: Gamry instrument set-up for electrochemical measurements

3.10.5 Electrochemical Impedance Spectroscopy Principle

The response of the corrosion system to an interfering signal was the current intensity signal, which is the effect of transferring electrical charge between the corrosive metal (electron conductor) and the electrolyte (ionic conductor). This response is described by the time-varying current signal $I(t) = I_o \cos(\omega t + \varphi)$, where I (t) =instantaneous current value, $\omega = 2\pi f$ pulsation, f =frequency and φ= phase shift. The measuring system digitally generates the excitation having the above sinusoidal form (Figure 3.10.3) and measures the current system response as a function of frequency.

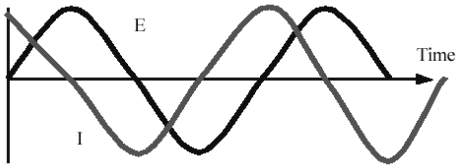

Figure 3.10.3: Sinusoidal behavior of AC current

The experimental results expressing the dependence of impedance spectra on the applied signal frequency were plotted as Bode plots and Nyquist plots. From the Bode plots (total impedance | Z | vs. frequency f), the solution resistance (R_s), Charge transfer resistance (Rct) and double layer capacitance (Cp) were found. In the Nyquist diagrams representing relationship Z"= f(Z'), Z' is a real component and Z"- imaginary component of input driving impedance $Z(j\omega) = Z' + jZ''$ of the corrosive systems investigated. Z' is the real part of the impedance and can be related to a pure resistance R, while Z" is the imaginary part that can be related to a capacitance of electrode-electrolyte interface. EIS data are displayed as Nyquist plot or Bode plot as shown in Figure 3.10.4.

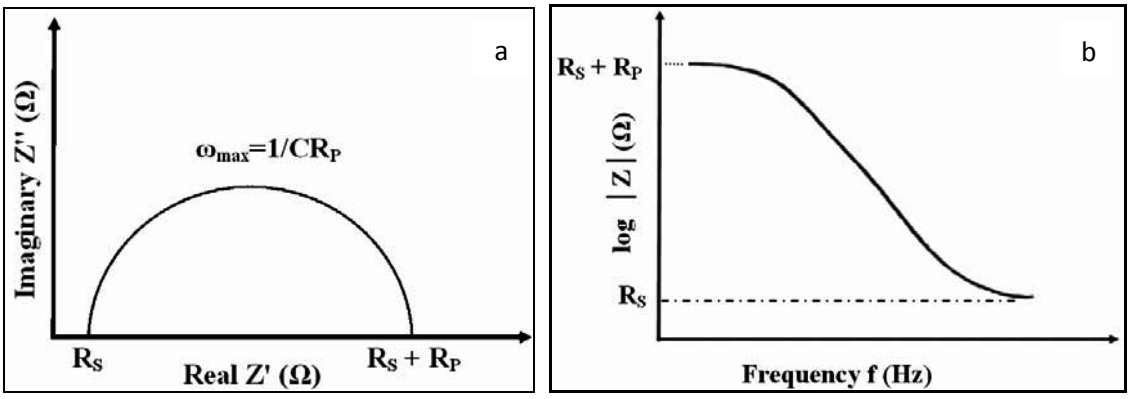

Figure 3.10.4: EIS data displayed as a) Nyquist plot and b) Bode plot

Under the simplest corrosion conditions, one semicircle appears in Nyquist plot, which means that probably only one process contributes to the polarization in the investigated frequency range. In Bode plot a high frequency domain gives the solution resistance and a low frequency domain gives some information regarding polarization resistance from the sample-solution interface, which is an indication of corrosion resistance.

3.10.6 Electrochemical Impedance Measurements

As in potentiodynamic polarization test, three electrode cell arrangement (Figure 3.10.5) was also used in electrochemical impedance measurements. Rectangular samples (10mm x 5mm) were connected with copper wire and adopted as working electrodes for impedance measurements. EIS tests were performed in 0.1M NaCl solution at room temperature over a frequency range of 100 kHz to 0.2 Hz using a 5mV amplitude sinusoidal voltage. The 10mm x 5mm sample surface was immersed in 0.1M NaCl solution (corrosion medium). All the measurements were performed at the open circuit potential (OCP). The test cells were maintained at room temperature and the NaCl solution was refreshed regularly during the whole test period. The impedance spectra were collected, fitting the experimental results to an equivalent circuit (EC) using the Echem Analyst ™ data analysis software and evaluating the solution resistance (Rs), polarization resistance or charge transfer resistance (Rct) and double layer capacitance(Cp) of the thermal treated alloys.

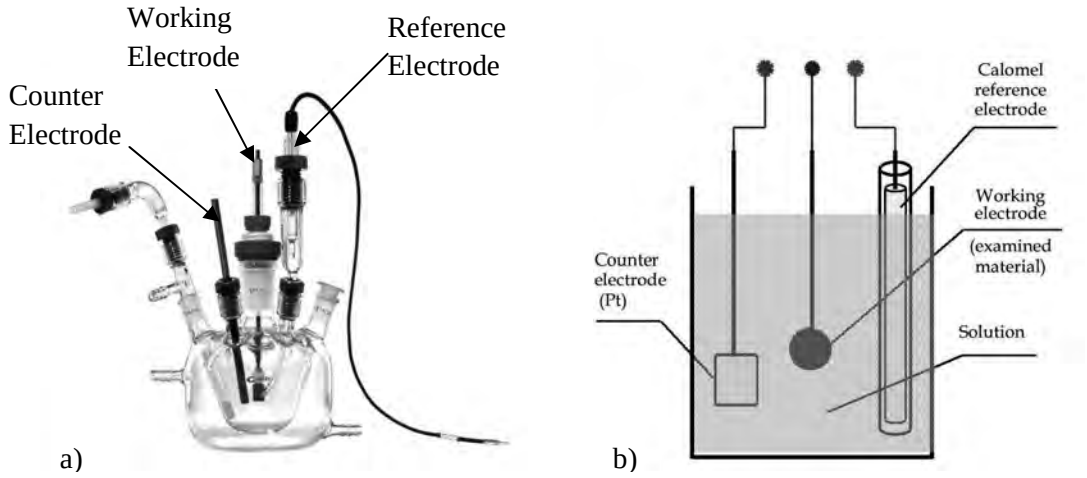

Figure 3.10.5: a) Gamry and b) schematic representation of the three electrode system cell

3.11 Material Characterizations

The metallurgical behaviour during thermal treatment was investigated by optical microscopy and scanning electron microscopy techniques. During ageing the evolution of precipitation was characterized using by thermal analysis and hardness and electrical resistivity measurements. The mechanical response of the material was measured by performing Rockwell hardness and tensile tests. Further details are given in the following sections.

3.11.1 Sample Preparation for Metallographic Observation

The as-cast, T4, T6 and T7 samples were taken for microstructural observation. All metallographic examinations were carried out on rectangular coupons. Starting from a grit size of 240, respectively 320, 400, 600, 800 and 1500 SiC emery papers were used for grinding and polishing. After every step of polishing and grinding the surface was rinsed with clean water to remove any excess particles and finally dried. After paper polishing, the samples were fine polished in cloth wheel with ultra fine alumina suspension. Afterwards the samples were cleaned with water, dried and wetted with acetone.

3.11.2 Optical Light Microscopy

The polished samples were first etched using Keller's reagent (1% hydrofluoric acid, 1.5% hydrochloric acid and 2.5% nitric acid in water) to improve the contrast between the various phases contained in the alloy microstructure. Afterwards, photomicrographs of the microstructures were taken using metallurgical microscope (OPTIKA, ITALY, B-600 MET series) equipped with a digital camera. The washed and dried samples were observed carefully in the microscope at X100, X200 and X500 magnifications and some selected photomicrographs were taken. Several microstructural characteristics were quantified by analyzing the 2-D micrographs.

3.11.3 Scanning Electron Microscopy

Structural characterization studies were done to observe the microstructure of as-cast, heat treated sample surface, tensile and impact fracture surface. The samples of different alloys were mechanically polished using standard metallographic techniques before the examination. Characterization is done in etched conditions. Etching was done using the Keller's reagent .The

SEM micrographs of the samples were obtained. The images were taken in secondary electron (SE) mode. This analysis was done by a scanning electron microscope equipped with Energy Dispersive X-Ray Spectroscopy (EDS) (Model: Inspect^{TM} S50 FEI Quanta**)** scanning electron microscope, Singapore).The compositional analysis of the base and intermetallic compounds were analyzed. The corrosion surface observations before and after corrosion were performed by JEOL JSM-7600F scanning electron microscope (SEM).

3.11.4 Thermal Analysis

Thermal analysis was carried out to study the phase transformation(s) during various stages of heat treatment. A phase transformation is accompanied by a release (exothermic) or absorption (endothermic) of thermal energy. An exothermic event results in a sudden increase in dT/dt value, whereas an endothermic event results in a sudden decrease in dT/dt value at the starting point of the transformation. Small samples 10-15 mg of each alloy were heated up in an IR-furnace to 640 °C. Then small samples placed on the sample holder of the device. The reference holder was left blank. Prior to each measurement the whole heating unit was cooled down. The samples were heated up to 640°C at a heating rate of 5°C /min, and then slowly cooled down. To prevent oxidation the experiment was carried out in an argon atmosphere. The Thermal analysis was carried out in SII EXSTAR 6000, TG/DTA6300.

3.11.5 XRD Analysis

Phase identification was confirmed by powder X-ray diffractometry (XRD) technique using BRUKER X-Ray Diffractometer of Model D8 Advance with CuK_{β} radiation (λ= 1.54 Å). For each sample a scan has been performed from 30˚ to 80˚. XRD analyses were carried out with the wear debris of alloys. The wear debris was directly put into the sample holder and then experiment was carried out. Gobel Mirror was the source of X-ray. Filter was used to remove CuK_{β} and soller slit to pass the parallel ray. The peaks obtained were used to determine the presence of major elements in the wear debris.

Chapter 4

Results and Discussion

4.1 Precipitation Treatment

4.1.1 Alloys Behaviour during Solution Treatment

The results of the solution treatment investigation on the various Cu and Ni content Al-6Si-0.5Mg alloys at 540^{o}C for 2 hours are presented. Optical Light Microscopy (OLM), Scanning Electron Microscopy (SEM), Rockwell (F scale) hardness and resistivity/conductivity measurements were used to investigate the structural changes of the alloys during solution treatment.

Figure 4.1.1 shows the change of hardness with an increase in Cu in the range 0.5 to 4 wt% Cu in the Al-6Si-0.5Mg alloys. The Cu free Al-6Si-0.5Mg alloy (Alloy-1) has the lowest hardness (59.5 HRF) among all the alloys under investigation. With the increase of Cu in the alloys the hardness increases from 59.5 HRF to 89.8HRF and 4wt% Cu content alloy (Alloy-5) has the highest hardness after solution treatment.

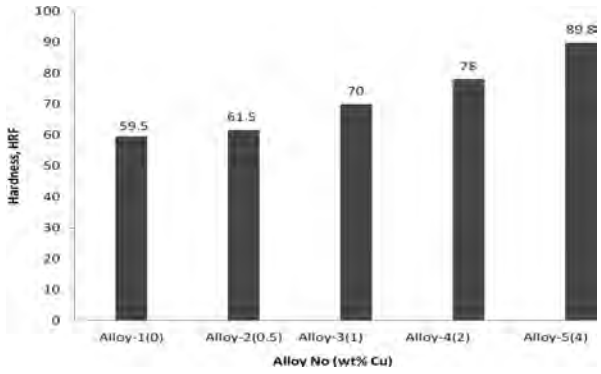

Figure 4.1.1: The change of hardness with Cu content in Al-6Si-0.5Mg alloys after solution treatment

Figure 4.1.2 shows the individual and combined effect of Cu and Ni on hardness of Al-6Si-0.5Mg alloys after solution treatment. The combined addition of Cu and Ni to Al-6Si-0.5Mg, Alloy-7 gives the highest hardness (82.5HRF). The alloy with 2wt% Cu (Alloy 4) has better hardness (78HRF) than the alloy containing the same amount of Ni, Alloy-6 (73HRF).Thus in the case of hardening, a specific amount of Cu addition is more effective than the addition of same amount of Ni to Al-6Si-0.5Mg.

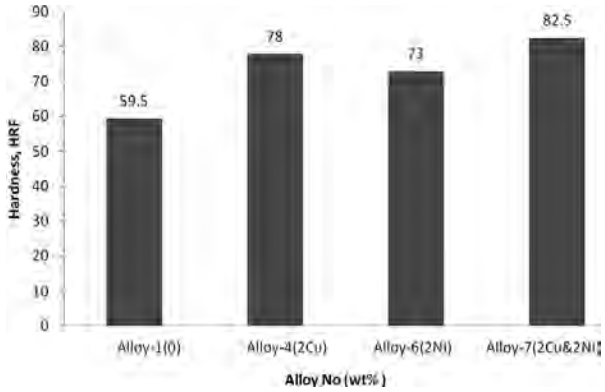

Figure 4.1.2: The change of hardness with Cu or/and Ni content in Al-6Si-0.5Mg alloys after solution treatment

4.1.2 Age Hardening Response

4.1.2.1 Alloys Behaviour during Natural Ageing

The natural ageing response of the solution treated alloys was investigated by performing hardness tests on specimens that were quenched after solution treatment and left for a period of time at room temperature. Normally the hardness increases with ageing time by means of fine precipitation. The hardness increases relative to the as-quenched state (0 days). The hardness of each as-quenched alloy was measured as a test of the solutionizing treatment. These values are given in Table 4.1.1.

Table 4.1.1: Natural ageing hardness of alloys

Alloy	Natural ageing hardness(HRF) as a function of days														
Name	0	1	2	3	4	5	7	10	15	20	35	50	60	75	90
Alloy-1	59.5	62.6	65.3	66.6	68.3	70.1	70.1	74.3	75.1	75.6	75.5	76.2	75.5	73.9	74.3
Alloy-2	61.5	68.1	70.6	71.5	72.8	73.3	74.7	76.5	77.3	78.4	78.9	80.7	80	82.2	80.1
Alloy-3	70	77.2	80.4	80.5	81.5	83.3	84.9	84.4	86.3	87.5	89.4	89.6	88	86.2	88.8
Alloy-4	78	84.2	84.6	85.3	86.6	88.6	89.9	89.4	89.7	89.3	89.5	90.8	90.7	90.4	91.3
Alloy-5	89.8	92.8	92.7	94.6	95.6	95.4	97.2	97.3	98.1	98.3	98.1	99.7	98	97	96.3
Alloy-6	73	74.3	75.3	77.2	78	78.4	79.3	78.4	81.6	82	82.5	81.9	82	83.6	82.6
Alloy-7	82.5	87.5	87.6	89.7	89.9	91.9	91.5	94.1	95.3	96.3	96.2	99.6	95.2	94.2	94.7

Figure 4.1.3 shows a plot of the hardness as a function of the Cu addition and ageing time at room temperature (25^{o}C) after solution treatment and quenching. The hardness just after solution treatment and quenching is smaller than after natural ageing, which implies that clusters formed during natural ageing are more effective obstacles to dislocation movement than those formed during the solution treatment and quenching.

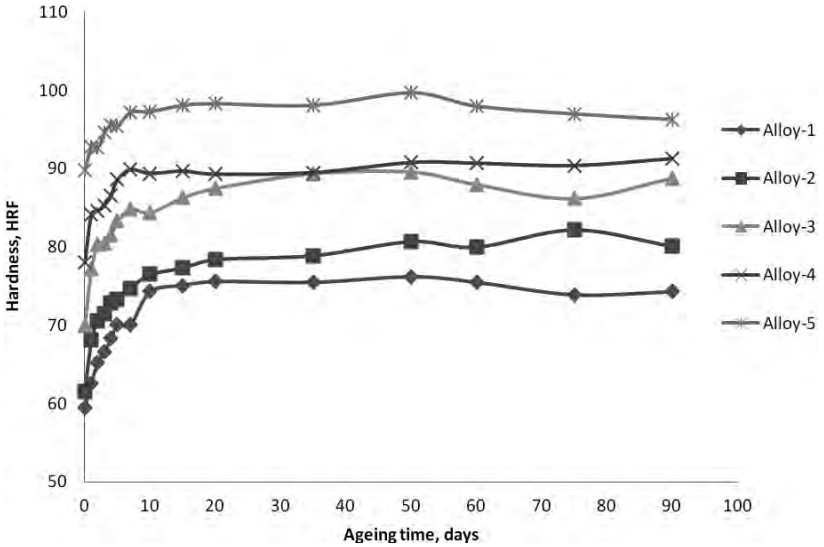

Figure 4.1.3: Natural ageing behaviour of Alloys 1 to 5 for 90 days at room temperature

Cu additions are seen to have many effects on the age-hardening behaviour. The first effect is the increased hardness in the as-quenched state; this increase has been shown to be beyond that expected from the additional solid-solution strengthening. Clusters formed in the Cu-containing alloys are almost always found to contain at least one Cu atom, and the Cu-containing alloys were found to contain a greater cluster number density than Cu-free material after natural ageing treatment. These observations seem to suggest that Cu aids nucleation at this early stage; however, clusters present in the as-quenched Cu-containing alloys must be taken into account [252].

The increase in hardness on natural ageing is seen to be larger in the Cu-containing alloys (Alloy-2 to Alloy-5).This observation suggests that Cu does have an effect, and that the effect is more pronounced when the kinetics are limited further as in the natural ageing treatment. Cu additions are seen to slightly increase the average Mg/Si ratio of small clusters seen after natural ageing. It is unclear whether this effect is due to Cu altering the kinetics, the thermodynamics or both. Mg-Cu vacancy complexes have lower mobility than Mg-vacancy complexes [253], which

would suggest that it is not simply a kinetic effect. It is intuitive that the small Cu atom might stabilize clusters containing higher levels of the larger Mg atom rather than the small Si atom. Such behaviour is consistent with Cu mainly affecting the chemistry of larger, elongated clusters where maintaining coherency along the needle direction is important.

The hardness data shows that 90 days long natural ageing treatment has effect on the hardness of naturally aged alloys (Figure 4.1.3). All the alloys are seen to show significant age hardening upto 15 days. The hardness of Cu free Alloy-1 increases from 59.5 HRF to 75.1HRF in 15 days, the subsequent changes of hardness are very insignificant. The hardness of 0.5 wt% Cu alloy (Alloy-2), increased from 61.5HRF to 77.3HRF in 15 days of natural ageing. The hardness of Alloy-3, Alloy-4 and Alloy-5 increased from 70HRF, 78HRF and 89.8HRF to 86.3HRF, 89.7HRF and 98.1HRF respectively. The further effect of natural ageing on these Cu content alloys is very insignificant.

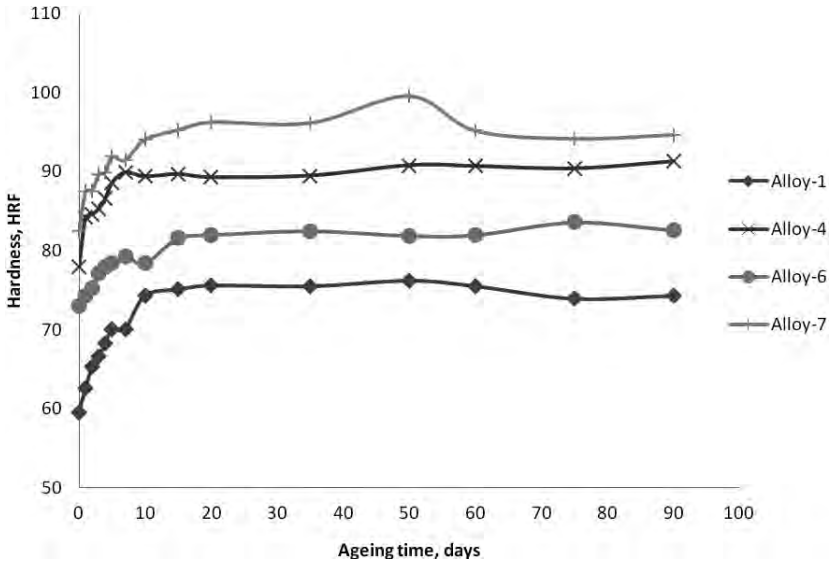

Figure 4.1.4: Natural ageing behaviour of the Alloys 1, 4, 6 and 7 for 90 days at room temperature

Figure 4.1.4 shows hardness of Alloy-1, Alloy-4, Alloy-6 and Alloy-7 in the as-quenched condition and after natural ageing at room temperature for 90 days. The only 2wt% Ni containing alloy (Alloy-6) shows an increase in hardness from 73 HRF in the as-quenched condition to 81.6 HRF after 15 days followed by a further increase to 82 HRF after 60 days, rising to 82.6 HRF after 90 days. The hardness of the alloy containing both 2wt%Ni and 2wt%Cu (Alloy-7) is 82.5 HRF in the as quenched condition. The hardness increases to

95.3HRF after 15 days of natural ageing. Further natural ageing for 90 days, raises the hardness to 94.7 HRF. Thus during natural ageing at room temperature, the maximum hardening occurred within 15 days for all the alloys. Further ageing, does not significantly improve the hardness.

4.1.2.2 Alloys Behavior during Artificial Ageing

4.1.2.2.1 Isochronal Ageing Characteristics of Alloys

Figure 4.1.5 and Figure 4.1.6 show the variation in Rockwell hardness (HRF) values of the alloys as a function of Cu content and ageing temperature at a constant time of 1 hr for different temperatures. The data points on the figures represent the average of at least seven repetitions. The curves show a typical precipitation-hardening behavior in which the hardness increases at first with increasing temperature, reaches a maximum, and finally slopes down.

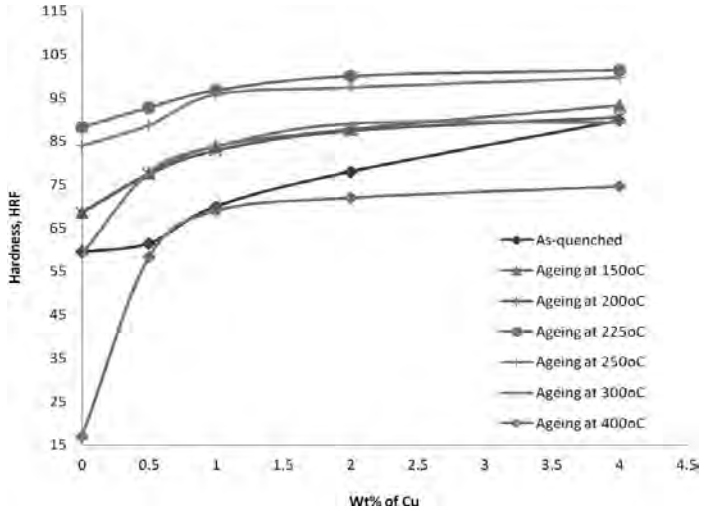

Figure 4.1.5: The change of hardness with Cu content in Al-6Si-0.5Mg alloys aged for different temperatures

Plots of hardness against Cu content of the alloys are plotted in Figure 4.1.5. Hardness in the as quenched conditions increases strongly with increase of Cu content. The increase of hardness in as quenched conditions with increase of Cu content indicates that the solid-solution strengthening of Al-6Si-0.5Mg-xCu (x= 0, 0.5, 1, 2 and 4) alloys is enhanced with increase of Cu content. In the as-solutionized [solution treated] condition, Alloy-1 (Al-6Si-0.5Mg) has the lowest hardness value of 59.5 HRF. Alloy-2, Alloy-3 and Alloy-4 have hardness of 61.5, 70 and 78 HRF respectively. The Alloy-5 has the highest as-quenched Rockwell hardness value of

89.8HRF. The isochronal ageing was conducted at 100, 150, 175, 200, 225, 250, 300, 350 and 400^{o}C for 1 hour and hardness values are presented in Figure 4.1.5. For all isochronal ageing conditions, the effect of Cu on hardness of Al-6Si-0.5Mg alloys is remarkable and maximum hardness was found for 4 wt% Cu addition after ageing at 225^{o}C.

With an increase in ageing temperature, hardness increases until it reaches the maximum peak strength, for all the alloys. From Figure 4.1.6, at the peak point, the alloys keep their as-solutionized hardness ranking. The Alloy-1 again has the lowest peak hardness of 88.3HRF. The Alloy-2 and Alloy-3 have a peak hardness of 92.8 and 96.8HRF respectively. Alloy-4 having a peak hardness of 100.1HRF gets closer to the Alloy-5. Among the Cu content alloys, the 4wt% Cu content alloy, Alloy-5 has the highest peak hardness of 101.5 HRF. Overageing of the alloys is observed in the material at artificial ageing temperatures higher than at 225^{o}C for 1 hour.

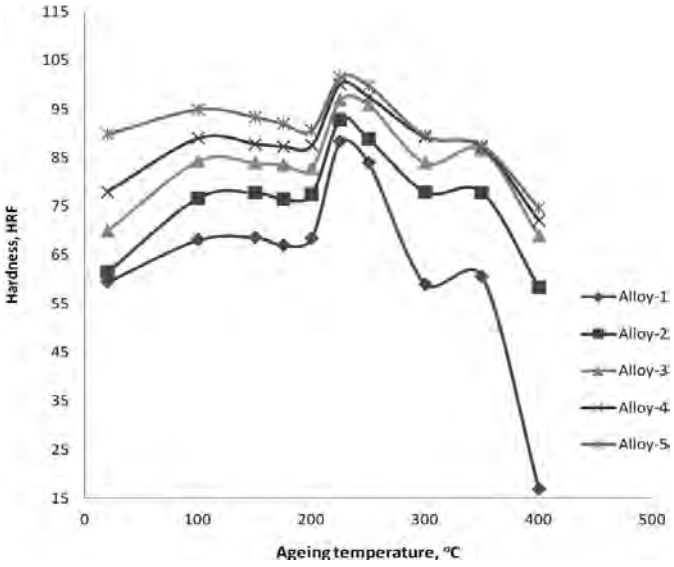

Figure 4.1.6: Evolution of hardness during artificial ageing of the Alloys 1 to 5 aged for 1 hour

Figure 4.1.7 shows the changes of electrical resistivity during isochronal ageing for 1 hour at as quenched condition to 400^{o}C for the both Cu-free and Cu-containing alloys. It is well known that the Cu-containing alloy shows higher number density of cluster than the Cu-free alloy [148]. Figure 4.1.6 shows the hardness results after solutionized (as quenched) in the both Cu-free and Cu-added alloys. As confirmed by the electrical resistivity, the Cu-added alloy represents the higher hardness than the Cu-free alloy.

Figure 4.1.7 also shows the effect of the chemical composition on the electrical resistivity. It can be seen that the electrical resistivity increases from Alloy-1 to Alloy-5, Alloy-5, with 4wt% of Cu, has the highest electrical resistivity. It is clear that, with an increase in the Cu content from 0.5wt% in Alloy 1 to 4wt% in Alloy 5 the electrical resistivity of the alloy increases by 22.20 % at 225^{o}C for 1 hour. Moreover, the electrical resistivity increases by 10.80 pct with increasing Cu content from 0.5 to 2 wt% at the peakaged condition.

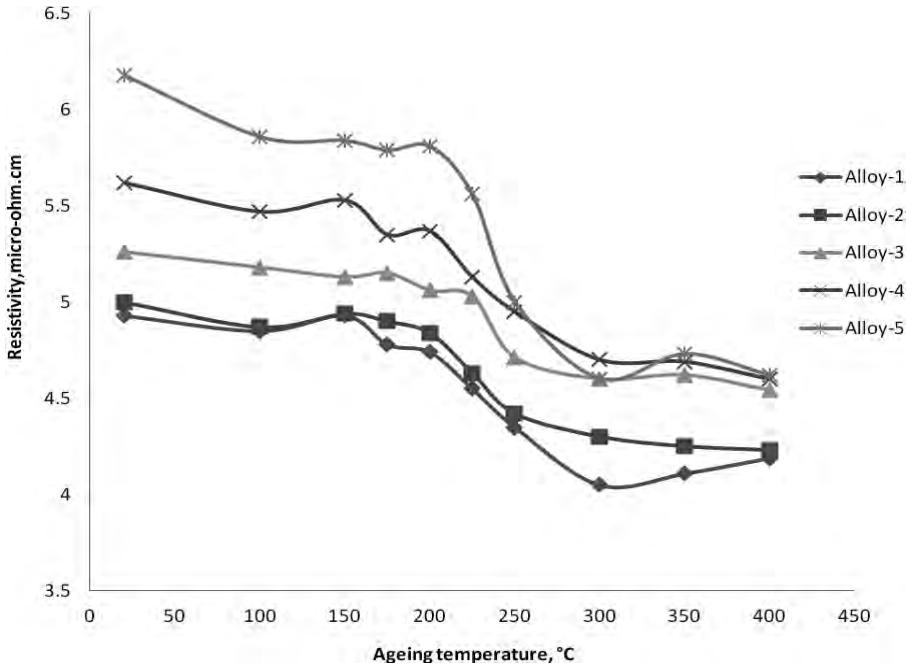

Figure 4.1.7: Evolution of resistivity during artificial ageing of Alloys 1 to 5 aged for 1 hour

Figure 4.1.8 shows the plots of hardness against ageing temperature during isochronal ageing for 1h of the as-quenched samples with additions of Cu and/or Ni. The addition of both Cu and Ni to the Al-6Si-0.5Mg base alloy strongly increases the hardness in both the as-quenched and the peak aged conditions. Peak aged (maximum hardness) condition is achieved at 225^{o}C for 1h artificial ageing for all alloys. The hardness value of 2 wt% Ni content alloy, Alloy-6 (92.6HRF) is lower than that of 2 wt% Cu content alloy, Alloy-4 (100.1HRF). So the effect of Cu on precipitation hardening on the Al-6Si-0.5Mg alloy is higher than that of Ni. When both Cu and Ni has been added (Alloy-7), the hardness value (102.3HRF) is slightly higher than that of Alloy-4 (2%Cu).

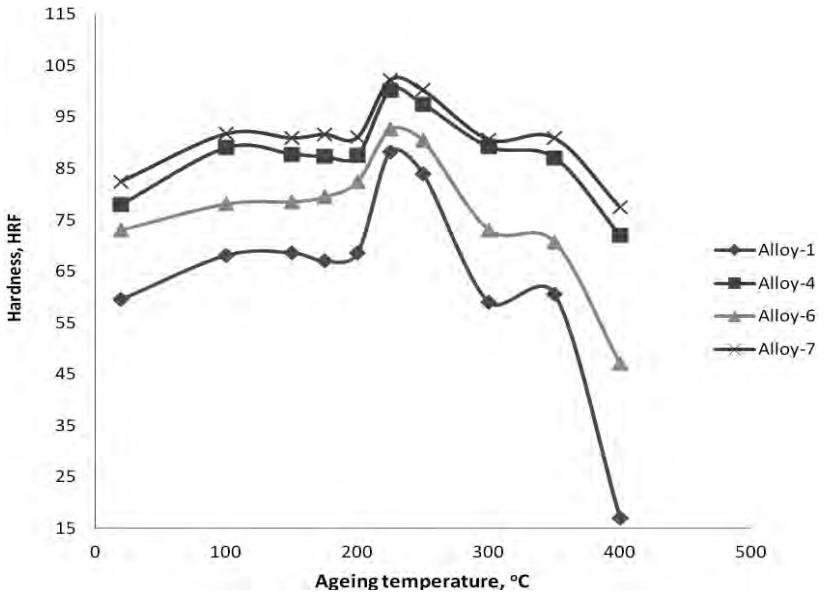

Figure 4.1.8: Evolution of hardness during artificial ageing of Alloys 1, 4, 6 and 7 aged for 1 hour

The electrical resistivity changes of Alloy-1, Alloy-4, Alloy-6 and Alloy-7 during isochronal ageing has shown in Figure 4.1.9. It also shows that the electrical resistivity in the solution treated condition depends on the chemical composition of the samples. The resistivity increases with the amount of alloying element added. Alloy-7 shows higher resistivity than the Alloy-4 or Alloy-6. It can also be seen that the electrical resistivity of the alloys decreased rather rapidly after ageing at 200^{o}C and this trend is exist till of ageing at 250^{o}C for the alloys.

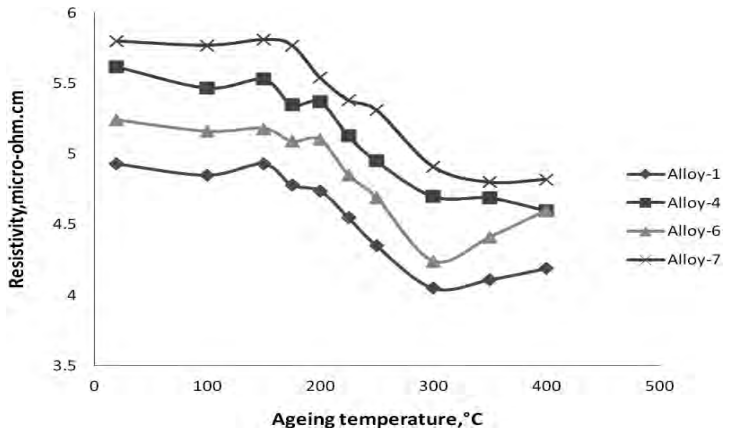

Figure 4.1.9: Evolution of resistivity during artificial ageing of Alloys 1, 4, 6 and 7 aged for 1 hour

4.1.2.2.2 Isothermal Ageing Characteristics of Alloys

4.1.2.2.2.1 Isothermal Ageing at 150^{o}C

Figure 4.1.10 shows the variation in hardness (HRF) values as a function of ageing time at a constant temperature of 150°C for different alloys. In the as-solutionized condition, the Cu free alloy (Alloy-1) has the lowest hardness value of 59.5HRF. The Alloy-2 (0.5wt% Cu) and Alloy-3 (1wt% Cu) have hardness of 61.5 HRF and 70 HRF respectively whereas the Alloy-4 with 2 wt% Cu has a hardness of 78 HRF. Alloy-5 (4 wt% Cu) has the highest as-quenched Rockwell hardness value at 89.8HRF. Significant improvement in hardness of the alloys occurs after ageing at 150^{o}C for 15 minute and 30 minute. The Cu-containing alloys, Alloy-2, Alloy-3, Alloy-4 and Alloy-5 maintain hardness values of 77.5, 83.9, 87.8 and 93.3 HRF after ageing of 60 minutes respectively. At the end of 360 minutes of ageing, the hardness value of the Cu free (Alloy-1) and Cu added alloys (Alloy-2 to Alloy-5) does not changes so significantly.

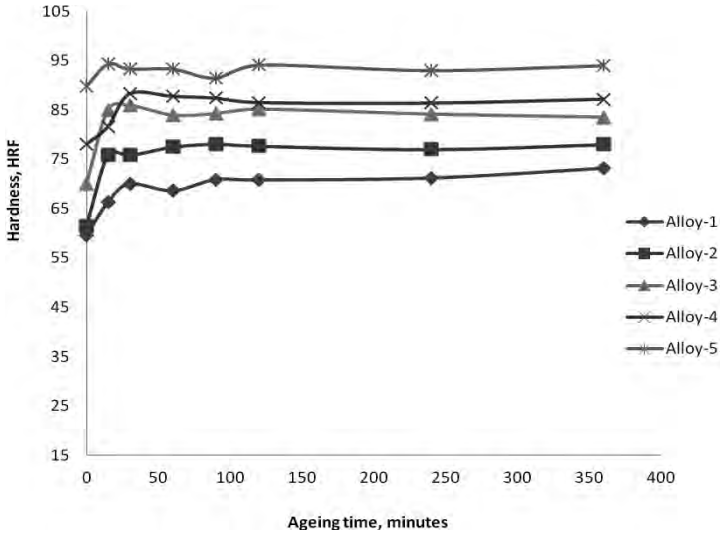

Figure 4.1.10: Evolution of hardness during artificial ageing of Alloys 1 to 5 aged at 150^{o}C

Figure 4.1.11 shows the changes of electrical resistivity during ageing at 150^{o}C in both the Cu-free and Cu-added alloys. The Cu added alloys (Alloy-2 - Alloy-5) show higher number density of cluster than the Cu-free alloy (Alloy-1). As confirmed by the electrical resistivity, the Cu-added alloy represents higher hardness than the Cu-free alloy. Cu enhances the formation of cluster [148-150]. The resistivity values of the alloys decrease slightly with increase of ageing time.

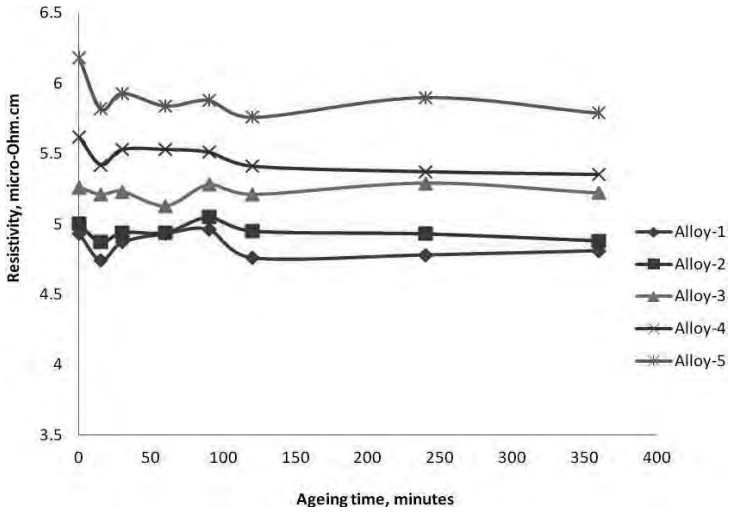

Figure 4.1.11: Evolution of resistivity during artificial ageing of Alloys 1 to 5 aged at 150^{o}C

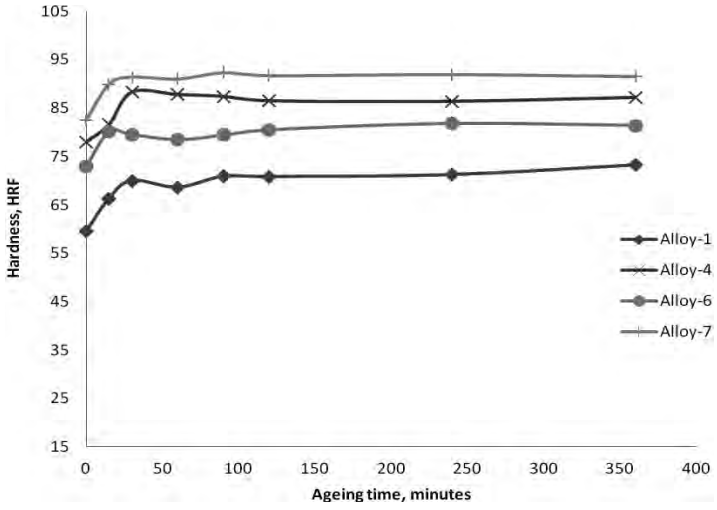

Figure 4.1.12: Evolution of hardness during artificial ageing of Alloys 1, 4, 6 and 7 aged at 150^{o}C

The hardness of Cu and Ni free alloy (Alloy-1) and Cu and/or Ni containing alloys (Alloys 4, 6 and 7), isothermally aged at 150^{o}C up to 360 minutes, and are shown in Figure 4.1.12. The significant improvement in hardness of Alloy-4, Alloy-6 and Alloy-7 over Alloy-1 in the as-solutionized state indicates that certain second phase hardening and solid solution strengthening occurred in these alloys due to Cu and/or Ni additions. Ageing from as-quenched condition to 30 minutes increases the hardness of the alloys significantly. At the end of 30 minutes of ageing,

the hardness values of these alloys remain almost unchanged. It is noted that the Alloy-1 has the lower hardness than the other alloys all over the ageing times. The combined effect of Cu and Ni (Alloy-7) on age hardening is greater than the individual effect of Cu or Ni all over the ageing conditions. But the 2wt% Cu addition to Al-6Si-0.5Mg alloy (Alloy-4) has a greater effect than 2wt% Ni (Alloy-6). The significant improvement in hardness of Alloy-4, Alloy-6 and Alloy-7 over Alloy-1 are maintained up to 30 minute of ageing.

Addition of Cu and/or Ni to Al-6Si-0.5Mg alloy increases the electrical resistivity (Figure 4.1.13). Alloy-7 has the highest electrical resistivity all over the ageing conditions among these alloys. It can be seen that Alloy-6 has lower electrical resistivity than Alloy-4.

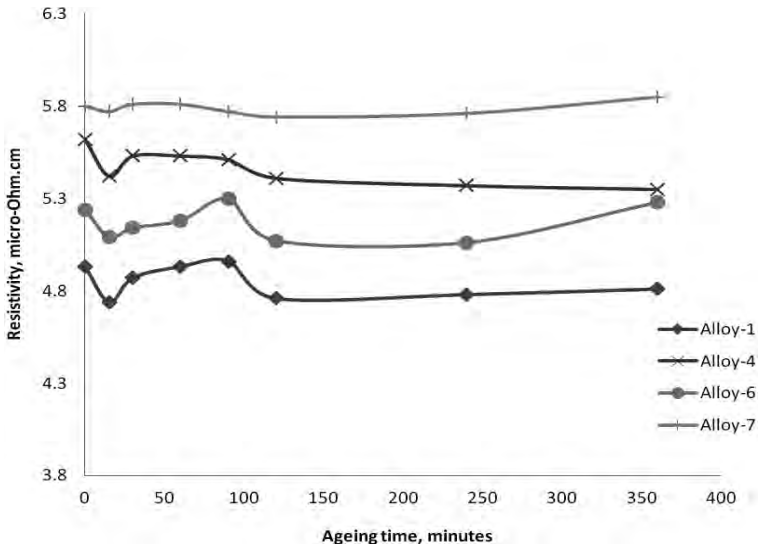

Figure 4.1.13: Evolution of resistivity during artificial ageing of Alloys 1, 4, 6 and 7 aged at 150^{o}C

4.1.2.2.2.2 Isothermal Ageing at 175^{o}C

The significant improvement in hardness of the five alloys (Alloys 1 to 5) in the as-solutionized state indicates that certain second phase hardening is occurring in these alloys due to the Cu additions. Figure 4.1.14 shows the age hardening curves of various Cu containing alloys aged at 175^{o}C for different times. The hardness of the alloys is lower in the as quenched condition. It can be seen that the artificial ageing treatment causes an obvious increase in hardness of as-quenched alloys and the hardness of artificial aged alloys increases with increasing ageing times. The age hardening curves of the alloys under all ageing conditions have a similar shape. Cu

addition improves the hardness as solution treated and all over the ageing conditions. The Cu free alloy, Alloy-1 has lower hardness all over the ageing condition. With the increase of Cu content the age hardening response increase significantly. 4wt% Cu content alloy, Alloy-5 has the highest hardness than the other Cu containing alloys at any stage of ageing.

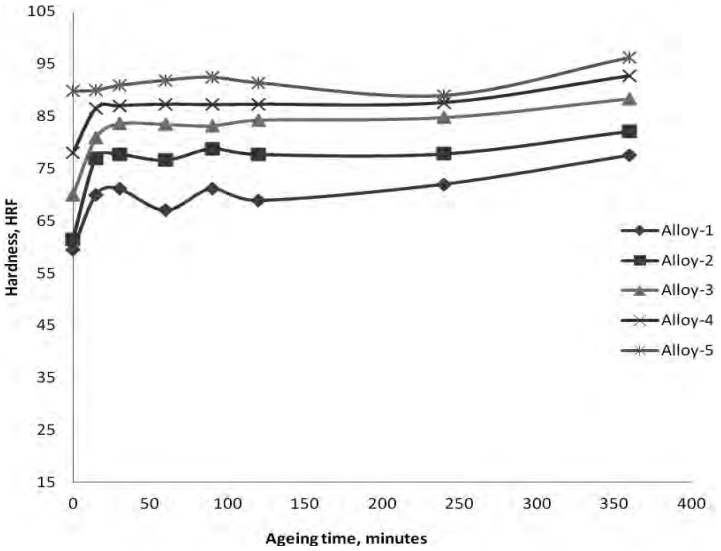

Figure 4.1.14: Evolution of hardness during artificial ageing of Alloys 1 to 5 aged at 175^{o}C

The Cu-added alloys, Alloy-2 to Alloy-5 show the higher increase of the electrical resistivity than the Cu-free alloy, Alloy-1 for the as-quenched condition at the initial stage of the isothermal ageing at 175^{o}C (Figure 4.1.15).

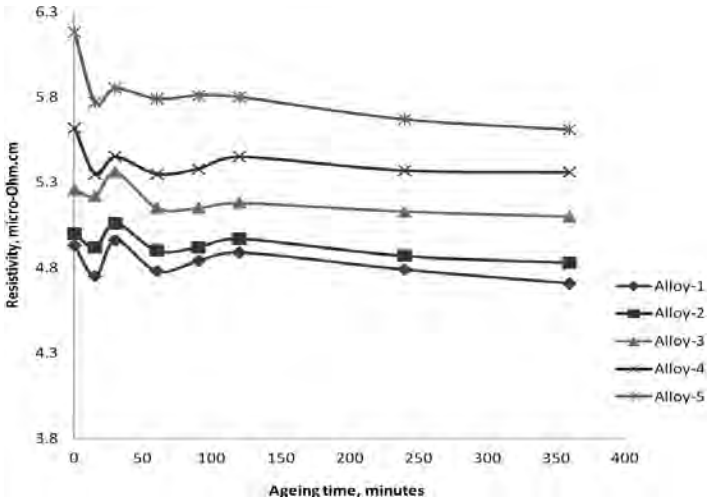

Figure 4.1.15: Evolution of resistivity during artificial ageing of Alloys 1 to 5 at 175^{o}C

The Cu-added alloys produce precipitates than the specimens keep about a constant value of the electrical resistivity in the both Cu-free and Cu-added alloys at the early stage of ageing at 175^{o}C. As introduced in the analysis method for the electrical resistivity, the substantial decrease of the electrical resistivity is caused by the decrease of number density with increase of the volume fraction of the precipitates with longer ageing times.

With an increase in ageing time, hardness increases until it reaches the maximum peak hardness, for all of the alloys. Figure 4.1.16 illustrates the Rockwell hardness of the samples against the ageing time. It could be found that the Cu and Ni containing Al-6Si-0.5Mg alloy, Alloy-7 was harder than the individual Cu added alloy (Alloy-4) or Ni added alloy (Alloy-6) during the whole ageing process even under the solution treated condition. For Alloy-4, Alloy-6 and Alloy-7, the hardness increased rapidly at the early stage (within the first 60 minutes) of artificial ageing. The hardness of the Cu and/or Ni alloys further increases after being aged for 360 minutes at 175^{o}C. The Alloy-1 has the lowest hardness of 77.5HRF ageing at 175^{o}C for 360minutes. The Alloy-4, with a hardness of 92.7HRF, gets closer to the Alloy-6 having a hardness of 94.4HRF. Among the four alloys, the Alloy-7 has the highest hardness of 98.1 HRF.

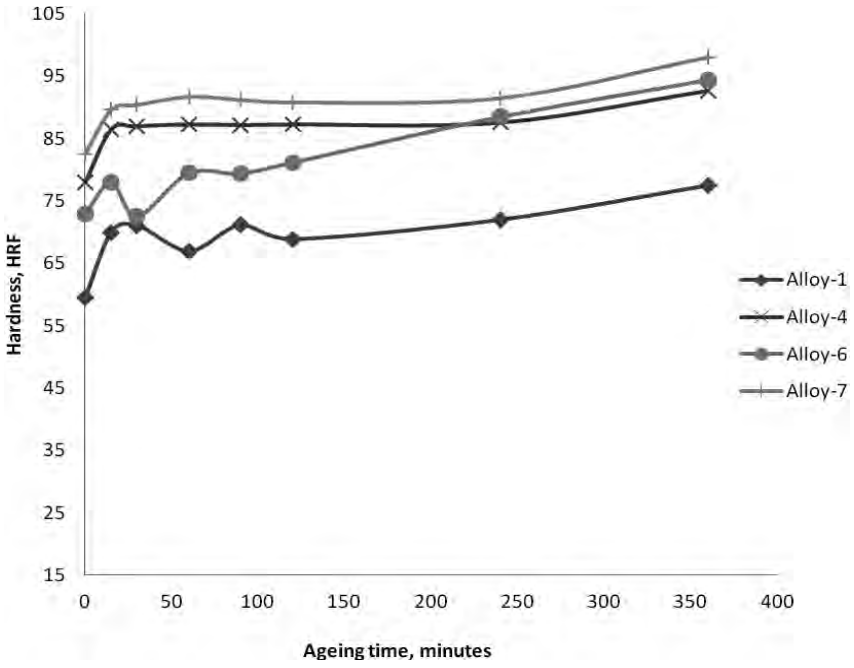

Figure 4.1.16: Evolution of hardness during artificial ageing of Alloys 1, 4, 6 and 7 aged at 175^{o}C

Figure 4.1.17 shows the resistivity changes with ageing times in the Cu and/or Ni added alloys. The 2wt% Cu and 2wt% Ni containing alloy (Alloy-7) shows higher resistivity than the 2 wt% Cu or 2wt% Ni containing alloys (Alloy-4 or Alloy-6). There is no resistivity increases during isothermal ageing at 175^{o}C for 120 minutes or longer times. The 2 wt% Cu containing alloy (Alloy-4) has better response than the 2 wt% Ni alloy (Alloy-6) in the case of age hardening.

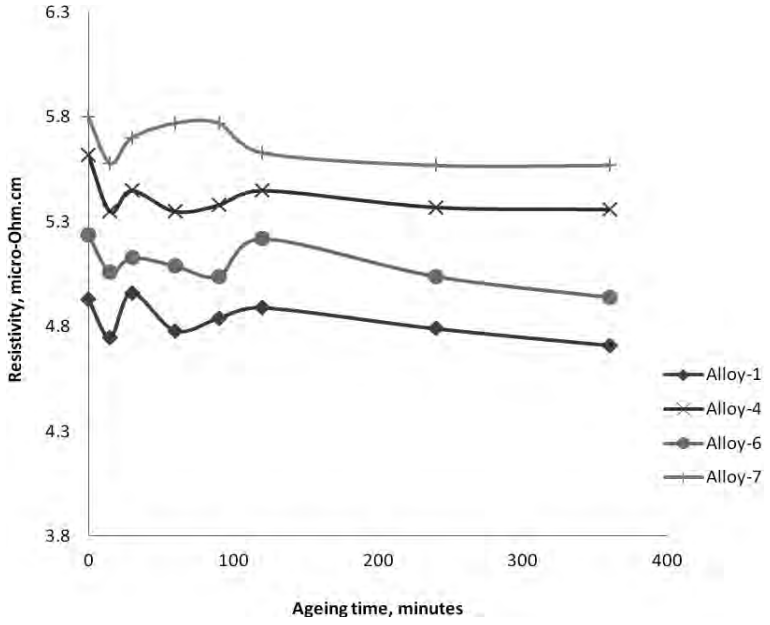

Figure 4.1.17: Evolution of resistivity during artificial ageing of Alloys 1, 4, 6 and 7 aged at 175^{o}C

4.1.2.2.2.3 Isothermal Ageing at 200^{o}C

The Cu containing alloys were aged at 200^{o}C. It can be seen (Figure 4.1.18) that there is an obvious age hardening phenomenon for each curve. However, another small hardness peak was observed following the first one in most of age-hardening curves. At the early stage of ageing, the hardness increases with ageing time until reaches the first peak. At intermediate stage of ageing, after a little decrease the hardness increases again and reaches the second peak (240 minutes at 200^{o}C). At the last stage of ageing (360 minutes at 200^{o}C), the hardness of the various Cu content Al-6Si-0.5Mg alloys decreases as a result of over-ageing. A hardness high plateau from 120 to 360 minutes is present in the age hardening curve of the Cu content Al-6Si-0.5Mg alloys.

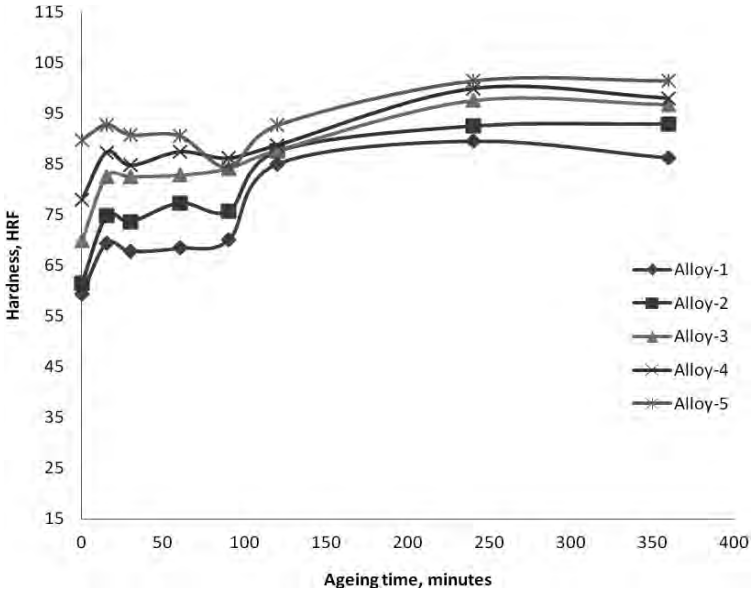

Figure 4.1.18: Evolution of hardness during artificial ageing of Alloys 1 to 5 aged at 200^{o}C

Figure 4.1.19 shows the changes of electrical resistivity during ageing at 200^{o}C in both the Cu-free and Cu-added alloys. Cu-added alloy represents higher resistivity than the Cu-free alloy. The substantial decrease of the electrical resistivity in the later part is caused by the decrease of number density with increase of the volume fraction of the precipitates. The decrease of the electrical resistivity is in order of Alloy-1, Alloy-2, Alloy-3, Alloy-4 and Alloy-5 alloys.

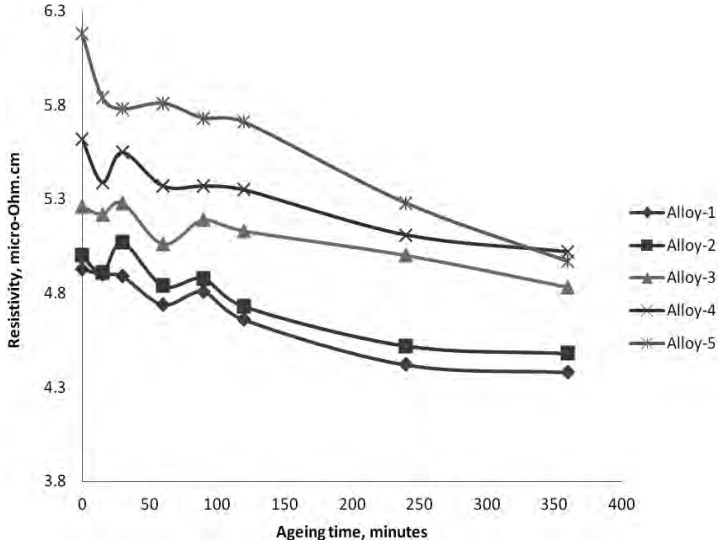

Figure 4.1.19: Evolution of resistivity during artificial ageing of Alloys 1 to 5 aged at 200^{o}C

The response of the Cu and /or Ni containing alloys during artificial ageing at 200^{o}C is shown in Figure 4.1.20. The hardness of the alloys aged at 200^{o}C for 15 minutes increases gradually and reaches the highest value. The highest hardness is identical for Alloy-4, Alloy-6 and Alloy-7. Alloy-1 has the lowest peak hardness of 89.6HRF. The Alloy-6, with a peak hardness of 96.1 HRF gets closer to the Alloy-7 having a peak hardness of 97.7 HRF. Among the four alloys, the Alloy-4 has the highest peak hardness of 100 HRF.

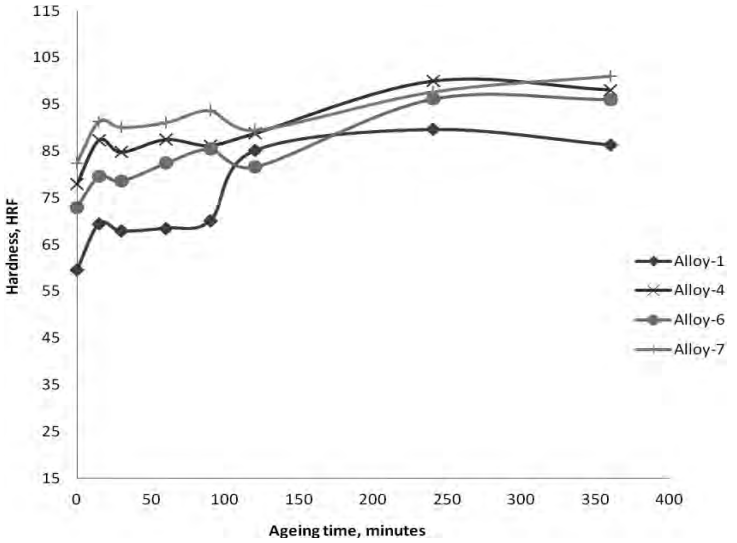

Figure 4.1.20: Evolution of hardness during artificial ageing of Alloys 1, 4, 6 and 7 aged at 200^{o}C

The evolution of resistivity during artificial ageing is shown in Figure 4.1.21.

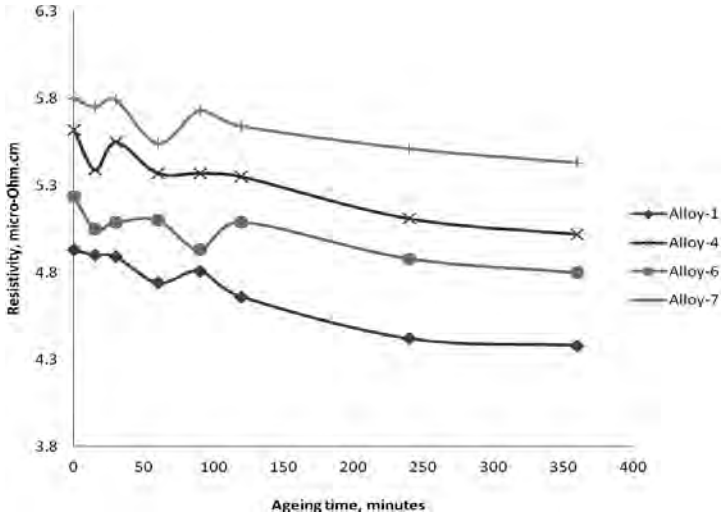

Figure 4.1.21: Evolution of resistivity during artificial ageing of Alloys 1, 4, 6 and 7 aged at 200^{o}C

These resistivity curves indicate the changes of precipitates size, shape and distribution with structural changes for different ageing times at 200^{o}C.The resistivity value of these alloys decreases with ageing. The combined addition of Cu and Ni shows higher resistivity all over the ageing treatment. The 2wt% Cu containing alloy, Alloy-4, has higher resistivity than the 2wt% Ni containing alloy, Alloy-6. The fall of resistivity with ageing time means that the total number of precipitates decreases but the sizes of precipitates increase. So a clear drop of resistivity was seen with longer time of ageing.

4.1.2.2.2.4 Isothermal Ageing at 225^{o}C

Figure 4.1.22 shows the evolution of hardness during artificial ageing of the Alloys 1 to 5 at 225^{o}C. With the increase of ageing time, hardness increases until it reaches the first peak, for all of the alloys. The maximum peak hardness was achieved after 60 minutes ageing at ~ 225^{o}C for all of the alloys. However, since the peak hardness ageing times (~60 minute) are identical, it can be postulated that the ageing sequence may be similar. At the peak point, the alloys maintain their as-solutionized hardness. The Alloy-1 again has the lowest peak hardness of 88.3HRF. The Alloy-2 and 3, have a peak hardness of 92.8 and 96.8HRF respectively. Alloy-4 having a peak hardness of 100.1HRF gets closer to the Alloy-5. Among the five alloys, the Alloy-5 has the highest peak hardness of 101.5 HRF.

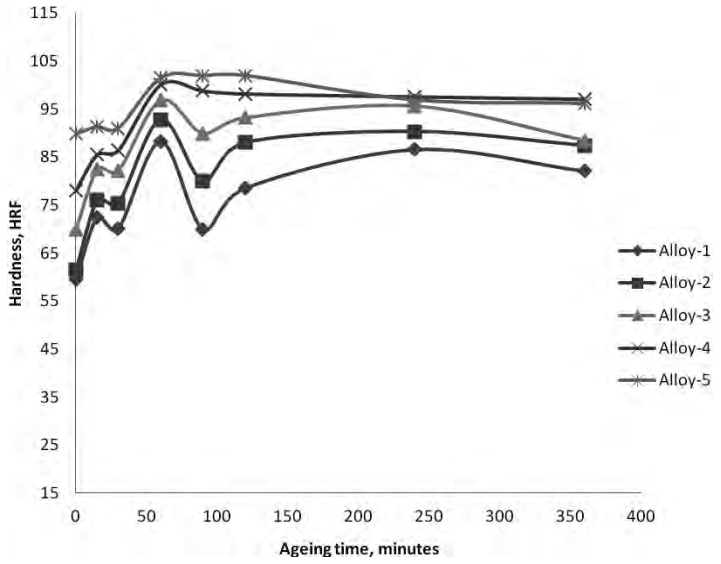

Figure 4.1.22: Evolution of hardness during artificial ageing of the Alloys 1 to 5 aged at 225^{o}C

The Cu additions significantly improve the ageing behavior of Al-6Si-0.5Mg alloy at all stage of ageing (Figure 4.1.23). The increase in the peak hardness might be due to the increased density of β'' and β' phases and the newly formed phases containing Cu such as λ' and θ' [89]. At longer ageing times, since the Mg-bearing phases lose their strength as in the Alloy-1, the growth of Cu-containing phases could provide strength through Orowan strengthening even in the over-aged state. Ageing times longer than the 120 minutes give a better idea on the overall over ageing behavior of the alloys. After 90 minutes of ageing, the Alloy-1 and Alloy-2 have low hardness values. On the other hand, the other Cu containing alloys, the Alloys 3, 4 and 5, maintain hardness values of 89.9, 98.8 and 102 HRF, respectively. At the end of 120 minutes of ageing, the hardness decreases further. However, Alloy-5 still has superior ageing behavior since the difference in hardness among the alloys is still maintained. At this end point, the alloys have low hardness value than the previous stage of ageing.

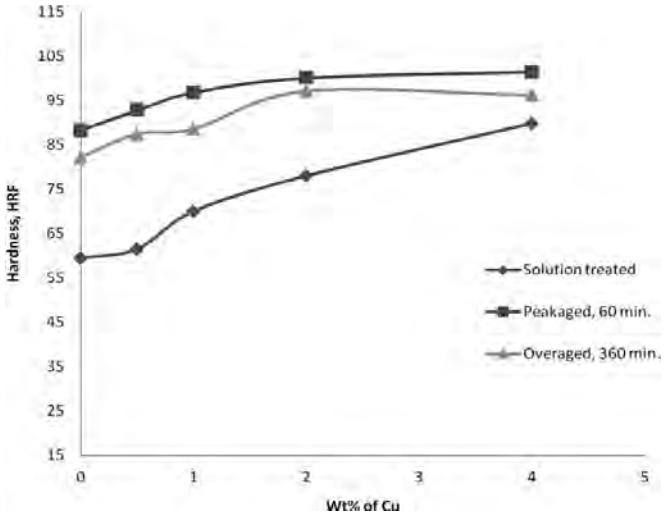

Figure 4.1.23: The change of hardness with Cu content in Al-6Si-0.5Mg alloys in solution treated, peakaged and overaged condition

In the presence of secondary particles, the primary elective parameters on the electrical resistivity are as follows: (1) the volume fraction of fine and coherent particles in the structure, (2) the particle interspacing, and (3) the concentration of elements in solid solution [155]. The formation of dispersoids leads to a decrease in the concentration of the corresponding elements in the matrix. If the elements precipitate out during a thermal process such as homogenization or precipitation hardening, the change in the electrical resistivity of the material depends on the size and the interface of the newly formed particles. If the new particles are small and coherent,

the electrical resistivity of the material increases and vice versa. The formation of the plateau in the electrical resistivity curve may be due to the balance of the increase in the concentrations of some elements, namely Si, Mg, and Cu in the matrix. When the rate of the increase in the electrical resistivity due to the dissolution of constitutive particles and therefore, the enrichment of the structure becomes equal to the rate of the decrease in the electrical resistivity due to the formation of dispersoids, a peak or plateau is observed in the electrical resistivity curve.

The effect of grain refinement of the alloys is clearly evident from the resistivity curves, which show a significant difference of resistivity values of the copper added alloy with that of the base alloy. The initial high resistivity of copper treated alloy is indicative of high electron scattering sites viz. grain boundary area to mean that grains in all those alloys are finer. Formation of supersaturated solid solution assures a high precipitation hardening effect upon decomposition of this solid solution with the formation of fine coherent precipitates. The softening of the alloys at higher temperature may be due to particle coarsening effect. The initial drop in resistivity is due to stress relieving in the alloys during ageing. The steeper drop at the initial period of isothermal ageing at 225^{o}C may be attributed to the formation solute atom vacancy complex. Transition metals are known to bind vacancies strongly. For this reason, the number density of scattering centers is reduced. This causes a sharp fall in resistivity (Figure 4.1.24). The subsequent increase in resistivity is due to the appearance of fine precipitates. When the ageing temperature is low, the resistivity continues to increase beyond the peak because the precipitation formation and reordering of atoms continues.

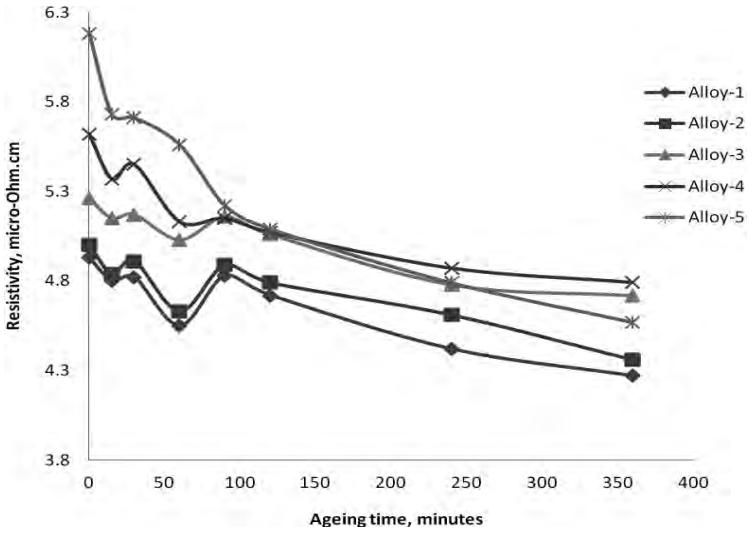

Figure 4.1.24: Evolution of resistivity during artificial ageing of the Alloys 1 to 5 aged at 225^{o}C

The Cu and/or Ni additions to the Alloy-1 gives the best ageing behavior (Figure 4.1.25) in the Alloy-4, Alloy-6 and Alloy-7 and this might be due to the combined effect of the alloying elements on the Cu and Ni containing second phases. The common observation from ageing at 225^{o}C of Cu containing Alloy-4 and Cu and Ni containing Alloy-7 is that the rate of decrease in hardness is lower than the Ni containing Alloy-6. This is mainly due to the Cu containing phases which retain their strength for longer times at 225°C [162-163].

The significant improvement in hardness of Alloy-4 and Alloy-7 over Alloy-1 and Alloy-6 in the peakaged condition indicates that most of the second phase hardening is occurring in these alloys due to the Cu and/or Ni additions into Alloy-1. However, this improvement disappears in Alloy-6 (gets closer to Alloy-1) when the alloy is exposed to ageing for longer times. Therefore, it can be concluded that the second phases including Ni in the Alloy-6 get coarsened with the increased duration of ageing at 225°C resulting in lower hardness values.

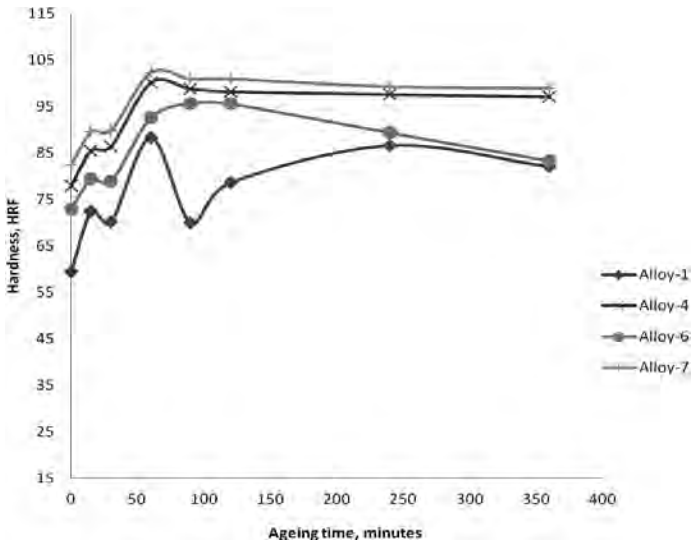

Figure 4.1.25: Evolution of hardness during artificial ageing of Alloys 1, 4, 6 and 7 aged at 225^{o}C

For the four alloys studied, the maximum peak strength occurs in the early stages of ageing, approximately within an hour, which is expected. This is mainly due to the temperature (225°C) at which the ageing is carried out. It is known that the lower ageing temperatures results in higher peak hardness values which are obtained at longer ageing times. After the first peak in the ageing curve, at the early intermediate stage of ageing, the hardness decreases until it reaches a plateau. Interestingly, this plateau is observed for all the alloys at the same ageing time ~1hours.

The alloys reach the plateau whereas the hardness of Alloy-4 and Alloy-7 tends to decrease after this point. The Alloy-4 and Alloy-7 have the highest hardness value of 100.1 and 102.3 HRF at 1 hour of ageing and 88.3HRF is the lower hardness value recorded for the Alloy-1 at peakaged condition. But the Alloy-6 reaches the maximum hardness 95.7HRF at the ageing time between 90-120 minutes.

Figure 4.1.26 shows the resistivity changes with ageing time of Cu and/or Ni containing alloys. The resistivity decrease is more pronounced for the alloys at longer ageing times. Alloy-1 and Alloy-6 (2wt% Ni) have lower resistivity all over the ageing treatment. But Alloy-7 (2 wt% Cu and Ni) and Alloy-4 (2wt% Cu) have stronger resistance to softening. The 2 wt% Cu containing alloy, Alloy-4 has higher resistivity than the 2 wt% Ni containing alloy, Alloy-6 all over the ageing times. So the Cu addition to Al-6Si-0.5Mg alloy is more effective than Ni in the case of hardening.

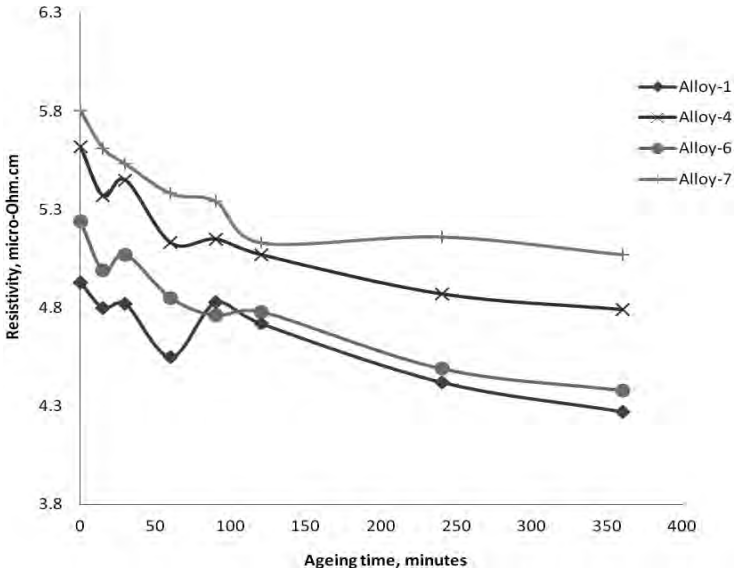

Figure 4.1.26: Evolution of resistivity during artificial ageing of Alloys 1, 4, 6 and 7 aged at 225^{o}C

4.1.2.2.2.5 Isothermal Ageing at 250^{o}C

Hardness change of alloys (Alloys 1 to 5) with time during ageing at 250°C is given in Figure 4.1.27 and Figure 4.1.28. It is found that increasing Cu content from 0.5% to 4% increases the hardness from 92.8HRF to 101.5HRF for 60 minutes ageing. This hardening mechanism

suggests the formation of GP zones in the early stage of ageing. In the course of ageing, this is followed by the precipitation of θ″ and θ ′. At long ageing time, over ageing occurs and the hardness drops due to extensive ageing, when the precipitation turns the equilibrium phase θ (Al_2Cu).

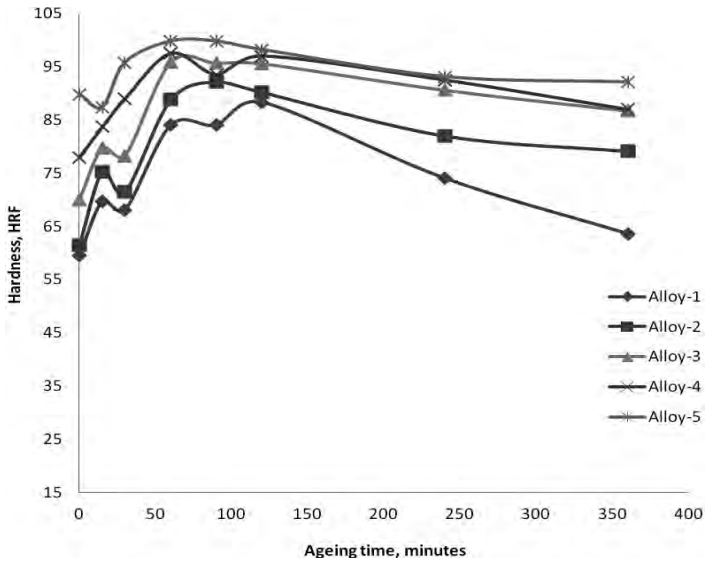

Figure 4.1.27: Evolution of hardness during artificial ageing of the Alloys 1 to 5 at 250^{o}C

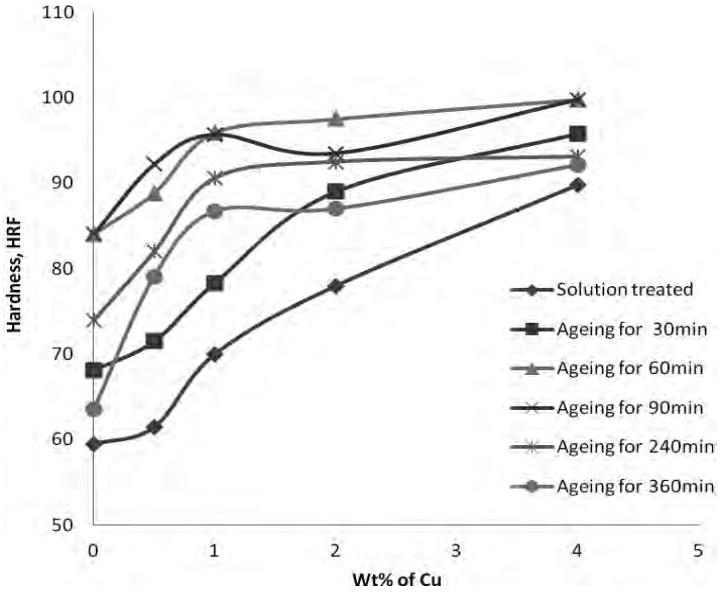

Figure 4.1.28: The change of hardness with Cu content in Al-6Si-0.5Mg alloys after aged at 250^{o}C for different times

Figure 4.1.27 shows the age hardening behaviour of the solution treated alloy in the as-quenched condition, and after artificial ageing at 250°C for various times. The Alloy-1 as-quenched hardness of 59.5HRF increases to 84HRF and 88.3HRF after 60 and 120 minutes respectively. The other alloys show the similar trend of increase of hardness with the increase of ageing time at 250^{o}C. The alloys show the maximum hardness achieved at 225^{o}C for 60-120 minutes of ageing. The Alloy-1, 2, 3, 4 and 5 show the maximum hardness 88.3(for 120min), 92.2(for 90min), 95.9(for 60min), 97.5 (for 60min), and 99.8HRF (for 60min) at 250^{o}C respectively. Overageing of the alloys is observed in the alloys at artificial ageing times longer than ~2 hours at 250^{o}C. The decrease in hardness of the Cu added alloys (Alloy-2 to Alloy-5) takes place very slowly compared with the Cu free alloy (Alloy-1) during overageing. During overageing the precipitated particles become larger, weaker and less able to prevent dislocation movement.

Figure 4.1.29 shows the resistivity changes at overageing conditions. The resistivity falls more pronounced ageing at 250^{o}C. At higher ageing temperature and longer time, overageing occurs i.e. the precipitates size increases but the total number of precipitates decreases, the grains are coarsen as a results the resistivity decreases. The resistivity drops rapidly up to 60 minutes at 250^{o}C.

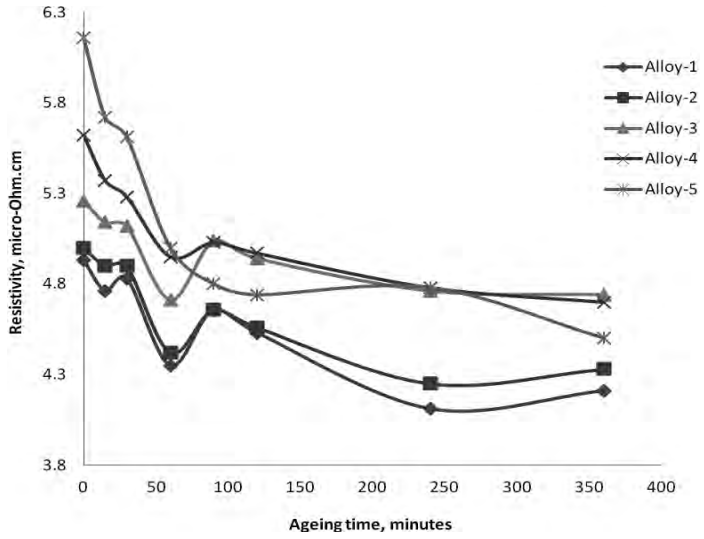

Figure 4.1.29: Evolution of resistivity during artificial ageing of Alloys 1 to 5 at 250^{o}C

The growth and coarsening of precipitates reduces the number of solute atoms in the matrix and releases the strain fields around those precipitates, which results in increasing electrical conductivity continuously during ageing. The change in electrical conductivity is related to

microstructural changes, especially the type and size of the matrix precipitates. During ageing, the amount of hardening phases that precipitates in the high Cu content alloy is more than that in the low content Cu alloy. The change in resistivity in the high content Cu alloy is therefore higher than that in the low content Cu alloy. The amount of the hardening precipitates increases with increasing Cu content in Al-6Si-0.5Mg alloy

Figure 4.1.30 shows the evolution of hardness of the Cu and/or Ni containing alloys during artificial ageing at 250°C. The hardness of the alloys in the as-quenched condition is lower than in the peak-aged condition. During artificial ageing at 250°C, the hardness value of 2wt% Cu containing Alloy-4 and 2wt% Cu and 2wt% Ni containing Alloy-7 increase rapidly from the as-quenched value to 78HRF and 82.5HRF after 1 hour, and subsequently reaches the maximum hardness of 97.5HRF and 100.3HRF after 1 hour. But the 2wt% Ni containing Alloy-6 increases the hardness as-quenched value to 73HRF after 1 hour, and subsequently reaches the maximum hardness of 90.4 HRF after 1 hour.

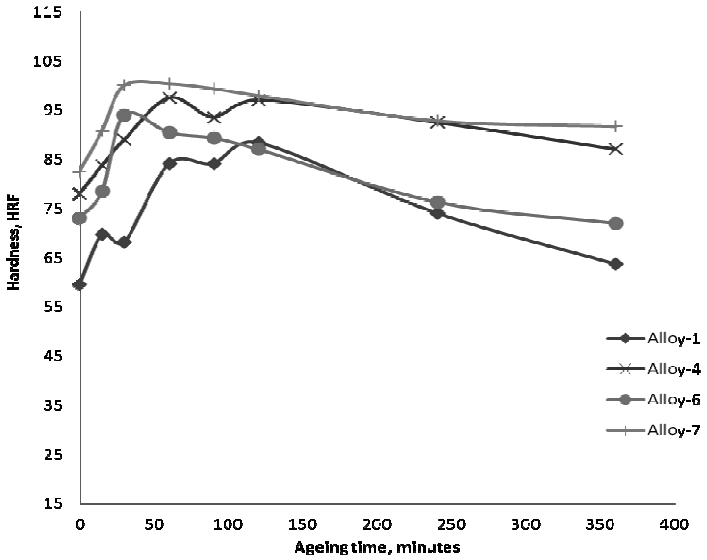

Figure 4.1.30: Evolution of hardness during artificial ageing of Alloys 1, 4, 6 and 7 aged at 250^{o}C

The significant improvement in hardness of Alloy-4 and Alloy-7 over Alloy-1 and Alloy-6 in the as-solutionized state indicates that certain second phase hardening is occurring in these alloys due to the individual Cu and combined Cu and Ni additions since the solubility limits of these elements in Al are low. However, this improvement disappears when the alloy is exposed to ageing for longer times. The combined Cu and Ni additions to the Alloy-1 gives the best

ageing behavior as shown in the Alloy-7 and this might be due to the alloying elements on the Cu and Ni containing second phases. The common observation from ageing of 2wt% Cu containing alloy (Alloy-4) and 2wt% Cu and 2wt% Ni containing alloy (Alloy-7) is that the rate of decrease in hardness is lower than the alloy containing only 2wt% Ni (Alloy-6). This is mainly due to the Cu and Cu & Ni containing phases which retain their strength for longer times at 250°C

Figure 4.1.31shows the effect of the ageing time on the electrical resistivity of the Alloy-1, 4, 6 and 7 aged for up to 360 minutes. It is clear that the electrical resistivity of the alloys decreased with increasing time during ageing. It can also be seen that the most significant decrease in the electrical resistivity occurs at the first 60 minutes of ageing. In addition, some differences are observed when different compositions of the materials are compared. The 2 wt% Cu and 2wt% Ni containing alloy, Alloy-7 the electrical resistivity shows a steep decrease (between 0 to 30 minutes) and then continuous decrease up to 360 minutes, while the 2 wt% Cu containing alloy, Alloy-4 the electrical resistivity shows a steep decrease (between 0 to 60 minutes) and then an increase leading to a peak (at 90 minutes), followed by a decrease (between 120 to 360 minutes). The 2 wt% Ni containing alloy, Alloy-6 show that, during ageing for longer times, the electrical resistivity steeply decreases till to 30 minutes, while the reduction in the electrical resistivity continues until the end of the process (360 minutes).

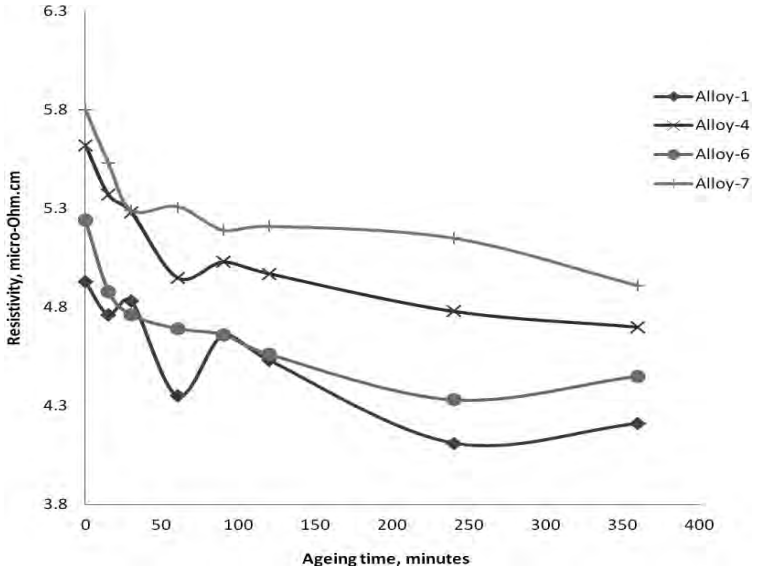

Figure 4.1.31: Evolution of resistivity during artificial ageing of Alloys 1, 4, 6 and 7 aged at 250^{o}C

4.1.2.2.2.6 Isothermal Ageing at 300°C

Ageing temperature at 300°C for different times give a better idea on the overall over ageing behavior of the Cu free and Cu added alloys (Figure 4.1.32). After 15 minutes of ageing, the hardness value of the Cu free Alloy-1 decreases very rapidly with the increases ageing times. The Cu free, Alloy-1 has very low hardness (17.2HRF) values after ageing 300°C for 240 minutes. On the other hand, the Cu-containing alloys, Alloy-2, Alloy-3, Alloy-4 and Alloy-5, maintain hardness values of 60.5, 67.9, 62 and 76.2HRF respectively. At the end of 360 minutes ageing, the hardness decreases further however, the Cu containing alloys, Alloy-2 to Alloy-5 still have better ageing behavior. The Alloy-5 has better hardness 72.2HRF difference in hardness whereas the Alloy-1, Alloy-2, Alloy-3 and Alloy-4 have 17.9, 55.2, 66 and 72.2HRF respectively.

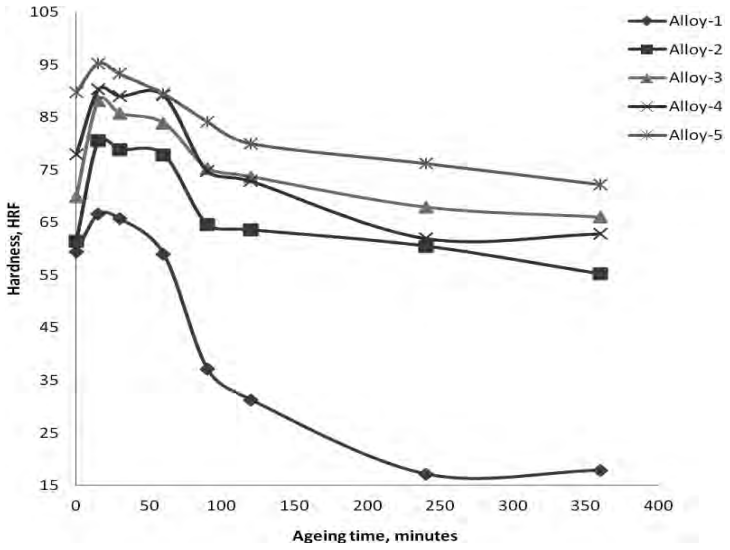

Figure 4.1.32: Evolution of hardness during artificial ageing of Alloys 1 to 5 at 300°C

Plots of hardness against Cu contents at various ageing time at 300°C for quenched samples of Al-6Si-0.5Mg-xCu alloys with 0 wt%Cu, 0.5 wt%Cu, 1 wt%Cu, 2 wt%Cu, and 4 wt% Cu are plotted in Figure 4.1.33. Hardness in both of the as quenched conditions and other ageing conditions increases strongly with increase of Cu content. The increase of hardness in as quenched conditions with increase of Cu content indicates that the solid-solution strengthening of Al-6Si-0.5Mg-xCu alloys is enhanced with increase of Cu content. For Cu-free alloy, hardness begins to increase in a few minutes and maximum hardness is obtained for about 15

min. For Cu containing Al-6Si-0.5Mg–xCu alloys, precipitation begin for at the very first time and maximum hardness is observed for about 15 min. The total increase in hardness 28.7HRF from Cu free Al-6Si-0.5Mg to 4wt% Cu added Al-6Si-0.5Mg (Alloy-5) ageing for 15minutes at 300^{o}C and this hardness of these alloys are better than longer time of ageing treatment.

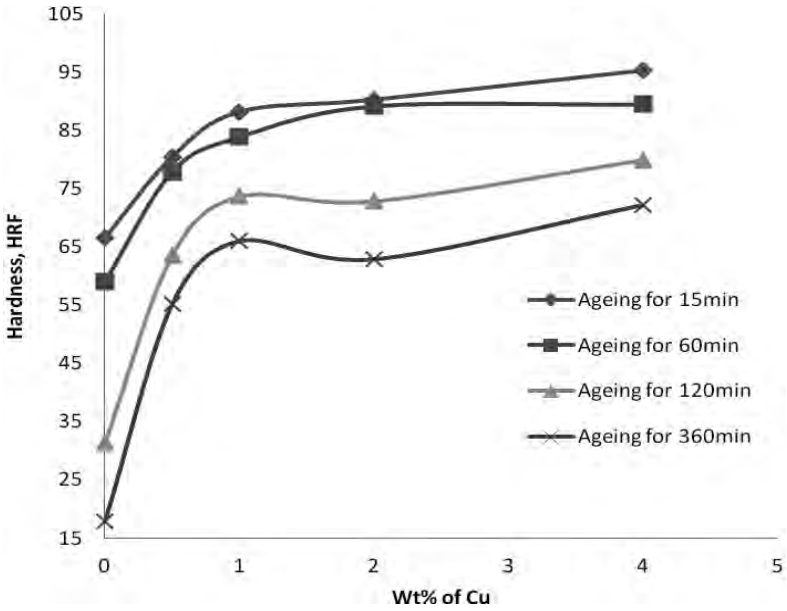

Figure 4.1.33: The change of hardness with Cu content in Al-6Si-0.5Mg alloys after aged at 300^{o}C for different times

The variation of electrical resistivity with the times in the range of 15-360 minutes at 300^{o}C was measured. It is observed that an increase in the ageing time (15-360 minutes) values lead to decrease in the electrical resistivity values for Cu free and Cu added Al-6Si-0.5Mg alloys. Comparison of electrical resistivity as a function of ageing time and Cu contents is given in Figure 4.1.34. For the times of ageing above 15 minutes the rate of changes of the electrical resistivity for the alloys was much higher than for the longer ageing times. For longer time of ageing the precipitates are larger in sizes but the total number of precipitates decreases, as a result the resistivity decreases. Form the age hardening curves at 300^{o}C for 30 minutes or higher times the ageing conditions are overaged conditions. So the resistivity decreases gradually. The Cu free alloy, Alloy-1 has lower resistivity than the Cu added alloys. Cu Added alloys, Alloys 2, 3, 4 and 5 contain 0.5, 1, 2 and 4 wt% Cu respectively and resulted higher number of precipitates which increases the resistivity.

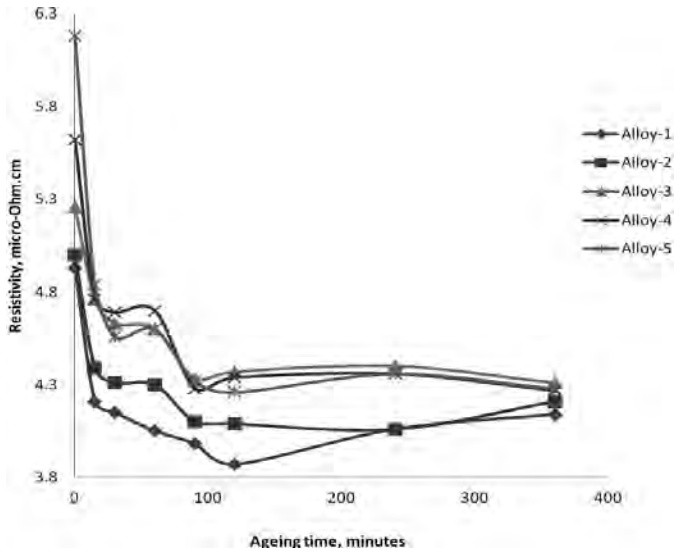

Figure 4.1.34: Evolution of resistivity during artificial ageing of Alloys 1 to 5 aged at 300^{o}C

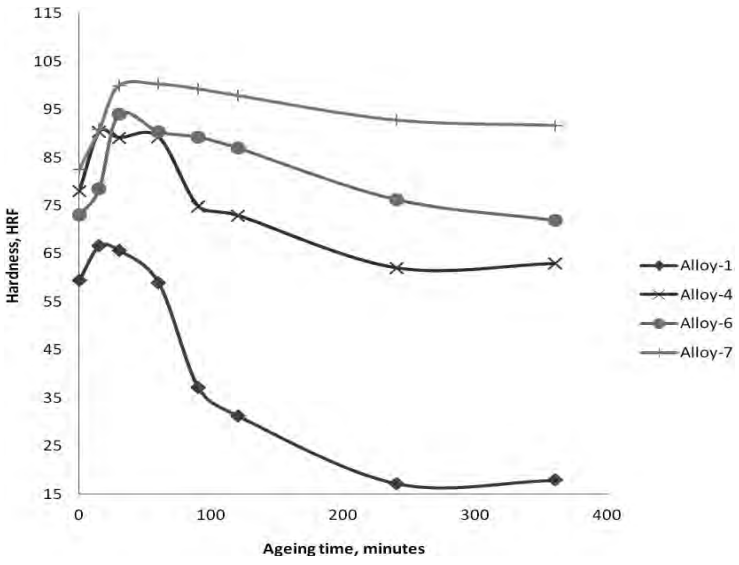

Figure 4.1.35: Evolution of hardness during artificial ageing of Alloys 1, 4, 6 and 7 aged at 300^{o}C

The ageing hardness at 300°C from as-quenched condition to 360 minutes of artificial ageing of Cu and/or Ni containing Al-6Si-0.5Mg alloys are shown in Figure 4.1.35. At first with the increase of ageing times the hardness increases up to 15 minutes for all alloys. The 2wt% Cu and Ni (Alloy-7) addition and alone 2wt% Cu (Alloy-4) seems to have a better effect than the 2 wt% Ni content alloy (Alloy-6) on the hardness for longer time of ageing. The hardness falls

with times due to the effect of long time overageing. The Alloy-7 has the higher hardness than the other alloys all over the ageing conditions but Alloy-4 has better hardness than Alloy-6.

The resistivity changes of the Alloy-1, Alloy-4, Alloy-6 and Alloy-7 with ageing times at 300^{o}C is shown in figure 4.1.36. Ageing at 300^{o}C the resistivity rapidly decreases at the very early stage of ageing. The resistivity decreases due to the overageing, overageing decreases the total number of precipitates but increases the precipitate size. Alloy-7 has better resistivity than other alloys all over the ageing conditions.Alloy-7 has strong resistance to lose resistivity with times whereas the Alloy-4 and Alloy-6 have lower resistivity. Alloy-1 has low resistivity than all other alloys all over the ageing treatments.

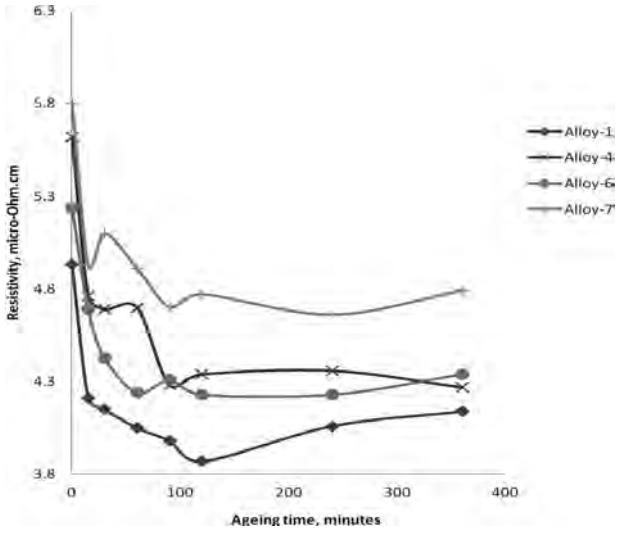

Figure 4.1.36: Evolution of resistivity during artificial ageing of Alloys 1, 4, 6 and 7 aged at 300^{o}C

4.1.3 Thermal Analysis (DTA Analysis) of the Alloys

DTA analyses are usually performed with a non-isothermal method (by heating the samples from room temperature up to 640°C), to determine the transition temperatures of the age-hardenable phases and the precipitation temperatures of the other phases. However, in this work, in order to elucidate the precipitation sequence, isothermal DTA analyses were conducted on the as-quenched samples.

In total, seven tests were performed (one for each alloy); however, the results obtained from each experiment were found to be inconclusive. The typical graphs obtained for each alloy are

given in Appendix B. The heat flows (μV) versus temperatures (^{o}C/min) graphs were acquired and the derivatives of the graphs were calculated to examine if there was any endothermic or exothermic reactions during the experiment. It was initially expected that the formation of the phases should give an exothermic peaks whereas the dissolution of the phases should cause an endothermic peak. However, no common peaks were observed within the alloys studied and the range of the heat change was not comparable.

One of the reasons for the inconclusive results could be the small mass (~15mg) of the samples. The amount of the phases that forms and dissolves in such a small volume could be insufficient for the heat detection or the phases could have been distributed non-homogeneously within the samples. Moreover, the amount of heat generated or absorbed during the isothermal test could be small and out of the sensitivity range of the calorimeter.

4.2 Microstructural Analysis of the Alloys

4.2.1 Effect of Alloying and Thermal Treatment on the Microstructures of Alloy-1

The results of the microstructural investigation are based on the four stages of the heat treatment cycle (as-cast, as-solutionized, peakaged and overaged). The "as-cast" condition means solidification of the liquid metal into a metal mould and air-quenched and the "as-solutionized" stage in this work, refers to solutionized and then water-quenched. Peakaged means the solutionized alloys are thermal treated (T6) at 225^{o}C for 1 hour and overaged refers to the solutionized alloys thermal treated (T7) at 300^{o}C for 1 hour.

4.2.1.1 Effect of Alloying on the As-Cast Microstructures of Alloy-1

The typical optical and SEM microstructures of the as-cast Alloy-1 are shown in Figure 4.2.1 and Figure 4.2.2 respectively. The microstructures of the alloy exhibit primary aluminum dendrites which are surrounded by a mixture of eutectic aluminum phase, eutectic silicon particles and other eutectic phases. It can be seen that as-cast microstructures also have casting defects such as porosity and inclusions which appear as dark spots in the optical microstructures. However, these features were not quantified in this study.

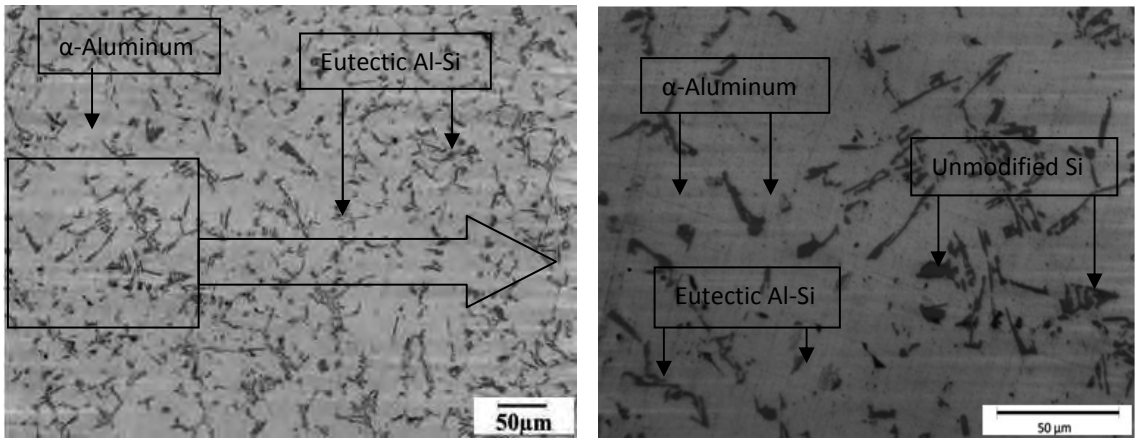

Figure 4.2.1: Optical micrographs of as-cast Alloy-1

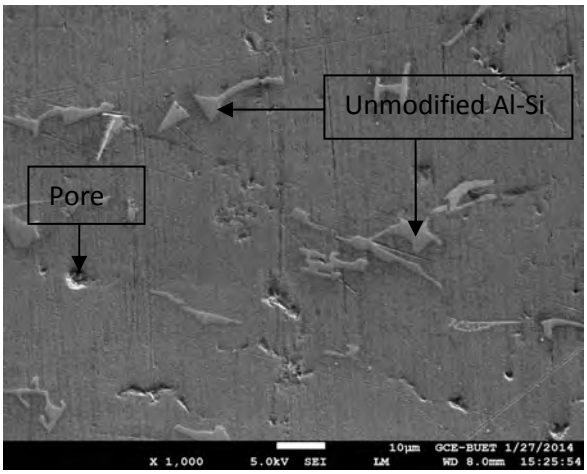

Figure 4.2.2: SEM micrograph of as-cast Alloy-1 showing unmodified Al-Si eutectic, porosity and α-aluminum matrix

4.2.1.2 Effect of Alloying and Solutionizing on the Microstructures of Alloy-1

Solution-treatment followed by quenching causes significant changes in the as-cast microstructure of Alloy-1. Figure 4.2.3 and Figure 4.2.4 show Optical Light and SEM microstructures of the as-solutionized Alloy-1. The heat treatment altered the morphology of the eutectic Si where the Si particles became more globular compared to as cast structure. Furthermore, the β-Mg_2Si and other intermetallic phases are dissolved during the solutionizing step. Therefore, the as-quenched microstructure consists of the eutectic Si and β phases with a matrix of super saturated solid solution of aluminum.

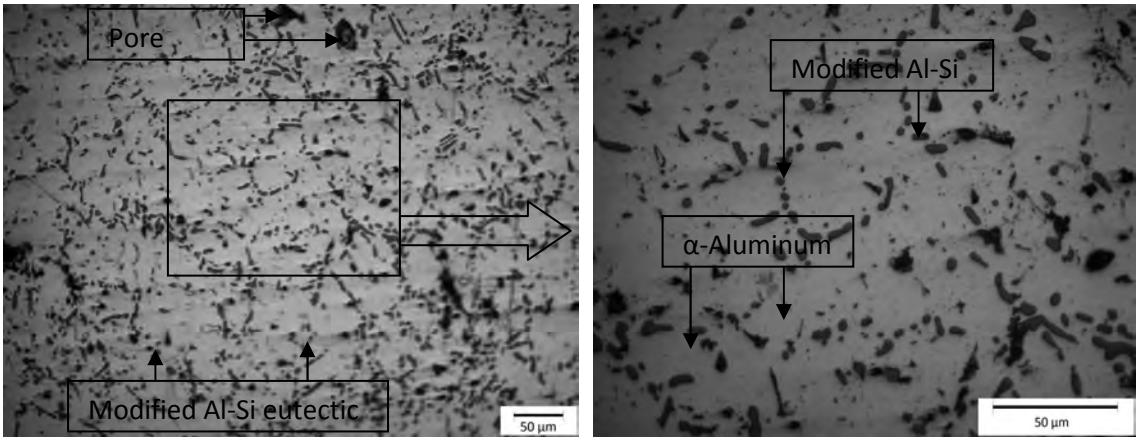

Figure 4.2.3: Optical micrographs of Alloy-1 after solution treatment at 540°C for 2 hours showing modified Al-Si eutectic and α-aluminum matrix

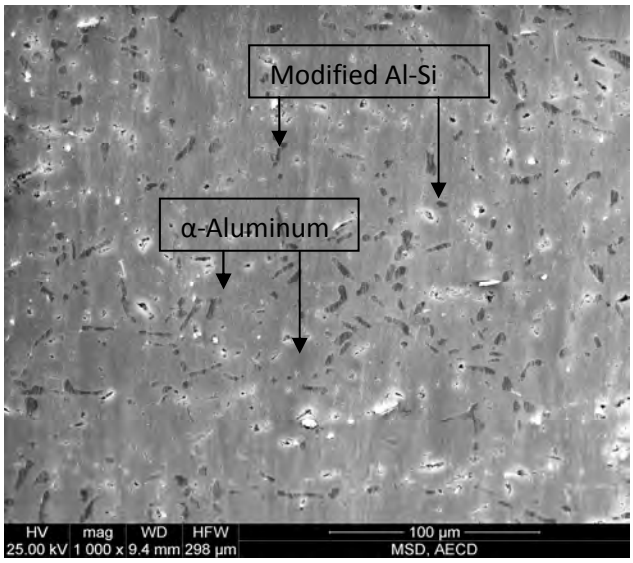

Figure 4.2.4: SEM micrograph of Alloy-1 after solution treatment at 540°C for 2 hours showing modified Al-Si eutectic and α-aluminum matrix

The EDS analyses revealed that the fine precipitates are α-(Al-Mg-Si) phase. The EDS spectra of the Al matrix, intermetallics and the precipitate inside the dendrite are shown in Figure 4.2.5. The signals from the precipitate were not very strong due to the small size of the precipitate and the large interaction volume created in the sample. It is believed that more signals from the Al matrix were acquired. However, the EDS analysis gives useful information about the qualitative identification of these precipitates. Figure 4.2.5 shows the EDS results of full frame scanning and Figure 4.2.6 shows the rod like (spot1) eutectic Al-Si phase where spot3 (Figure 4.2.7) indicates modified globular type Si phase.

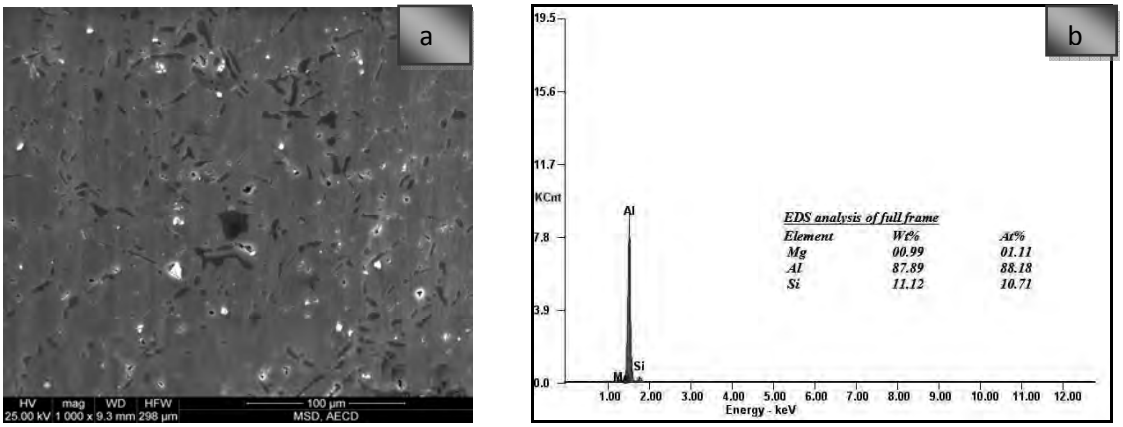

Figure 4.2.5: a) SEM micrograph of Alloy-1 after solution treatment at 540°C for 2 hours showing modified Al-Si eutectic and α-aluminum matrix; b) The corresponding EDS spectra of the full frame

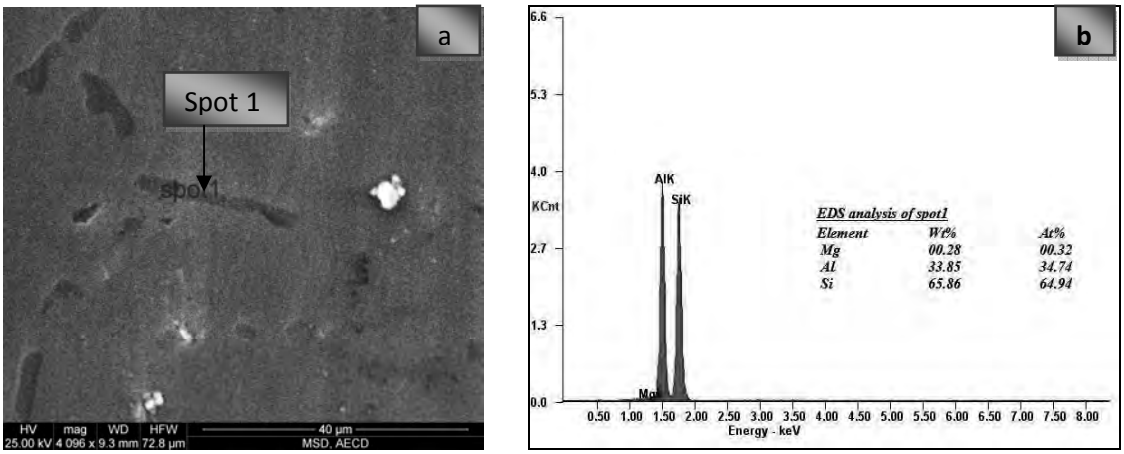

Figure 4.2.6: a) SEM micrograph of Alloy-1 after solution treatment at 540°C for 2 hrs; b) The corresponding EDS spectra of spot1

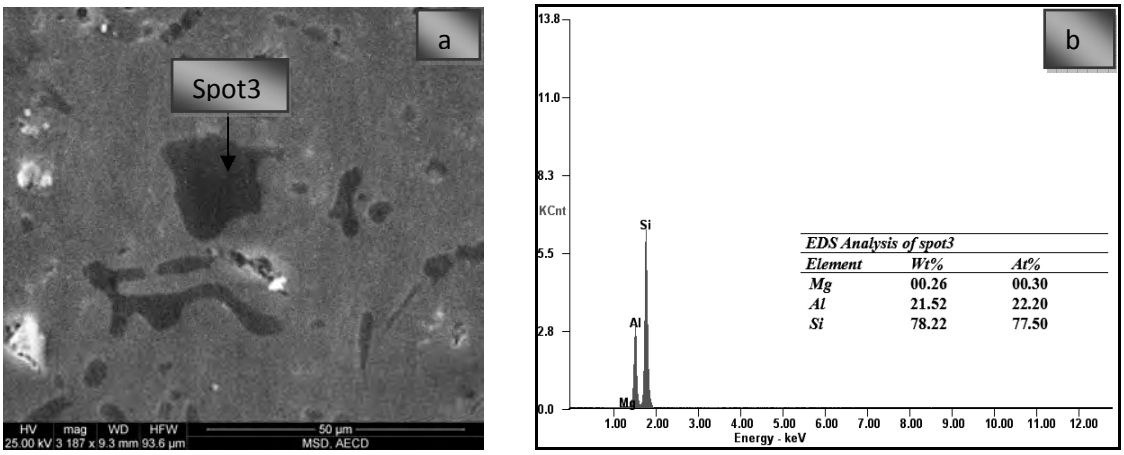

Figure 4.2.7: a) SEM micrograph of Alloy-1 after solution treatment at 540°C for 2 hours; b) The corresponding EDS spectra of spot3

4.2.1.3 Effect of Alloying and Peak Ageing on the Microstructures of Alloy-1

Figure 4.2.8 shows the peakaged optical microstructure of Alloy-1.The ageing at 225^{o}C for 1 hour (peakaged) represents the defragmentation of Al-Si eutectic phases. The Si phases are more rounded than the as-solutionized condition. The Al-Si eutectic networks are more modified and precipitates are more visible.

Figure 4.2.9 shows the chemical components of full frame after ageing at 225^{o}C for 1 hour and sopt2 (Figure 4.2.11) EDS analysis refers to the matrix composition of the Alloy-1. Spot1 is the lamellar type eutectic Si (Figure 4.2.10) and spot3 (Figure 4.2.12) EDS result shows the thermally modified globular type eutectic Si phase.

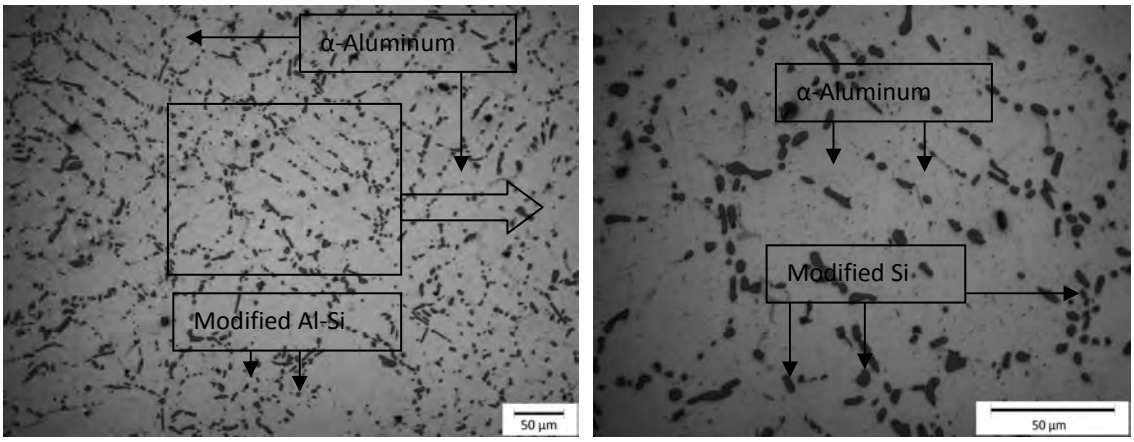

Figure 4.2.8: Optical micrographs of Alloy-1 after peakaged at 225°C for 1 hour showing modified Al-Si eutectic and α-aluminum matrix

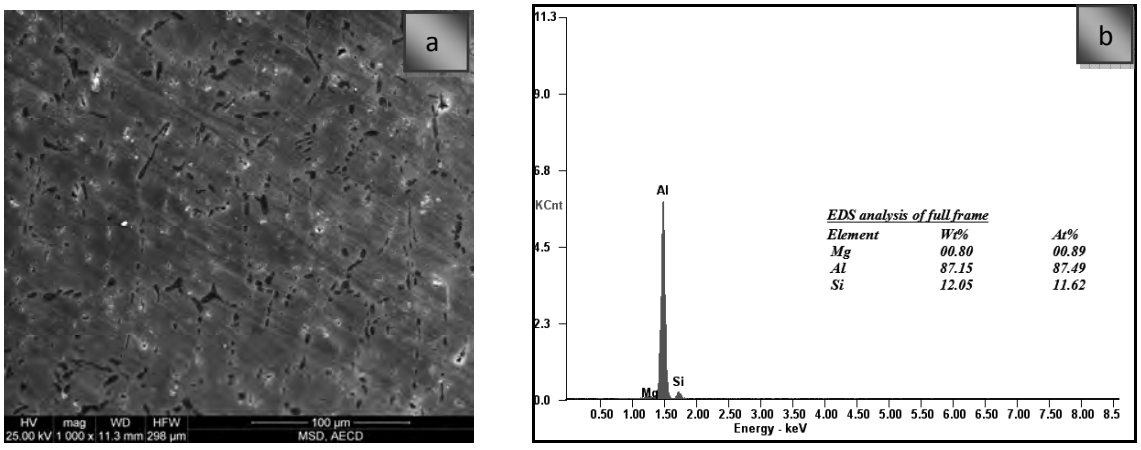

Figure 4.2.9: a) SEM micrograph of Alloy-1 after peakaged at 225°C for 1 hour showing modified Al-Si eutectic and α-aluminum matrix; b) The corresponding EDS spectra of full frame

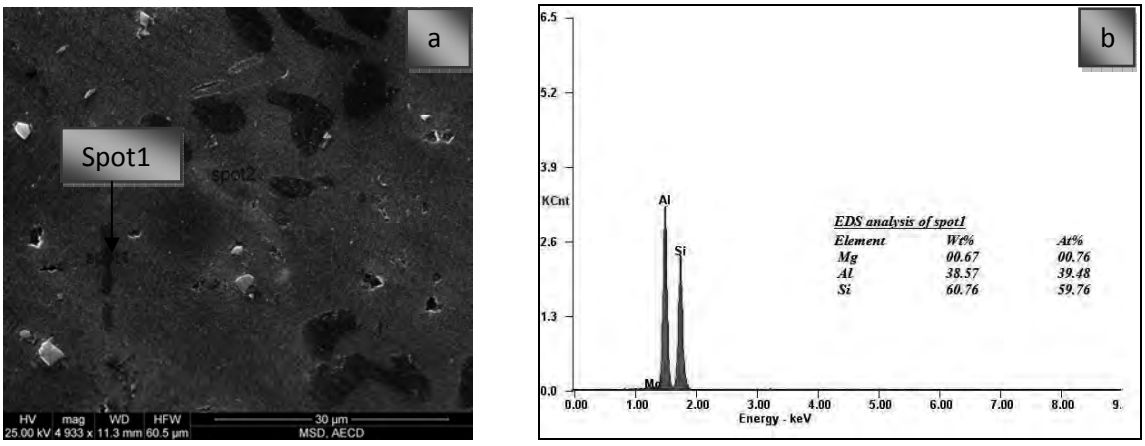

Figure 4.2.10: a) SEM micrograph of Alloy-1 after peakaged at 225°C for 1 hour; b) The corresponding EDS spectra of spot1

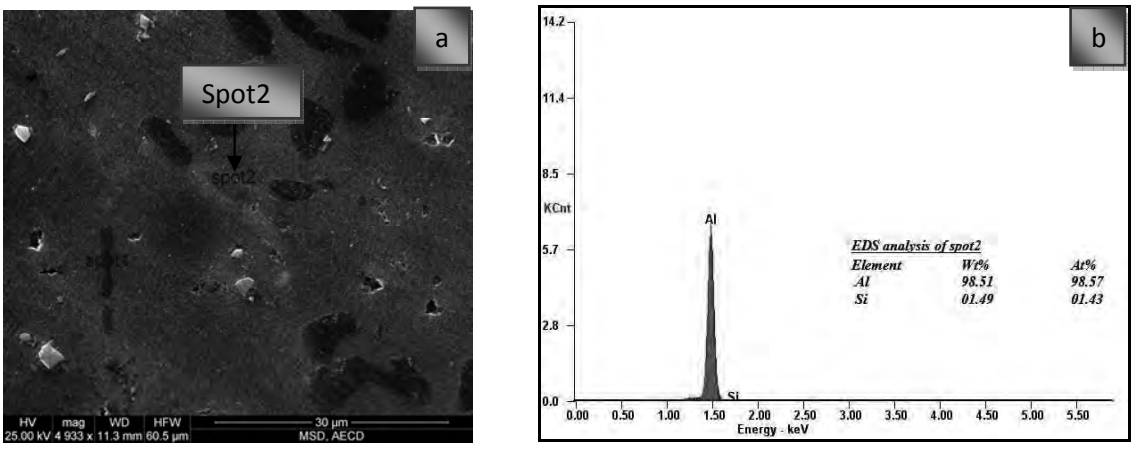

Figure 4.2.11: a) SEM micrograph of Alloy-1 after peakaged at 225°C for 1 hour; b) The corresponding EDS spectra of spot2

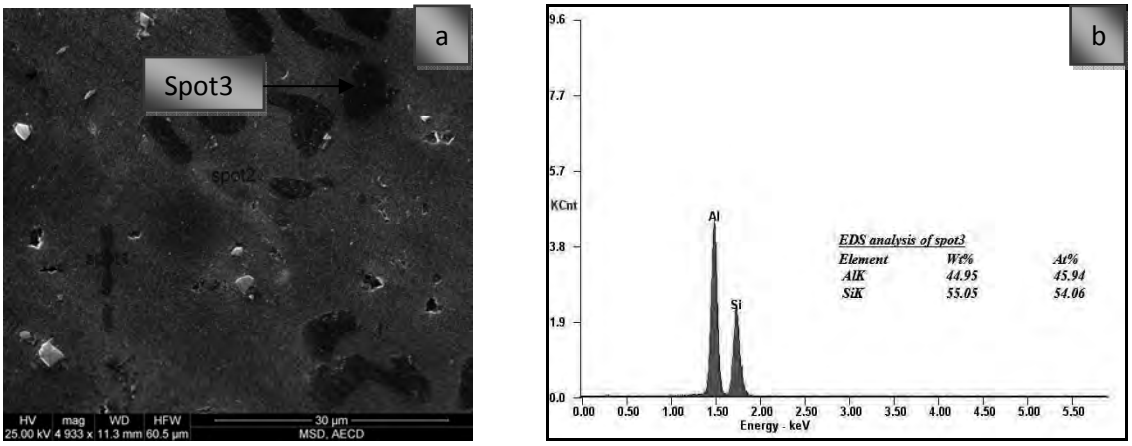

Figure 4.2.12: a) SEM micrograph of Alloy-1 after peakaged at 225°C for 1 hour; b) The corresponding EDS spectra of spot3

4.2.1.4 Effect of Alloying and Over Ageing on the Microstructures of Alloy-1

After solutionizing and quenching, an over-aging for 1 hour at 300°C causes further microstructural evolution. Figures 4.2.13 shows the typical optical microstructures of the overaged alloy. It can be seen that the Al-Si eutectic and alumina matrix with precipitates phase is common at overaged condition. Moreover, the eutectic Si is very globular when compared the as-cast condition.

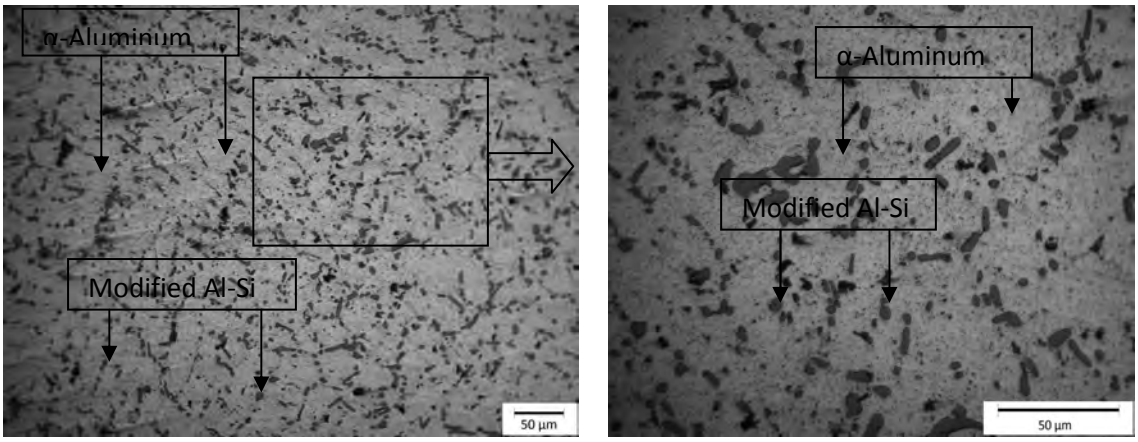

Figure 4.2.13: Optical micrograph of Alloy-1 after overaged at 300°C for 1 hour showing modified Al-Si eutectic and α-aluminum matrix

Figure 4.2.14 shows the overaged SEM microstructures of the Alloy-1. The needle like eutectic Si phases is observed in the Alloy-1. No other coarse eutectic phases that were previously dissolved during solutionizing can be seen. The coarser α-(Al-Mg-Si) precipitates are also seen near the eutectic Si in the alloy. Again, no Mg-containing coarse phases are observed in inter-dendritic region. The EDS analysis of spot1 (Figure 4.2.15) and spot3 (Figure 4.2.17) represents the thermal modified Al-Si eutectic where as spot2 (Figure 4.2.16) EDS results is mainly the α-aluminum matrix. Furthermore, the equilibrium β-Mg_2Si precipitates as well as the Si clusters are also likely to be present in the overaged state of the Alloy-1; however, there is no sufficient evidence to support this statement. It can be concluded that the phase identification of the fine precipitates (less than 500nm) is very challenging due to the resolution of the SEM.

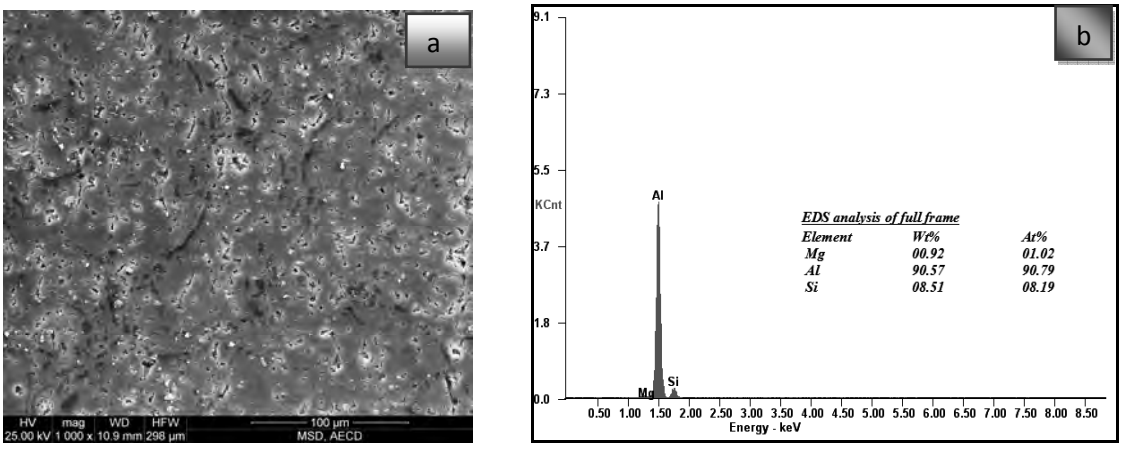

Figure 4.2.14: a) SEM micrograph of Alloy-1 after overaged at 300°C for 1 hour showing modified Al-Si eutectic and α-aluminum matrix; b) The corresponding EDS spectra of full frame

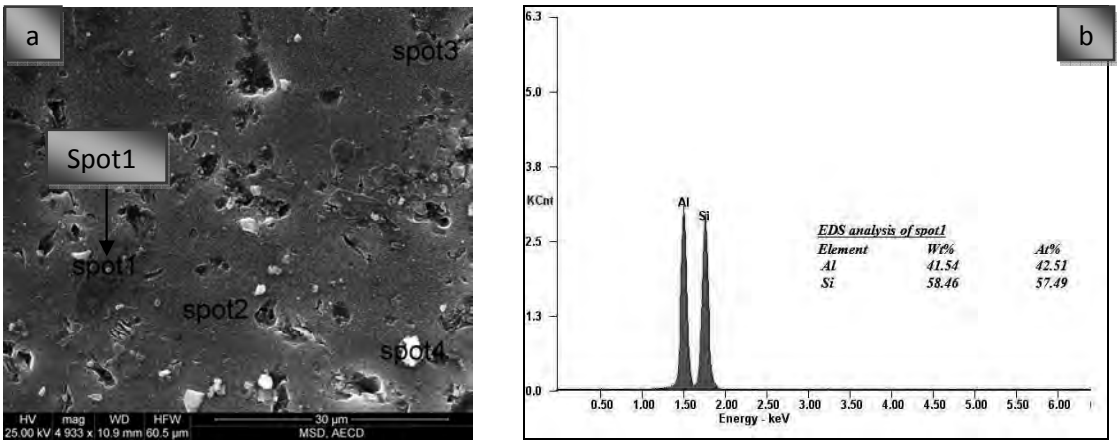

Figure 4.2.15: a) SEM micrograph of Alloy-1 after overaged at 300°C for 1 hour; b) The corresponding EDS spectra of spot1

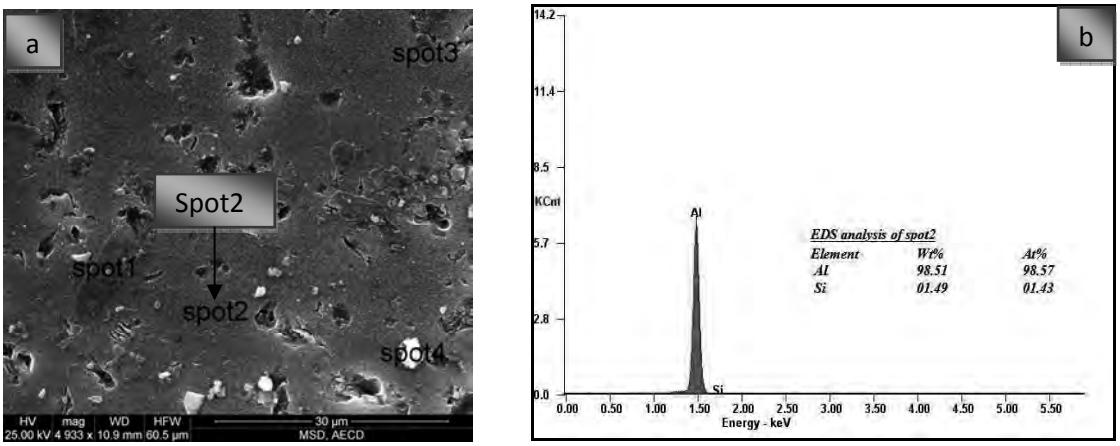

Figure 4.2.16: a) SEM micrograph of Alloy-1 after overaged at 300°C for 1 hour; b) The corresponding EDS spectra of spot2

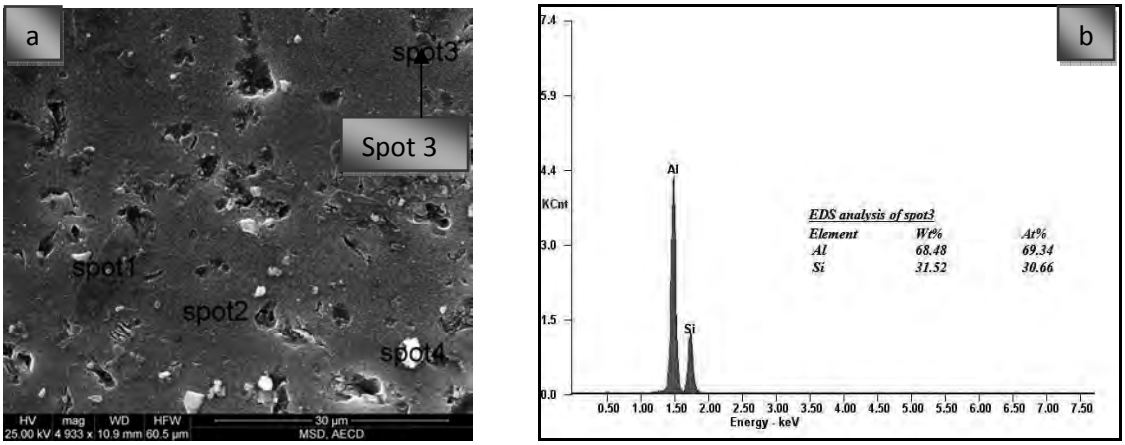

Figure 4.2.17: a) SEM micrograph of Alloy-1 after overaged at 300°C for 1 hour; b) The corresponding EDS spectra of Spot3

4.2.2 Effect of Alloying and Thermal Treatment on the Microstructures of Alloy-2

4.2.2.1 Effect of Alloying on the As-Cast Microstructures of Alloy-2

Figure 4.2.18 shows the typical microstructures of the as-cast Alloy-2 (0.5% Cu). It can be seen that 0.5% Cu addition to Al-6Si-0.5Mg forms a new phase, θ-$CuAl_2$. The Cu-containing phases are presented in Figure 4.2.18. The θ phase usually coexists with other eutectic phases but it forms independently in inter dendritic region as well [162]. It has more rounded blocky type morphology and sometimes appears as many pockets connected to each other.

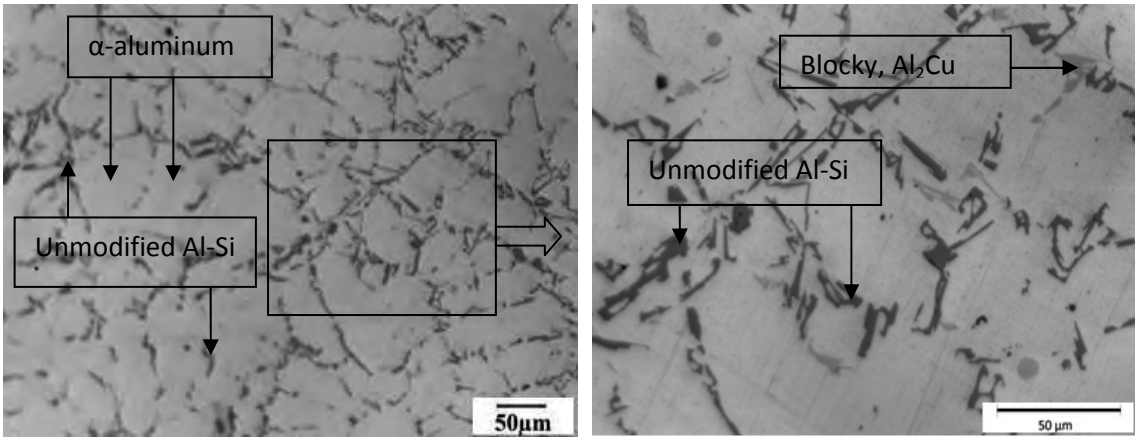

Figure 4.2.18: Optical micrographs of the as- cast Alloy-2

4.2.2.2 Effect of Alloying and Solutionizing on the Microstructures of Alloy-2

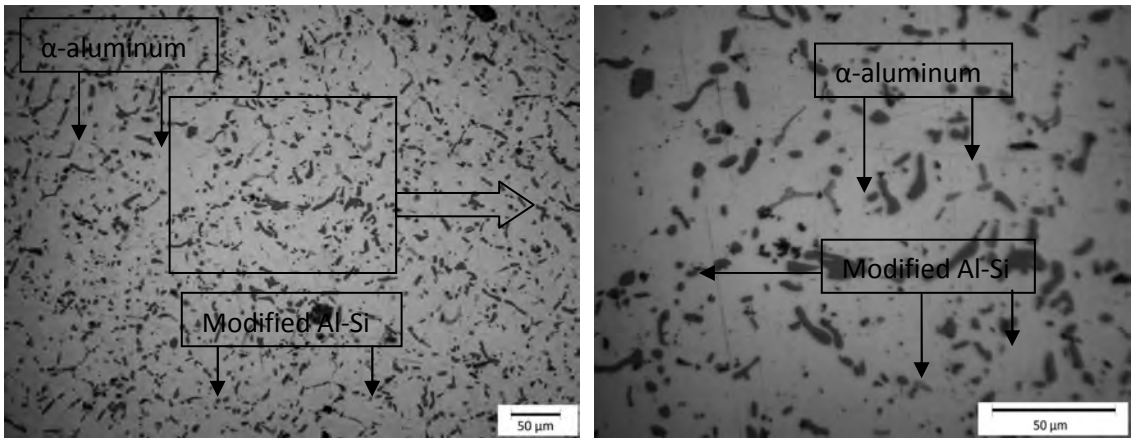

Figure 4.2.19: Optical micrographs of Alloy-2 after solution treatment at 540°C for 2 hours showing modified Al-Si eutectic and α-aluminum matrix

The as-solutionized microstructure of Alloy-2 is very similar to that of Alloy-1, as shown in Figure 4.2.19 and Figure 4.2.20. This is basically due to the dissolution of the Cu and Mg-containing phases (θ, Q and π) during the solutionizing treatment. The spherodize and globular eutectic Si are the second phases observed in the microstructure. After solutionizing, all of the Cu is expected to enter into the solid solution of Al (Al-matrix). Therefore, it can be concluded that Cu does not form a new Fe-rich intermetallic after the solutionizing treatment. Garat et al. [157] also observed that 0.5% Cu addition complicated the phase identification of the new phases.

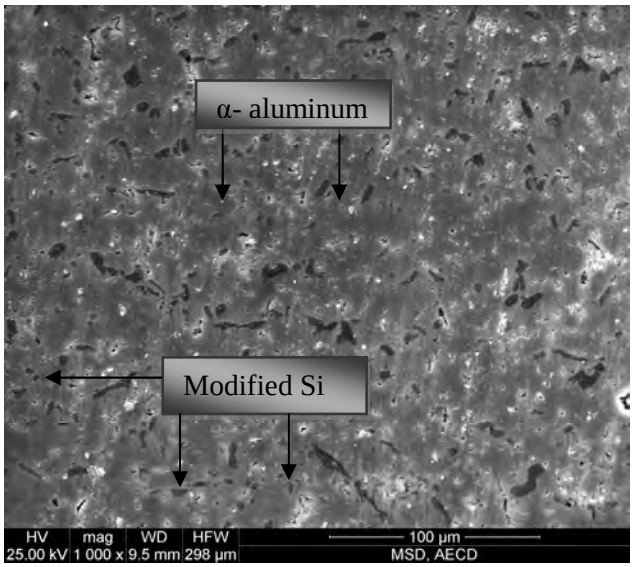

Figure 4.2.20: SEM micrograph of the Alloy-2 after solution treatment at 540°C for 2 hours showing the modified Al-Si eutectic and α-aluminum matrix

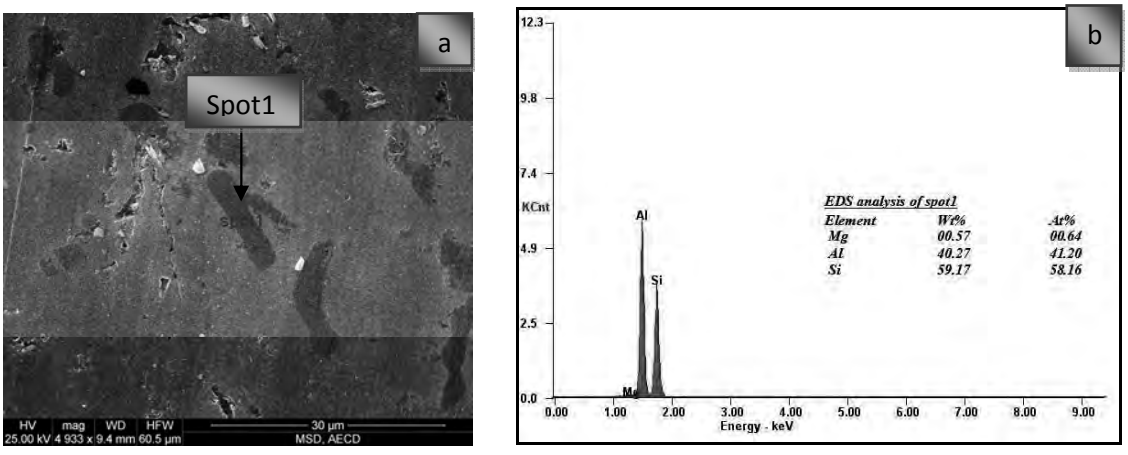

Figure 4.2.21: a) SEM micrograph of Alloy-2 after solution treatment at 540°C for 2 hours; b) The corresponding EDS spectra of spot1

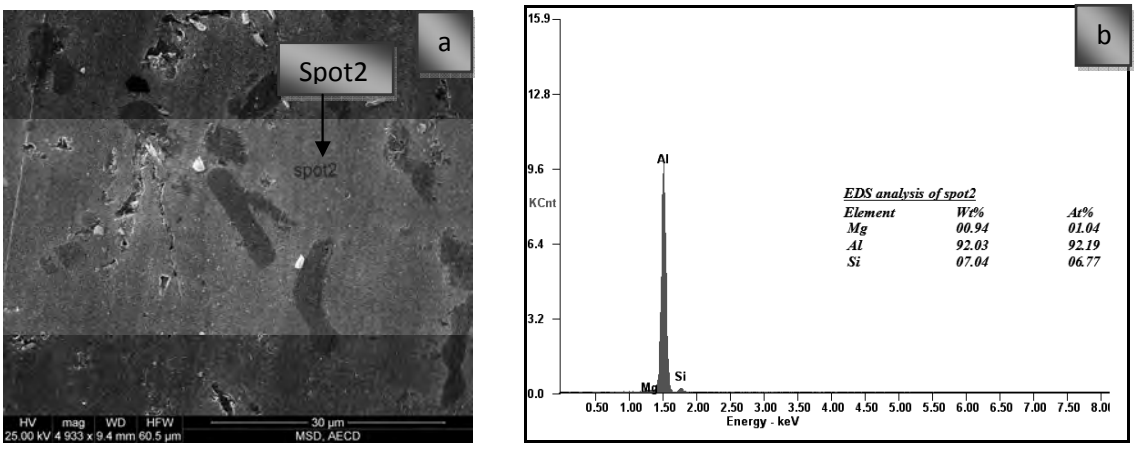

Figure 4.2.22: a) SEM micrograph of Alloy-2 after solution treatment at 540°C for 2 hours; b) The corresponding EDS spectra of spot2

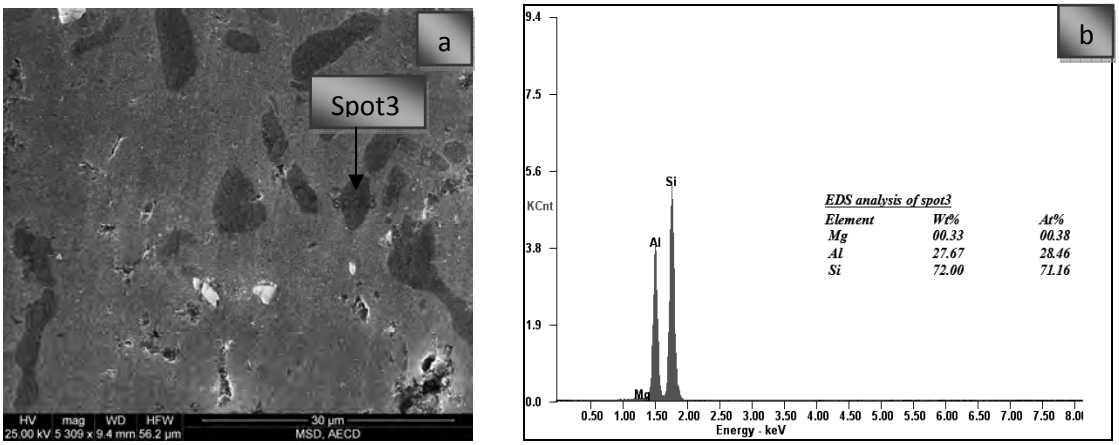

Figure 4.2.23: a) SEM micrograph of Alloy-2 after solution treatment at 540°C for 2 hours; b) The corresponding EDS spectra of spot3

The EDS analysis of spot1 (Figure 4.2.21) and spot3 (Figure 4.2.23) on the fibrous like intermetallic shows the Al-Si eutectic of as solutionized alloys. The chemical components of spot2 (Figure 4.2.22) indicate the α-aluminum matrix composition.

4.2.2.3 Effect of Alloying and Peak Ageing on the Microstructures of Alloy-2

After ageing at 225^{o}C for 1 hour, the microstructural changes show that the spherodize Si particles are more fragmented (Figure 4.2.24). The intermetallic particles are more homogenous.

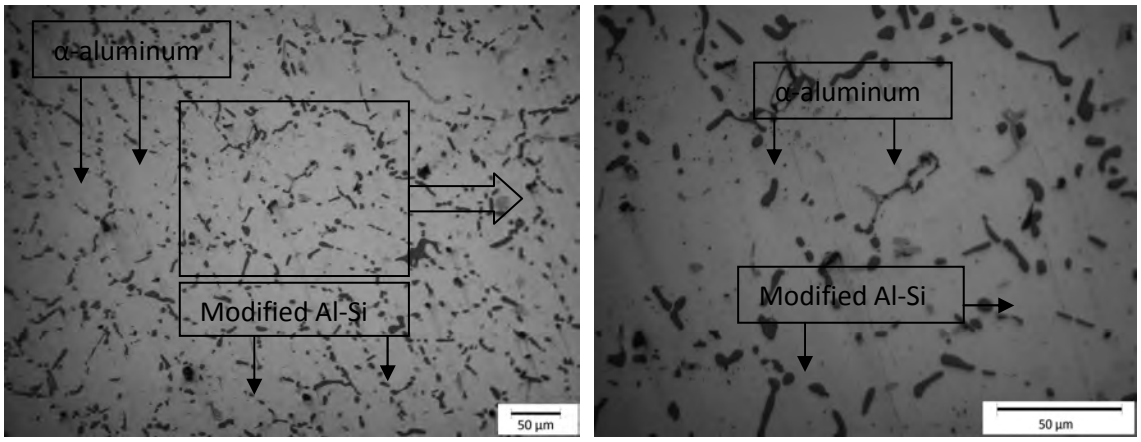

Figure 4.2.24: Optical micrographs of Alloy-2 after peakaged at 225°C for 1 hour showing modified Al-Si eutectic and α-aluminum matrix

4.2.2.4 Effect of Alloying and Over Ageing on the Microstructures of Alloy-2

After solutionizing and quenching, an over-aging for 1 hour at 300°C causes further microstructural evolution. Figure 4.2.25 shows the typical optical microstructures of the over aged Alloy-2. It can be seen that the spherodize Si phase is common in the Alloy-2. Moreover, in all alloys the eutectic Si is very globular. The coarse eutectic Si phases can be seen in the peakaged alloy.

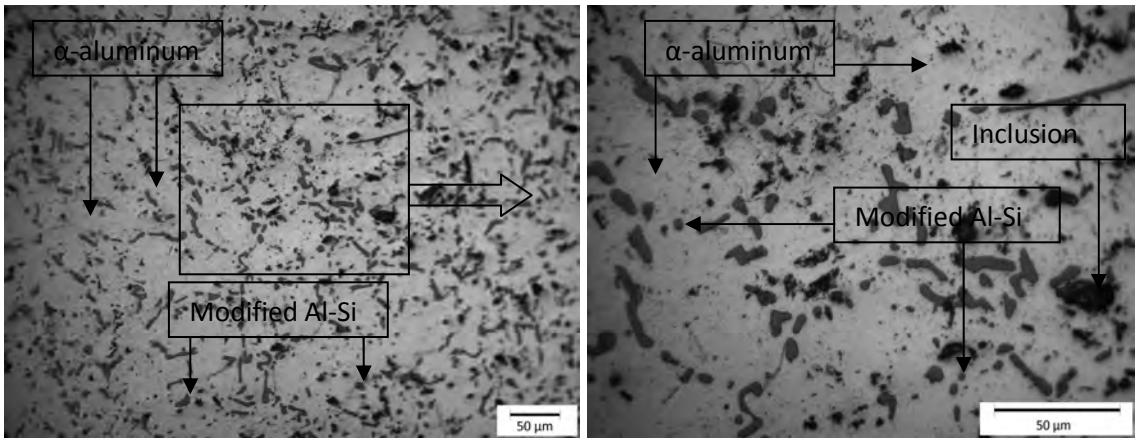

Figure 4.2.25: Optical micrograph of Alloy-2 after overaged at 300°C for 1 hour showing modified Al-Si eutectic and α-aluminum matrix

4.2.3 Effect of Alloying and Thermal Treatment on the Microstructures of Alloy-3

4.2.3.1 Effect of Alloying on the As-Cast Microstructures of Alloy-3

Figure 4.2.26 represents the optical micrograph of as-cast microstructure of Alloy -3. α (Al) solid solution is the predominant phase (light grey) in the as-cast microstructure of these alloys. α-phase forms dendritic network, usually cores, and also participates in several multiphase eutectic reactions. The silicon-phase which is soluble into aluminium and the other alloying elements form a binary eutectic with α (Al). In the as-cast alloys, the morphology and orientation of dendritic α (Al) are non-uniform. There are some primary silicon particles, whereas the eutectic silicon is present as coarse plates. The microstructure of as-cast alloy consists of large grains, including the dendrites of the aluminium matrix; inter dendritic networks of eutectic silicon plates and other large intermetallic compound particles present between the aluminium dendrite arms.

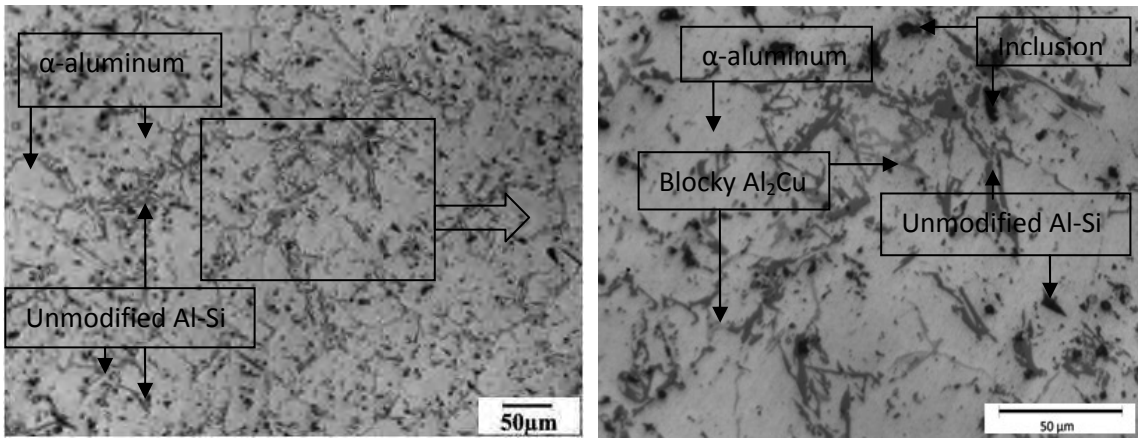

Figure 4.2.26: Optical micrographs of as-cast Alloy-3

4.2.3.2 Effect of Alloying and Solutionizing on the Microstructures of Alloy-3

As seen from Figure 4.2.27, many intermetallic phases dissolve and the eutectic silicon particles tend to spheroidize after the solution treatment. The mechanical properties of Al-Si alloys not only depend on the chemical composition, but also on the microstructural features such as morphologies of dendritic α(Al), spheroidization of eutectic silicon and other intermetallics within the microstructure. The improvement in mechanical properties is generally attributed to the variation of the morphology and size of the eutectic silicon phase particles. The

microstructural investigations show that the shape of the eutectic Si particles changes to granular type in all alloy after heat treatment.

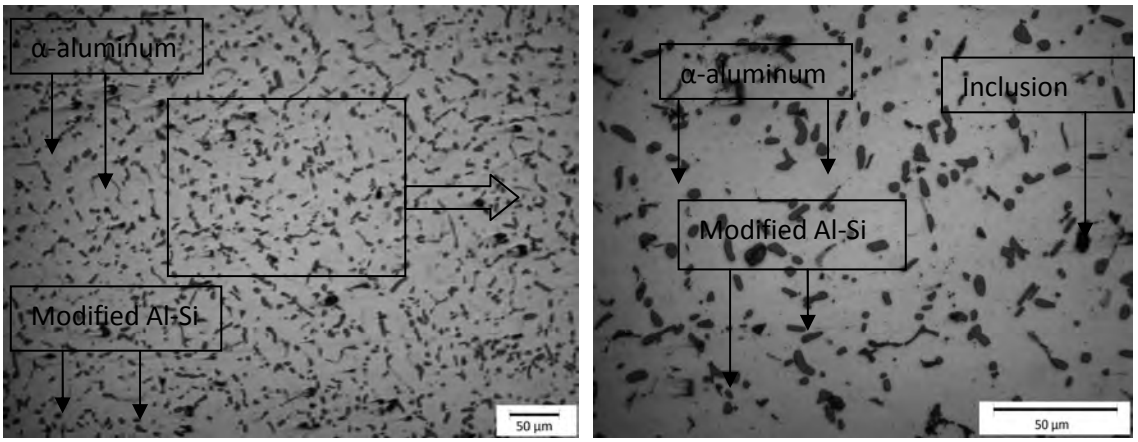

Figure 4.2.27: Optical micrographs of Alloy-3 after solution treatment at 540°C for 2 hours showing modified Al-Si eutectic and α-aluminum matrix

4.2.3.3 Effect of Alloying and Peak Ageing on the Microstructures of Alloy-3

Microstructural examination reveals that in the absence of Cu, Alloy-1 shows a coarse columnar α-Al dendritic structure and unmodified needle/plate like eutectic Si (Figure 4.2.1). However, with addition of 1% Cu results in fine and well distributed eutectic Si phase and conversion of coarse columnar α-Al dendritic structure to coarse equiaxed structure (Figure 4.2.28). This is due to the partial refinement of α-Al dendrites with increasing Cu addition [8].

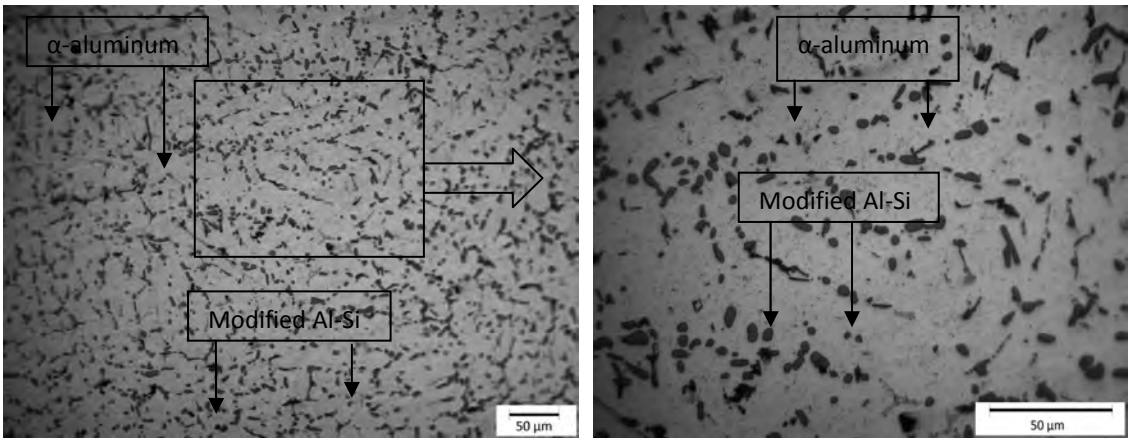

Figure 4.2.28: Optical micrographs of Alloy-3 after peakaged at 225°C for 1 hour showing modified Al-Si eutectic and α-aluminum matrix

During peak ageing the Al_2Cu precipitates forms which are fully coherent with the α-aluminum matrix. 0.5%Mg addition results in conversion of unmodified acicular Si to lamellar, a partially rounded and even fibrous structure. This could be due to the depression of eutectic temperature [160-162] accompanied by increased undercooling. Both the morphology of the silicon phase and the depression of the eutectic temperature, as well as the increased undercooling suggest that high levels of Mg act to slightly modify the silicon phase of Al-6Si-0.5Mg alloy. These changes suggest the formation of Mg_2Si which is semi coherent with the α-aluminium matrix.

4.2.3.4 Effect of Alloying and Over Ageing on the Microstructures of Alloy-3

Figure 4.2.29 shows the comparatively coarse eutectic Si phase and fine precipitates inside the dendrites of each alloy. There are some fine precipitates in the Alloy-3.The precipitates could be the equilibrium β-Mg_2Si and Al_2Cu phase. Moreover, due to high over-ageing temperature, Si clusters might have also precipitated. The amount of precipitates inside the dendrites is higher than the Cu free Alloy-1.

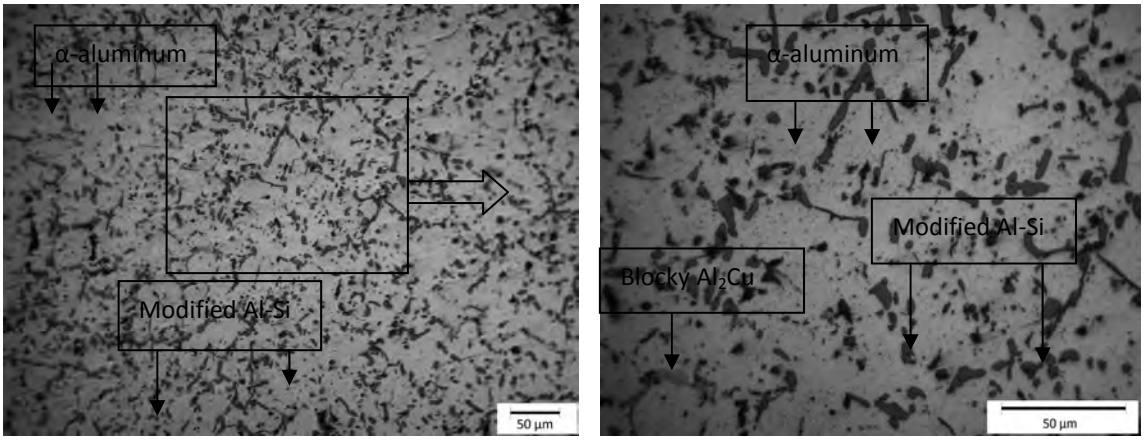

Figure 4.2.29: Optical micrograph of Alloy-3 after overaged at 300°C for 1 hour showing modified Al-Si eutectic and α-aluminum matrix

4.2.4 Effect of Alloying and Thermal Treatment on the Microstructures of Alloy-4

4.2.4.1 Effect of Alloying on the As-Cast Microstructures of Alloy-4

The microstructure of as-cast Alloy-4 consists of large grains, including the dendrites of the aluminium matrix, inter-dendritic networks of eutectic silicon plates and other large intermetallic compound particles present between the aluminium dendrite arms, as shown in Figure 4.2.30 and Figure 4.2.31.Cu is soluble to a low concentration in α-Al (5.65% in the

binary alloy) and is a major constituent in the intermetallic phase $CuAl_2$ (θ-phase). After the excess precipitation of $CuAl_2$ at α-grain boundaries in Al-6Si-0.5Mg-4Cu alloy, the microstructure becomes brittle and fails inter-granularly [57, 73].

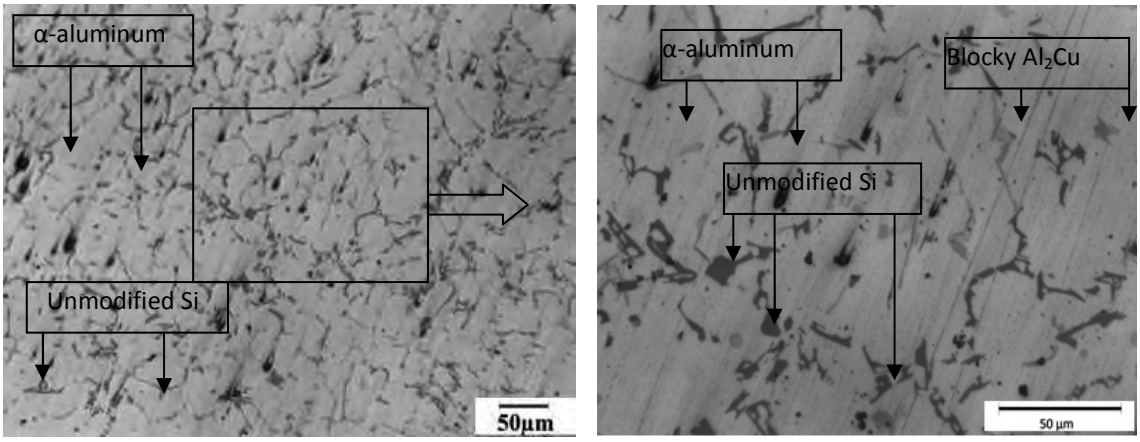

Figure 4.2.30: Typical microstructures of the as-cast Alloy-4

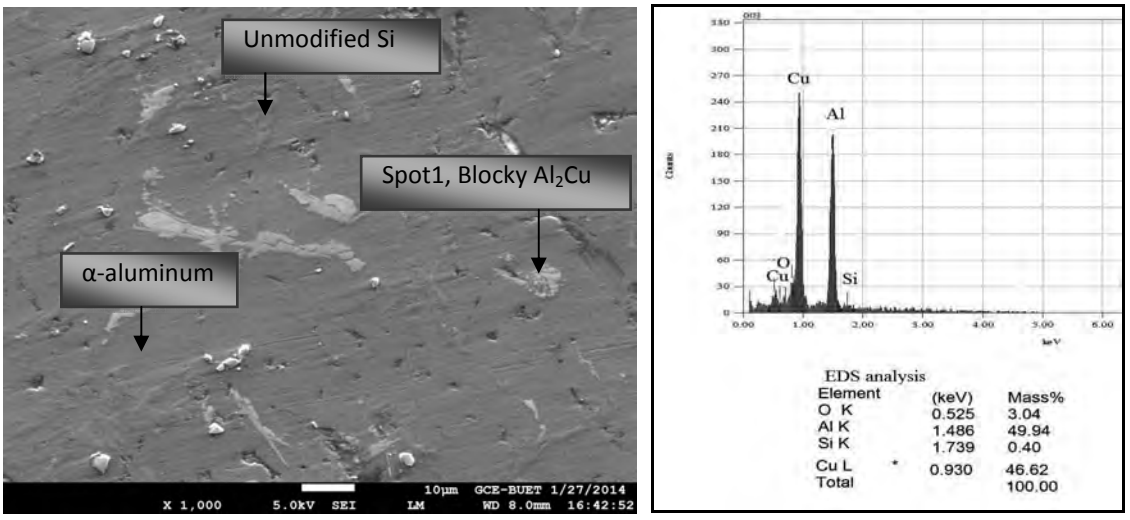

Figure 4.2.31: a) SEM micrograph of as-cast Alloy-4 showing unmodified Al-Si eutectic, blocky Al_2Cu, and α-aluminum matrix; b) The corresponding EDS spectra of spot1

4.2.4.2 Effect of Alloying and Solutionizing on the Microstructures of Alloy-4

As seen from Figure 4.2.32, many intermetallic phases dissolve and the eutectic silicon particles tend to spheroidize after the heat treatment. The mechanical properties of Al-Si alloys not only depend on the chemical composition, but also on the microstructural features such as

morphologies of dendritic α(Al), spheroidization of eutectic silicon and other intermetallics within the microstructure. The improvement in mechanical properties is generally attributed to the variation of the morphology and size of the eutectic silicon phase particles [8]. The microstructural investigations show that the shape of the eutectic Si particles changes to granular type in all alloys after heat treatment. It is observed a very remarkable spheroidization of eutectic Si particle in comparison to plate shaped in as-cast specimen. The particle distribution including eutectic silicon and intermetallic compounds is more homogenous after heat treatment.

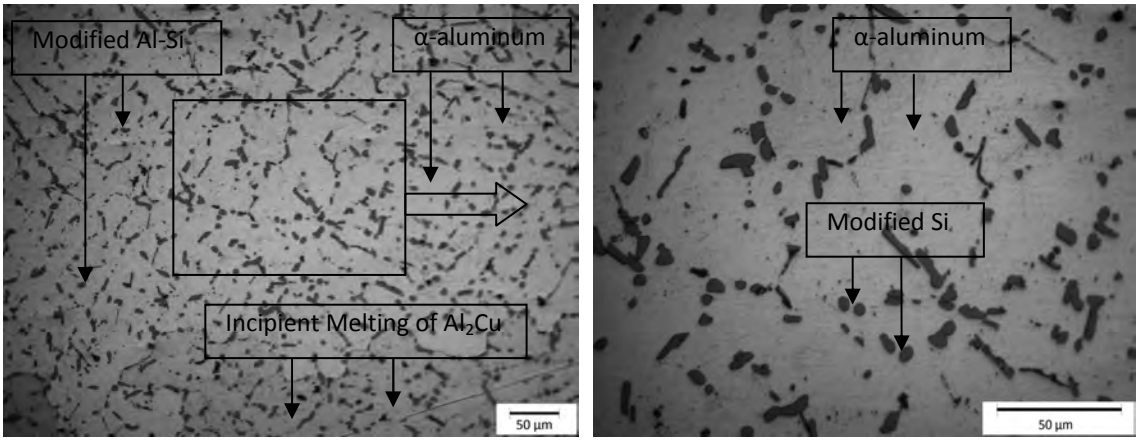

Figure 4.2.32: Optical micrographs of Alloy-4 after solution treatment at 540°C for 2 hours showing the modified Al-Si eutectic and α-aluminum matrix

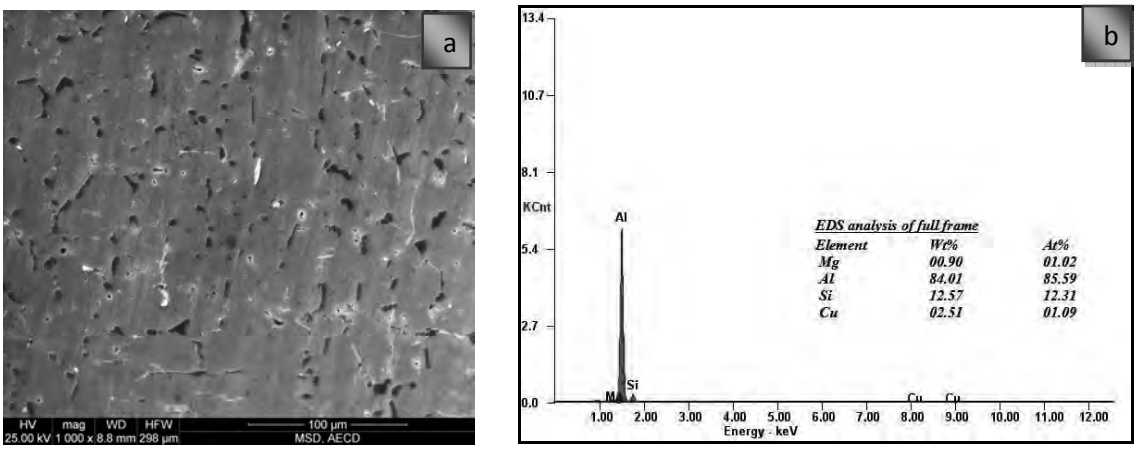

Figure 4.2.33: a) SEM micrograph of Alloy-4 after solution treatment at 540°C for 2 hours showing the modified Al-Si eutectic and α-aluminum matrix; b) The corresponding EDS spectra of full frame

After the solution treatment, most of the intermetallic phases dissolve. As known in Al-Cu alloys, rapid cooling after a solution treatment makes GP zones form disc shape and consist of

about 90% Cu. These zones with a uniform distribution in the α(Al) matrix form preferentially with copper atoms in the aluminium lattice. A general characteristic of these zones is to have a coherent interface within the matrix, which results in local strain and provides higher hardness. As Cu content increases, the formation of GP zone is promoted due to rapidly cooling with homogenous nucleation [254]. Figure 4.2.33 represents the SEM micrographs of heat-treated microstructure of Alloy-4 and full frame EDX analysis results. Some network structures are observed. The bright particles ($CuAl_2$ phases) appear at the boundaries of eutectic cells.

Figures 4.2.34 to 4.2.37 show the SEM micrograph and spot analyses EDX spectrum of Allloy-4. This is basically due to the dissolution of the Cu and Mg containing phases (θ, Q and π) during the solutionizing treatment. The rod like and globular eutectic Si are the second phases observed in the microstructure. During some of the spot analyses of the β phase, Cu is also found in the EDS spectra, however, when an elemental mapping is performed; Cu is only seen in the matrix and not inside the β intermetallic. It is likely that the β phase does not have Cu and the Cu signals are coming from the Al matrix. After solutionizing, all of the Cu is expected to enter into the solid solution of Al. Therefore, it can be concluded that Cu does not form a new Fe- rich intermetallic after the solutionizing treatment.

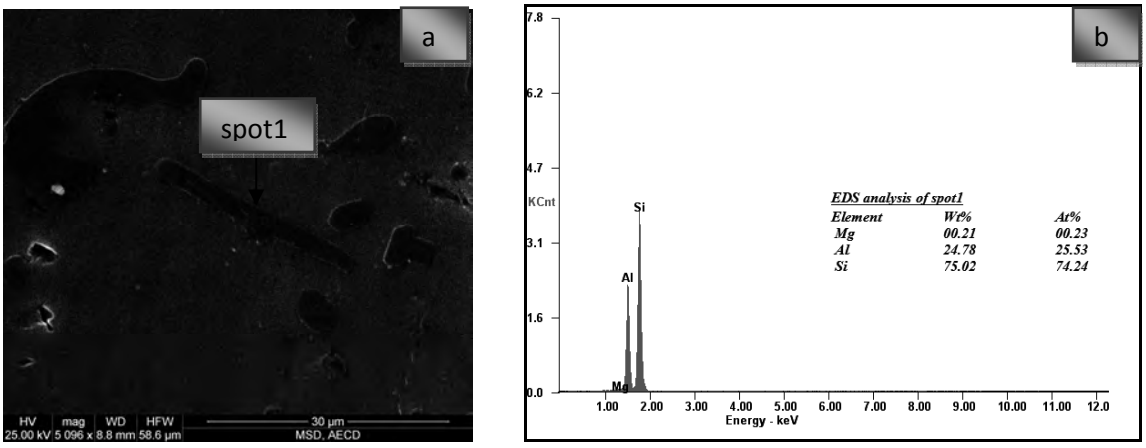

Figure 4.2.34: a) SEM micrograph of Alloy-4 after solutionizing at 540°C for 2 hour; b) The corresponding EDS spectra of spot4

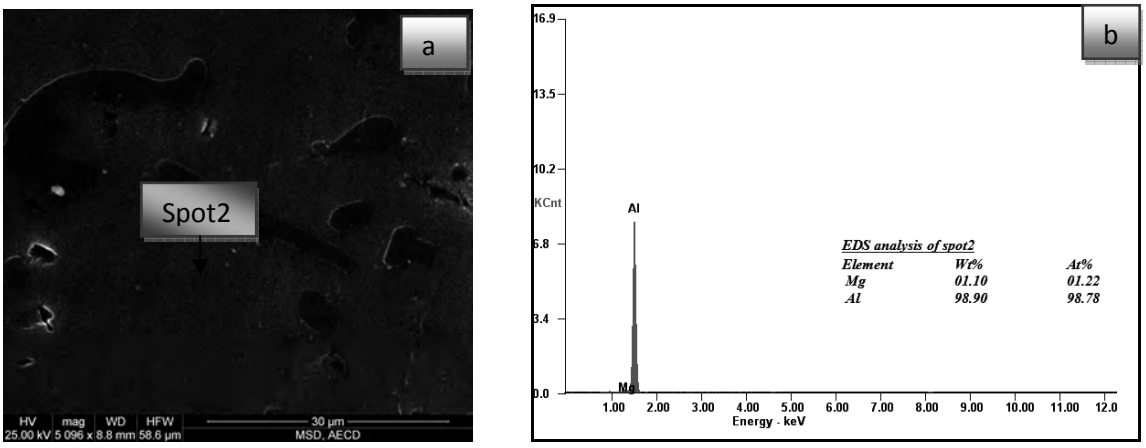

Figure 4.2.35: a) SEM micrograph of Alloy-4 after solutionizing at 540°C for 2 hour; b) The corresponding EDS spectra of spot2

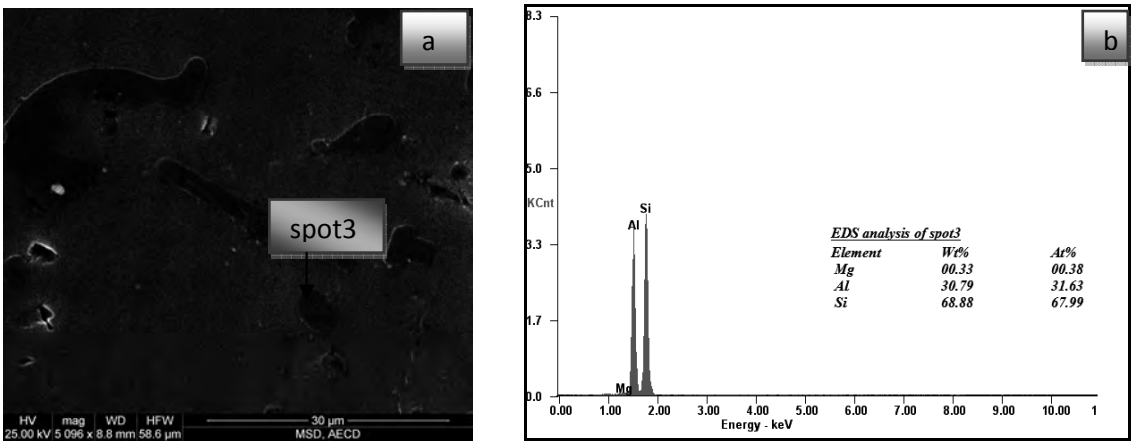

Figure 4.2.36: a) SEM micrograph of Alloy-4 after solutionizing at 540°C for 2 hour; b) The corresponding EDS spectra of spot3

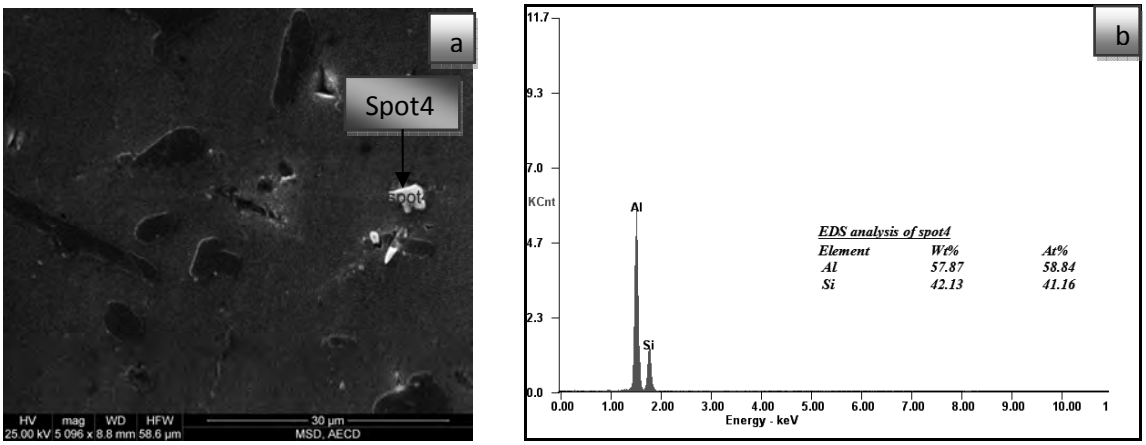

Figure 4.2.37: a) SEM micrograph of the Alloy-4 after solutionizing at 540°C for 2 hour; b) The corresponding EDS spectra of spot4

4.2.4.3 Effect of Alloying and Peak Ageing on the Microstructures of Alloy-4

The as-solutionized and peakaged microstructure (Figure 4.2.38) of the Alloy-4 is very similar to the Alloy-2 and Alloy-3 as same thermal history. This is basically due to the precipitates Cu and Mg containing phases during the solutionizing and ageing treatment. The spherodize and globular eutectic Si are the second phases observed in the microstructure.

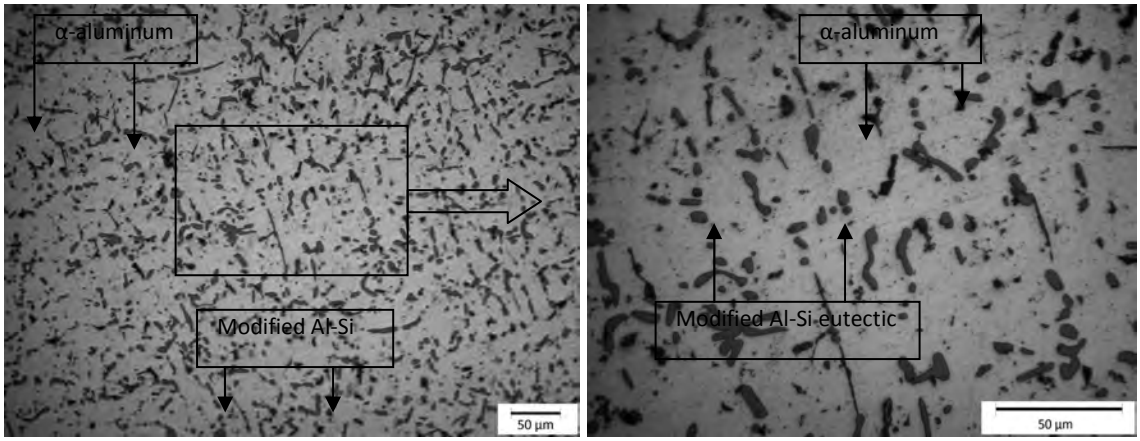

Figure 4.2.38: Optical micrographs of Alloy-4 after peakaged at 225°C for 1 hour showing the modified Al-Si eutectic and α-aluminum matrix

The full frame EDS analysis of the SEM microstructure (Figure 4.2.39) shows the presence of Al, Si, Mg and Cu. Spot1 (Figure 4.2.40) and spot3 (Figure 4.2.42) EDS analysis show the fibrous like intermetallic the Al-Si eutectic inside the aluminum matrix. The chemical components of spot2 (Figure 4.2.41) indicate the α-aluminum matrix composition. Spot4 (Figure 4.2.43) shows the Al-Mg-Cu containing intermetallics.

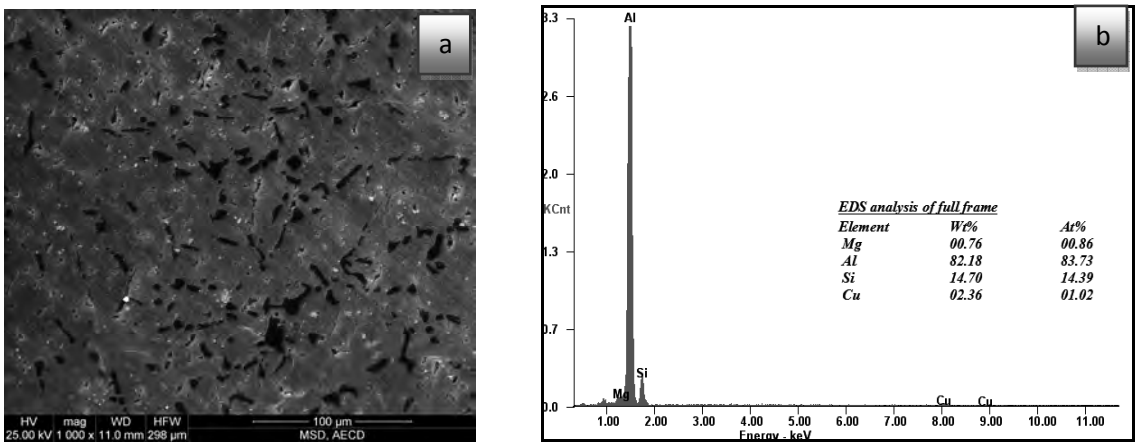

Figure 4.2.39: a) SEM micrograph of Alloy-4 after peakaged at 225°C for 1 hour; b) The corresponding EDS spectra of full frame

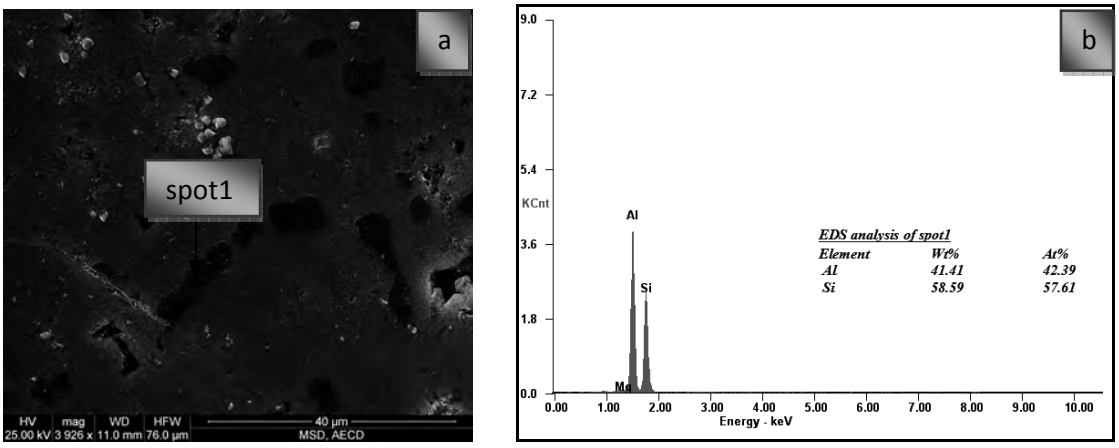

Figure 4.2.40: a) SEM micrograph of Alloy-4 after peakaged at 225°C for 1 hour; b) The corresponding EDS spectra of spot1

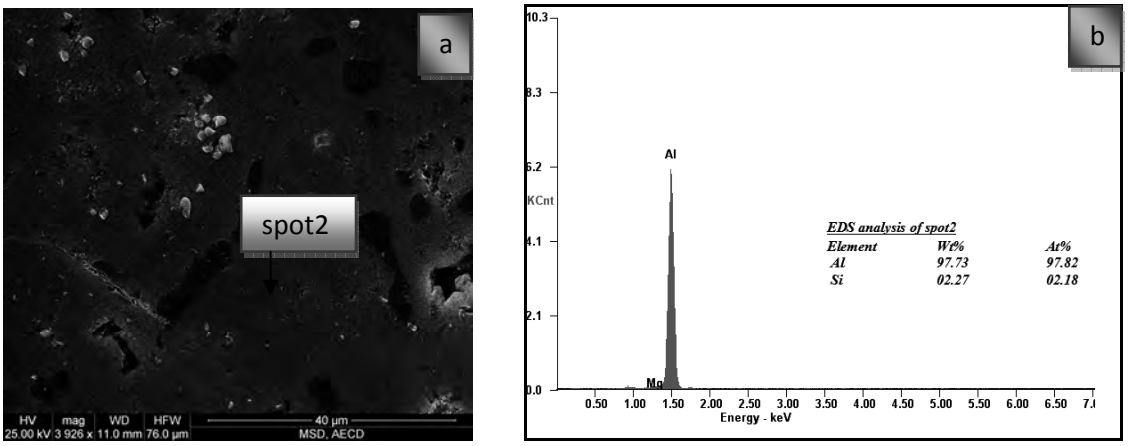

Figure 4.2.41: a) SEM micrograph of Alloy-4 after peakaged at 225°C for 1 hour; b) The corresponding EDS spectra of spot2

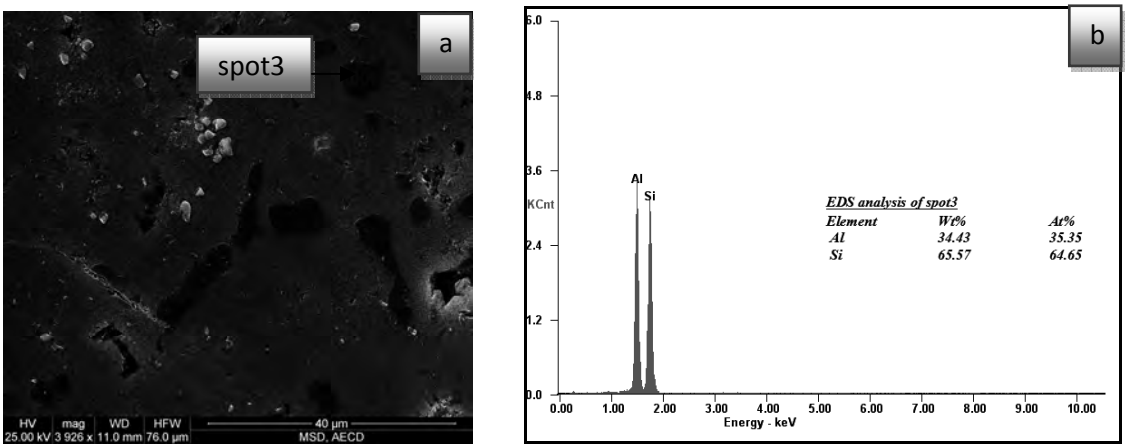

Figure 4.2.42: a) SEM micrograph of Alloy-4 after peakaged at 225°C for 1 hour; b) The corresponding EDS spectra of spot3

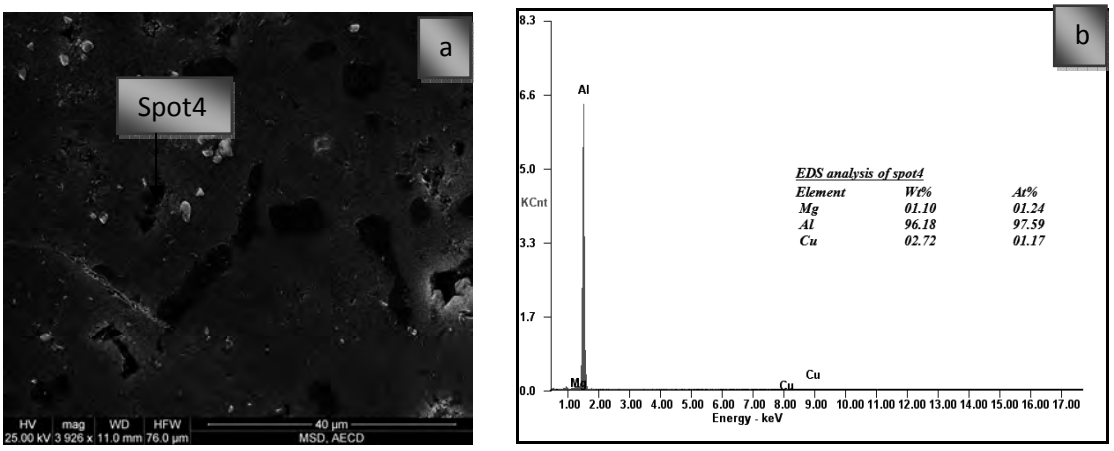

Figure 4.2.43: a) SEM micrograph of Alloy-4 after peakaged at 225°C for 1 hour; b) The corresponding EDS spectra of spot4

4.2.4.4 Effect of Alloying and Over Ageing on the Microstructures of Alloy-4

Figure 4.2.44 shows the typical optical microstructures of the over-aged Alloy-4. Moreover, the eutectic Si is very globular when compared the as-cast condition. Figure 4.2.45 shows the SEM microstructures of the over-aged Alloy-4. The needle like and eutectic Si phases are observed in the Alloys 1-5. No other coarse eutectic phases that were previously dissolved during solutionizing can be seen. No Cu- or Mg-containing coarse phases are observed in the inter-dendritic region.

Figure 4.2.45 shows fine precipitates inside the dendrites of the alloy. It can be seen that there are some fine precipitates in the Alloy-4, however, the amount is higher than in Alloys 1-3 and due to the contrast the observation is difficult. It is likely that these precipitates are the equilibrium β-Mg_2Si phase. Moreover, due to the high over-aging temperature, Si clusters might have also precipitated.

The amount of precipitates inside the dendrites is higher in Alloy-4 possibly due to the 4wt% Cu addition. From literature it is known that the Q'-($Al_5Mg_8Cu_2Si_6$) and the β"-(Mg_2Si) phases coexist inside the primary aluminum dendrites in Cu-added (below 1%) A356 alloys at T6 condition [89]. However, the alloys were analyzed in the over-aged condition in this work and the precipitation sequence has not been investigated. It is likely that the β" phase was converted to the equilibrium β phase due to the T7condition (1 hours at 300°C) in this study. A firm conclusion for the Q’ phase is more difficult to make since the Cu-containing alloys show

slower aging response at 300°C. Therefore, the high hardness of the Cu-containing phases in the aging curves could be due to the Q' phase which still exist at 300°C (and results in higher hardness than the Q phase) and/or due to nature of the Cu-containing phases in general which are harder than the only Mg-containing phases.

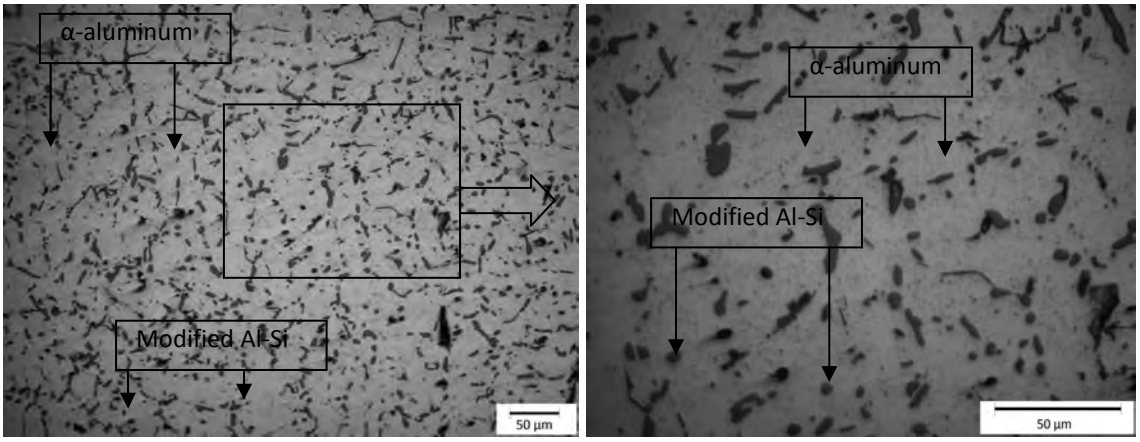

Figure 4.2.44: Optical micrograph of Alloy-4 after overaged at 300°C for 1 hour showing modified Al-Si eutectic and α-aluminum matrix

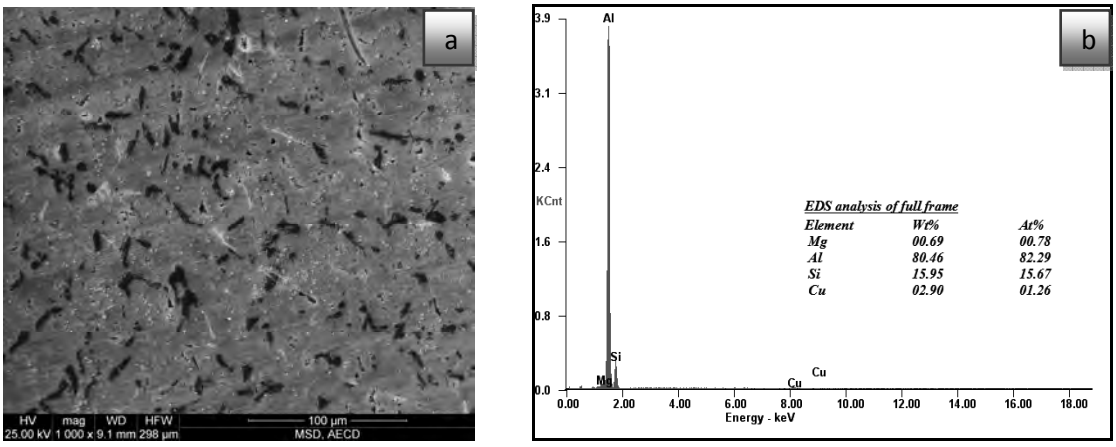

Figure 4.2.45: a) SEM micrograph of Alloy-4 after overaged at 300°C for 1 hour showing the modified Al-Si eutectic and α-aluminum matrix; b) The corresponding EDS spectra of full frame

The EDS analyses on these reveal that these are the fine α-(Al-Mg-Si) precipitates. Further spot analyses on the precipitates showed that modified eutectics. Spot1 (Figure 4.2.46), spot3 (Figure 4.2.48) and spot4 (Figure 4.2.49) show the modified Al-Si eutectics. The EDS analysis of the spot2 represents the α-aluminum matrix.

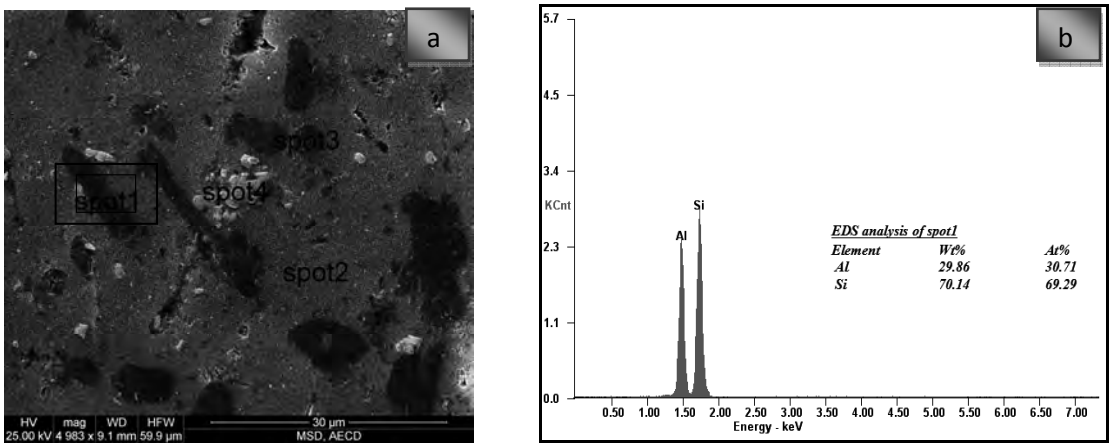

Figure 4.2.46: a) SEM micrograph of Alloy-4 after overaged at 300°C for 1 hour; b) The corresponding EDS spectra of spot1

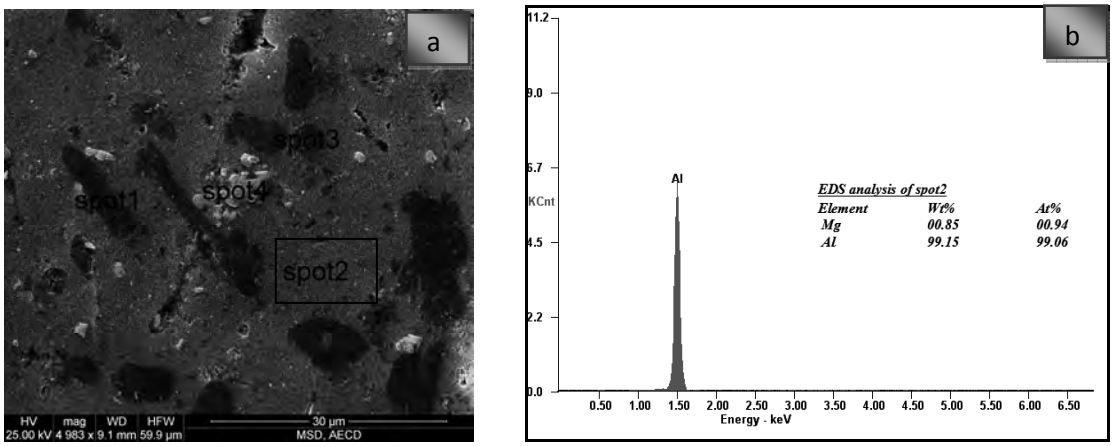

Figure 4.2.47: a) SEM micrograph of Alloy-4 after overaged at 300°C for 1 hour; b) The corresponding EDS spectra of spot2

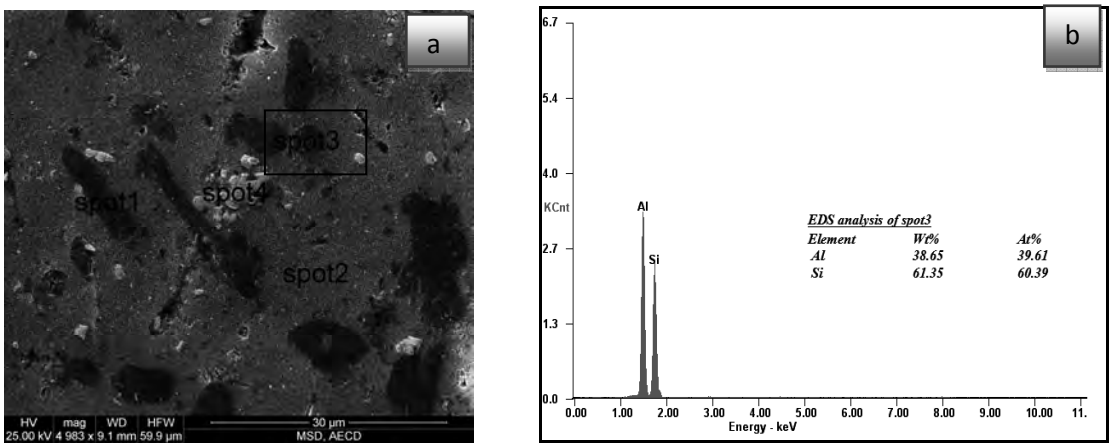

Figure 4.2.48: a) SEM micrograph of Alloy-4 after overaged at 300°C for 1 hour; b) The corresponding EDS spectra of spot3

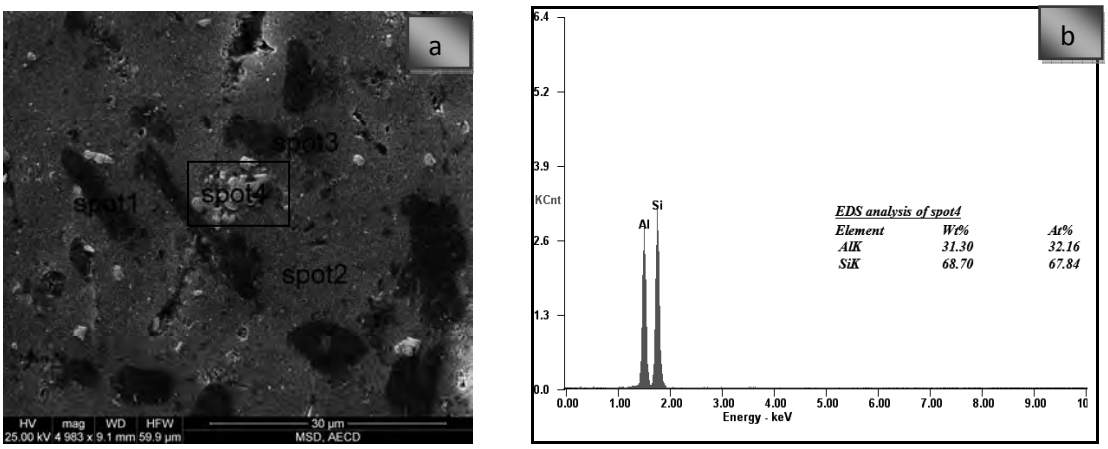

Figure 4.2.49: a) SEM micrograph of Alloy-4 after overaged at 300°C for 1 hour; b) The corresponding EDS spectra of spot4

4.2.5 Effect of Alloying and Thermal Treatment on the Microstructures of Alloy-5

4.2.5.1 Effect of Alloying on the As-Cast Microstructures of Alloy-5

The microstructures of the alloy are shown in Figure 4.2.50. In the micrographs, the silicon eutectic and primary particles are dark grey. The Al_2Cu phase cannot be seen as well; it appears in the form of small particles, slightly darker than the white aluminum matrix. The Alloy-5 shows eutectic acicular silicon and very few coarse primary silicon particles embedded in the dendritic aluminum matrix. The Al_2Cu particles are rather coarse, mainly elongated along the grain boundaries and also forming small pockets. The distribution of the intermetallic phase is rather homogeneous.

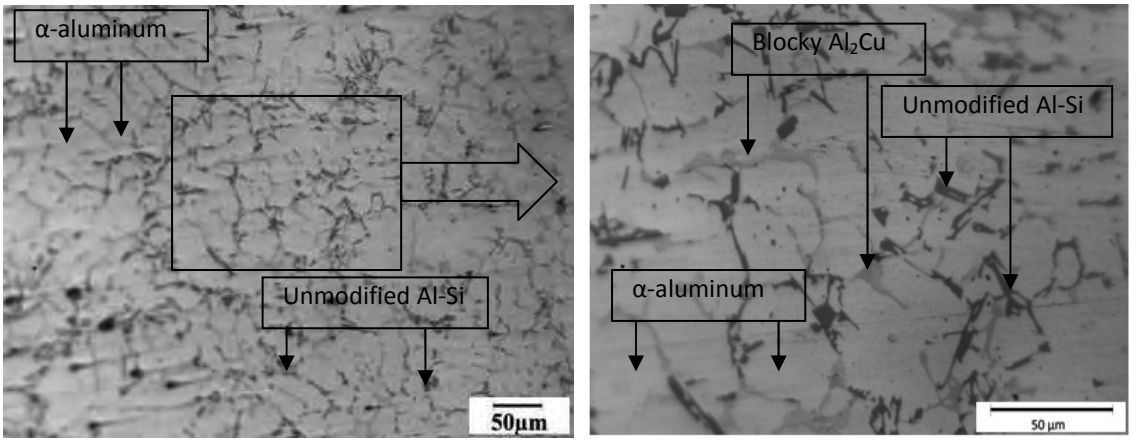

Figure 4.2.50: Optical micrographs of as-cast Alloy-5

4.2.5.2 Effect of Alloying and Solutionizing on the Microstructures of Alloy-5

Figure 4.2.51 shows the microstructures of the solution treated samples. For samples solution treated at 540℃, the α-aluminum dendrite network did not undergo much change, even with a prolonged solution time of 2 hr at a solution temperature of 540℃. However, the dendrite network disappeared completely (Figure 4.2.51). The morphology change of the eutectic Si is obvious after solution treatment. The plate-like eutectic Si in as-cast case (shown in Figure 4.2.50) was broken into small particles. The fragmentation process was accelerated rapidly by higher the solutionizing temperature.

When the concentration of Cu is greater than 3.5wt%, there is a risk of incipient melting during solution heat treatment in the temperature range of 505°C to 515°C, as shown by region in contrast, there is no risk of incipient melting during solution heat treatment at 515°C, when the Cu concentration is less than 3.5wt% since only solid state reactions take place. The white grey region is the incipient melting of Al_2Cu.

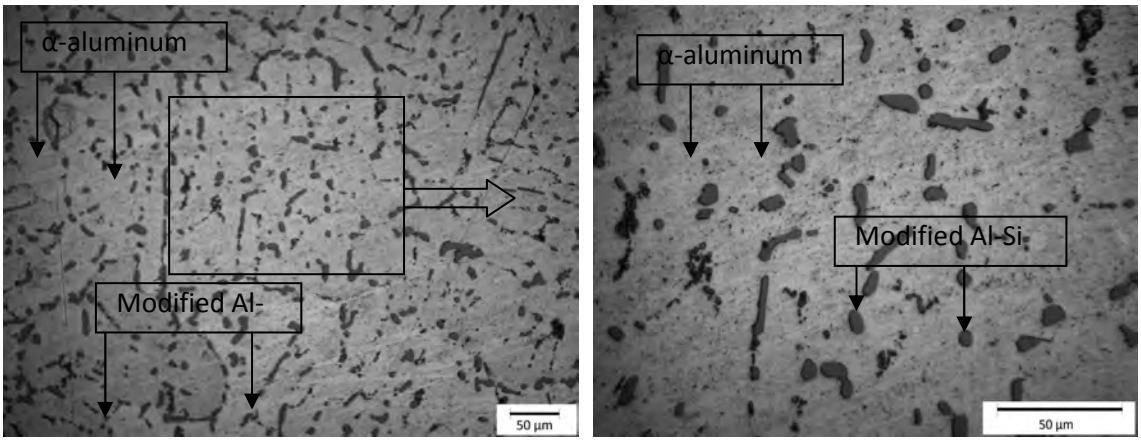

Figure 4.2.51: Optical micrographs of Alloy-5 after solution treatment at 540°C for 2 hours showing modified Al-Si eutectic and α-aluminum matrix

4.2.5.3 Effect of Alloying and Peak Ageing on the Microstructures of Alloy-5

Figure 4.2.52 shows the typical microstructures of the as-solutionized and peakaged Alloy-5.The fragmentation of Si particles are about same as the solutionized condition. But the spherodize Si particles are more coarsened than the solution treated condition. The Cu and Mg containing precipitates are reveals in the peakaged condition.

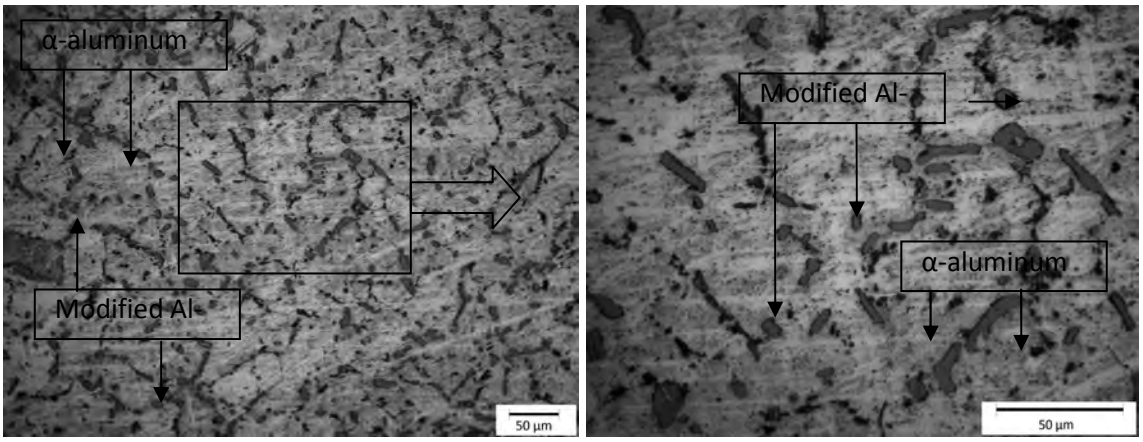

Figure 4.2.52: Optical micrographs of Alloy-5 after peakaged at 225°C for 1 hour showing modified Al-Si eutectic and α-aluminum matrix

Figure 4.2.53 shows the EDS analysis of the full frame SEM image. The characteristic of the intermetallic phases after solution treatment and peak ageing are detects by EDS analysis. The full frame chemical compositions are the intermetallic, precipitated and solid solution constituents. The complex eutectic mixture experienced fragmentation in the early stage of solution treatment, and a large number of individual particles were formed. EDS analysis of spot1 (Figure 4.2.54) revealed that the Cu containing phase and fibrous eutectic Si phase where spot2 (Figure 4.2.55) EDS results indicate the aluminum matrix with 0.82wt% Mg and 1.39wt% Si content solid solution. Spot3 (Figure 4.2.56) EDS results confirm the spherodize eutectic Si phase.

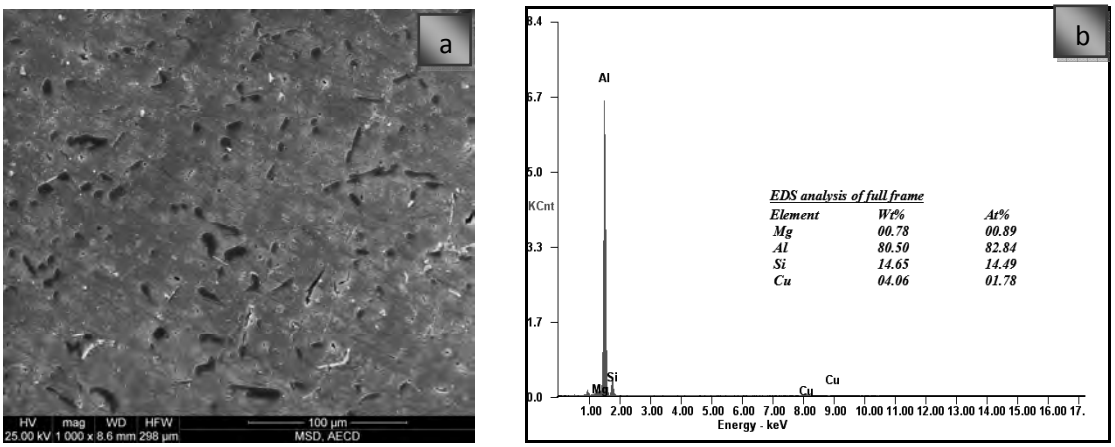

Figure 4.2.53: a) SEM micrograph of Alloy-5 after peakaged at 225°C for 1 hour showing modified Al-Si eutectic and α-aluminum matrix; b) The corresponding EDS spectra of full frame

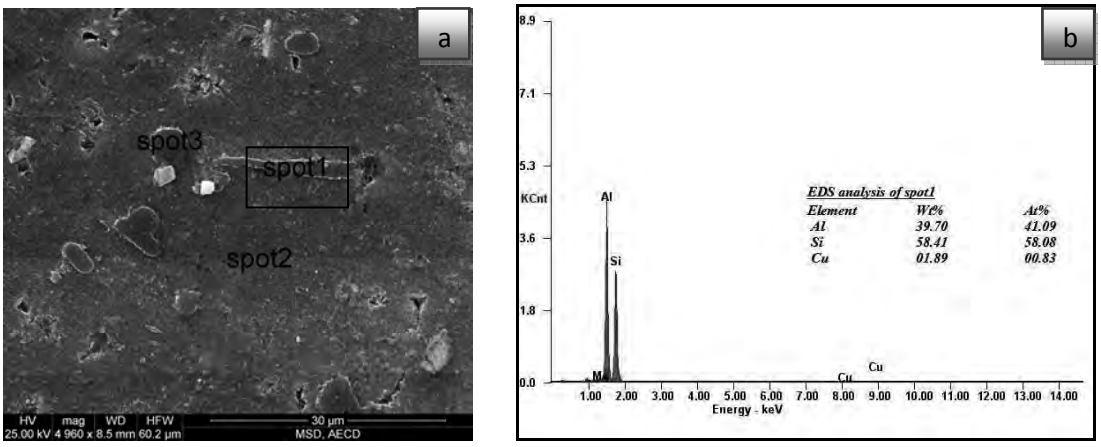

Figure 4.2.54: a) SEM micrograph of the Alloy-5 after peakaged at 225°C for 1 hour; b) The corresponding EDS spectra of spot1

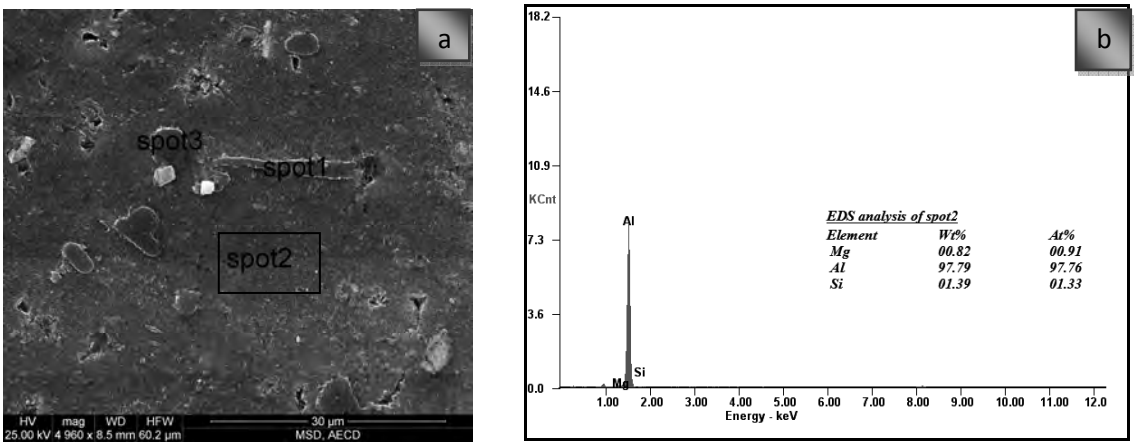

Figure 4.2.55: a) SEM micrograph of Alloy-5 after peakaged at 225°C for 1 hour; b) The corresponding EDS spectra of spot2

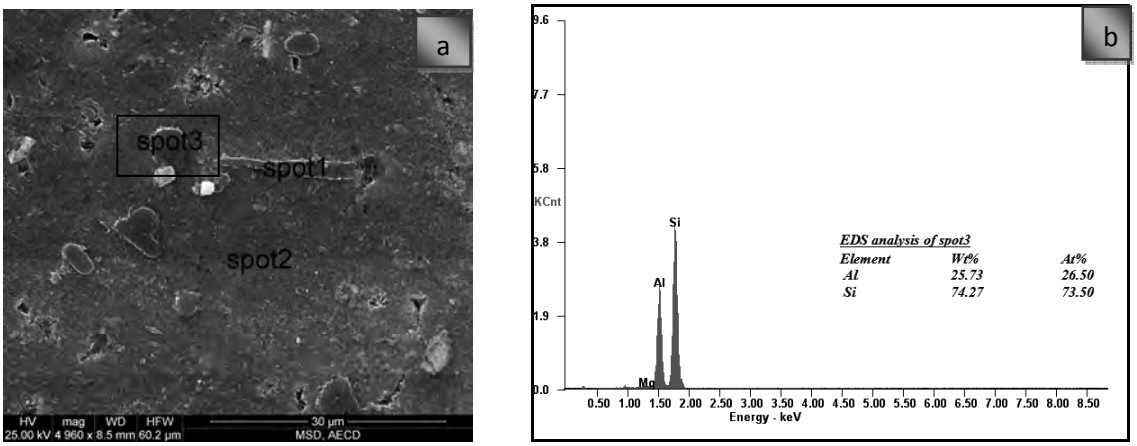

Figure 4.2.56: a) SEM micrograph of Alloy-5 after peakaged at 225°C for 1 hour; b) The corresponding EDS spectra of spot3

4.2.5.4 Effect of Alloying and Over Ageing on the Microstructures of Alloy-5

Figure 4.2.57 shows the typical optical microstructures of the over-aged Alloy-5. It can be seen that the spherodize Si particles are more rounded than the as solutionized condition and density of spherodize Si phase decreases. The eutectic Si is modified.

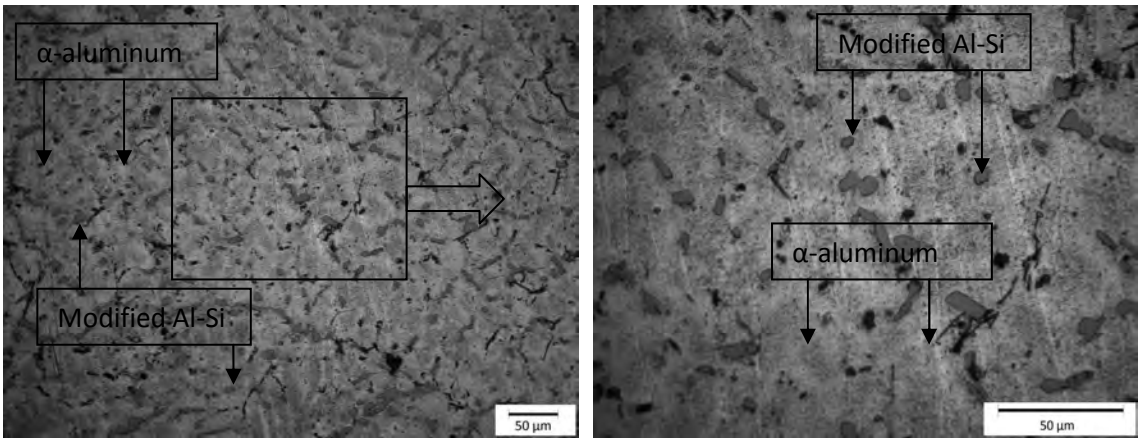

Figure 4.2.57: Optical micrograph of Alloy-5 after overaged at 300°C for 1 hour showing modified Al-Si eutectic and α-aluminum matrix

4.2.6 Effect of Alloying and Thermal Treatment on the Microstructures of Alloy-6

4.2.6.1 Effect of Alloying on the As-Cast Microstructures of Alloy-6

Figure 4.2.58 and Figure 4.2.59 show the optical and SEM microstructure of as cast Al-6Si-0.5Mg-2Ni alloy which consisted of the eutectic Si, $NiAl_3$ (gray), Mg_2Si (black) and other intermetallic phases on α-Al matrix. It should be noted that the sample was produced by the non-modification and rapid solidification in the steel mold. It can be seen that the eutectic Si phase is flake-like and acicular morphologies. The $NiAl_3$ phase is the plate-like morphologies. According to the manufacturing practice, it has been well known that the casting product has very low mechanical properties due to the casting product was contained much micro-segregation in solid solution state. Therefore, it is necessary for following by homogenization or heat treatment processes

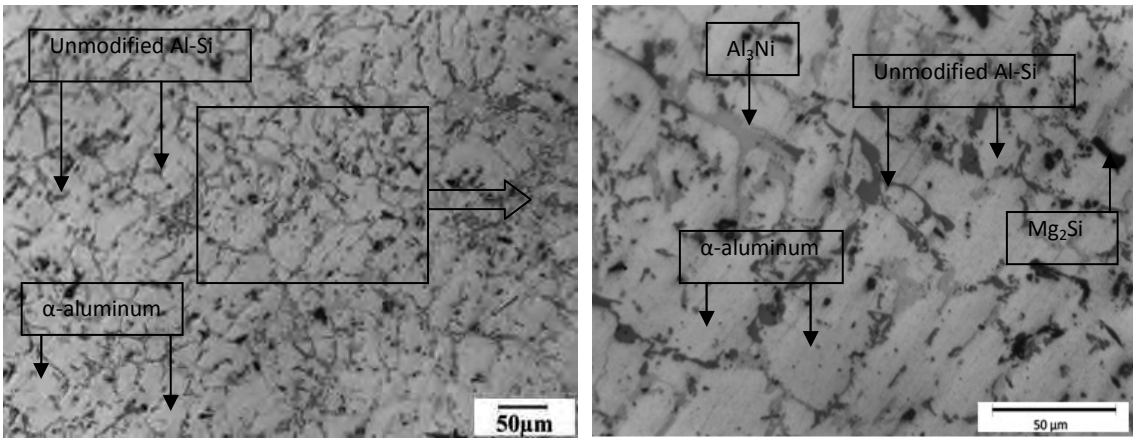

Figure 4.2.58: Optical micrographs of as-cast Alloy-6

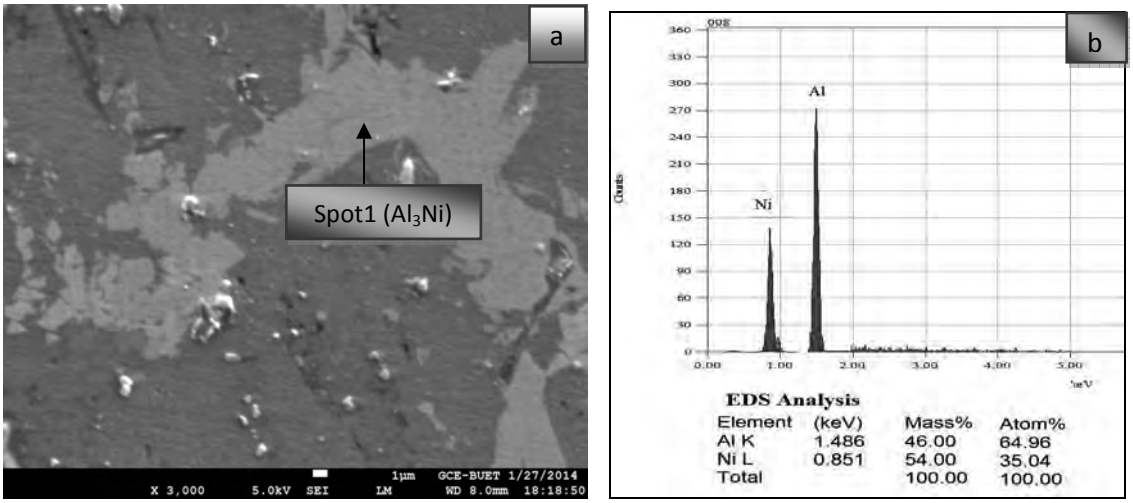

Figure 4.2.59: a) SEM micrograph of as-cast Alloy-6 showing the Al_3Ni intermetallic; b) The corresponding EDS spectra of spot1

4.2.6.2 Effect of Alloying and Solutionizing on the Microstructures of Alloy-6

In Ni containing Al-6Si-0.5Mg-2Ni alloy (Alloy-6), the eutectic phase consists of more or less soft 'eutectic Al 'and hard 'eutectic, Mg_2Si, Si and Al_3Ni'. In order to form a strong or hard eutectic phase, the hard 'eutectic Mg_2Si, Si and Al_3Ni' needs to be connected three-dimensionally (Figure 4.2.60 and Figure 4.2.61). Before discussing the contiguity of the 'eutectic Si and Al_3Ni' depending on the Ni content, some additional issues regarding the thermal stability of eutectic Si and eutectic Al_3Ni need to be addressed.

During solution treatment, the eutectic Si platelets spheroidise and their aspect ratio decreases, which may result in a loss of the interconnectivity of the eutectic phases. In Ni free alloys

(Alloys 1-5), the Si contiguity is completely lost after solution treatment at 540°C for 2h, and the eutectic Al_3Ni does not significantly change its shape during the course of solution treatment, as can be metallographically observed. In the presence of Ni aluminides, the loss of eutectic Si interconnectivity is significantly reduced. The Ni phase in combination with eutectic Si forms a strongly interconnected three-dimensional structure, whose contiguity is strongly preserved even after solution treatment for 2h. As a result of solution treatment spheroidization of the eutectic Si takes place and its aspect ratio decreases. In contrast, the Ni containing phases do not significantly change their shape. The EDS analysis (Figure 4.2.61) shows the compositions exist into the full frame scanning area which is the major constituents of the SEM image frame.

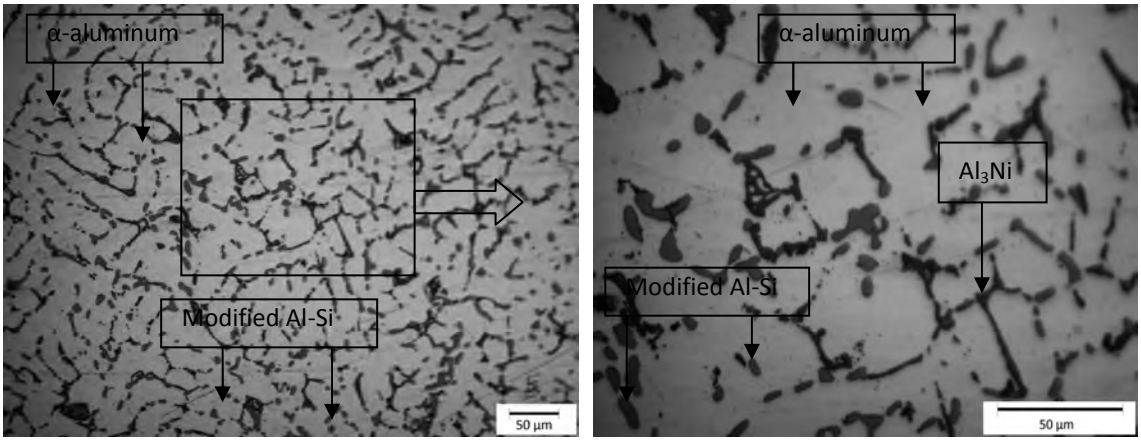

Figure 4.2.60: Optical micrographs of Alloy-6 after solution treatment at 540°C for 2 hours showing modified Al-Si, Mg_2Si, Al-Al_3Ni eutectic and α-aluminum matrix

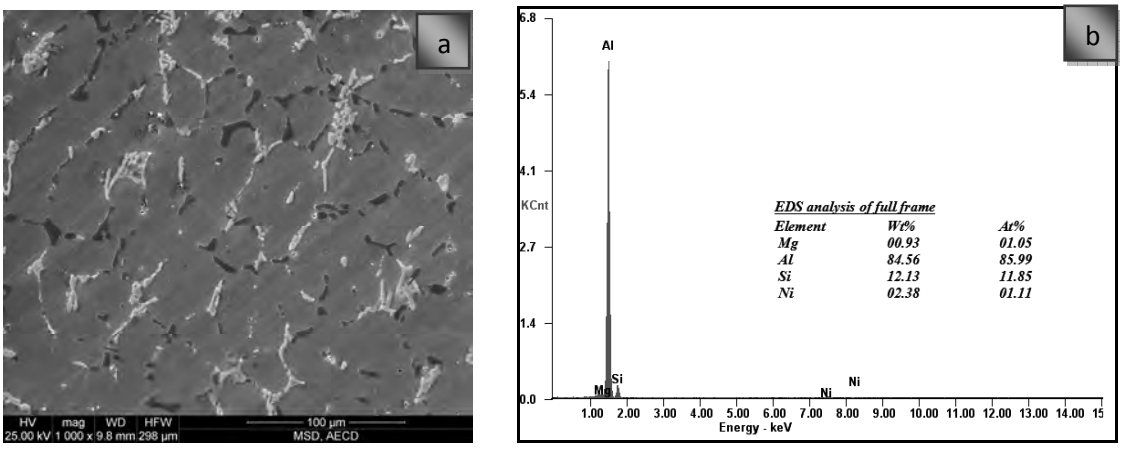

Figure 4.2.61: a) SEM micrograph of Alloy-6 after solution treatment at 540°C for 2 hours showing modified Al-Si eutectic, Al_3Ni and α-aluminum matrix; b) The corresponding EDS spectra full frame

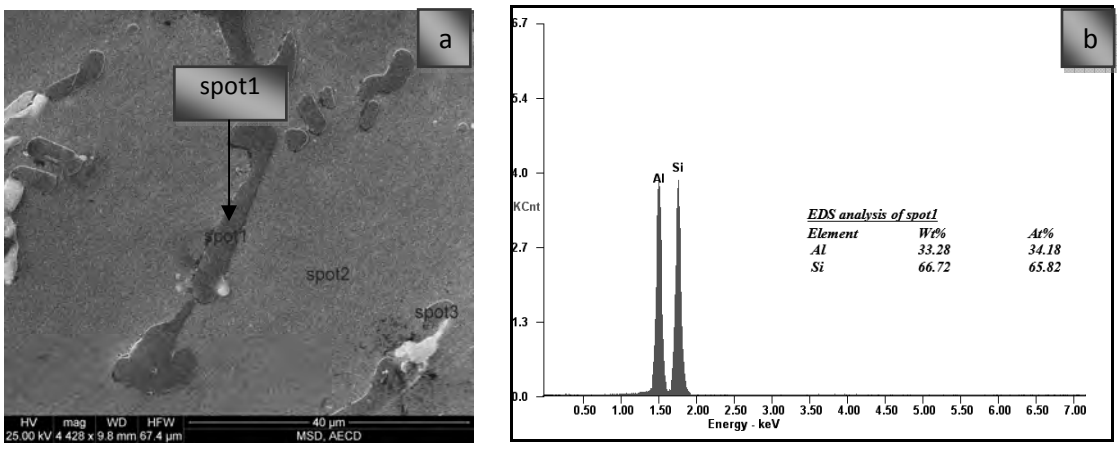

Figure 4.2.62: a) SEM micrograph of Alloy-6 after solution treatment at 540°C for 2 hours; b) The corresponding EDS spectra of spot1

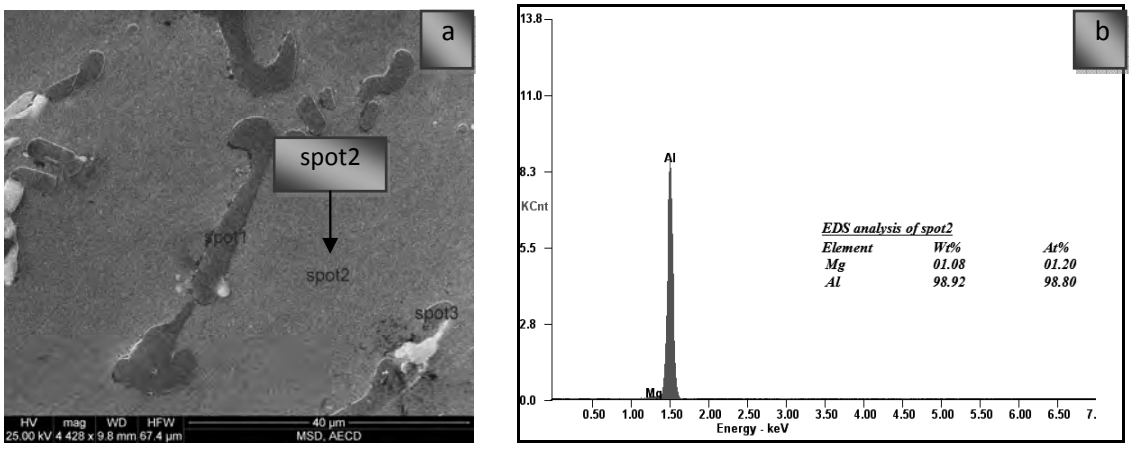

Figure 4.2.63: a) SEM micrograph of Alloy-6 after solution treatment at 540°C for 2 hours; b) The corresponding EDS spectra of spot2

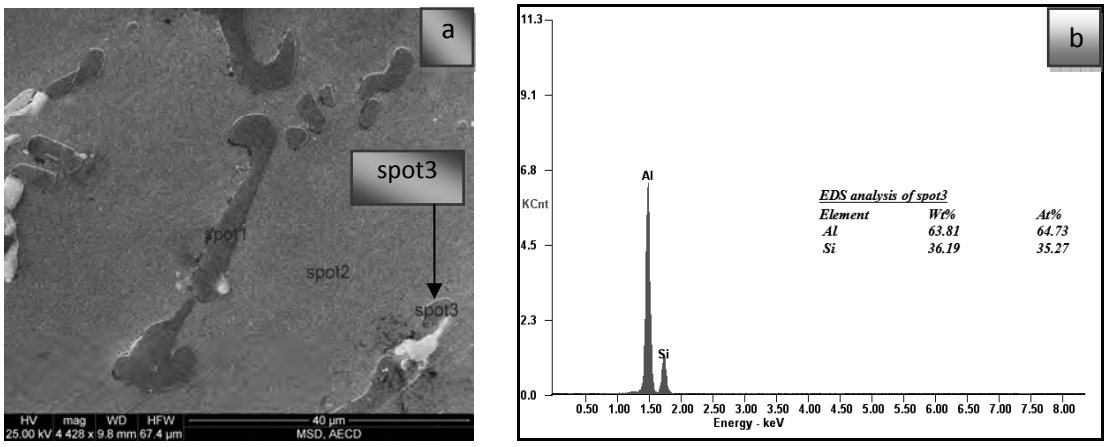

Figure 4.2.64: a) SEM micrograph of Alloy-6 after solution treatment at 540°C for 2 hours; b) The corresponding EDS spectra of spot3

Figure 4.2.62 to Figure 4.2.64 show the spot analysis of the intermetallics or matrix elements. The spot1 (Figure 4.2.62) is the fibrous like structure and the end surfaces are well smooth. The EDS results of spot1 indicate the Al-Si eutectic. EDS analysis of spot2 (Figure 4.2.63) is the Aluminum matrix with 1.08 wt% Mg content. The spot3 (Figure 4.2.64) is globular or rounded and the EDS spectra of its chemical composition indicate the eutectic Al-Si phase into the Aluminum matrix.

4.2.6.3 Effect of Alloying and Peak Ageing on the Microstructures of Alloy-6

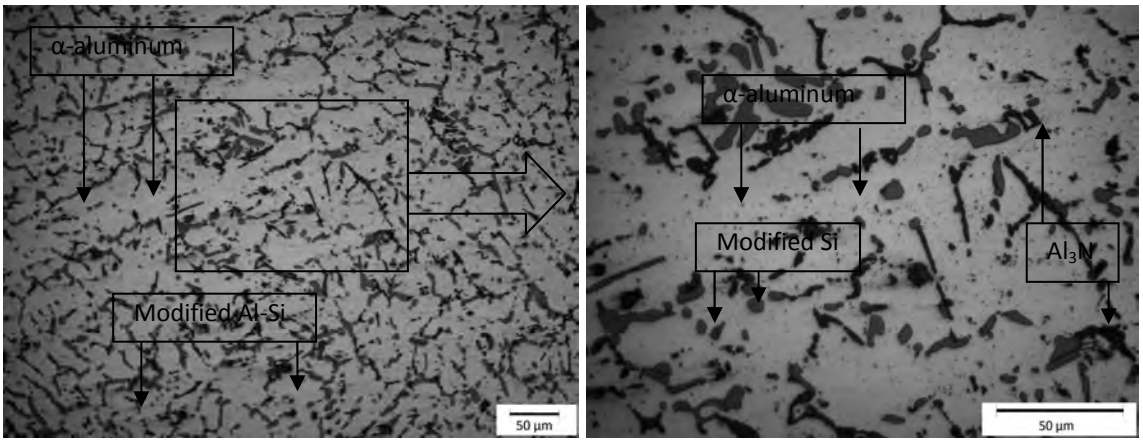

Figure 4.2.65: Optical micrographs of Alloy-6 after peakaged at 225°C for 1 hour showing modified Al-Si, Al_3Ni eutectic and α-aluminum matrix

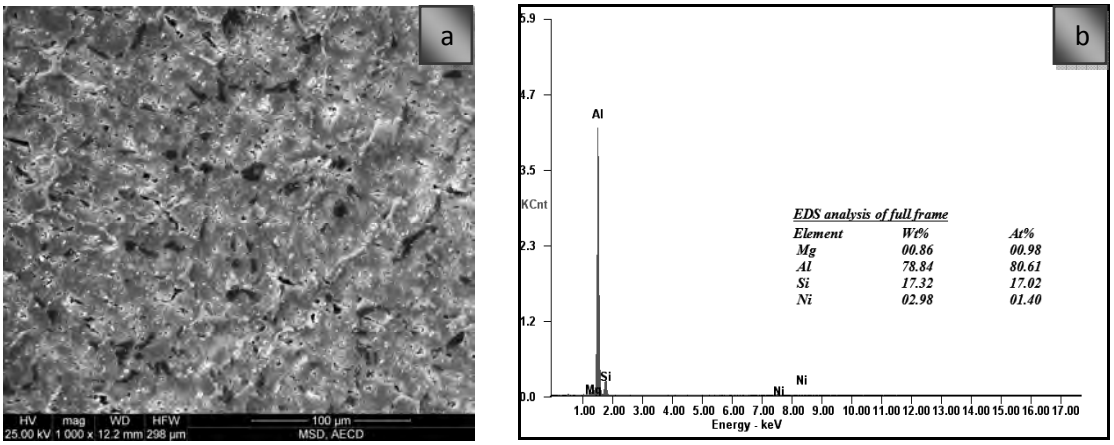

Figure 4.2.66: a) SEM micrograph of Alloy-6 after peakaged at 225°C for 1 hour showing modified Al-Si eutectic, Al_3Ni and α-aluminum matrix; b) The corresponding EDS spectra of full frame

Figure 4.2.65 shows optical micrographs of the Ni-containing Alloy-6 at two magnifications. Four different phases can be observed: α-Al, eutectic Si and Ni-containing phases. By means of

EDX-analysis the latter were identified to be Al_3Ni phases. The full frame EDX analysis (Figure 4.2.66) content Al, Si, Mg and Ni which are the major compositions of Alloy-6.

The Figure 4.2.67, Figure 4.2.68, Figure 4.2.69 and Figure 4.2.70 illustrate the scanning electron image with EDS spot analysis of the peakaged Al-6Si-0.5Mg-2Ni alloy. Al is present both in solid solution with the matrix and precipitates. Mg and Si combine to form a compound of Mg_2Si, which in turn forms a simple eutectic system. The spot1 EDS result (Figure 4.2.67) indicates the Al-Si eutectic as fibrous like modified structure. The spot2 (Figure 4.2.68) is mainly 1.10 wt% Mg containing aluminum solid solution. The EDS analysis of spot3 (Figure 4.2.69) shows the rounded like eutectic Si phase and spot4 (Figure 4.2.70) indicates the presence of Ni containing compound Al_3Ni.

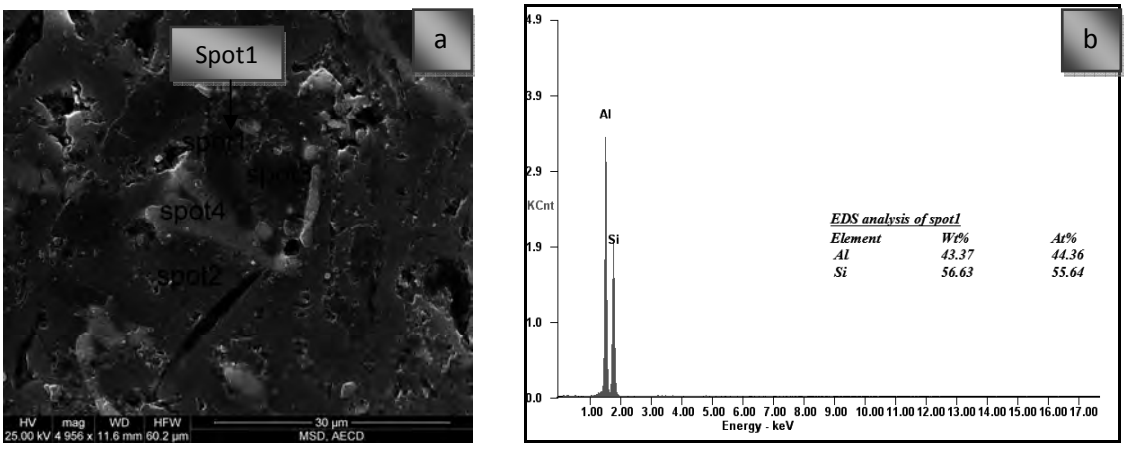

Figure 4.2.67: a) SEM micrograph of Alloy-6 after peakaged at 225°C for 1 hour; b) The corresponding EDS spectra of spot1

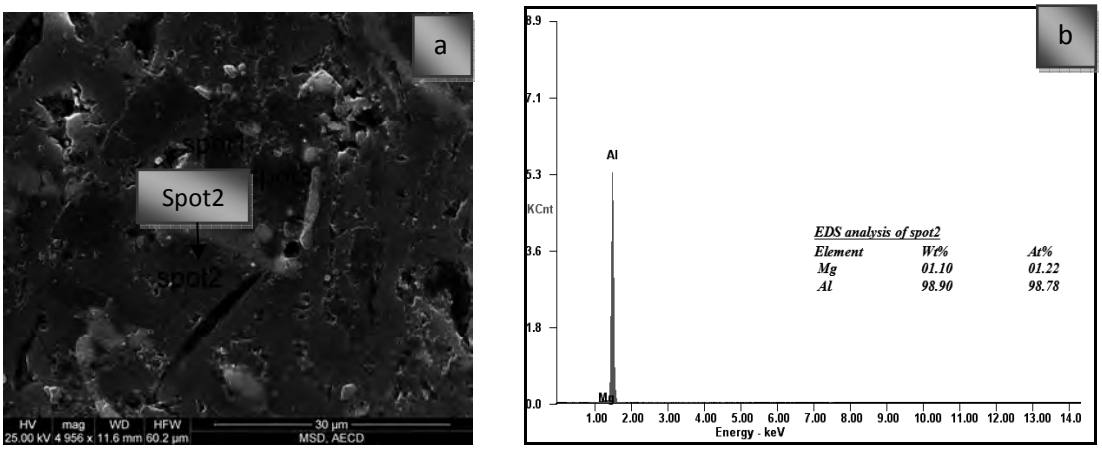

Figure 4.2.68: a) SEM micrograph of Alloy-6 after peakaged at 225°C for 1 hour; b) The corresponding EDS spectra of spot2

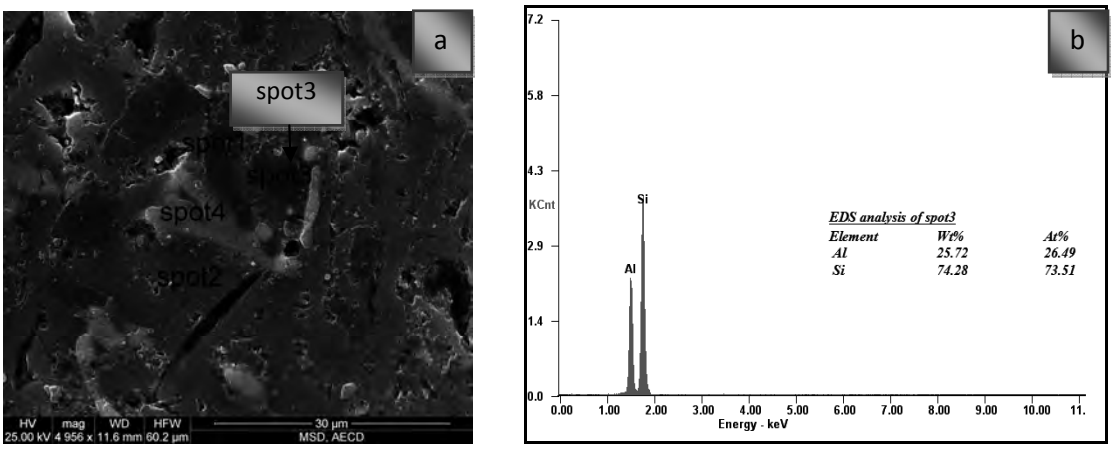

Figure 4.2.69: a) SEM micrograph of Alloy-6 after peakaged at 225°C for 1 hour; b) The corresponding EDS spectra of spot3

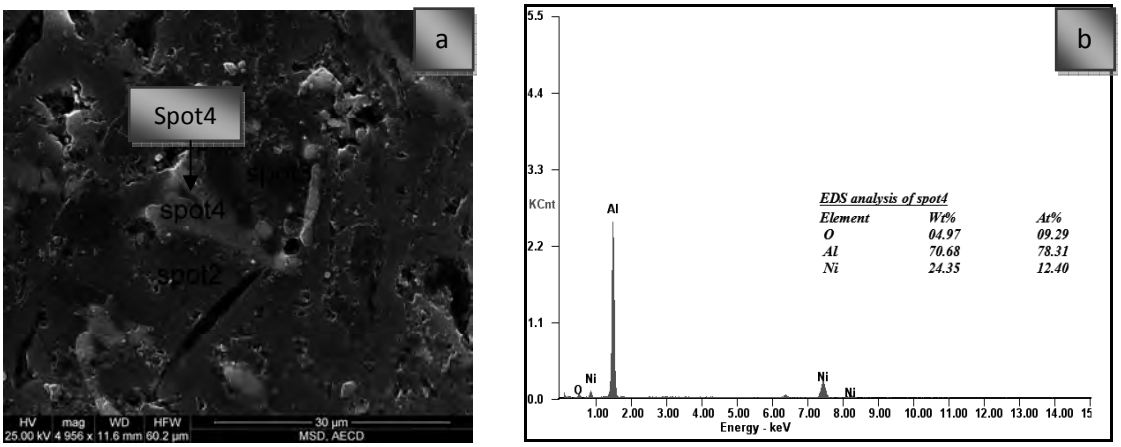

Figure 4.2.70: a) SEM micrograph of Alloy-6 after peakaged at 225°C for 1 hour; b) The corresponding EDS spectra of spot4

4.2.6.4 Effect of Alloying and Over Ageing on the Microstructures of Alloy-6

Figure 4.2.71 and Figure 4.2.72 show the OLM and SEM typical microstructures of the overaged Alloy-6 respectively. The eutectic Si is very globular when compared the as cast condition and Al_3Ni are about same as the solution treated condition. The Ni containing intermetallics are partially fragmented and no significant modification occurs.

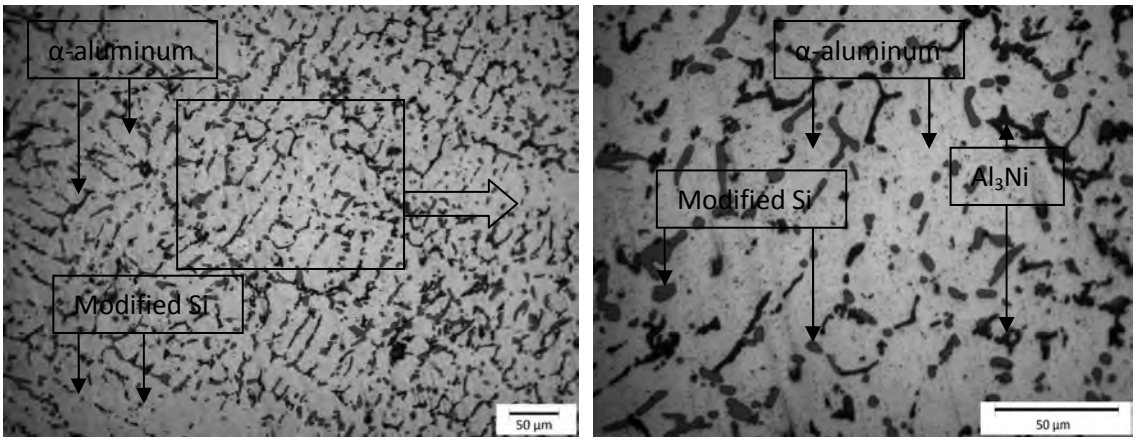

Figure 4.2.71: Optical micrograph of Alloy-6 after overaged at 300°C for 1 hour showing modified Al-Si, Al_3Ni eutectic and α-aluminum matrix

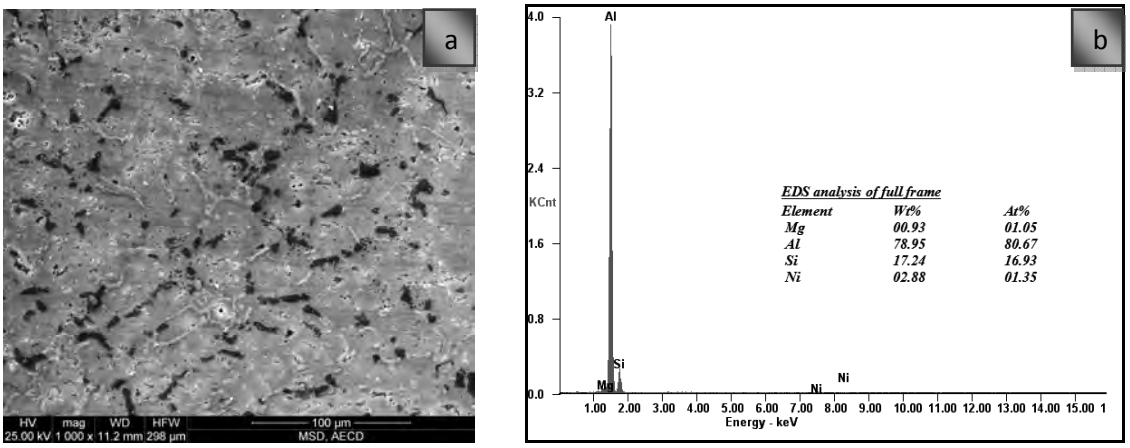

Figure 4.2.72: a) SEM micrograph of Alloy-6 after overaged at 300°C for 1 hour showing modified Al-Si eutectic, Al_3Ni and α-aluminum matrix; b) The corresponding EDS spectra of full frame

To study the complex eutectic mixture, EDS analysis using the scanning electron microscope (SEM) was carried out to identify the finer intermetallic compounds. As shown in Figure 2.4.73 to Figure 4.2.75, three spots were quantified and the EDS analysis reveals its chemical composition. The EDS analysis of spot1 (Figure 2.4.73) represents the eutectic Al-Si phase which is more modified than the as cast structure. The chemical composition of the eutectic is 46.55wt% Al and 53.45wt% Si. Spot2 (Figure 2.4.74) is the mainly aluminum matrix with 1.01wt% Mg. And spot3 (Figure 2.4.75) is mainly the aluminium matrix with 1.01wt% Mg and spot4-white color is the Ni content (Al_3Ni) intermetallic compound.

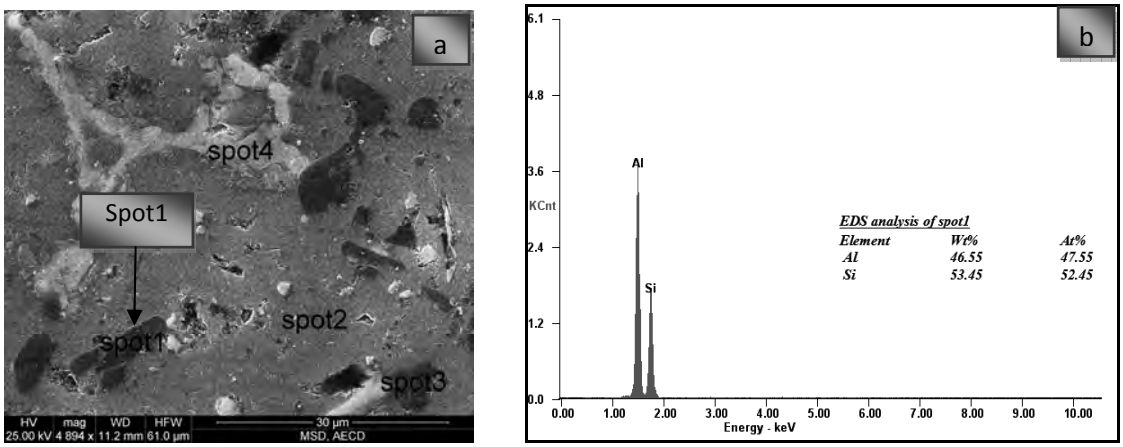

Figure 4.2.73: a) SEM micrograph of Alloy-6 after overaged at 300°C for 1 hour; b) The corresponding EDS spectra of spot1

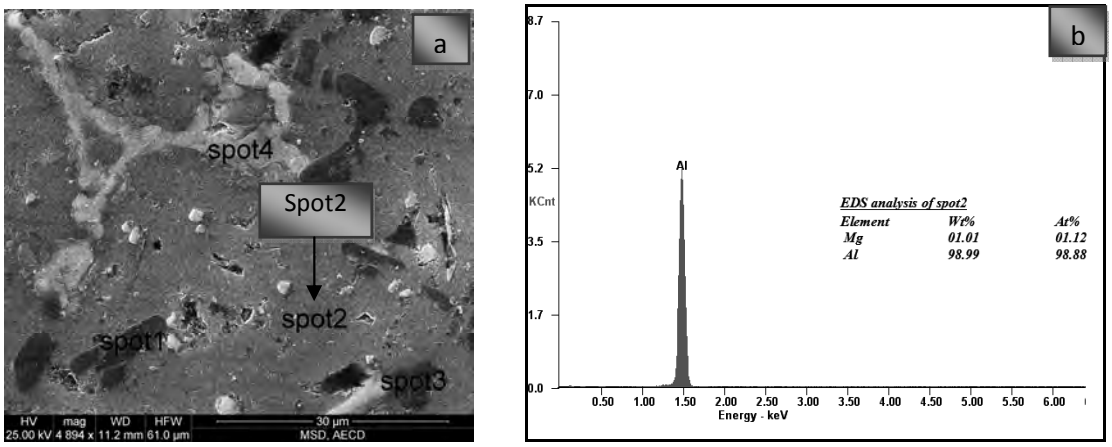

Figure 4.2.74: a) SEM micrograph of Alloy-6 after overaged at 300°C for 1 hour; b) The corresponding EDS spectra of spot2

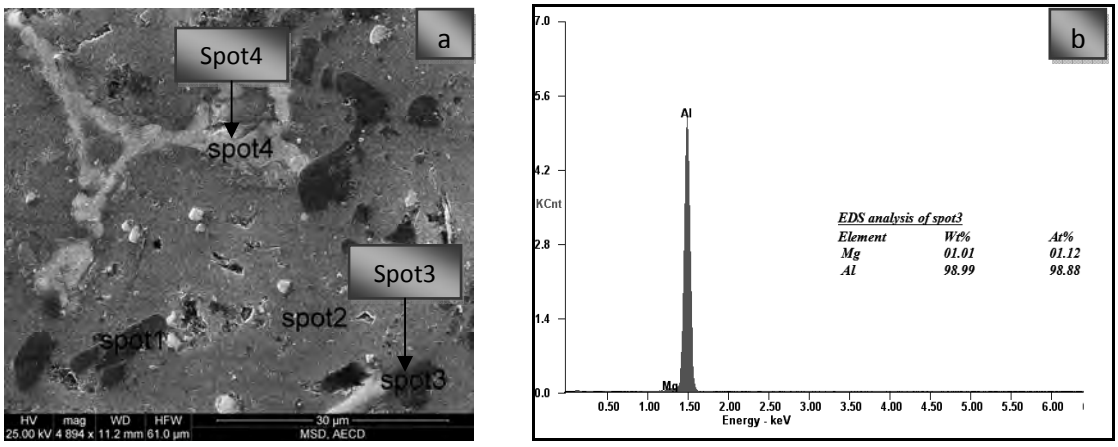

Figure 4.2.75: a) SEM micrograph of Alloy-6 after overaged at 300°C for 1 hour; b) The corresponding EDS spectra of spot3

4.2.7 Effect of Alloying and Thermal Treatment on the Microstructures of Alloy-7

4.2.7.1 Effect of Alloying on the As-Cast Microstructures of Alloy-7

Figure 4.2.76 shows the as-cast microstructure of Al-6Si-0.5Mg-2Cu-2Ni alloy (Alloy-7). It consists of primary Si and α-aluminum dendritic cells with eutectic Si and complex intermetallic compounds segregated into the inter-dendritic regions. The primary Si particles and irregular eutectic Si are dark grey, while the intermetallic phases are light grey in color. The EDS (Figure 4.2.77) analysis represents the Ni containing intermetallics.

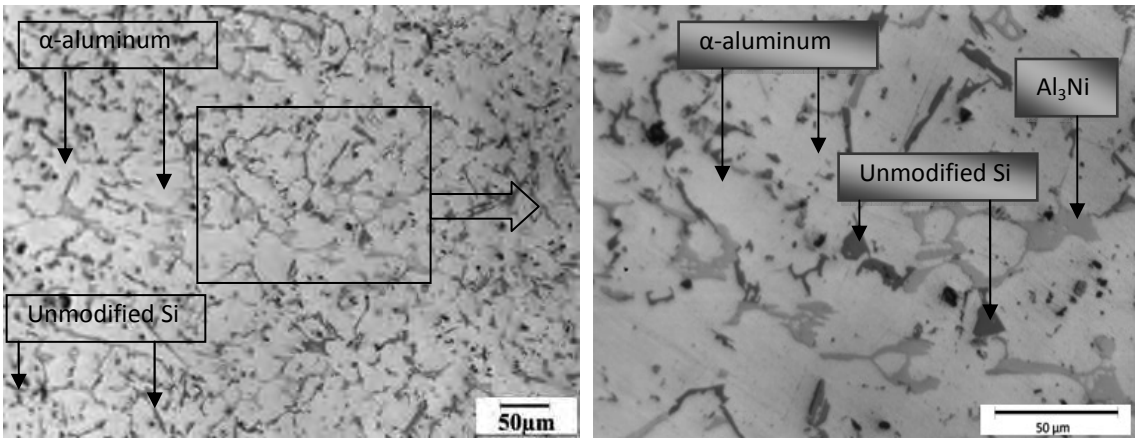

Figure 4.2.76: Optical micrographs of the as cast Alloy-7

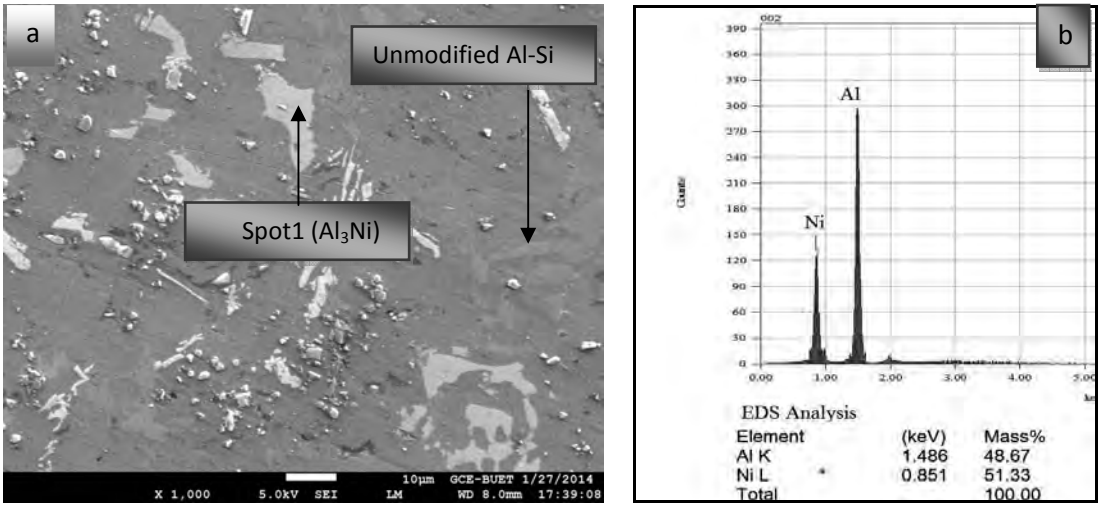

Figure 4.2.77: a) SEM micrograph of as-cast Alloy-7; b) The corresponding EDS spectra of spot1

4.2.7.2 Effect of Alloying and Solutionizing on the Microstructures of Alloy-7

Figure 4.2.78 shows the typical optical light microstructures and Figure 4.2.79 shows the SEM image of the as-solutionized Alloy-7. It is very similar to the as-solutionized Alloy-6. The coarse Cu- and Mg-containing phases (θ, π and Q) dissolved during the solutionizing treatment and the second phases observed are the eutectic Si, Al_3Ni α-(Al-Cu-Mg-Ni-Si). Very fine α-(Al-Cu-Mg-Ni-Si) precipitates can be seen inside the aluminum dendrites (Figure 4.2 78), as well as in the intra dendritic regions. However, it is very difficult to draw firm conclusions due to the small size of the precipitates. Moreover, similar to the Alloy-1, only α precipitates are observed in the as-solutionized stage.

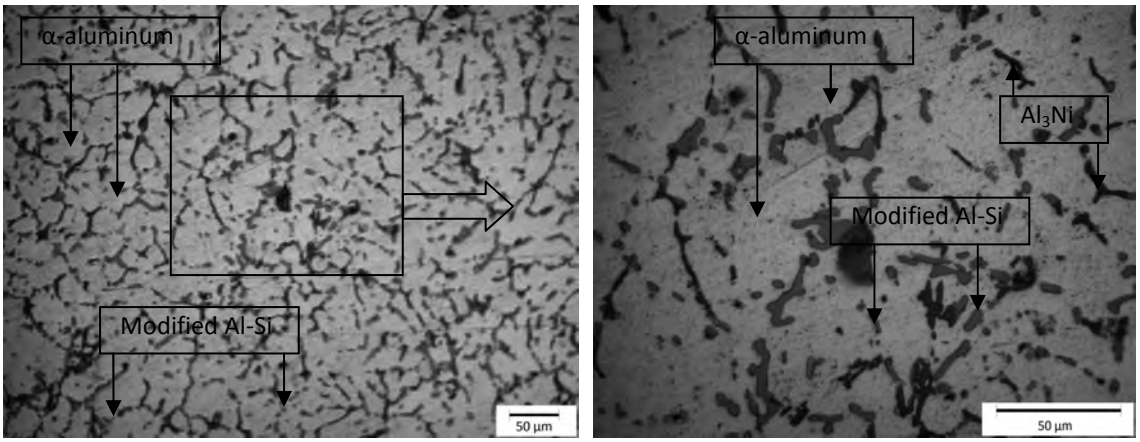

Figure 4.2.78: Optical micrographs of Alloy-7 after solution treatment at 540°C for 2 hours showing modified Al-Si, Al3Ni eutectic and α-aluminum matrix

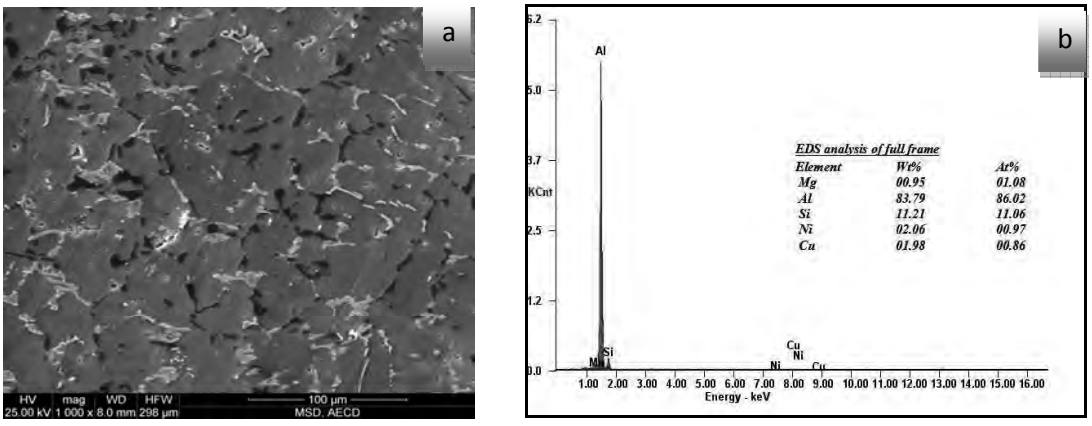

Figure 4.2.79: a) SEM micrograph of Alloy-7 after solution treatment at 540°C for 2 hours showing modified Al-Si eutectic, Al_3Ni and α-aluminum matrix; b) the corresponding EDS spectra of the full frame

The EDS analysis reveals the chemical composition of the full frame SEM image (Figure 4.2.79). However, the uniform distribution of particles can clearly observed from prolonged the solution treatment samples. Moreover, it was found that the $NiAl_3$ phase was also partially dissolved by prolonged the solution treatment time.

Figure 4.2.80, Figure 4.2.81 and Figure 4.2.82 show the SEM photomicrograph and three spot analyses of EDS spectra of Alloy-7. The EDS spectrum spot analyses clearly reveal the peaks of Al, Si and Mg indicating the presence of this eutectic. Mg is completely dissolved into the Aluminum matrix. Spot1 (Figure 4.2.80) EDS results indicate the Si eutectic, spot2 (Figure 4.2.81) aluminum matrix with Mg and spot3 (Figure 4.2.82) is eutectic Al-Si phase. The white intermetallics are mainly the Al-Ni intermetallic eutectic phases.

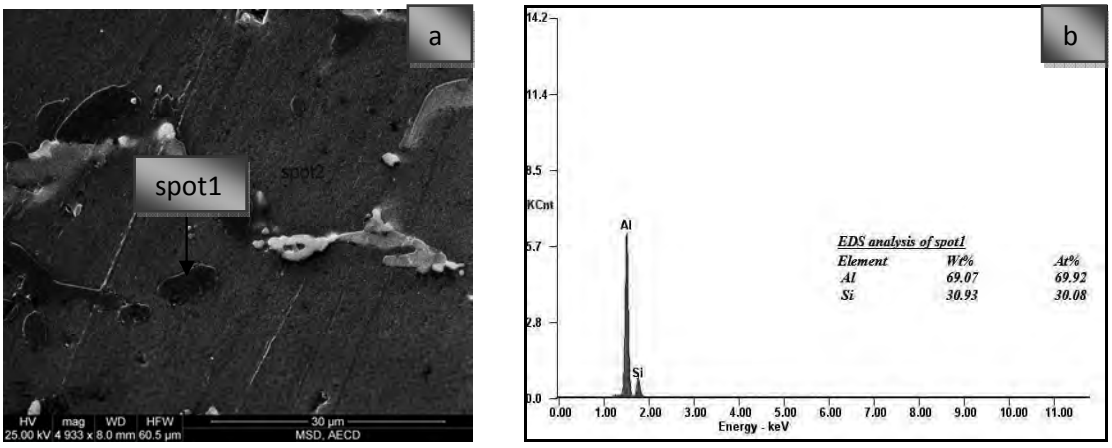

Figure 4.2.80: a) SEM micrograph of Alloy-7 after solution treatment at 540°C for 2 hours; b) The corresponding EDS spectra of spot1

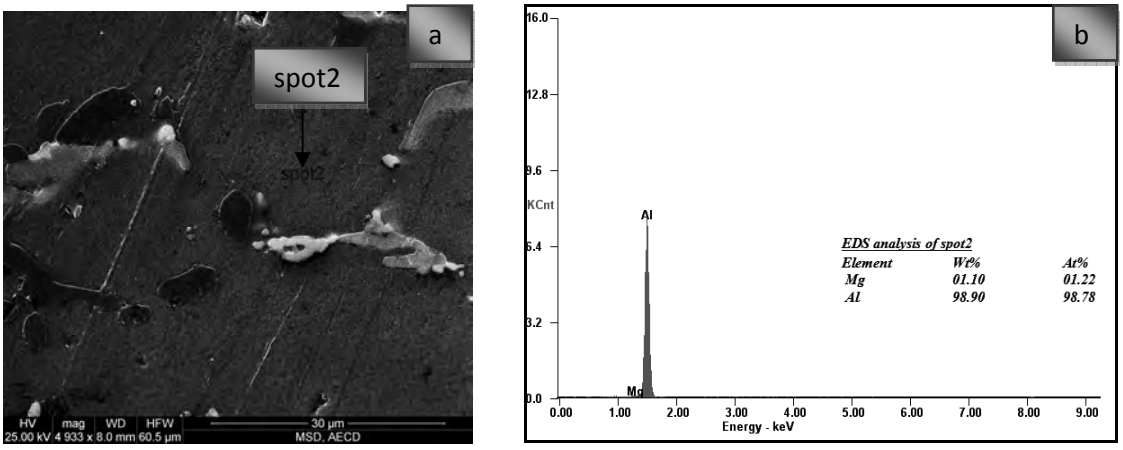

Figure 4.2.81: a) SEM micrograph of Alloy-7 after solution treatment at 540°C for 2 hours; b) The corresponding EDS spectra of spot2

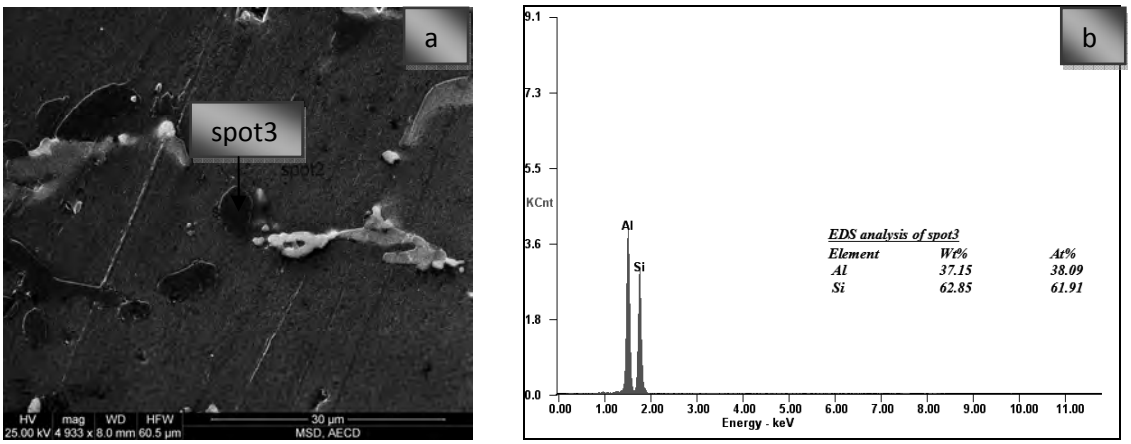

Figure 4.2.82: a) SEM micrograph of Alloy-7 after solution treatment at 540°C for 2 hours; b) The corresponding EDS spectra of spot3

4.2.7.3 Effect of Alloying and Peak Ageing on the Microstructures of Alloy-7

Figure 4.2.83 shows the microstructure of the peakaged Alloy-7. The matrix of the alloy shows the modified eutectic Al-Si and Al_3Ni eutectic and α-solid solution of Al. Cu in combination with Ni forms Cu-Ni aluminides, which are thermally stable and cannot be dissolved in the course of solution treatment. For this reason, a certain amount of Cu is found in intermetallic phases and is missing when it comes to the precipitation of secondary Al_2Cu phases during over aging. Thus, the contribution of precipitation hardening to the alloys' high temperature strength decreases. However, the number of thermally stable intermetallic phases increases, which leads to better interconnectivity of the eutectic network (contiguity).Therefore, all in all, the strength is only slightly increased, where upon it is noticeable that the addition of Ni becomes more inefficient at higher Cu concentrations.

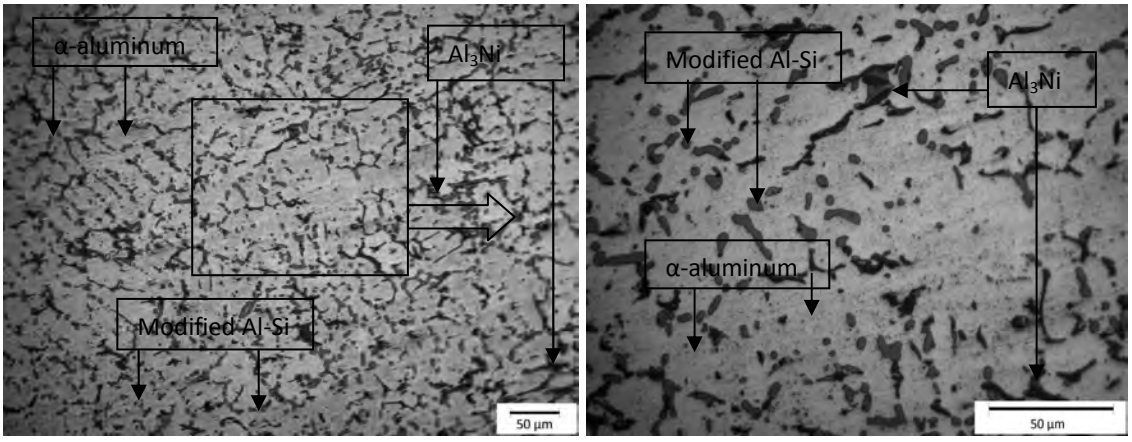

Figure 4.2.83: Optical micrographs of Alloy-7 after peakaged at 225°C for 1 hour showing modified Al-Si eutectic, Al3(Cu/Ni) and α-aluminum matrix

The full frame EDS analysis of the SEM image (Figure 4.2.84) indicates the Al, Si, Mg, Cu and Ni content intermetallics and precipitates.

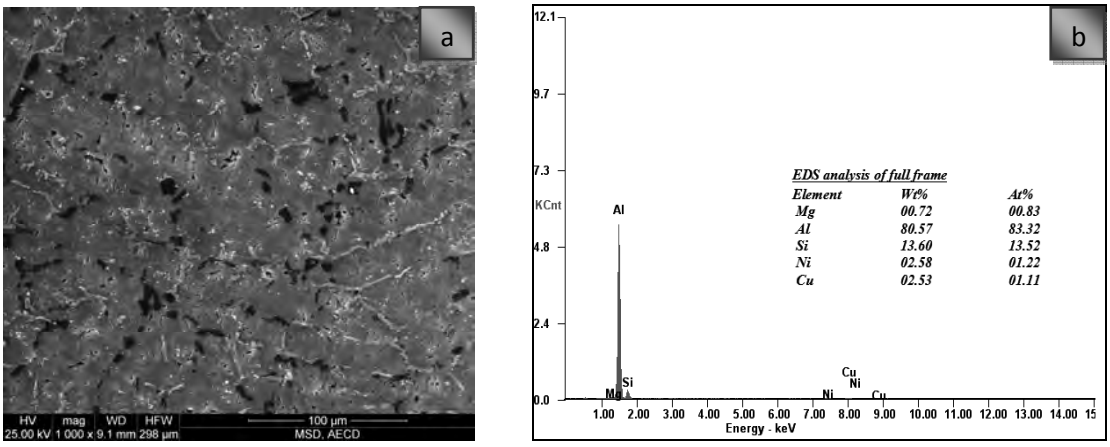

Figure 4.2.84: SEM micrograph of Alloy-7 after peakaged at 225°C for 1 hour showing modified Al-Si eutectic, Al_3Ni and α-aluminum matrix; b)The corresponding EDS spectrum of full frame

Figure 4.2.85 to Figure 4.2.88 show the characteristic of the intermetallic phases and some spots after solution treatment and peakaged. The complex eutectic mixture experienced fragmentation in the early stage of solution treatment, and a large number of individual particles were formed. EDS analysis revealed that the θ phase dissolved completely after solution treatment for 2 h at 540℃, whereas the γ phase was substituted by the Al_3Ni or Al_3CuNi phase. The EDS spectra of spot1 (Figure 4.2.85) and spot3 (Figure 4.2.87) indicate the modified Al-Si eutectics and spot2 (Figure 4.2.86) confirm the aluminium matrix with 1.13wt% of Mg. EDS analyses of spot4 (Figure 4.2.88) indicates the Al-Cu-Ni-Mg containing complex intermetallics.

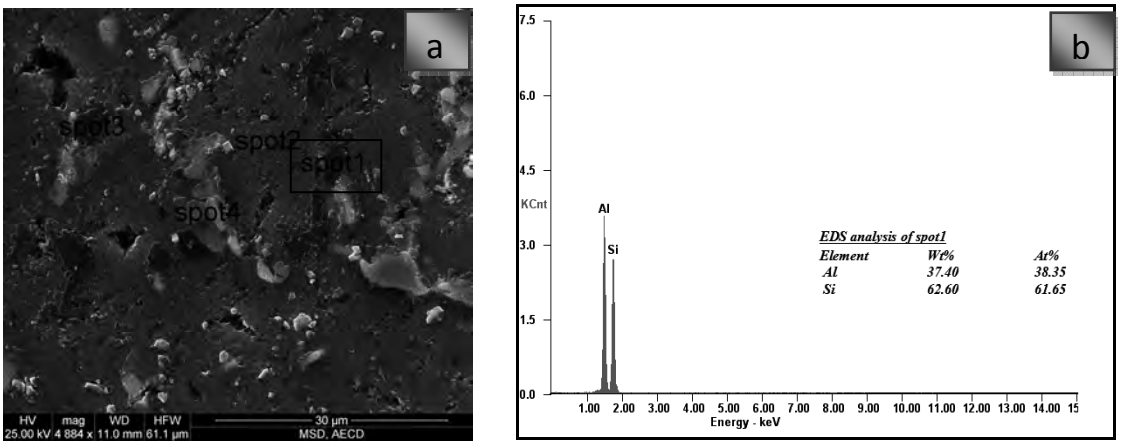

Figure 4.2.85: a) SEM micrograph of Alloy-7 after peakaged at 225°C for 1 hour; b) The corresponding EDS spectra of spot4

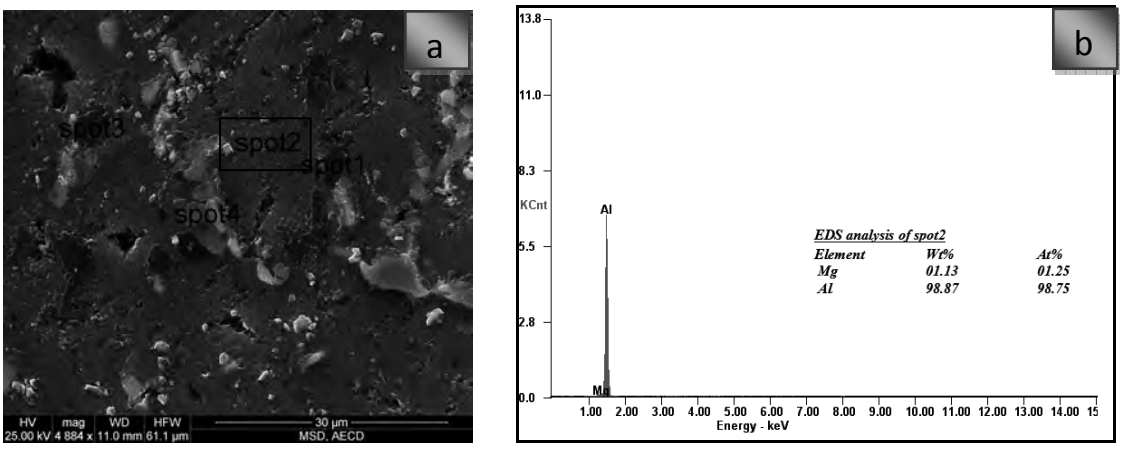

Figure 4.2.86: a) SEM micrograph of Alloy-7 after peakaged at 225°C for 1 hour; b) The corresponding EDS spectra of spot2

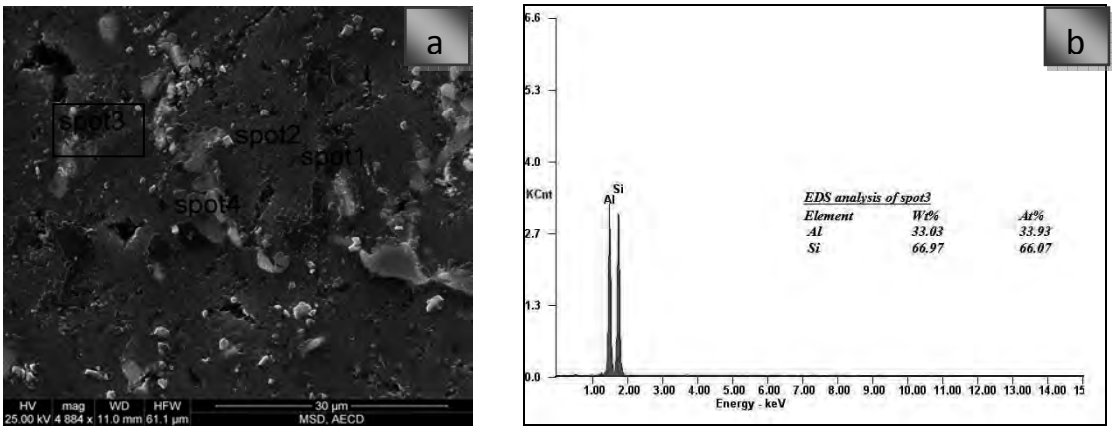

Figure 4.2.87: a) SEM micrograph of Alloy-7 after peakaged at 225°C for 1 hour; b) The corresponding EDS spectra of spot3

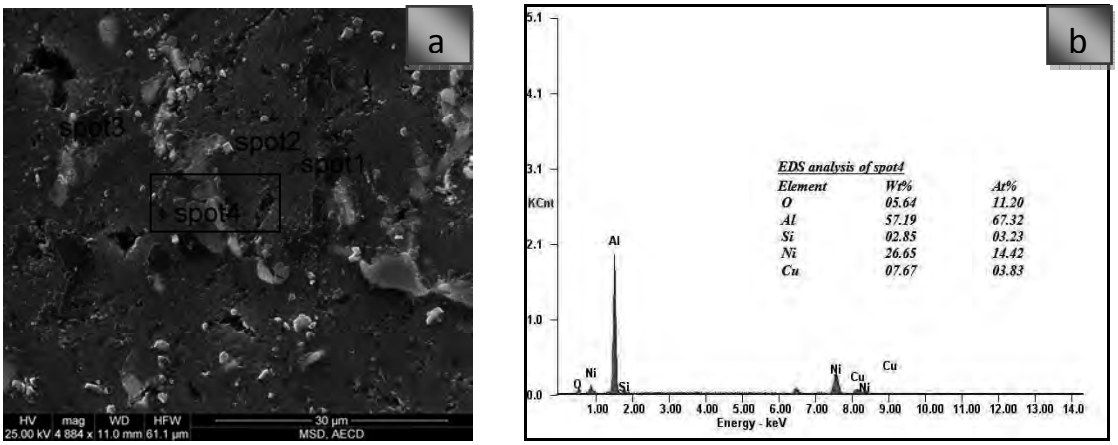

Figure 4.2.88: a) SEM micrograph of Alloy-7 after peakaged at 225°C for 1 hour; b) The corresponding EDS spectra of spot4

4.2.7.4 Effect of Alloying and Over Ageing on the Microstructures of Alloy-7

Figure 4.2.89 shows the microstructure of the solution treatment and overaged Alloy-7. The Ni phase in combination with eutectic Si forms a strongly interconnected three-dimensional structure, whose contiguity is strongly preserved even after overageing at 300^{o}C for 1h. It was found that after 2 hr of solution treatment at 540^{o}C and overaged at 300^{o}C for 1 hr, the flake-like and acicular eutectic silicon appear to be fragmented compared to the as cast sample. However, the particle distribution is widely in size between the flake-like and fine spherical particles. After 2 h of solution treatment, the eutectic silicon was clearly fragmented and more spherical as demonstrated in Figure 4.2.90. After overageing, the inter particle spacing was increased.

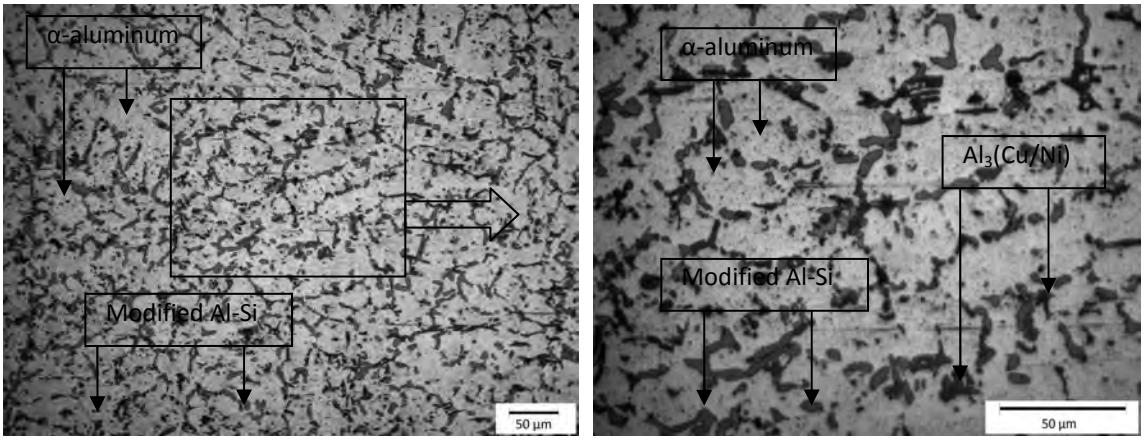

Figure 4.2.89: Optical micrograph of Alloy-7 after overaged at 300°C for 1 hour showing modified Al-Si, Al3(Cu/Ni) eutectic and α-aluminum matrix

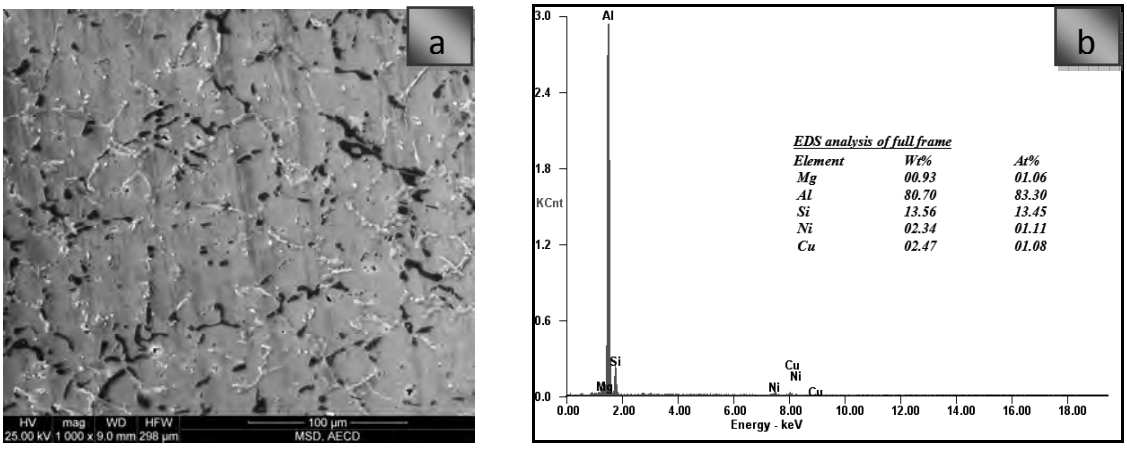

Figure 4.2.90: a) SEM micrograph of Alloy-7 after overaged at 300°C for 1 hour showing modified Al-Si eutectic, Al_3(Cu, Ni) and α-aluminum matrix; b) The corresponding EDS analysis of full frame

To study the complex eutectic mixture, EDS analysis using the scanning electron microscope (SEM) was carried out to identify the finer intermetallic compounds. The SEM results and EDS data shown in Figure 4.2.91, demonstrate that the intermetallic compound exhibited the Al_3(Ni,Cu) structure. A certain amount of solute was found dissolved in it, mainly Fe. The EDS analysis of spot1 (Figure 4.2.91) and spot3 (Figure 4.2.93) indicates the modified Al-Si eutectic where spot2 (Figure 4.2.92) is the α-aluminum matrix with 1.06wt% Mg. The corresponding spot4 (Figure 4.2.94) analysis indicates the Al-Cu-Fe-Ni-O content complex compounds.

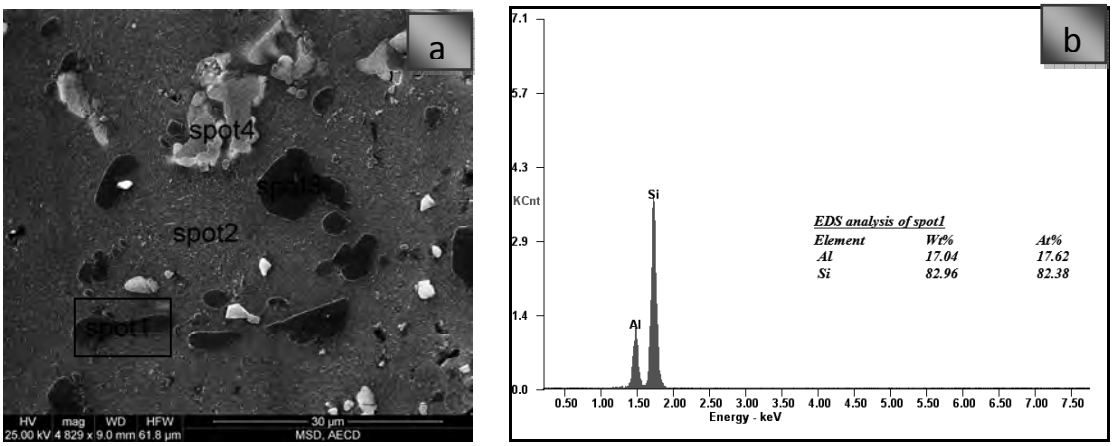

Figure 4.2.91: a) SEM micrograph of Alloy-7 after overaged at 300°C for 1 hour; b) The corresponding EDS spectra of spot1

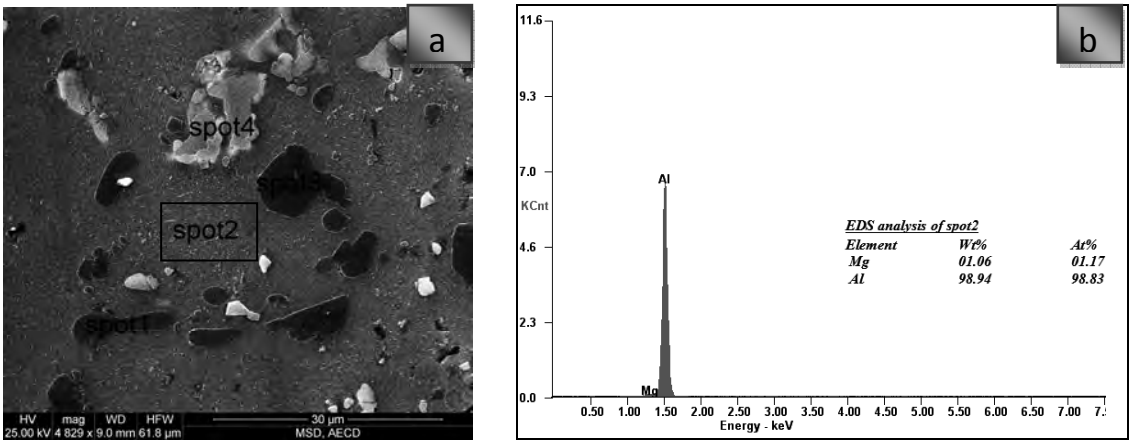

Figure 4.2.92: a) SEM micrograph of Alloy-7 after overaged at 300°C for 1 hour; b) The corresponding EDS spectra of spot2

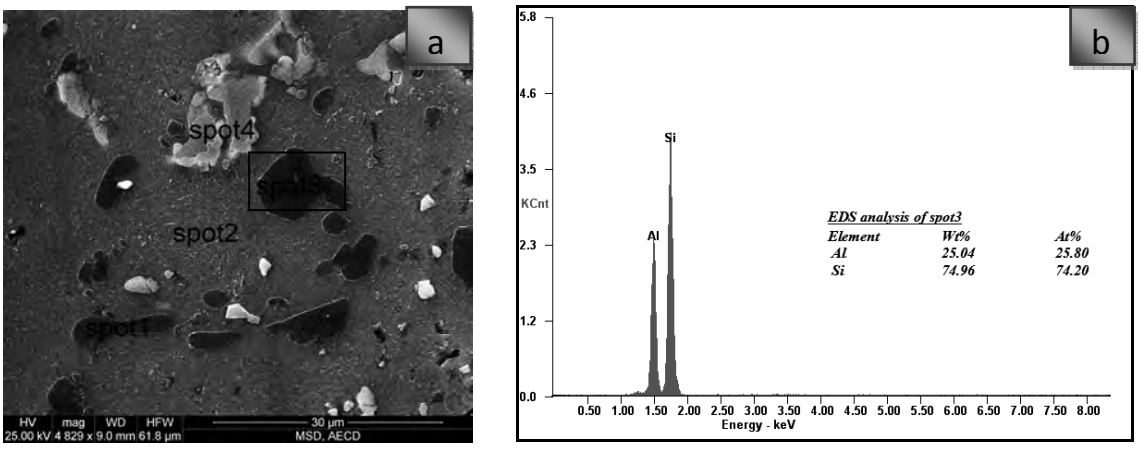

Figure 4.2.93: a) SEM micrograph of Alloy-7 after overaged at 300°C for 1 hour; b) The corresponding EDS spectra of spot3

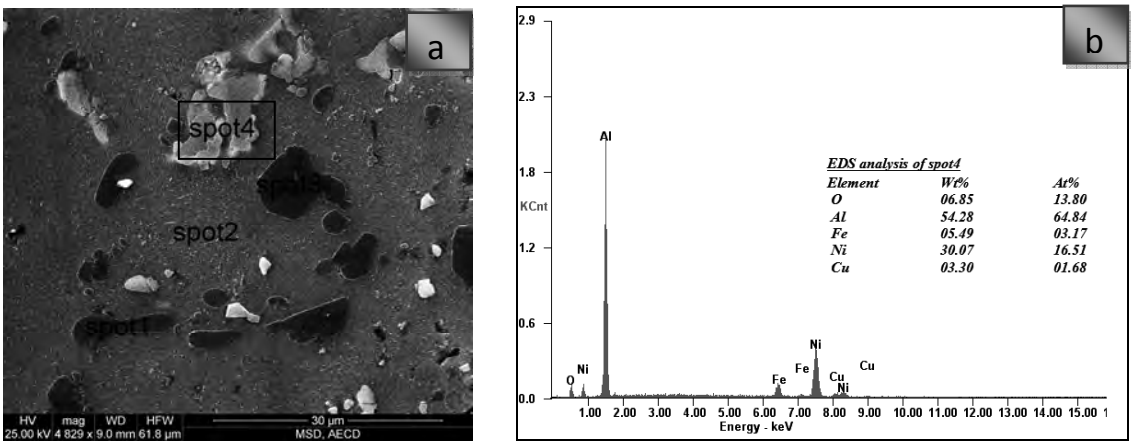

Figure 4.2.94: a) SEM micrograph of Alloy-7 after overaged at 300°C for 1 hour; b) The corresponding EDS spectra of spot4

4.3 Tensile Properties of the Alloys

For each alloy, tensile tests were conducted for six conditions, i.e. as solution treated, two underaged (1hr at 150^{o}C and 1hr at 200^{o}C), peakaged (1hr at 225^{o}C), and two overaged (1hr at 250^{o}C and 1hr at 300^{o}C) conditions. In solution treated condition, tensile tests were conducted to evaluate the solution strengthening contribution due to Mg, Cu and Ni. The age hardening trends for the alloys observed by the tensile tests are generally consistent with the observations in the hardness and resistivity tests. That is, all alloys show age hardening during artificial ageing.

The results of the tensile tests at room temperature are explained here. The tensile properties, UTS, Y.S and % elongation are extracted from the stress-strain curves for each alloy after solutionizing and artificial ageing. The results show the average values of the three repeats. The ultimate tensile strengths, yield strength (0.2% offset proof strengths) and percentage elongations were determined from the engineering stress vs. engineering strain curves. The results of the variation of ultimate tensile strength, yield strength and percentage elongation under various aging conditions of the Alloy-1 to Alloy-7 are shown in Figure 4.3.1 to Figure 4.3.6. The test values obtained at a common strain rate of testing $10^{-3}s^{-1}$ are used to plot the graphs. The peakaged (1hr at 225^{o}C) alloys were also tested other two strain rate of $10^{-2}s^{-1}$ & $10^{-4}s^{-1}$.

4.3.1 Effect of Ageing Temperature on Tensile Properties of Cu Content Al-6Si-0.5Mg Alloys

The tensile properties i.e. ultimate tensile strength (UTS), yield strength(YS) and percent elongation (%E) of different Cu content Al-6Si-0.5Mg alloys were shown in Figure 4.3.1, Figure 4.3.2 and Figure 4.3.3 respectively. These properties were evaluated at as-quenched and artificial ageing at 150, 200, 225, 250 and 300^{o}C. The strength of the alloys increases with the increase of Cu addition to Al-6Si-0.5Mg alloy and ageing temperature. Maximum strength was found for 2wt% Cu addition to Al-6Si-0.5Mg alloy (Alloy-4) and ageing at 225^{o}C and the ductility pass through minima.

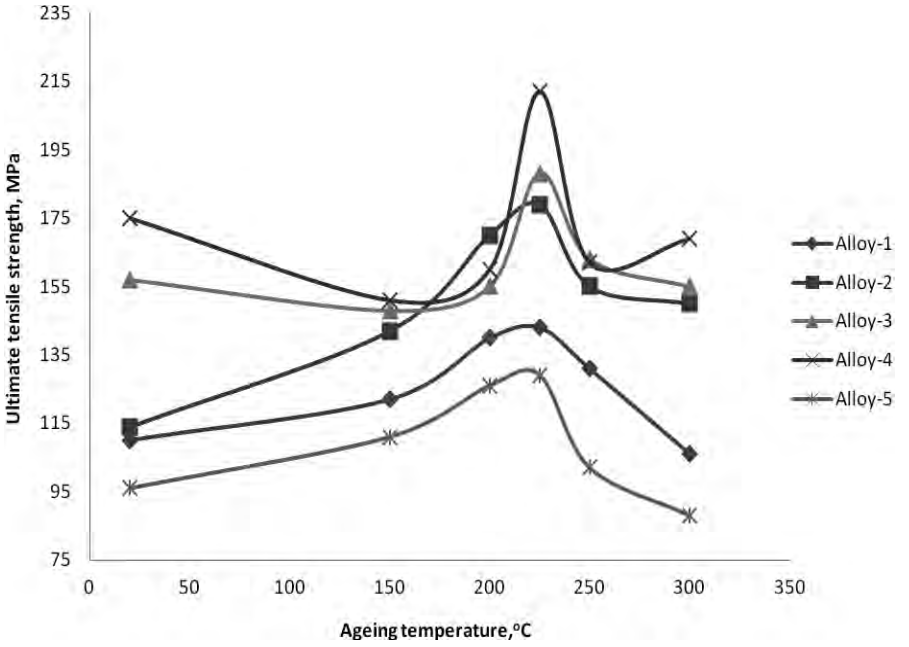

Figure 4.3.1: Evolution of ultimate tensile strength with ageing temperature of various Cu content alloys (Alloys 1 - 5) at a strain rate of $10^{-3}s^{-1}$

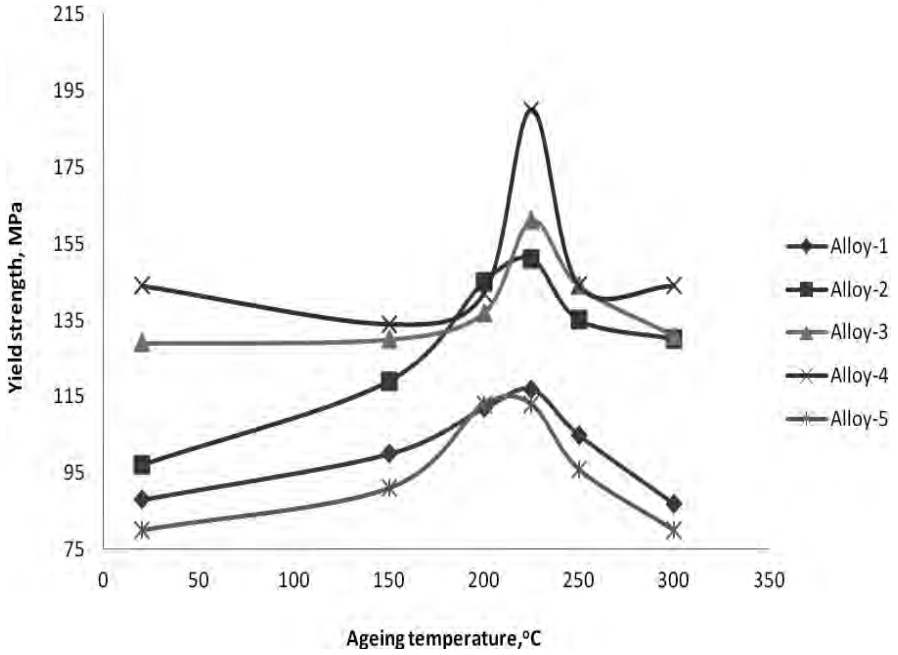

Figure 4.3.2: Evolution of yield strength with ageing temperature of various Cu content alloys (Alloys 1 - 5) at a strain rate of $10^{-3}s^{-1}$

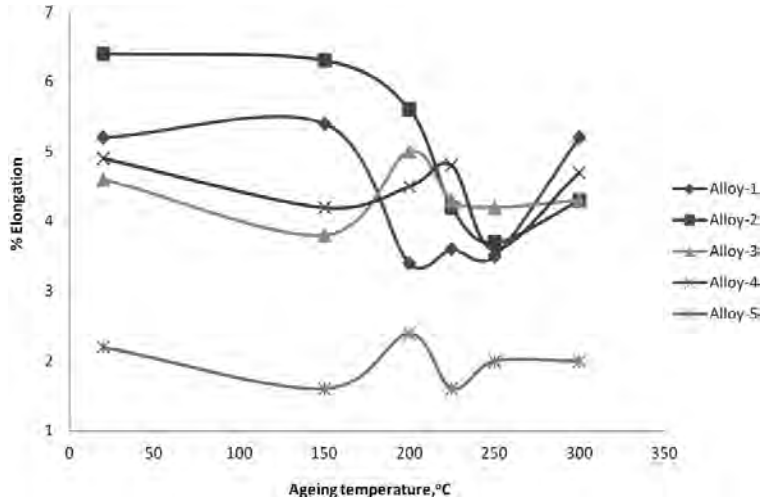

Figure 4.3.3: Evolution of ductility (%elongation) with ageing temperature of various Cu content alloys (Alloys 1 - 5) at a strain rate of $10^{-3}s^{-1}$

4.3.2 Effect of Ageing Temperature on Tensile Properties of Cu or/and Ni Content Al-6Si-0.5Mg Alloys

The results obtained during tensile tests show the ultimate tensile strength, yield strength and percentage elongation are affected by ageing (Figure 4.3.4 to Figure 4.3.6).

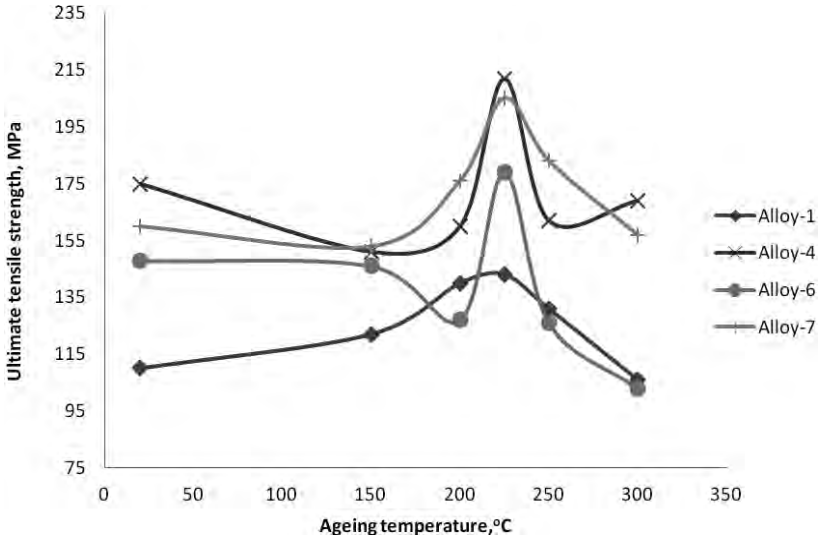

Figure 4.3.4: Evolution of ultimate tensile strength with ageing temperature of Cu and/Ni content alloys at a strain rate of $10^{-3}s^{-1}$

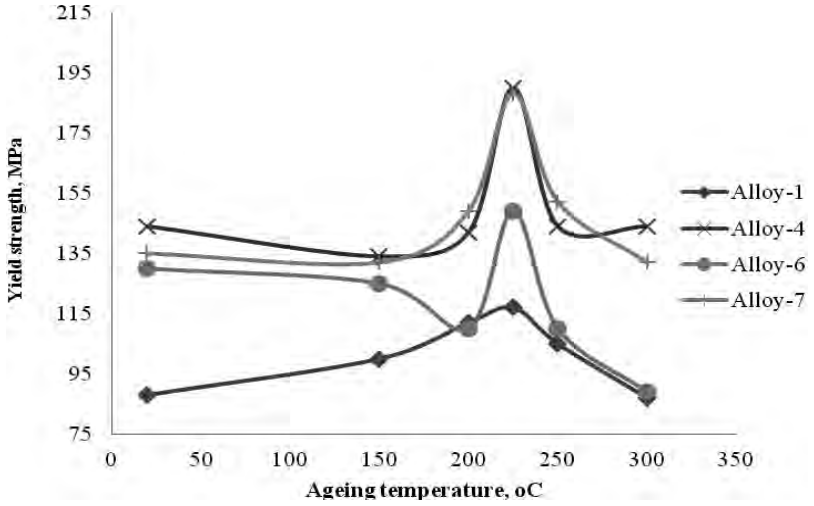

Figure 4.3.5: Evolution of yield strength with ageing temperature of Cu and/or Ni content alloys at a strain rate of $10^{-3}s^{-1}$

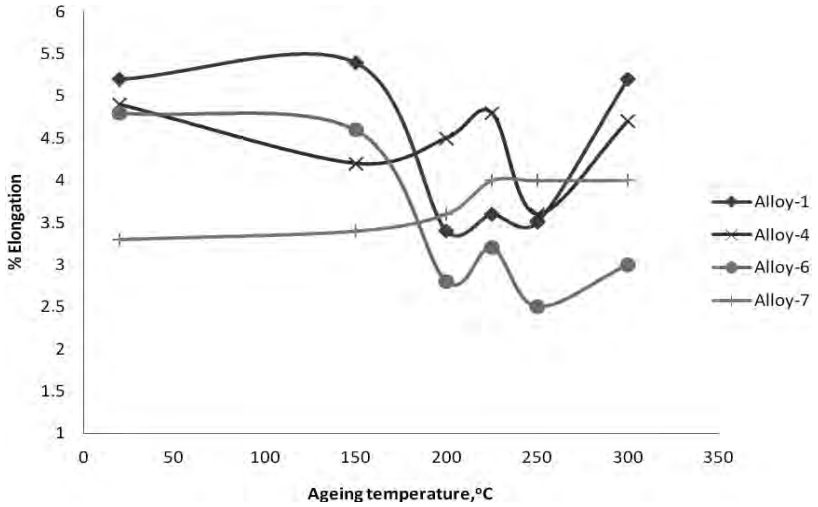

Figure 4.3.6: Evolution of ductility (%elongation) with ageing temperature of Cu and/or Ni content alloys at a strain rate of $10^{-3}s^{-1}$

During artificial ageing, the yield and ultimate tensile strengths were found to increase with ageing temperature; the maximum being attained at peak aged condition. Ductility of the alloys, on the other hand decreased with ageing temperature reaching the minimum at the peak strength. From the experimental results it is clear that Alloy-4 show maximum strength ageing at 225^{o}C. This ageing condition, Alloy-7 tensile strength is very close to Alloy-4. The ductility maximum drops at peakaged of Alloy-6. The addition of only 2wt%Cu into Al-6Si-0.5Mg alloy resulted in increase the better tensile properties.

4.3.3 Tensile Properties at Thermal Treated Conditions

4.3.3.1 Tensile Properties at Solution Treated Condition (Room Temperature)

Mechanical property data from tensile testing of solution treated specimens in the as-quenched condition and the results of the tensile tests of the alloys at room temperature are given in Figure 4.3.7. The tensile properties i.e. UTS, YS and % elongation are extracted from the strain–stress curves for each alloy at different ageing temperatures for 1 hour. The results show the average values of the three repeat tests.

Alloy-1 has UTS of 110 MPa and a YS of 88 MPa. The Cu additions have a significant effect on the solutionizing strength of the Al-6Si-0.5Mg alloy as the UTS and YS of the Alloy-2, Alloy-3 and Alloy-4 are 114 MPa and 97 MPa, 157 MPa and 129MPa, and 175 MPa and 144 MPa respectively. Among the alloys, Alloy-4 has the highest yield strength of 144 MPa (Figure 4.3.7). Its UTS (175 MPa) is higher than of the rest alloys (Figure 4.3.7), mainly due to the optimum Cu addition.

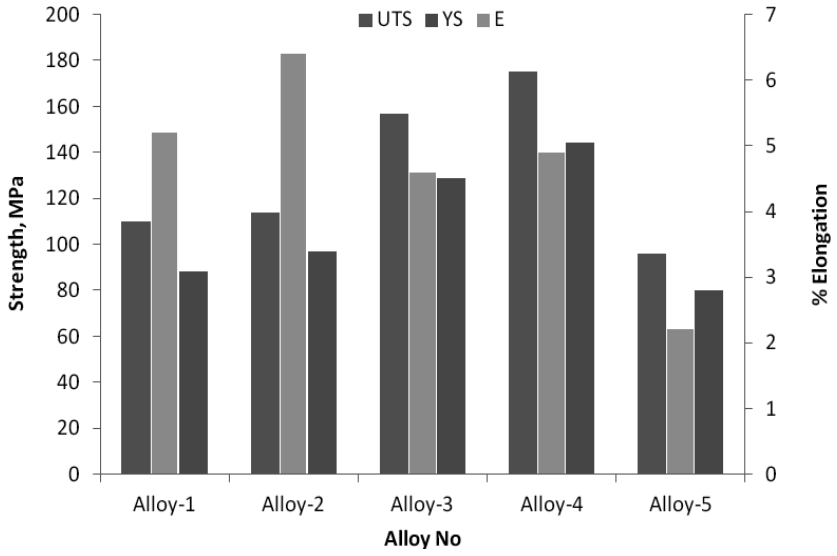

Figure 4.3.7: UTS, YS and %E of Alloys 1-5 at solution treated condition

The % elongation values at solution treated condition are 5.2 (Alloy-1), 6.4 (Alloy-2), 4.6 (Alloy-3), 4.9(Alloy-4) and 2.2% (Alloy-5) (Figure 4.3.7). The addition of 0.5%wt.Cu (Alloy-2) seems to have a positive effect on the ductility on the Al-6Si-0.5Mg alloy (Alloy-1) at solutionized and quenched state. 1- 4 %wt. Cu additions to Al-6Si-0.5Mg alloy have markedly

reduced the elongation at solution treated and quenched condition for the rest alloys (Alloy-2 to Alloy-5). One reason for this could be the increased amount of microporosity with additions of Cu, although microporosity studies have not been performed yet. Secondly, the Cu additions may have formed brittle second phases that influence the crack initiation and cause early fracture.

From the experimental results (Figure 4.3.8) it is clear that the Cu and/or Ni added Al-6Si-0.5Mg alloys (Alloys 4, 6 and 7) show better strengths (UTS and YS) than Cu and Ni free alloy (Alloy-1). It can be observed that addition of 2wt% Cu (Alloy-4) to the Al-6Si-0.5Mg alloy has a better UTS of 175 MPa and YS of 144 MPa than addition of 2wt% Ni (Alloy-6). The highest values of strength were obtained for Alloy-4 at solution treated condition. The strength of Alloy-4 has better strength than both the Alloy-6 (UTS: 148 MPa and YS: 130 MPa) and the Alloy-7 (UTS: 160 MPa and YS: 135 MPa).

Figure 4.3.8 shows the variation of percent elongation with Cu and/or Ni content at solutionized and quenched condition. Moderate elongation is found at this solution treated and quenched condition for all alloys. Alloy-1 shows the maximum ductility than others. The ductility (4.9%) of 2wt. %Cu containing alloy (Alloy-4) and the ductility (4.8%) 2wt. %Ni containing alloy (Alloy-6) were about same at solution treated condition. The percent elongation (3.3%) of 2 wt% Cu and 2 wt % Ni containing alloy (Alloy-7) has lower than other alloys (1, 4 and 6).

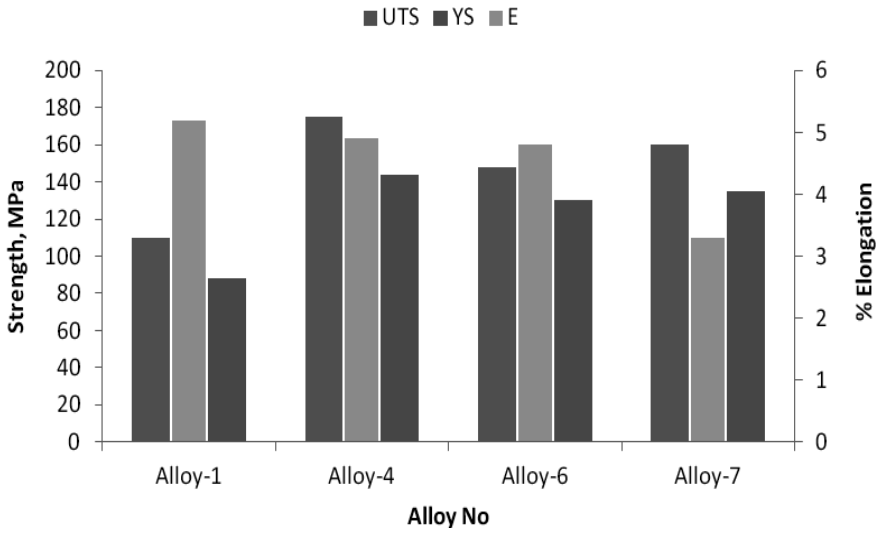

Figure 4.3.8: UTS,YS and %E of the Alloys 1, 4, 6 and 7 at solution treated condition

4.3.3.2 Tensile Properties of Alloys Aged for 1 hour at 150°C

The results of the tensile tests at 150°C are given in Figure 4.3.9. The data show the average values of the three repeat tests. It can be seen that the strength values ageing at 150°C of Alloy-3 (Except YS) (UTS: 148 MPa and YS: 130 MPa) and Alloy-4 (UTS: 151 MPa and YS: 134 MPa) are lower than the solutionized and quenched state values. It is noted that aged at 150°C, the Alloy-5 has the lowest UTS (111 MPa) and YS (91 MPa). The Alloy-2, Alloy-3 and Alloy-4 have the higher UTS of 142, 148 and 151 MPa and YS of 119, 130 and 134 MPa than the Alloy-1 and Alloy-5. Alloy-4 has the highest strength aged at 150°C, with a UTS of 151 MPa and YS of 134 MPa.

The Alloy-1 and Alloy-2 have about similar elongation at solution treated and ageing at 150°C for 1 hour (Figure 4.3.9). On the other hand, the Alloy-3 and Alloy-4 seem to lower the % elongation (3.8% and 4.2%) values than the Alloy-1 and Alloy-2 (5.4% and 6.3%). Alloy-5 has the lowest elongation (1.6%) among the investigated alloys ageing at 150°C for 1 hour. Therefore, aged at 150°C the Cu addition does not seem to positive affect the elongation very much. When a high ductility is desired, the Alloy-2 (0.5wt% Cu) seems the best candidate whereas the Alloy-4 offers the highest strength at 150°C.

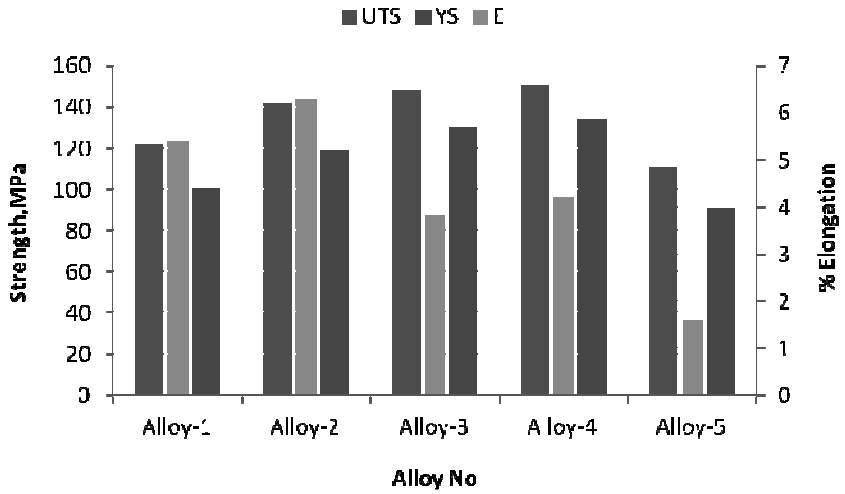

Figure 4.3.9: UTS, YS and %E of the Alloys 1 - 5 aged at 150°C

From the Figure 4.3.10, it is clear that the Cu and /or Ni added alloys (Alloy-4, Alloy-6 and Alloy-7) show the better strength (UTS and YS) than Cu and Ni free alloy (Alloy-1). It can be observed that Alloy-4 has a better UTS of 151 MPa and YS of 134 MPa than Alloy-6. Alloy-4

(UTS: 151 MPa and YS: 134 MPa) and Alloy-7 (UTS: 153 MPa and YS: 132 MPa) have the highest values of strength were obtained ageing at 150^{o}C for 1 hour. The strength of Alloy-6 has better strength (UTS: 146 MPa and YS: 125 MPa) than the Alloy-1 (UTS: 122 MPa and YS: 100 MPa).

Figure 4.3.10 also shows the variation of percent elongation with Cu and/or Ni content Al-6Si-0.5Mg alloys aged at 150^{o}C. Cu and Ni free alloy (Alloy-1) has the maximum elongation aged at 150^{o}C over the alloys of aged at 150^{o}C. The ductility (4.2%) of Alloy-4 and the ductility (4.6%) of Alloy-6 were higher than the ductility (3.4%) of Alloy-4. Alloy-6 shows the highest ductility among the Cu or/Ni content Al-6Si-0.5Mg alloys under investigation.

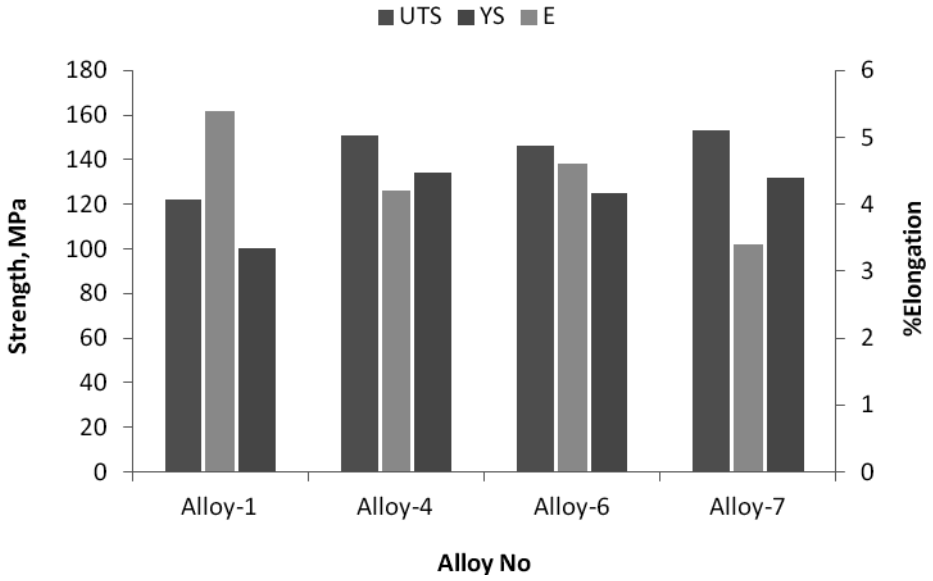

Figure 4.3.10: UTS, YS and %E of the Alloys 1, 4, 6 and 7 aged at 150^{o}C

4.3.3.3 Tensile Properties of Alloys Aged for 1 hour at 200^{o}C

The results of the tensile tests at 200°C are given in Figure 4.3.11. It can be seen that the strength values ageing at 200^{o}C of Cu free Alloy-1 (UTS: 140 MPa and YS: 112 MPa), Alloy-2 (UTS: 170 MPa and YS: 145 MPa), Alloy-3 (UTS: 155 MPa and YS: 137 MPa), Alloy-4 (UTS:160 MPa and YS: 142 MPa) and Alloy-5 (UTS: 126 MPa and YS: 113 MPa) are higher than the solutionized and as-quenched and aged at 150^{o}C values. It is noted that at 200°C, the Alloy-5 has the lowest UTS (126 MPa) and YS (113 MPa) among the Cu containing alloys. The Cu-containing Alloy-2, Alloy-3 and Alloy-4 have the higher UTS and YS than the Cu free

Alloy-1 and Alloy-5. Alloy-2 gives the highest strength aged at 200°C, with a UTS of 170 MPa and YS of 145 MPa.

Alloy-1 and Alloy-2 have lower elongation aged at 200^{o}C than as-quenched and aged at 150^{o}C for 1 hour (Figure 4.3.3). On the other hand, the Alloy-3 and Alloy-5 seem to higher the % elongation (5% and 2.4%) values over the as-quenched and aged at 150^{o}C. The ductility of the Alloy-4 decreases than the as quenched condition but increases the previous treatment (1 hr at 150^{o}C). Alloy-5 has the lowest elongation (2.4%) among the examined alloys aged at 200^{o}C but it (2.4%) is the maximum elongation for this alloy all over the thermal treatments. Therefore, aged at 200°C the Cu addition does not seem to positive affect the elongation very much.

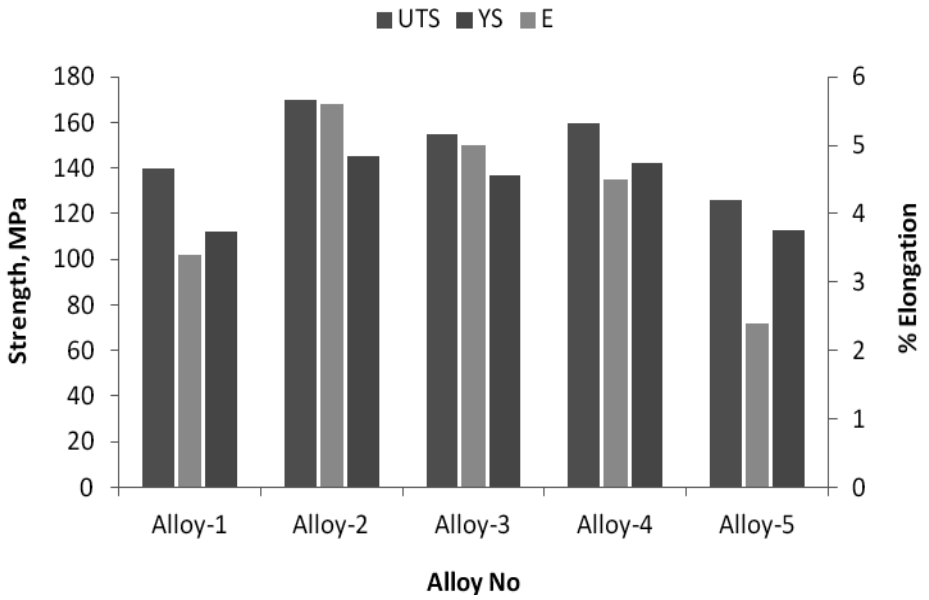

Figure 4.3.11: UTS,YS and %E of the Alloys 1-5 aged at 200^{o}C

From the experimental results (Figure 4.3.12), the strength of Alloy-4 (UTS: 160 MPa and YS: 142 MPa) and Alloy-7 (UTS: 176 MPa and YS: 149 MPa) are higher than the strength of Alloy-1 (UTS: 140 MPa and YS: 112 MPa) and Alloy-6 (UTS: 127 MPa and YS: 110 MPa). It can be observed that Alloy-7 has a better UTS of 176 MPa and YS of 149 MPa Alloy-6 (UTS: 127 MPa and YS: 110 MPa) and Alloy-4 (UTS: 160 MPa and YS: 142 MPa). Alloy-6 (UTS: 127 MPa and YS: 110 MPa) has the lowest values of tensile strength were obtained ageing at 200^{o}C for 1 hour. Alloy-1 has better strength (UTS: 140 MPa and YS: 112 MPa) than the Alloy-6.

Figure 4.3.12 also shows the variation of percent elongation of Cu and/or Ni content Alloy-1, 4, 6 and 7 aged at 200^{o}C. Alloy-4 has the maximum elongation over the alloys ageing at 200^{o}C. The ductility (4.5%) of Alloy-4 and the ductility (3.6%) Alloy-7 has higher than the ductility (2.8%) of Alloy-6 and Alloy-1.

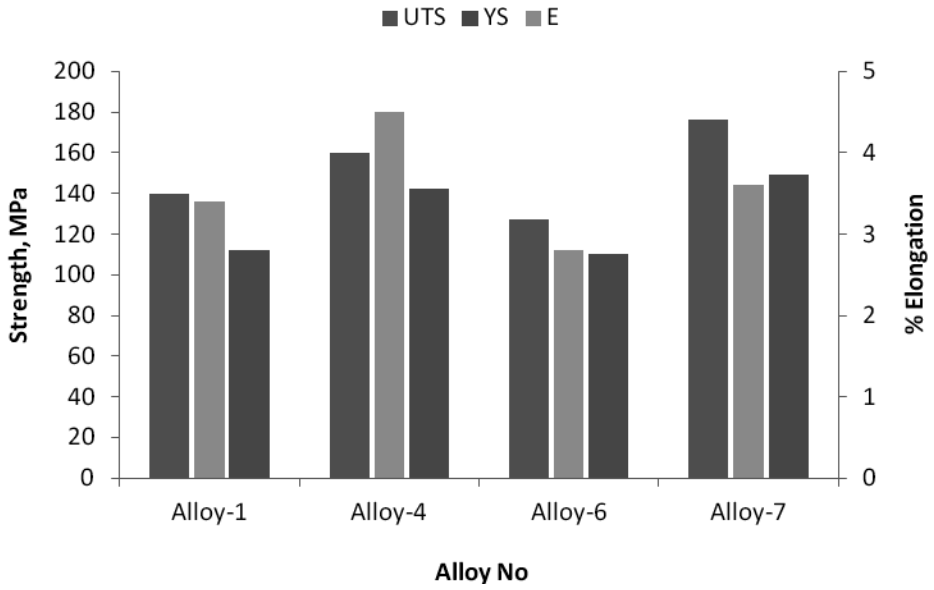

Figure 4.3.12: UTS,YS and %E of the Alloy-1, 4, 6 and 7 aged at 200^{o}C

4.3.3.4 Tensile Properties of Alloys Aged for 1 hour at 225^{o}C

It can be seen (Figure 4.3.1) that the tensile strength values aged at 225^{o}C of the alloys are higher than all over the ageing conditions. It is noted (Figure 4.3.13) that at 225°C, the 4wt% Cu containing Alloy-5, has the lowest UTS (129 MPa) and YS (113 MPa) among the Cu content alloys. But the other Cu containing Alloy-2, Alloy-3 and Alloy-4 have the highest UTS of 179, 188 and 212 MPa and YS of 151, 161 and 190 MPa than the other thermal treatment. The Alloy-4, 2wt.%Cu addition to Al-6Si-0.5Mg give the highest strength at 225°C, with a UTS of 212 MPa and YS of 190 MPa. So ageing at 225^{o}C, 2wt% Cu addition to Al-6Si-0.5Mg is most effective in the case of strengthening.

Figure 4.3.13 also shows the % elongation values at peakaged condition: 3.6 (Alloy-1), 4.2 (Alloy-2), 4.3 (Alloy-3), 4.8 (Alloy-4) and 1.6% (Alloy-5). The addition of 2wt% Cu seems to have a positive effect on the ductility of the Al-6Si-0.5Mg alloy at the peakaged condition. The 0.5, 1 and 4 %wt. Cu additions to the Al-6Si-0.5Mg alloy have markedly reduced the elongation

aged at 225°C. Ageing at 225°C, Alloy-4 has the highest ductility and Alloy-5 (4wt% Cu) has the lowest ductility among the investigated Cu content alloys. The 4 wt% Cu additions have formed more brittle second phases that influence the crack initiation and cause early fracture.

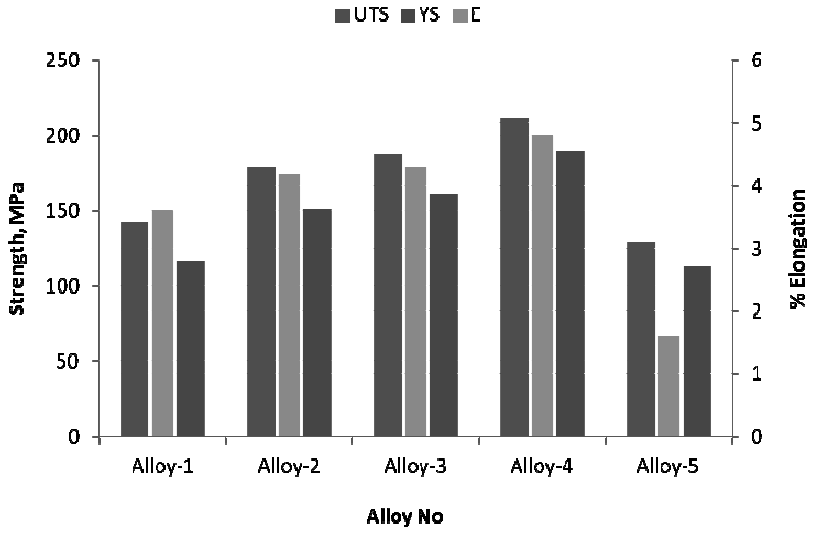

Figure 4.3.13: UTS,YS and %E of Alloys 1 - 5 aged at 225°C

The tensile properties of Cu and/or Ni added alloys (Alloy-4, Alloy-6 and Alloy-7) are presented in Figure 4.3.14. Alloy-4 and Alloy-7 show better strength (UTS and YS) than Alloy-1 and Alloy-6. It can be observed that Alloy-4 has a better strength (UTS: 212 MPa and YS: 190 MPa) than Alloy-6 (UTS of 179 MPa and YS of 149 MPa) and Alloy-7 (UTS: 205 MPa and YS: 188 MPa). Alloy-6 (UTS: 179 MPa and YS: 149 MPa) has higher value of strength than Alloy-1 (UTS: 143 MPa and YS: 117 MPa) aged at 225°C.

The % elongation values at 225°C (Figure 4.3.14) are 3.6 (Alloy-1), 4.8 (Alloy-4), 3.2 (Alloy-6) and 4% (Alloy-7). 2wt% Ni addition alone (Alloy-6) seems to have a negative effect on the ductility on Alloy-1. The ductility of Alloy-6 is close to the Alloy-1, where as the Alloy-7 has lower elongation but still better than the Alloy-1 and Alloy-6. From these results, it can be stated that aged at 225°C the individual and combined addition of 2wt%Cu and 2wt%Ni to the Al-6Si-0.5Mg (Alloy-1) are less detrimental for the elongation values than the other ageing conditions. Alloy-4 (2 wt% Cu) addition to Alloy-1 has a great effect on the increasing ductility among the investigated alloys.

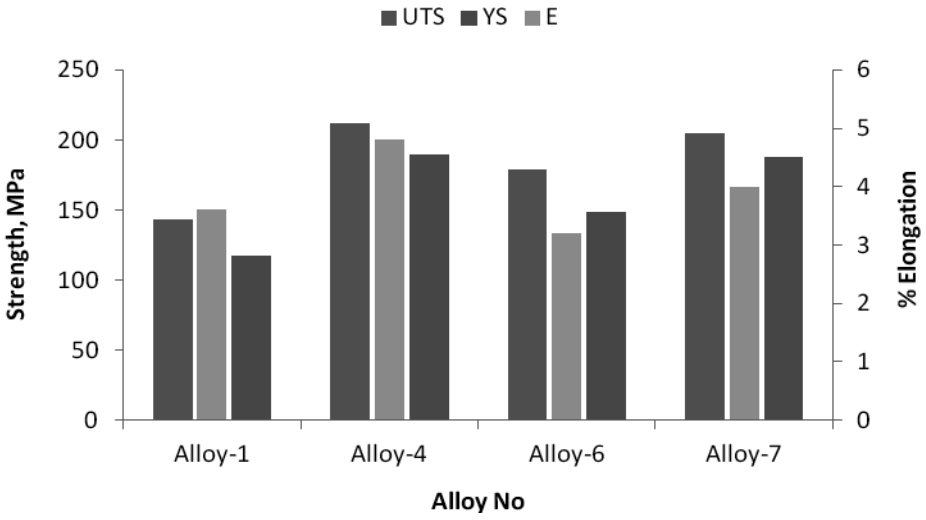

Figure 4.3.14: UTS,YS and %E of Alloys 1, 4, 6 and 7 aged at 225^{o}C

4.3.3.5 Tensile Properties of Alloys Aged for 1 hour at 250^{o}C

The results of the tensile tests at 250°C are shown in Figure 4.3.15. It can be seen that the strength values and elongations are lower than the tensile properties at 225°C. At 250°C, the alloy-1 has UTS of 131 MPa and a YS of 105 MPa. The UTS and YS of Alloy-2, Alloy-3 and Alloy-4 are 155 MPa and 135 MPa, 163 MPa and 144 MPa and 162 and 144 MPa respectively. Alloy-3 and Alloy-4 have better strength than other Cu containing alloys.

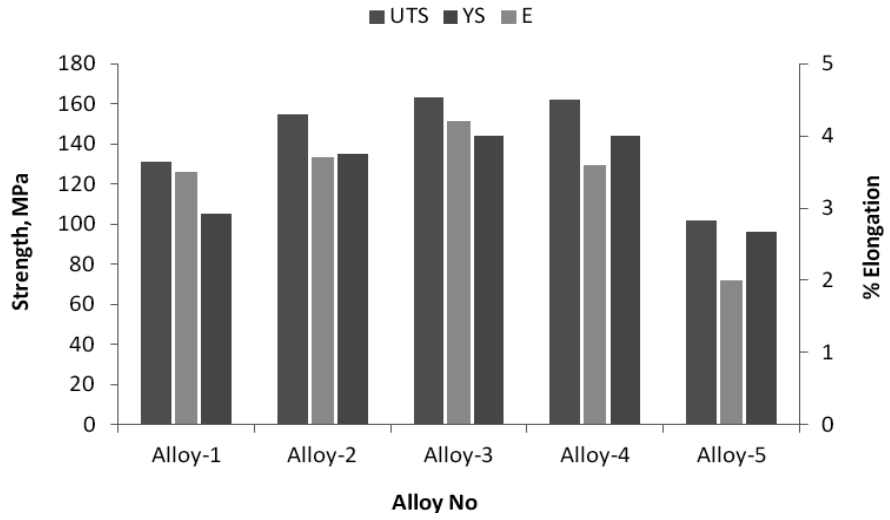

Figure 4.3.15: UTS,YS and %E of Alloys 1 - 5 aged at 250^{o}C

The % elongation values at 250°C (Figure 3.4.15) are: 3.5 (Alloy-1), 3.7 (Alloy-2), 4.2 (Alloy-3), 3.6 (Alloy-4) and 2% (Alloy-5). The 1wt% Cu addition seems to have significant effect on the ductility on the Al-6Si-0.5Mg alloy. The ductility value of Alloy-2 and Alloy-4 are very close to the Alloy-1, whereas the Alloy-5 has lower elongation. Alloy-3 has better ductility than the other alloys at 250^{o}C. This could be due to the increased of Cu-containing phases, which are harder but more brittle than the other phase.

Figure 4.3.16 shows that Cu and/or Ni added alloys (Alloys-4, 6 and 7) show better strength (UTS and YS) than Cu and Ni free alloy (Alloy-1). It can be observed that addition of 2wt% Cu and 2wt% Ni (Alloy-7) has a better UTS of 183 MPa and YS of 152 MPa than the addition of only 2wt% Ni (Alloy-6) or only 2 wt% Cu (Alloy-4). When aged at 250^{o}C for 1 hour, Alloy-4 (UTS: 162 MPa and YS: 144 MPa) has the higher values of strength than Alloy-1 and Alloy-6. The strengths of Alloy-6 and Alloy-1 have about equal UTS (131 and 126 MPa) and YS (105 and 110 MPa).

The variation of percent elongation with Cu and/or Ni addition is shown in Figure 4.3.16. The elongation values are 3.5 (Alloy-1), 3.6 (Alloy-4), 2.5 (Alloy-6) and 4% (Alloy-7). Alloy-7 has the maximum elongation. The ductility of 2wt. %Cu containing alloy (Alloy-4) and the ductility of Cu and Ni free alloy (Alloy-1) are about same but higher than the ductility (2.5) of 2wt% Ni containing alloy (Alloy-6).

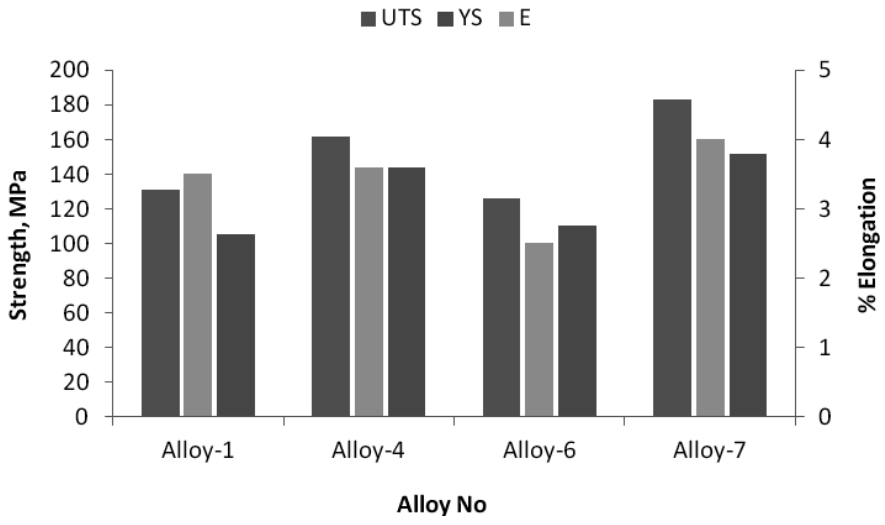

Figure 4.3.16: UTS, YS and %E of the Alloys 1, 4, 6 and 7 aged at 250^{o}C

4.3.3.6 Tensile Properties of Alloys Aged for 1 hour at 300°C

The results of the tensile tests of alloys aged for 1 hour at 300°C are given in Figure 4.3.17. It can be seen that the strength values of Alloy-1 (UTS: 106 MPa and YS: 87 MPa), Alloy-2 (UTS: 150 MPa and YS: 130 MPa), and Alloy-3 (UTS: 155 MPa and YS: 131 MPa), Alloy-4 (UTS: 169 MPa and YS: 144 MPa) and Alloy-5(UTS: 88 MPa and YS: 80 MPa) are lower than the peakaged condition values. Alloy-5 has the lowest UTS (88 MPa) and YS (80 MPa) among the alloys. The Alloy-4 has the highest UTS of 169 MPa and YS of 144 MPa than the other alloys.

Figure 4.3.17 shows that Alloy-2 and Alloy-3 have similar elongation (4.3%) values. On the other hand, the Alloy-4 has lower % elongation (4.3%) values than the Alloy-1 (5.2%). Alloy-5 has the lowest elongation (2%) among the alloys overaged at 300°C for 1 hour. Therefore, at 300°C the Cu addition does not seem to positive affect the elongation. When a high ductility is desired, Alloy-1 seems the best candidate whereas the Alloy-4 offers the highest strength ageing at 300°C

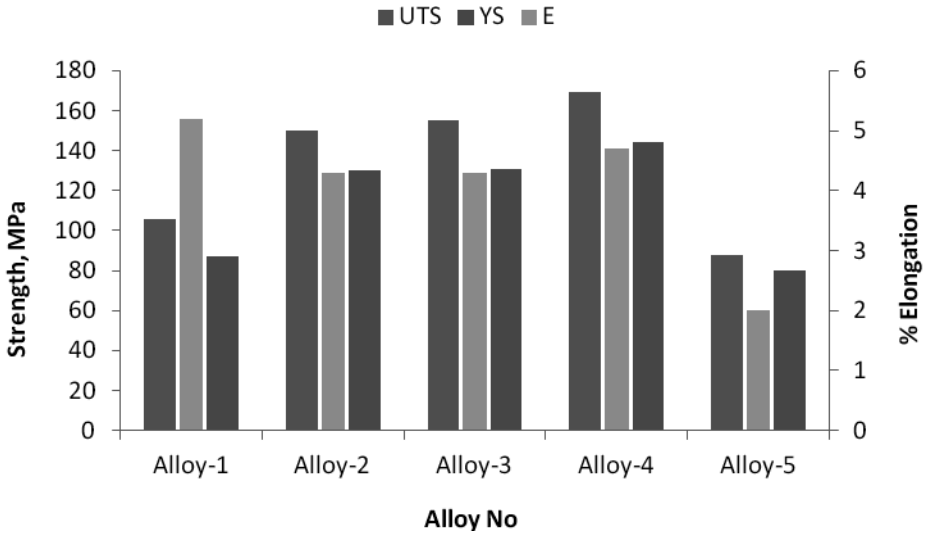

Figure 4.3.17: UTS, YS and %E of Alloys 1 - 5 aged at 300°C

The Cu and/or Ni added alloys (Alloy-4 and Alloy-7) show better strength (UTS and YS) than Alloy-1 and Alloy-6 (Figure 4.3.18). It can be observed that Alloy-4 has a better UTS of 169 MPa and YS of 144 MPa than Alloy-6 (UTS: 103 MPa and YS: 89 MPa) and Alloy-7 (UTS: 157 MPa and YS: 132 MPa). Alloy-4 has the highest values of strength among the alloys.

Figure 4.3.18 also shows the % elongation values of Alloy-4 (4.7%) and Alloy-7 (4%) are lower than those of Alloy-1 (5.2%) and Alloy-6 (3%). Alloy-6 has the minimum elongation among the investigated alloys.

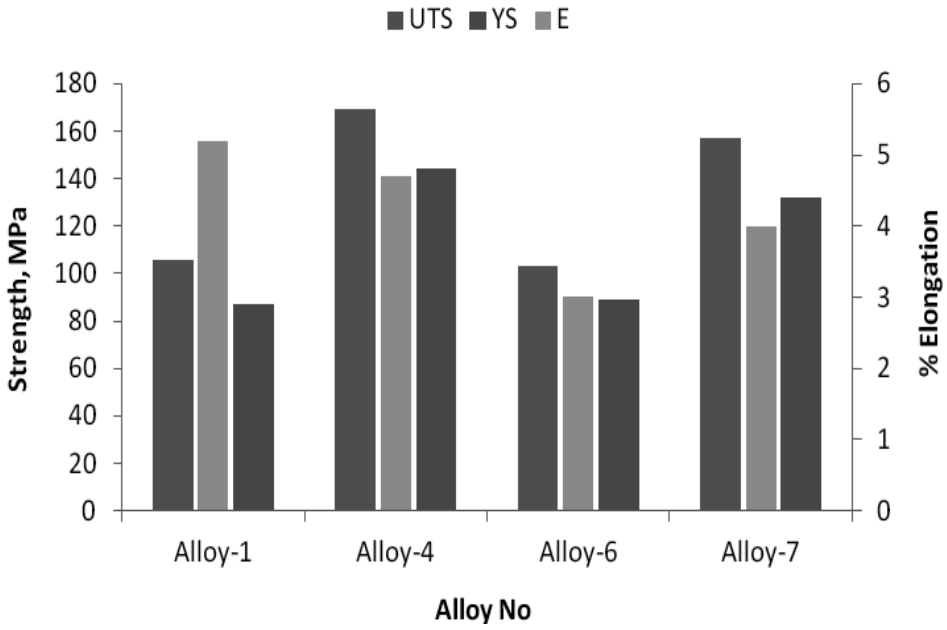

Figure 4.3.18: UTS, YS and %E of the Alloys 1, 4, 6 and 7 aged at 300^{o}C

4.3.4 Effect of Strain Rate on Tensile Properties in the Peakaged Condition

4.3.4.1 Effect of Strain Rate on Ultimate Tensile Strength of Cu Content Alloys

Typical tensile stress - strain rates curves of the alloys at 225^{o}C are plotted in Figure 4.3.19. Tensile test experiments were conducted at three different crosshead speeds 0.25, 2.5 and 25 mm/min which are equal to the nominal strain rates of 10^{-4} (0.0001), 10^{-3} (0.001) and 10^{-2} (0.01) s^{-1}. Enhancing strain rates results in an obvious increase in fracture strength. When the strain rates are below 10^{-3} s^{-1}, work hardening decreases strongly. Work hardening decreases strongly during the plastic deformation of sample at $10^{-4}s^{-1}$, and sometimes necking phenomenon is observed in this strain rate before fracture. Alloy-4 shows the highest ultimate tensile strength at all strain rates while Alloy-5 shows the lowest ultimate tensile strength at all strain rates.

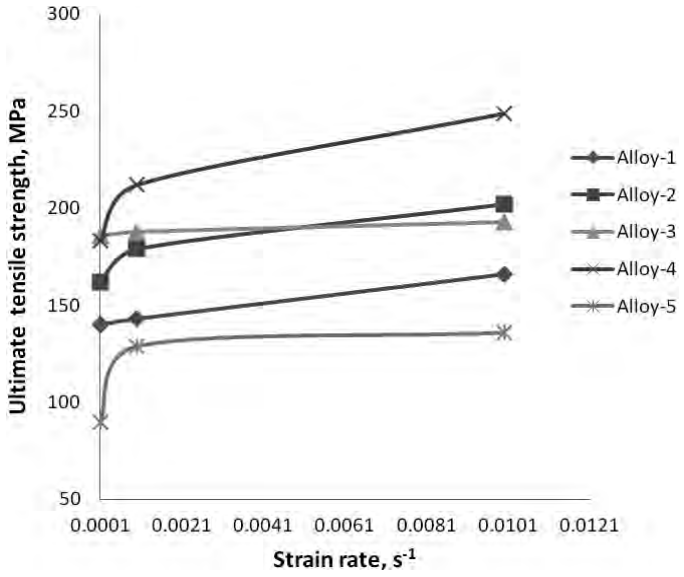

Figure 4.3.19: UTS - strain rate curves of Alloys 1-5 aged for 1hr at 225^{o}C

Figure 4.3.20 shows the UTS at different strain rates as a function of Cu content of the alloys. The tensile strength increases with increasing Cu at the examined strain rates and maximum strength was found for 2 wt% Cu addition to Al-6Si-0.5Mg alloy. A further addition of Cu to Al-6Si-0.5Mg alloy lowers the tensile strength at all strain rates.

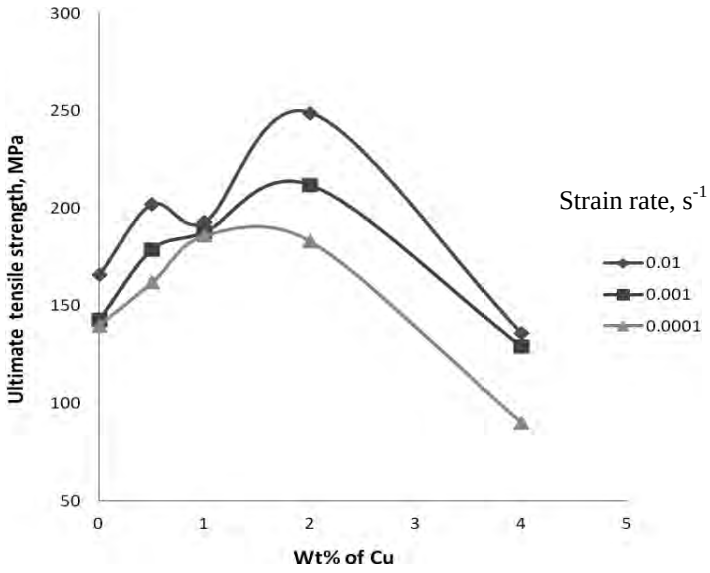

Figure 4.3.20: The change of ultimate tensile strength with Cu content in Al-6Si-0.5Mg alloys at different strain rates

4.3.4.2 Effect of Strain Rate on Ultimate Tensile Strength of Cu or/and Ni Content Alloys

The ultimate tensile stress - strain rates curves of the Cu or/& Ni content Al-6Si-0.5Mg alloys (aged at 225^{o}C for 1 hour) are plotted in Figure 4.3.21. The tensile test experiments are conducted at three different strain rates (10^{-4}, 10^{-3} & 10^{-2} s^{-1}) for evaluation the effects strain rate. Enhancing strain rates results in an obvious increase in fracture strength. When the strain rates are below 10^{-3} s^{-1}, work hardening decreases strongly for the alloys. In the case of Alloy-6 and Alloy-7, work hardening decrease strongly during the plastic deformation of sample at 10^{-4} s^{-1}. The tensile strength increases more pronounced with the increase of strain rates and Cu content alloys. 2 wt% Cu containing alloy, Alloy-4 shows the highest ultimate tensile strength all over the strain rates among the investigated alloys. But Alloy-7 (2 wt% Cu & 2wt% Ni) shows lower strength than Alloy-4. The ultimate tensile strength of Alloy-1 and Alloy-6 (2wt% Ni) does not show significant change of strength with the increase of strain rates.

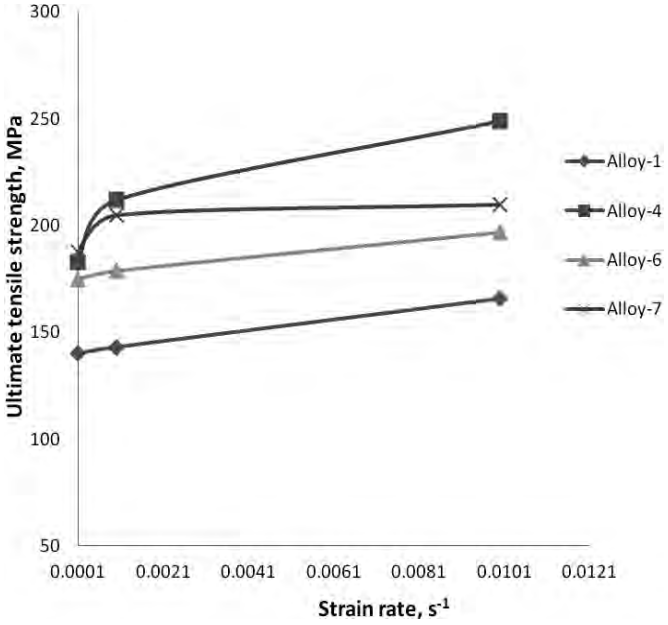

Figure 4.3.21: UTS - strain rate curves of Alloys 1, 4, 6 and 7 aged for 1hr at 225^{o}C

4.3.4.3 Effect of Strain Rate on Yield Strength of Cu Content Alloys

Figure 4.3.22 shows the yield strength (0.2% proof strength) vs. strain rates of the Cu content alloys. The increase in proof strengths with strain rates of the alloys is very similar to the

ultimate tensile strengths. The maximum yield strength is attained at $10^{-2}s^{-1}$. Alloy-5 shows the lowest yield strength at all the strain rates investigated while Alloy-4 is found to show the highest yield strength among the alloys. The intermetallic particles could contribute a reinforcement effect in the Al alloy matrix. The higher yield strength is due to the effect of precipitation hardening and higher strain hardening.

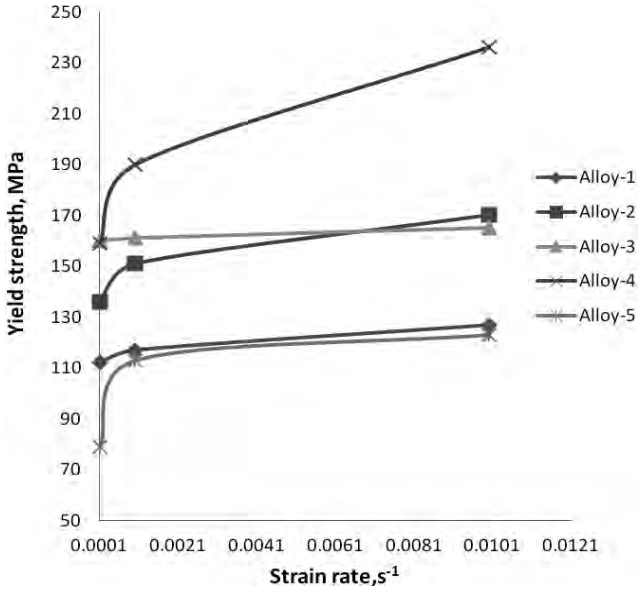

Figure 4.3.22: Yield strength- strain rate curves of Alloys 1 - 5 aged for 1hr at 225^{o}C

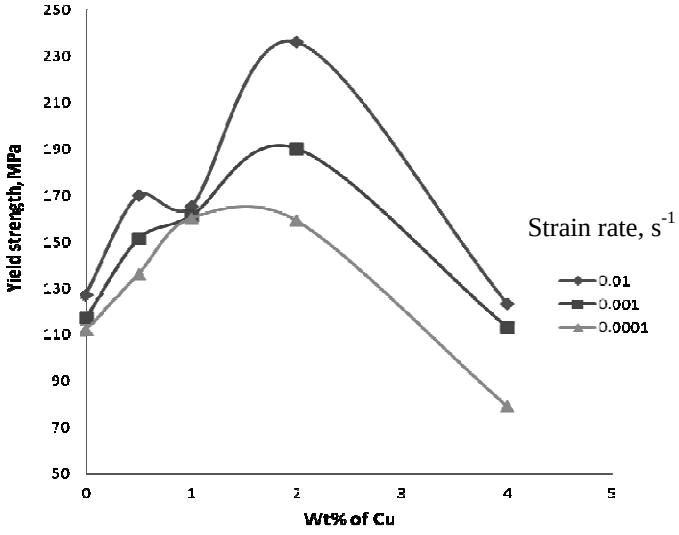

Figure 4.3.23: The change of yield strength with Cu content in Al-6Si-0.5Mg alloys at different strain rates

Figure 4.3.23 shows the yield strength of Al-6Si-0.5Mg alloys as a function of Cu content. Yield strength increases with an increase of Cu in the alloys and maximum yield strength was found for 2 wt% Cu addition to Al-6Si-0.5Mg alloy in all strain rates. With further addition of Cu, the yield strength of Al-6Si-0.5Mg alloys decreased very rapidly.

4.3.4.4 Effect of Strain Rate on Yield Strength of Cu or/and Ni Content Alloys

Figure 4.3.24 shows the yield strength (0.2% proof strength) vs. strain rates of the Alloys 1, 4, 6 and 7. The increase in proof strengths of the alloys with strain rates is very similar to the ultimate tensile strengths. With the increase of strain rate the yield strength increases and the maximum being attained at 10^{-2} s^{-1}. The combined effect of 2 wt% Cu and 2 wt% Ni (Alloy-7) is very similar to that of 2 wt% Cu (Alloy-4). But 2wt% Ni containing Alloy-6 shows lower strength than Alloy-4 and Alloy-7 at all strain rates.

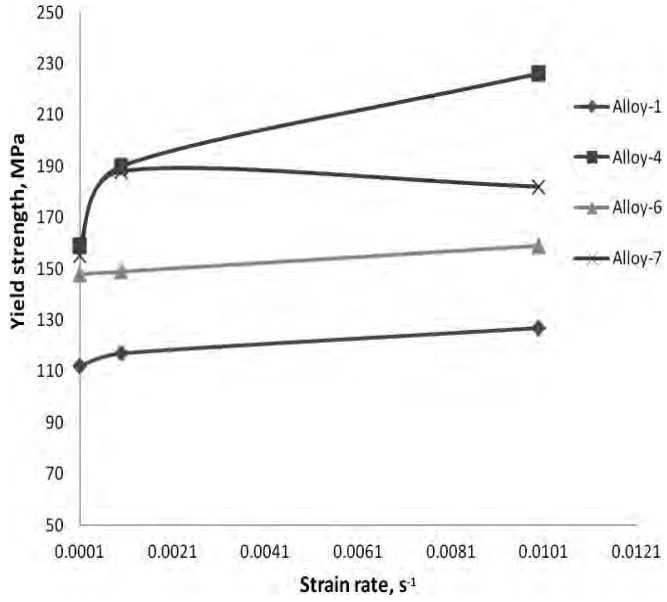

Figure 4.3.24: Yield strength-strain rate curves of Alloys 1, 4, 6 and 7 aged for 1 hr at 225^{o}C

4.3.4.5 Effect of Strain Rate on % Elongation of Cu Content Alloys

Figure 4.3.25 shows the variation of % elongation of the alloys with strain rates. It is observed that at the strain rate for which strength is maximum ($10^{-2}s^{-1}$), the ductility values of the alloys

pass through minima. The ductility value of the peak aged Alloy-5 (4wt % Cu) is found to be less than all other alloys in the examined strain rates.

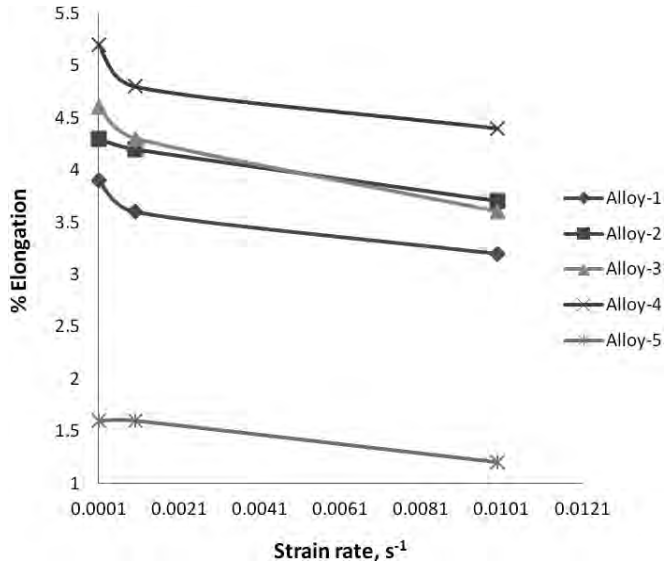

Figure 4.3.25: Ductility (% elongation) - strain rate curves of Alloys 1-5 aged for 1hr at 225^{o}C

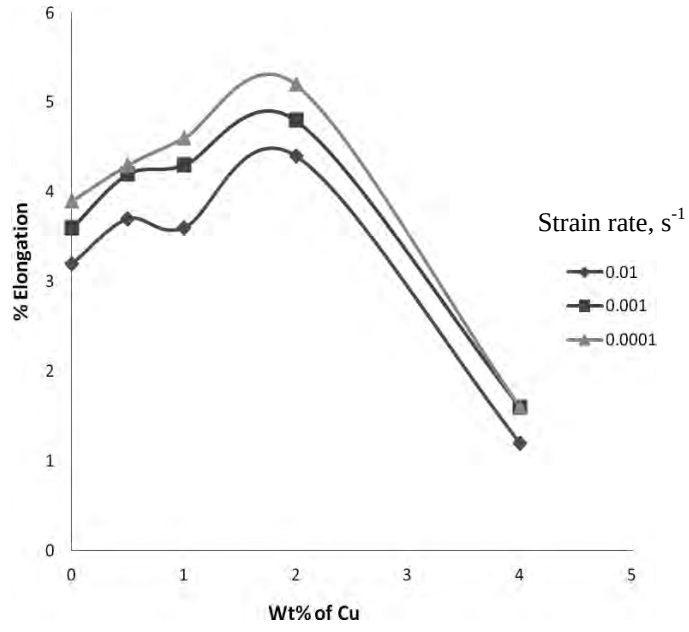

Figure 4.3.26: The change of Ductility (% Elongation) with Cu content in Al-6Si-0.5Mg alloys at different strain rates

The elongation increased markedly with the increasing content of Cu in all strain rates. Figure 4.3.26 shows the elongation of Al-6Si-0.5Mg alloys as a function of Cu contents. For 2 wt% Cu addition to Al-6Si-0.5Mg alloy, maximum ductility was found at all strain rates. With further additions of Cu, ductility drops very quickly.

4.3.4.6 Effect of Strain Rate on % Elongation of Cu or/and Ni Content Alloys

Elongation versus strain rates of Cu and/or Ni containing alloys has been plotted in Figure 4.3.27. The elongation of the alloys decreases with increasing the strain rate. The ductility value of peakaged Alloy-6 (2 wt.% Ni) is found to be less than all other alloys (Alloys 1, 4 and 7) at all strain rates. It was recorded maximum ductility at the strain rate of 10^{-4} s^{-1} and this trend is followed for all alloys. Alloy-2 (2wt% Cu) shows the maximum ductility at all strain rates, so Cu has a significant effect on ductility than individual Ni (Alloy-6) or combined Cu &Ni (Alloy-7) additions to Al-6Si-0.5Mg alloy.

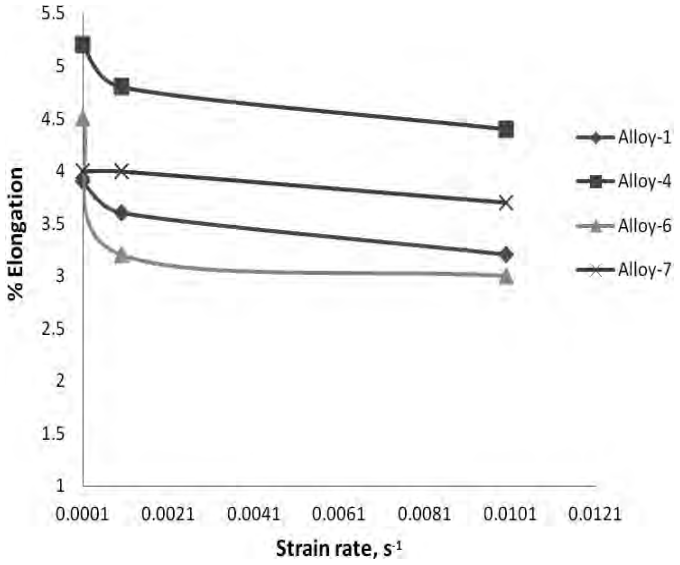

Figure 4.3.27: Ductility (%elongation) - strain rate curves of Alloys 1, 4, 6 and 7 aged for 1hr at 225^{o}C

4.4 Impact Properties of the Alloys

4.4.1 Effect of Ageing Temperature on Impact Strength of Cu Content Al-6Si-0.5Mg Alloys

Figure 4.4.1 shows the impact strength (absorbed energy) as a function of the artificial ageing temperature. As-quenched condition, the alloys have shown higher toughness than in the peakaged (1hr at 225^{o}C) condition. The absorbed energy decreased to a minimum due to the precipitation of intermediate phases at peak aged condition. The impact strength increases with the ageing temperature; this is expected because the stiffness of the samples increases with the ageing temperature.

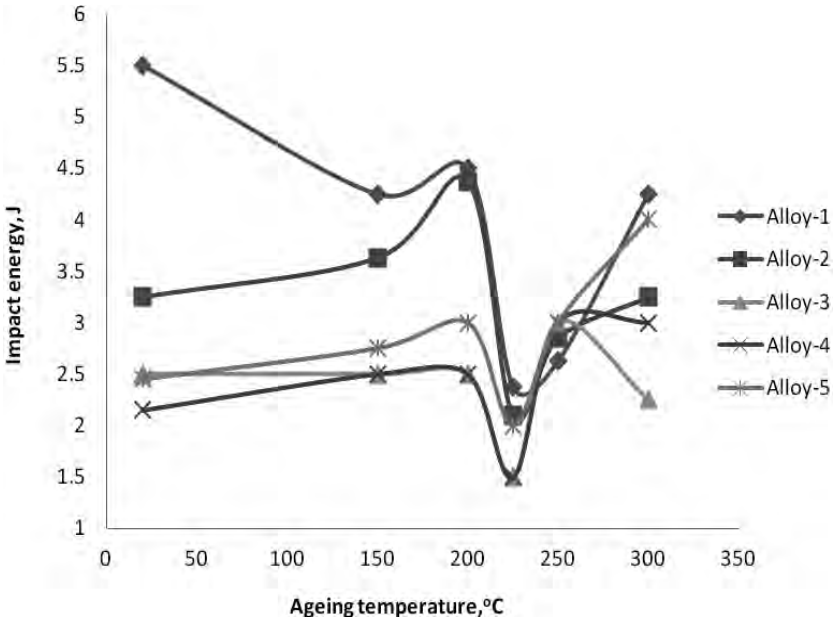

Figure 4.4.1: Effects of ageing temperatures on the impact strength of Alloys 1-5 (Isochronally aged for 1 hour)

4.4.2 Effect of Ageing Temperature on Impact Strength of Cu or/ and Ni Content Al-6Si-0.5Mg Alloys

Figure 4.4.2 shows the effects of ageing temperature on the impact strength (absorbed energy) of Cu or/ and Ni containing alloys. During artificial ageing the impact strength of alloys 4, 6, and 7 first increased or remained about constant, and then decreased to a minimum at the peakaged condition. The Cu and Ni free alloy, Alloy-1 shows the highest absorbed energy. The impact behavior of Alloy-4 and Alloy-6 are about same. The combined effect of 2%Cu and 2%Ni

(Alloy-7) has, in general, the lowest capacity to absorb energy. All the alloys have minimum impact strength at peakaged condition (1hr at 225^{o}C). For all alloys, overageing at 250 and 300^{o}C raises the impact strength rapidly.

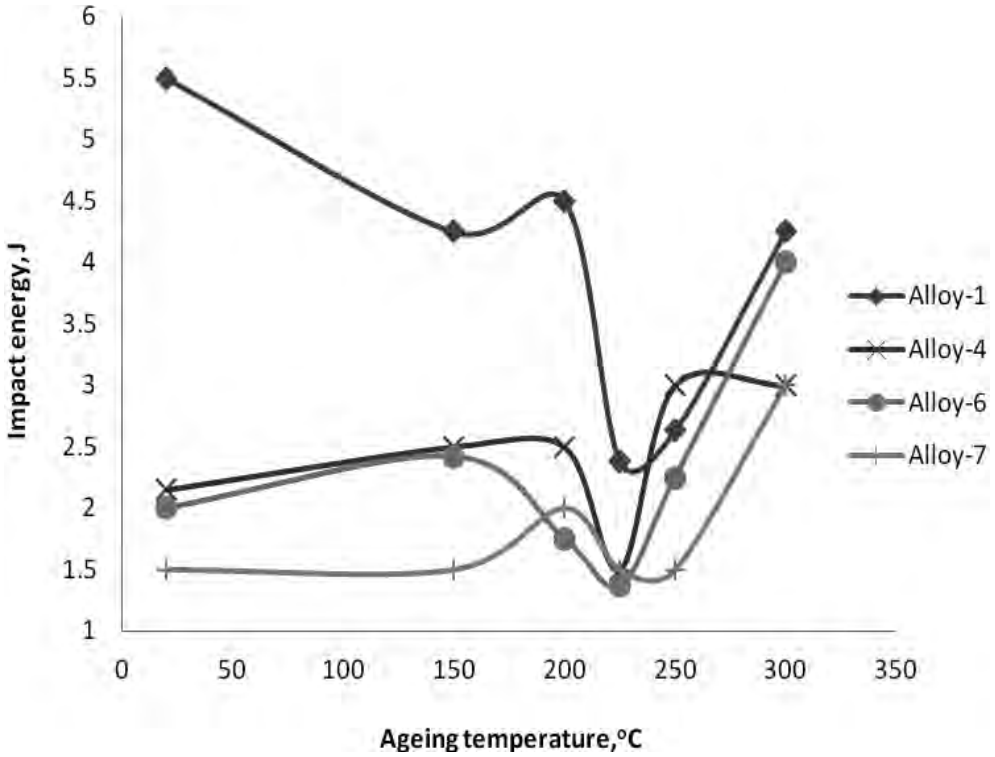

Figure 4.4.2: Effects of ageing temperature on the impact strength of Alloys 1, 4, 6 and 7 (Isochronally aged for 1 hour)

4.4.3 Impact Strength of Alloys at Thermal Treated Conditions

4.4.3.1 Impact Strength of Alloys at Solution Treated Condition (Room Temperature)

Figures 4.4.3 shows the impact strength (absorbed energy) of Alloys 1 – 5 in the solution treated condition. It can be seen that the Alloy-1 has the impact strength of the alloys. With the increase of Cu in Alloy-1, the absorbed energy decreases and minimum (absorbed) energy was found for the Alloy-4 and Alloy-5. Cu additions to Al-6Si-0.5Mg alloy decrease the impact strength of the alloys.

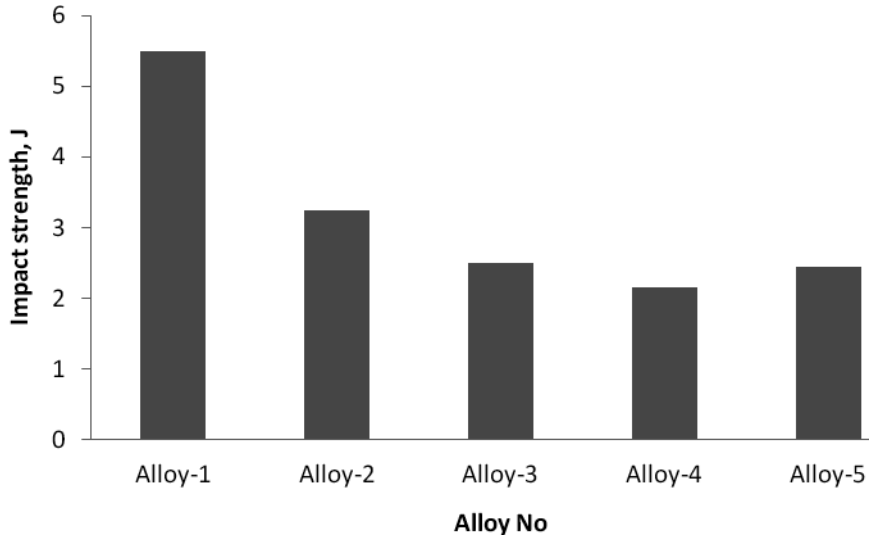

Figure 4.4.3: Impact strength of Alloys 1 - 5 at solution treated condition

In the solution treated condition, the Alloy-1 has impact strength of 5.5 J (Figure 4.4.4). The individual and combined addition of Cu and Ni to Al-6Si-0.5Mg alloy reduces the impact strength. The impact strength (2.15 J) of Alloy - 4 (2wt% Cu) is close to the impact strength (2.00J) of 2wt% Ni content alloy (Alloy-6) whereas the Alloy-7 (2 wt. % Cu and 2 wt% Ni) has lower impact strength (1.5J). From these results, it can be said that at solution treated condition the Cu and/or Ni additions to the Al-6Si-0.5Mg (Alloy-1) alloy, are detrimental on the impact strength by any of them alloying element additions.

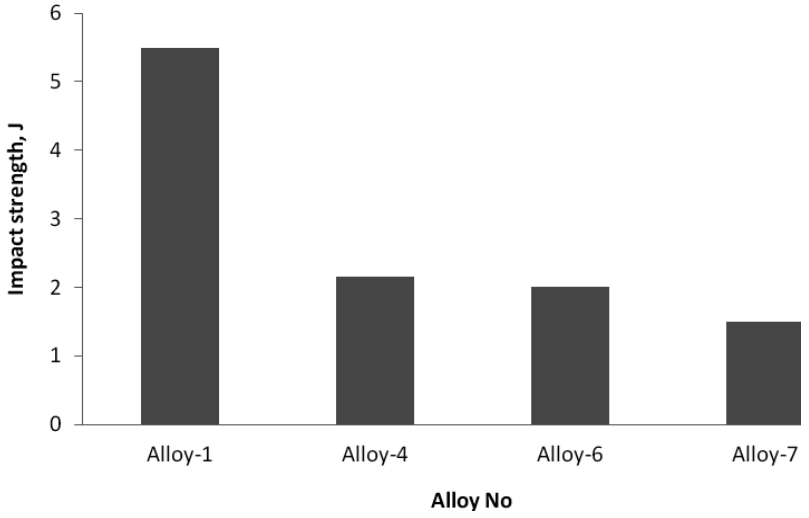

Figure 4.4.4: Impact strength of Alloys 1, 4, 6 and 7 at solution treated condition

4.4.3.2 Impact Strength of Alloys Aged for 1 hour at 150^{o}C

The impact strength of Cu free alloy, Alloy-1 (4.25J) is higher than any of the Cu containing alloys. Thus, when aged at 150°C Cu addition affect the impact absorbed energy significantly. In an earlier section we have seen that addition of Cu improves both YS and UTS regardless of the other additions. When high impact strength is desired, the Alloy-1 seems the best candidate whereas the Alloy-4 offers the highest strength at 150°C.

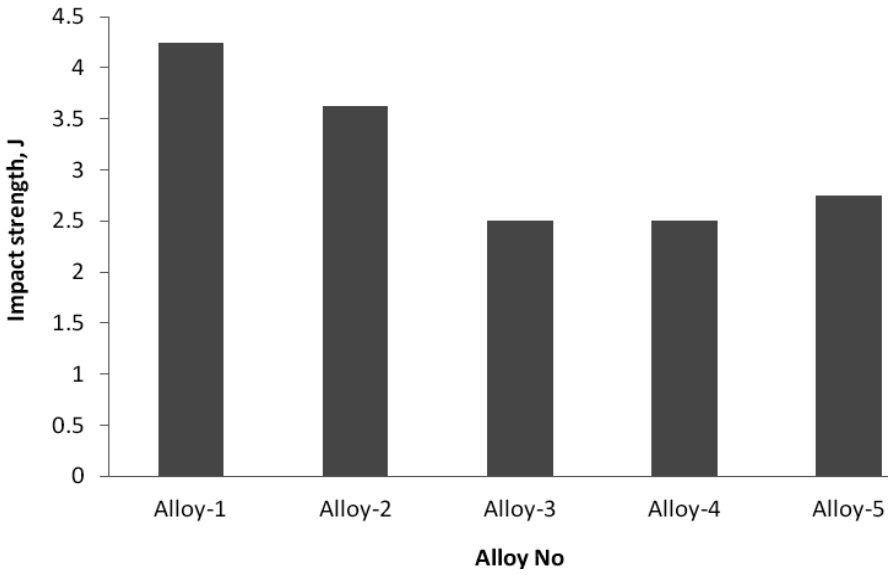

Figure 4.4.5: Impact strength of Alloys 1 - 5 isochronally aged at 150^{o}C for 1 hour

Slightly higher impact properties are obtained by means of Cu and/or Ni addition to Al-6Si-0.5Mg and ageing at 150^{o}C for 1 hour rather than solution treatment. The impact strength values at 150°C are 4.25 (Alloy-1), 2.5 (Alloy-4), 2.42 (Alloy-6) and 1.5J (Alloy-7) shown in Figure 4.4.6. The 2wt% Cu addition (Alloy-4) alone seems to have a negative effect on the ductility of the Alloy-1. The Alloy-6 is close to the Alloy-4, whereas the Alloy-7 has lower impact strength. From these results, it can be said that at 150°C the combined 2wt% Cu and 2wt% Ni additions to Alloy-1 are more detrimental on the impact strength than the individual 2wt% Cu or 2wt% Ni additions. This could be due to the increased formed Cu-Ni containing phases, which are harder but more brittle than the other phases at 150°C.

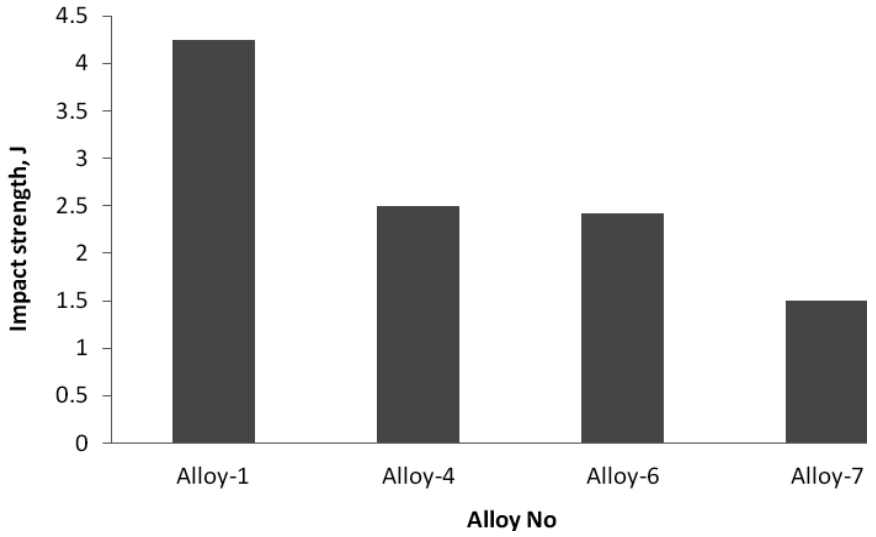

Figure 4.4.6: Impact strength of Alloys 1, 4, 6 and 7 isochronally aged at 150^{o}C for 1 hour

4.4.3.3 Impact Strength of Alloys Aged for 1 hour at 200^{o}C

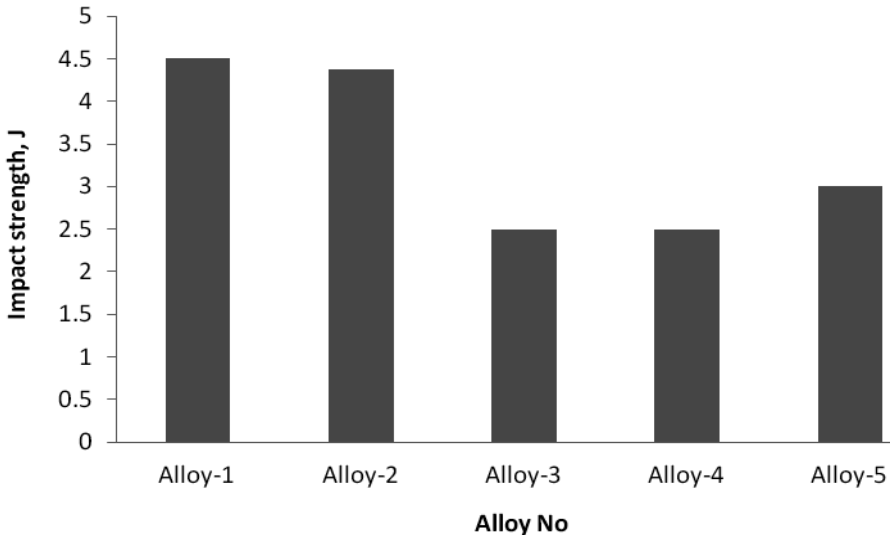

Figure 4.4.7: Impact strength of Alloys 1 – 5 isochronally aged at 200^{o}C for 1 hour

Figure 4.4.7 shows that when aged at 200°C the impact strength in five alloys decreases with the increase of Cu content into Alloy-1, which is expected. The Cu addition reduces the impact strength of the Al-6Si-0.5Mg alloy (Alloy-1). Although the impact strength of Alloy-2 has strength similar to that of Alloy-1, the alloys having 1wt%, 2wt% and 4wt% Cu have very close

impact strengths. Cu additions above 0.5wt% significantly reduce the impact strength of Al-6Si-0.5Mg alloys after ageing at 200^{o}C.

The Charpy impact energy values of alloys aged at 200^{o}C are shown in Figure 4.4.8. The impact strength values at 200°C are 4.5 (Alloy-1), 2.5 (Alloy-4), 1.75 (Alloy-6) and 2J (Alloy-7). The 2wt% Cu addition (Alloy-4) alone seems to have a negative effect on the impact strength on the Al-6Si-0.5Mg alloy. The impact strength of Alloy-6 is close to the Alloy-7, whereas the Alloy-4 has lower impact strength but still better than the Alloy-6 and Alloy-7. From these results, it can be said that at 200°C the 2wt% Cu (Alloy-4) additions to the Al-6Si-0.5Mg is less detrimental effect on the impact strength than the individual 2wt% Ni (Alloy-6) or combined 2wt% Cu and 2wt% Ni (Alloy-7) additions. This could be due to the optimum grain refinement with the Cu addition.

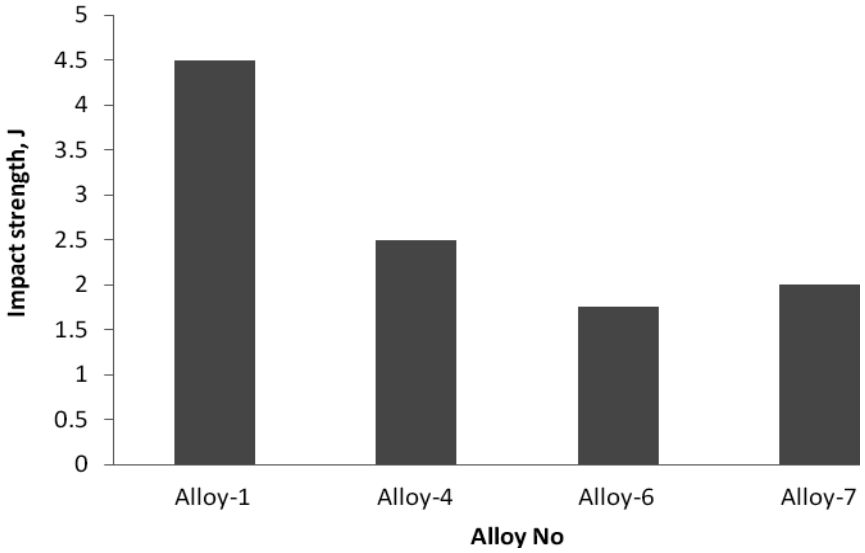

Figure 4.4.8: Impact strength of Alloys 1, 4, 6 and 7 isochronally aged at 200^{o}C for 1 hour

4.4.3.4 Impact Strength of Alloys Aged for 1 hour at 225^{o}C

Figure 4.4.9 shows the impact strength values of alloys isochronally aged at 225^{o}C. The results show that when aged at 225^{o}C, the impact strength of the alloys decrease with increased Cu content of the alloy, which is expected. Additions of Cu into the Alloy-1, reduces the absorbed energy of the alloys in a consisted manner. The Alloy-3 and Alloy-4 have similar impact strength at 1.5 J. On the other hand, the Alloy-5 has to lower impact strength value (2J) of the

Alloy-1(2.38J) and Alloy-2 (2.1J). Therefore, at 225°C the Cu additions affect the Charpy impact absorbed energy very much but it improves hardness, YS and UTS. When high impact strength is desired, the Alloy-1 seems the best candidate whereas the Alloy-4 offers the highest strength at 225°C.

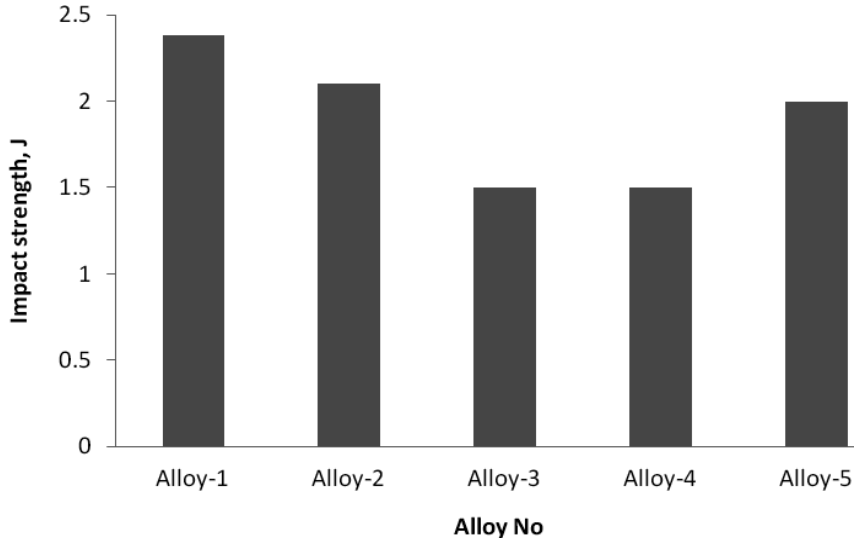

Figure 4.4.9: Impact strength of Alloys 1 -5 isochronally aged at 225^{o}C for 1 hour

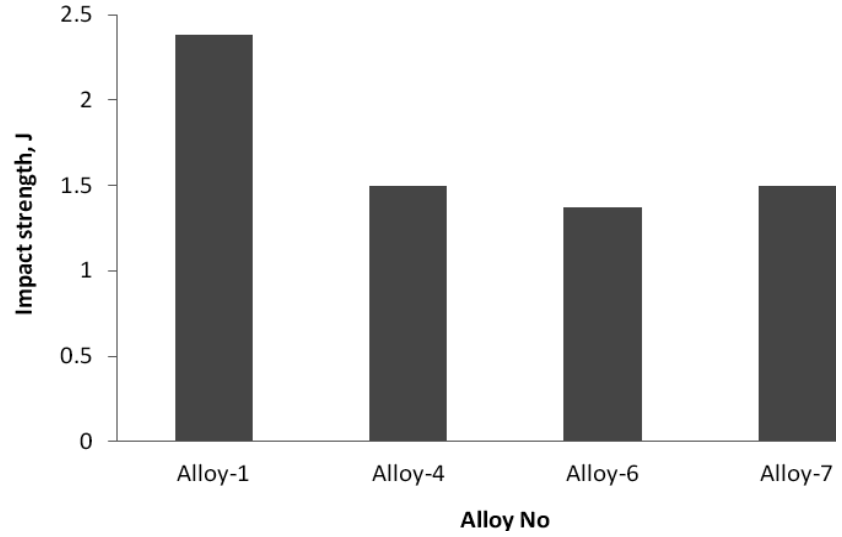

Figure 4.4.10: Impact strength of Alloys 1, 4, 6 and 7 isochronally aged at 225^{o}C for 1 hour

The effect of peak ageing treatment on the Charpy impact energy is shown in Figure 4.4.10. The impact strength values at 225°C are 2.38J (Alloy-1), 1.5 J (Alloy-4), 1.37 J (Alloy-6) and 1.5 J (Alloy-7). Addition of 2wt% Cu (Alloy-4) alone seems to have a negative effect on the impact

strength of the Alloy-1. The impact strength of Alloy-6 is lower than that of Alloy-4, whereas the Alloy-7 has slightly higher impact strength. From these results, it can be said that at 225°C the combined effect of Cu and Ni additions to the Alloy-1 are less detrimental on the impact strength than the individual Cu and Ni additions.

4.4.3.5 Impact Strength of Alloys Aged for 1 hour at 250^{o}C

As noted from Figure 4.4.11, the Alloy-3, Alloy-4 and Alloy-5 have same Charpy impact strength at 3J. The Cu additions have a positive effect on the ageing temperature impact strength of the Alloy-1 as the impact strength of the Alloy-1 is 2.63J. The 0.5 wt% Cu-containing Alloy-2 has better impact strength (2.85J) than the Alloy-1. Among the five alloys, Alloy-3, Alloy-4 and Alloy-5 have the maximum similar impact strength aged at 250^{o}C.

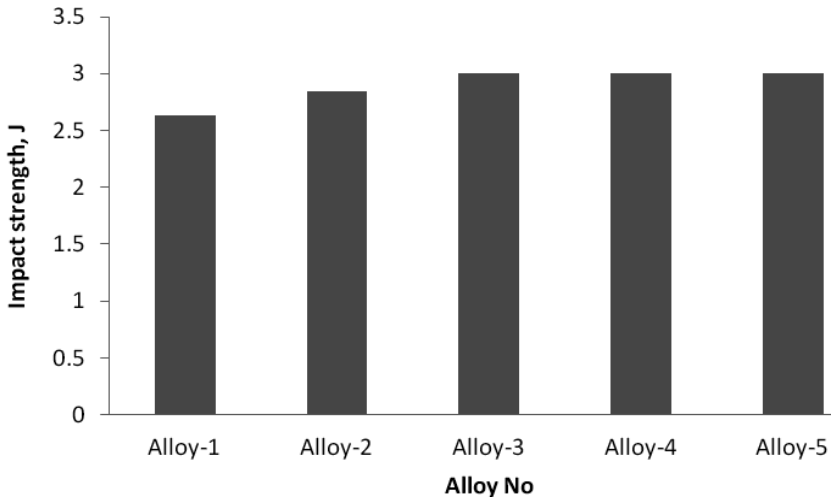

Figure 4.4.11: Impact strength of Alloys 1 - 5 isochronally aged at 250^{o}C for 1 hour

The increase in Charpy impact strength attained through the overageing treatment at 250^{o}C for 1 hour (T7) is shown in Figure 4.4.12. The Charpy impact strength values at 250^{o}C are 2.63J (Alloy-1), 3J (Alloy-4), 2.25J (Alloy-6) and 3J (Alloy-7). The addition of only 2wt% Cu seems to have a positive effect on the impact strength of the Alloy-1. The additions of only 2wt% Ni (Alloy-6) have markedly reduced the impact energy of the Alloy-1. The combined addition of Cu and Ni (Alloy-7) to the Alloy-1 markedly reduces the impact strength than individual additions Cu or Ni.

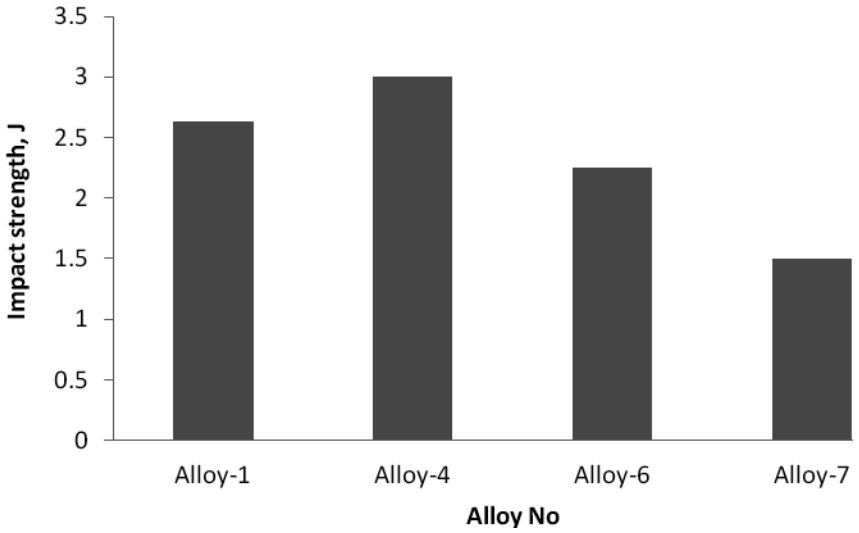

Figure 4.4.12: Impact strength of Alloys 1, 4, 6 and 7 isochronally aged at 250^{o}C for 1 hour

4.4.3.6 Impact Strength of Alloys Aged for 1 hour at 300^{o}C

Figures 4.4.13 shows the Charpy impact strength of Alloys 1 - 5 overaged at 300^{o}C (T7). It can be seen that the Alloy-1 has the maximum stiffness among the alloys investigated. With increase of Cu in Alloy-1, the absorbed energy decreases initially and minimum energy was found for the 1wt% Cu addition to Al-6Si-0.5Mg (Alloy-3). But additions of more than 1wt% Cu to Al-6Si-0.5Mg alloy, the impact energy of the alloys increases.

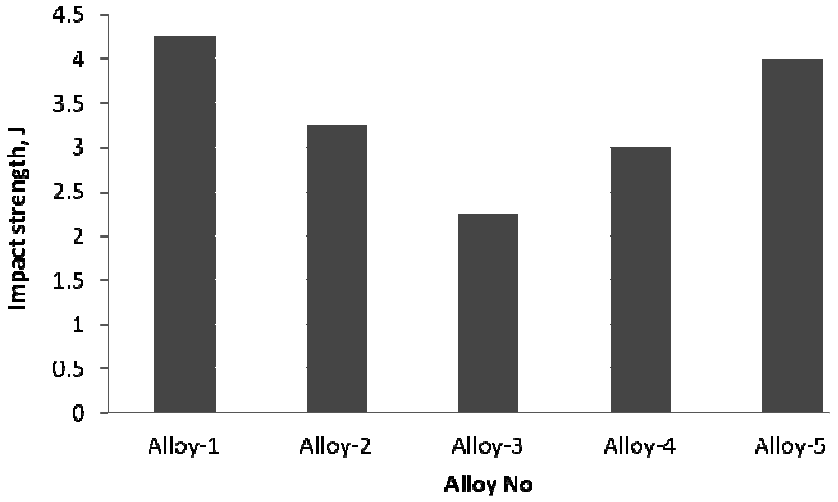

Figure 4.4.13: Impact strength of Alloy-1 - 5 isochronally aged at 300^{o}C for 1 hour

The Charpy impact strength values of Alloy-1, 4, 6 and 7 after ageing at 300^{o}C for 1 hour (T7) are shown in Figure 4.4.14. The effect of over ageing on the impact energy is better. At 300^{o}C, the Cu and Ni free Al-6Si-0.5Mg alloy, Alloy-1 has impact strength of 4.25 J. The individual and combined addition of 2wt% Cu and 2wt% Ni reduces the impact strength of the Al-6Si-0.5Mg alloy at overaged condition too. The impact strength of 2wt% Cu containing Alloy-4, is close to 2wt% Cu and 2wt% Ni containing Alloy-7, whereas the Alloy-6 (4 J) has higher impact strength. From these results, it can be said that overaged at 300^{o}C the 2wt% Cu and/or 2wt% Ni additions to the Alloy-1(Al-6Si-0.5Mg) are detrimental on the impact strength.

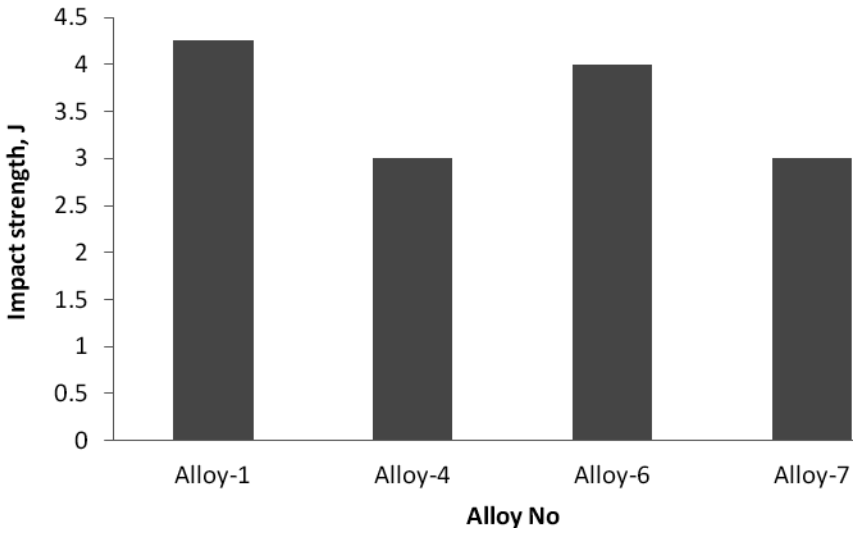

Figure 4.4.14: Impact strength of Alloys 1, 4, 6 and 7 isochronally aged at 300^{o}C for 1 hour

4.5 Fracture Behavior of the Alloys

Fractography studies were conducted on to the solutionized samples at the common strain rate of $10^{-3}s^{-1}$ after tensile test. The peakaged alloys were also subjected to fractographic observation after uniaxial tensile test at the three strain rates of $10^{-4}s^{-1}$, $10^{-3}s^{-1}$ & $10^{-2}s^{-1}$. After Charpy impact testing, only the fracture surfaces of the peakaged alloys were investigated in SEM at BAEC, Dhaka.

4.5.1 Tensile Fracture Behavior of Solutionized Alloy-1

Figure 4.5.1 shows the fracture surface morphology of Alloy-1 with a strain rate of $10^{-3}s^{-1}$. It can be seen that the fracture surface shows a quasi-cleavage fracture at solution treated condition. A mixture of quasi-cleavage fracture with a high density of micro-cracks of the silicon platelets and other brittle constituent particles can be observed.

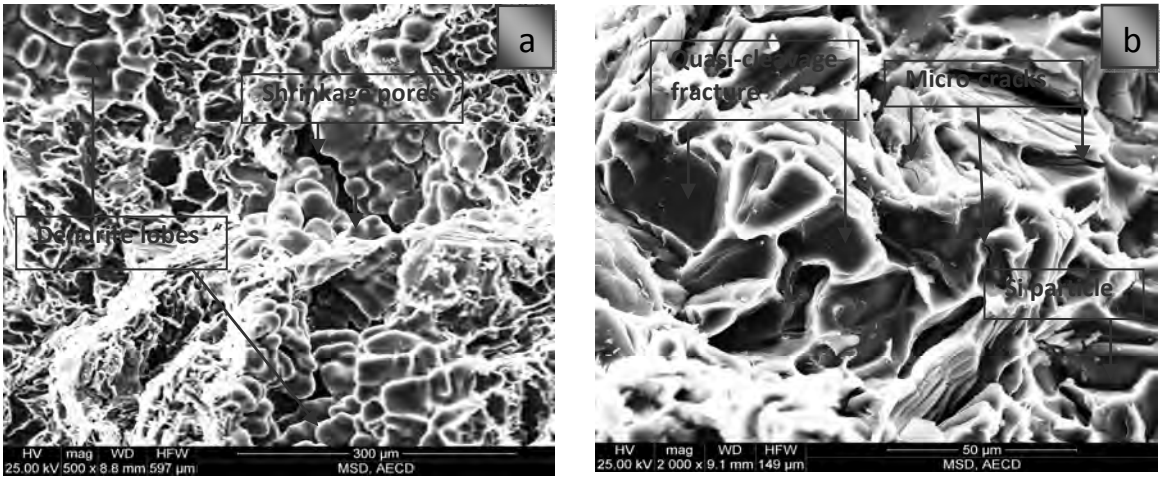

Figure 4.5.1: Fracture surface morphology of the solutionized Alloy-1 at different magnifications at a uniaxial tensile strain rate of $10^{-3}s^{-1}$

In the Figure 4.5.1a, the regions of shrinkage porosity, contain dendrite lobes, which existed as "free surfaces" within the cavities after the available liquid metal solidified. This behavior can be caused by an excessively high pouring temperature (which exaggerates total contraction in freezing) or by failure to provide proper risers. Figure 4.5.1b shows a complicated array of facets separated in many instances by indications of isolated dimples. Transcrystalline cleavage fractures are visible in the SEM image. Among the eutectic Si phase on the interface between α-

aluminium and Si, the regions of well-retained cohesion are visible. Some small cleavage steps are present on the cleavage facets in the Si. Micro-crack inside the silicon particle and crack linkage between eutectic silicon particles were observed on the fracture surfaces. The degree of flow in microvoid coalescence, however, did not contribute materially to ductility, and overall fracture was brittle in nature.

4.5.2 Tensile Fracture Behavior of Peakaged Alloy-1 at Various Strain Rates

Figures 4.5.2, 4.5.3 and 4.5.4 show the SEM tensile fracture surfaces of peakaged Alloy-1 at the strain rates of $10^{-4}s^{-1}$, $10^{-3}s^{-1}$ and $10^{-2}s^{-1}$ respectively. Structural defects, such as shrinkage porosity exists in the fracture surfaces and it may acts as fracture initiation sites in this case. After initiation the crack progresses by cracking the eutectic Si particles, which is responsible for generation of facets in the fracture surface. Presence of dimples in the fractograph signifies the void initiations at thermally modified eutectic Si particles. The void coalescence are more pronounced at lower strain rates, as a results larger and deeper sizes dimples are produced during failure.

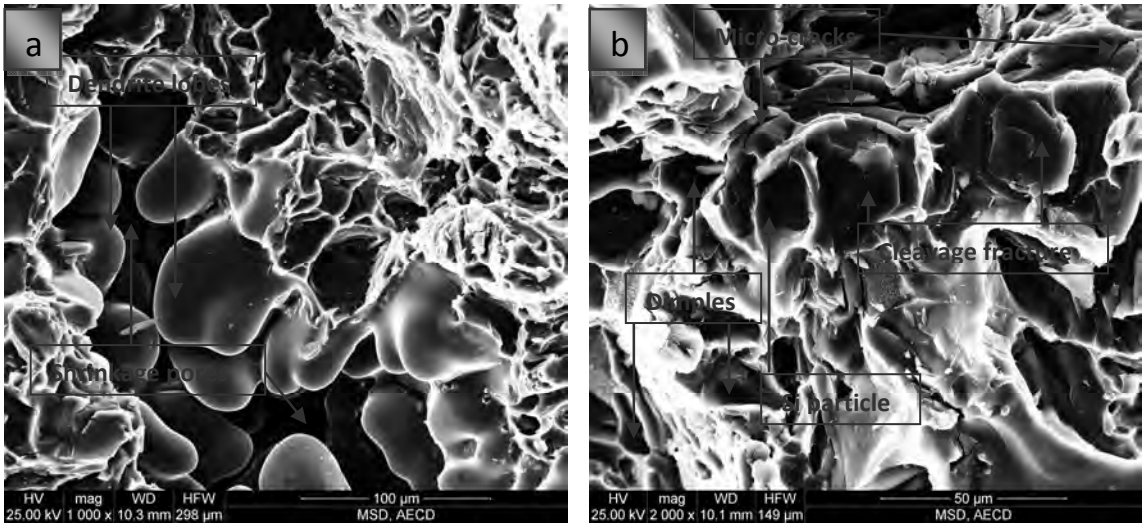

Figure 4.5.2: Fracture surface morphology of peakaged Alloy-1at a uniaxial tensile strain rate of $10^{-4}s^{-1}$

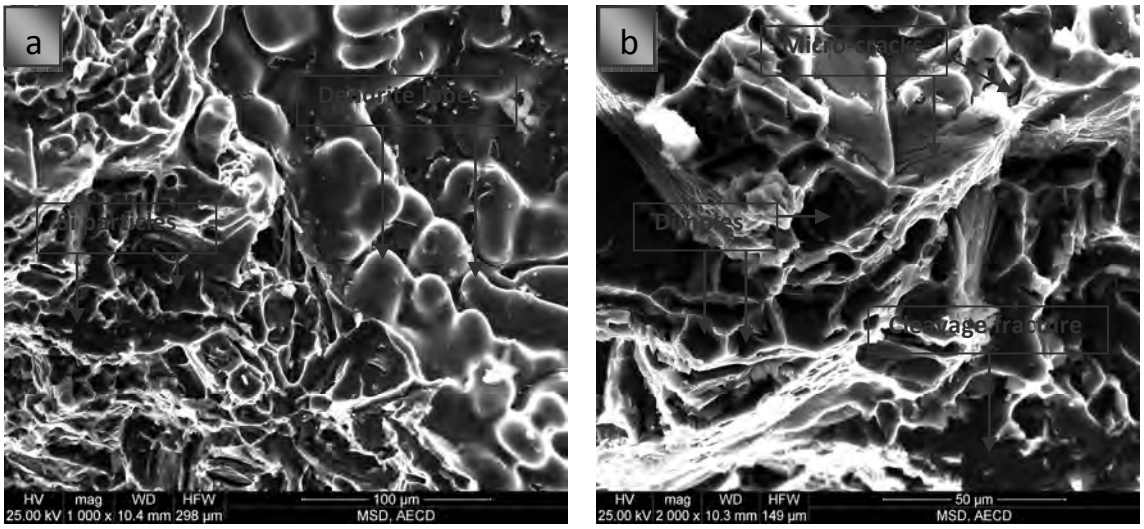

Figure 4.5.3: Fracture surface morphology of peakaged Alloy-1at a uniaxial tensile strain rate of $10^{-3}s^{-1}$

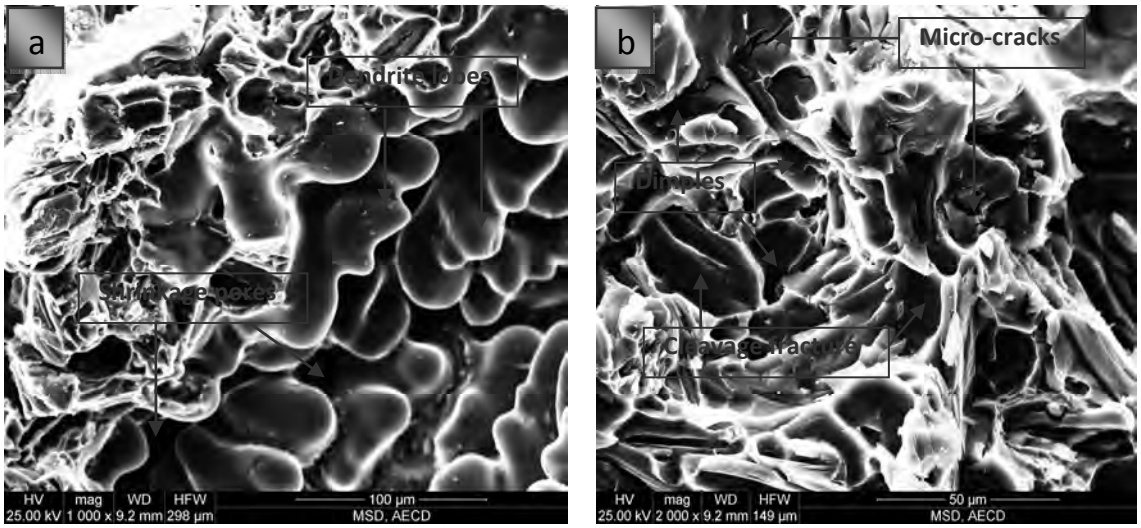

Figure 4.5.4: Fracture surface morphology of peakaged Alloy-1 at a uniaxial tensile strain rate of $10^{-2}s^{-1}$

4.5.3 Tensile Fracture Behavior of Solutionized Alloy-2

Fractographs of the specimens after solution treatment are documented in Figure 4.5.5. By solution treatment at 540°C the Si platelets were fragmented into smaller platelets with spherical edges. The morphology from transcrystalline brittle fracture (cleavage) is rare visible, but some degree of plastic deformation in the aluminium solid solution (α-Al matrix) also may be noticed in the form of shallow dimples. Most of the Si particles were found to contain cracks and the

fractured primary Si particles show clear cracks running through their centres. This indicates that the crack initiates in the primary Si particle.

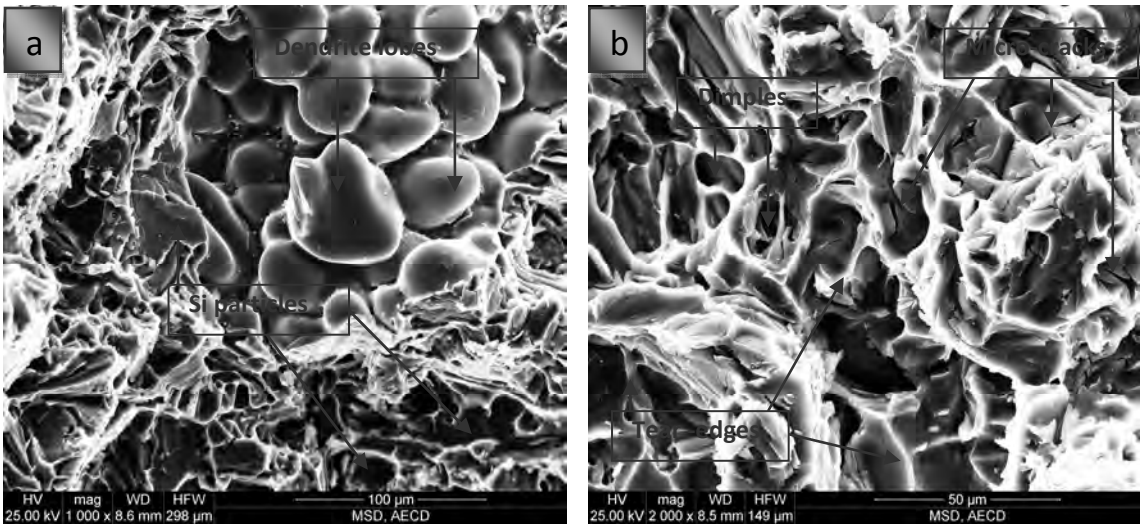

Figure 4.5.5: Fracture surface morphology of the solutionized Alloy-2 at a uniaxial tensile strain rate of $10^{-3}s^{-1}$

4.5.4 Tensile Fracture Behavior of Peakaged Alloy-2 at Various Strain Rates

Figures 4.5.6, 4.5.7 and 4.5.8 show the fracture surface of the specimen of Alloy-2 (0.5% Cu) in the peak aged condition after uniaxial tensile test at the mentioned strain rates.

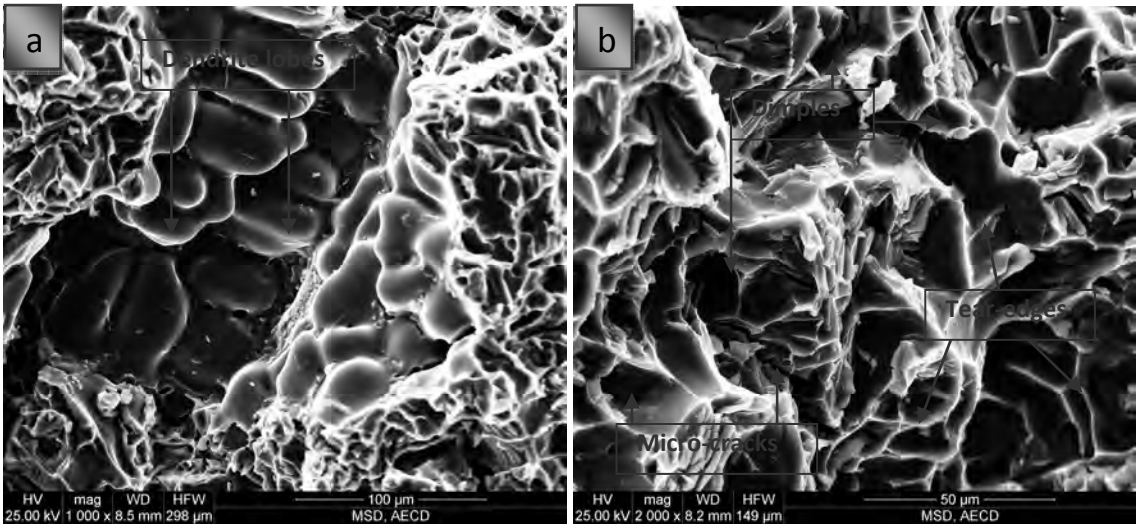

Figure 4.5.6: Fracture surface morphology of the peakaged Alloy-2 at a uniaxial tensile strain rate of $10^{-4}s^{-1}$

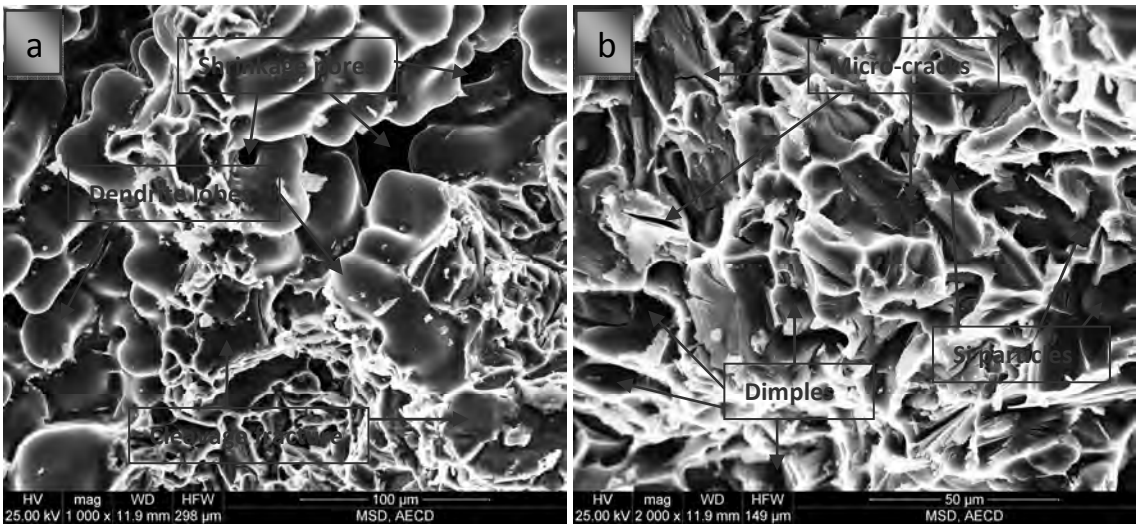

Figure 4.5.7: Fracture surface morphology of the peakaged Alloy-2 at a uniaxial tensile strain rate of $10^{-3}s^{-1}$

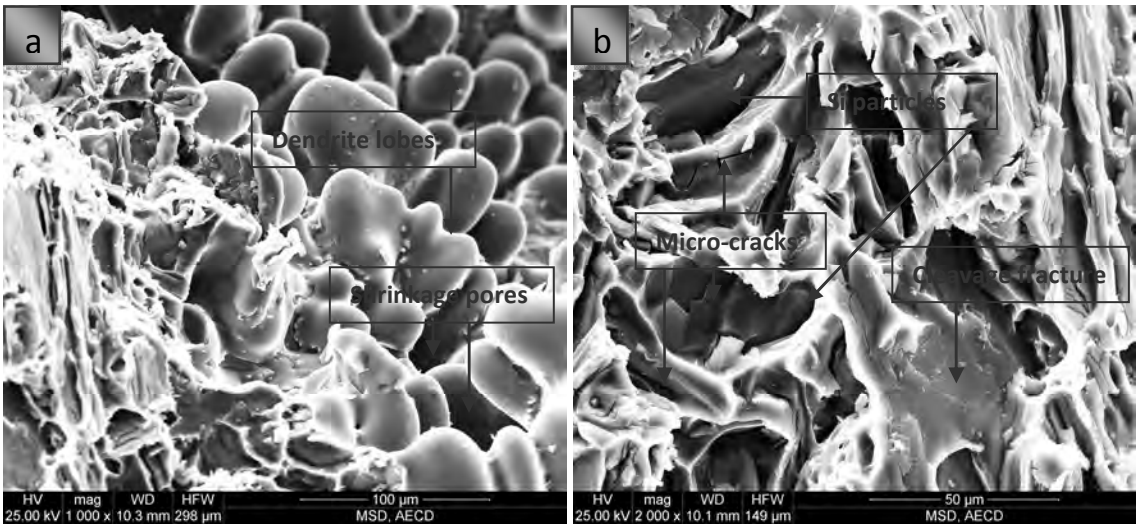

Figure 4.5.8: Fracture surface morphology of the peakaged Alloy-2 at a uniaxial tensile strain rate of $10^{-2}s^{-1}$

Figure 4.5.6 presents the classical ductile profile with existence of dimples with different sizes which can be related to the presence of the two populations of voids. At lower strain rate ($10^{-4}s^{-1}$) the dimples are larger and deeper than the higher strain rates ($10^{-3}s^{-1}$, $10^{-2}s^{-1}$) tensile testing samples. There are many cracks in the Si particles; these cracks are mainly responsible for initiating the brittle fracture. Both the micrographs (Figures 4.5.8(a) and (b)) show a combination of cleavage fracture through the particle and ductile tearing of the (thin) matrix at the higher strain rate ($10^{-2}s^{-1}$). The cleavage facets are mainly created at high strain hardening tensile testing.

4.5.5 Tensile Fracture Behavior of Solutionized Alloy-4

Fractograph of the specimen after solution treatment at the 540°C is documented in Figure 4.5.9. The fracture mechanism was identified as transcrystalline ductile with dimples morphology accompanied by plastically transformed walls. Figure 4.5.9 is an example of a transcrystalline ductile fracture of Cu-rich phase after solution treatment at the 540 °C. The fracture is transcrystalline ductile with fine dimples morphology. The size of the dimples shows the size of eutectic silicon.

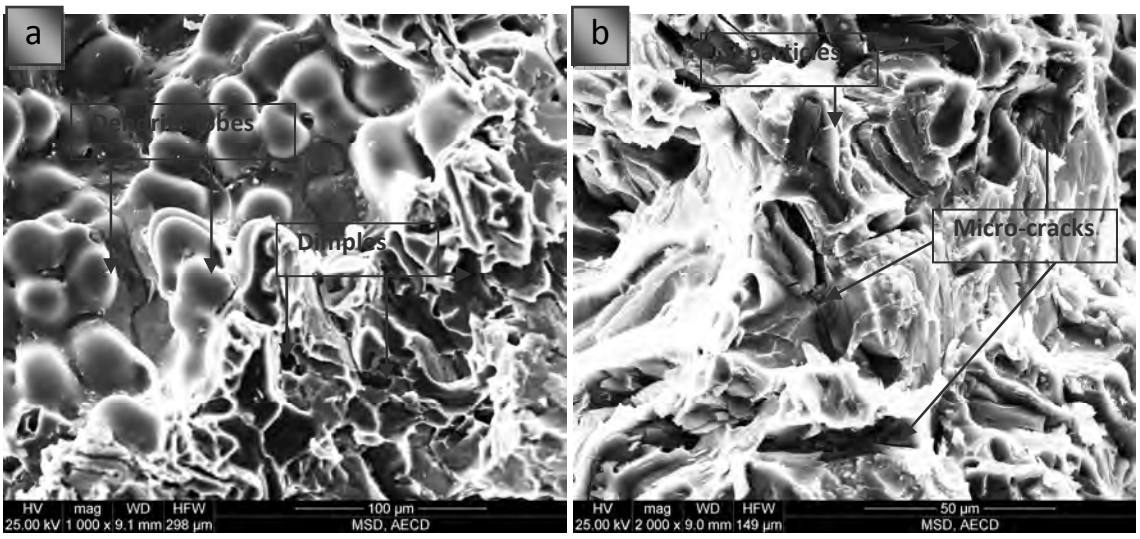

Figure 4.5.9: Fracture surface morphology of the solutionized Alloy-4 at a uniaxial tensile strain rate of $10^{-3}s^{-1}$

4.5.6 Tensile Fracture Behavior of Peakaged Alloy-4 at Various Strain Rates

Figures 4.5.10, 4.5.11 and 4.5.12 show cracking of primary Si particles on the tensile fracture surfaces at three the strain rates. The typical fracture surface consists of a distribution of large and small dimples associated with primary Si particles. It may be noted that fracture of the Al-6Si-0.5Mg-2Cu alloys occurs through ductile fracture of the Al matrix and brittle fracture of primary Si particles. Thus, it may be concluded that the fracture of the primary Si particles is the major one responsible for the relatively low ductility of the alloys. Most of the primary Si particles were found to contain cracks and the fractured primary Si particles show clear cracks running through their centers. This indicates that the crack initiates in the primary Si particle, thus leading to typical brittle fracture. The dimple sizes are more shallow at the higher strain rate ($10^{-2}s^{-1}$) compared to the lower strain rate ($10^{-4}s^{-1}$). There is severe crack initiation in Si particles

into α-Al matrix at lower strain rate during tensile testing. The more deeper dimples at lower strain rate indicates the ductile tearing but at higher strain rate a combination of cleavage fracture through the particle and ductile tearing of the α-Al matrix.

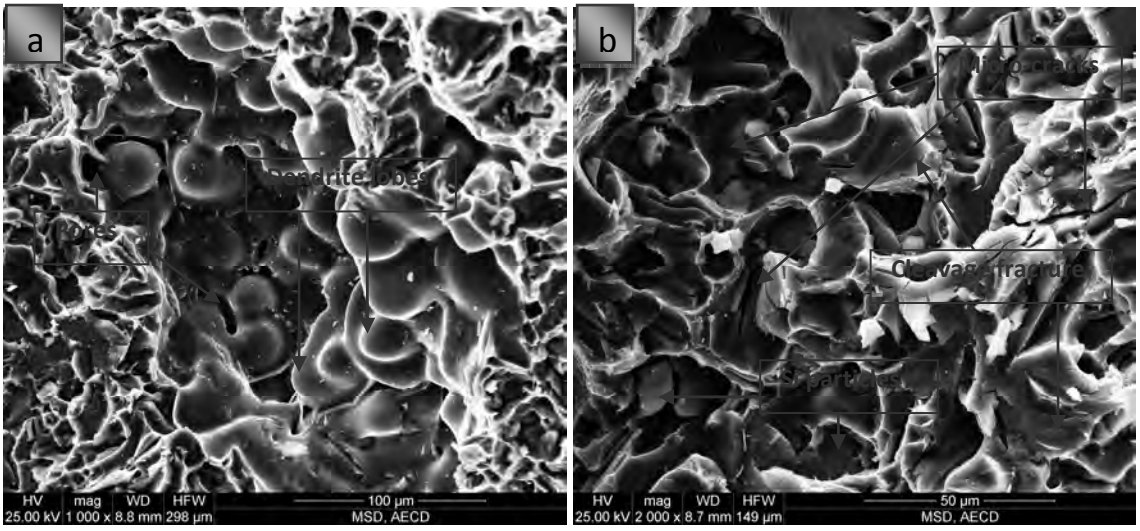

Figure 4.5.10: Fracture surface morphology of the peakaged Alloy-4 at a uniaxial tensile strain rate of $10^{-4}s^{-1}$

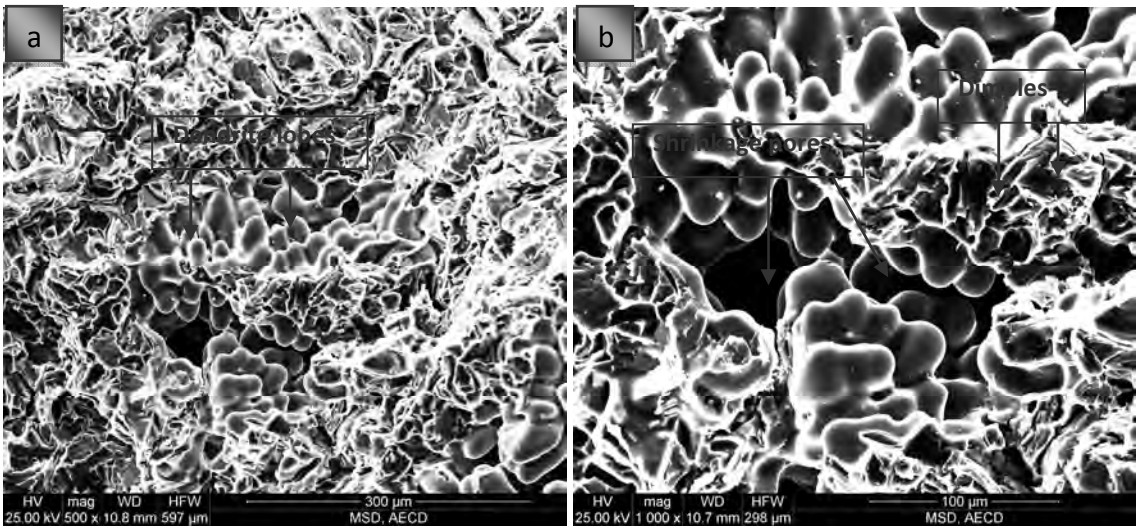

Figure 4.5.11: Fracture surface morphology of the peakaged Alloy-4 at a uniaxial tensile strain rate of $10^{-3}s^{-1}$

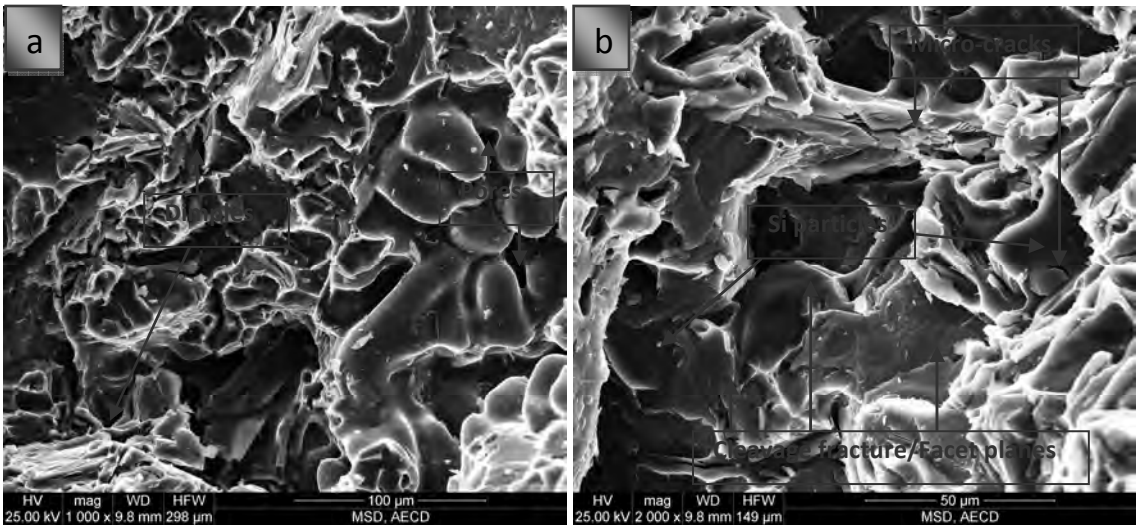

Figure 4.5.12: Fracture surface morphology of the peakaged Alloy-4 at a uniaxial tensile strain rate of $10^{-2}s^{-1}$

4.5.7 Tensile Fracture Behavior of Solutionized Alloy-6

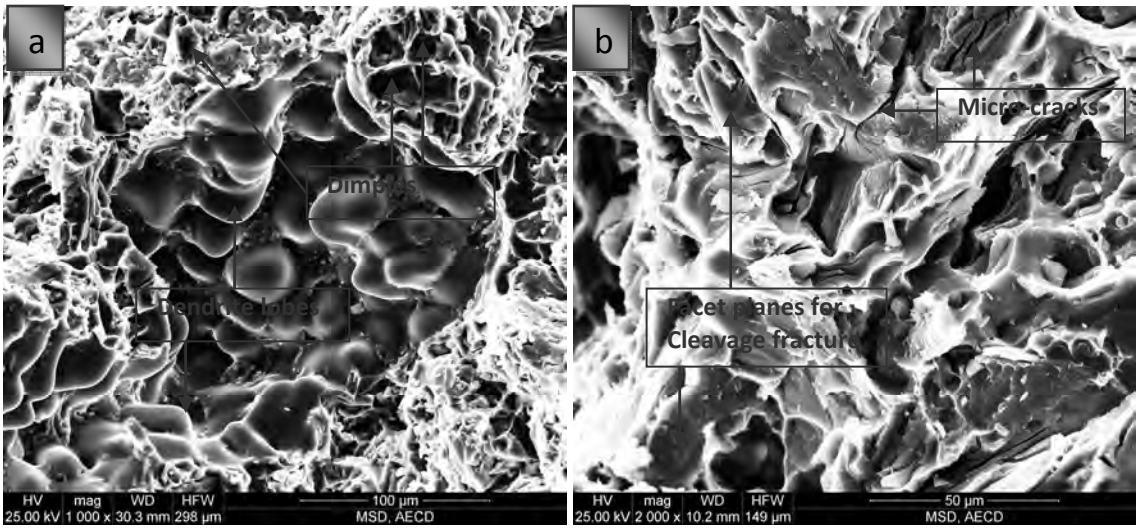

Figure 4.5.13: Fracture surface morphology of the solutionized Alloy-6 at a uniaxial tensile strain rate of $10^{-3}s^{-1}$

Figure 4.5.13 shows the tensile fracture morphology of solution treated Al-6Si-0.5Mg-2Ni alloy at strain rate of $10^{-3}s^{-1}$ in tension test. The fracture surface has some cleavage planes, cleavage steps and river patterns, there are also a few tearing ridges and very few dimples exist. It can be seen the fracture morphology of this alloy is similar the previous solution treated alloys. The fracture surface has a large number of tiny quasi-cleavage planes, a few tearing ridges and few

dimples. Cleavage steps formed in the intermetallic particles and Si phases and numerous secondary cracks are visible in these brittle phase. The cleavage step system is a result of the crack front propagation on the successive cleavage planes.

4.5.8 Tensile Fracture Behavior of Peakaged Alloy-6 at Various Strain Rates

Figures 4.5.14, 4.5.15 and 4.5.16 show the tensile fracture morphology of thermal treated (peakaged) Alloy-6 at tensile test in different strain rates. The fracture surface has some cleavage planes, cleavage steps and river patterns.

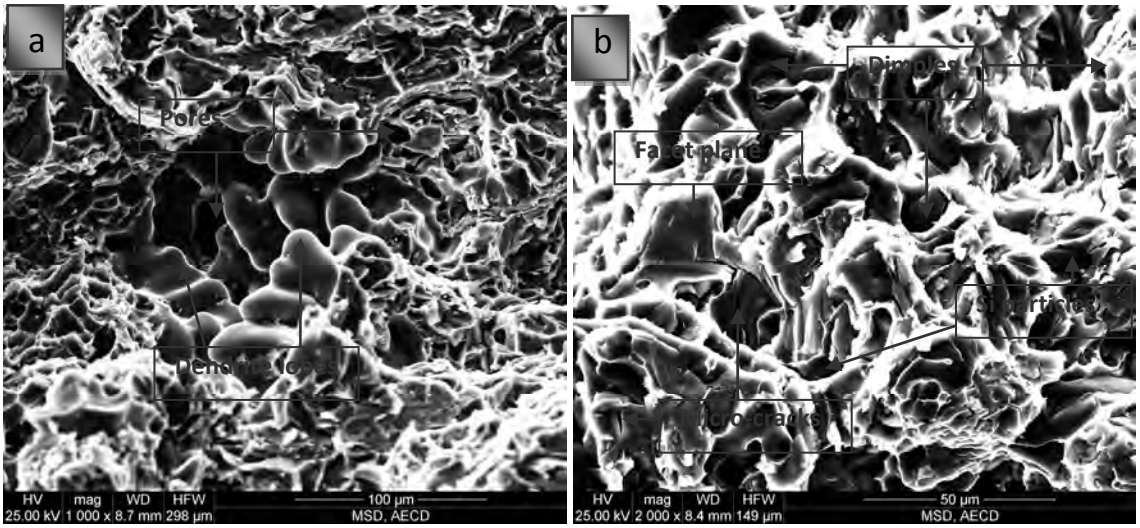

Figure 4.5.14: Fracture surface morphology of the peakaged Alloy-6 at a uniaxial tensile strain rate of $10^{-4}s^{-1}$

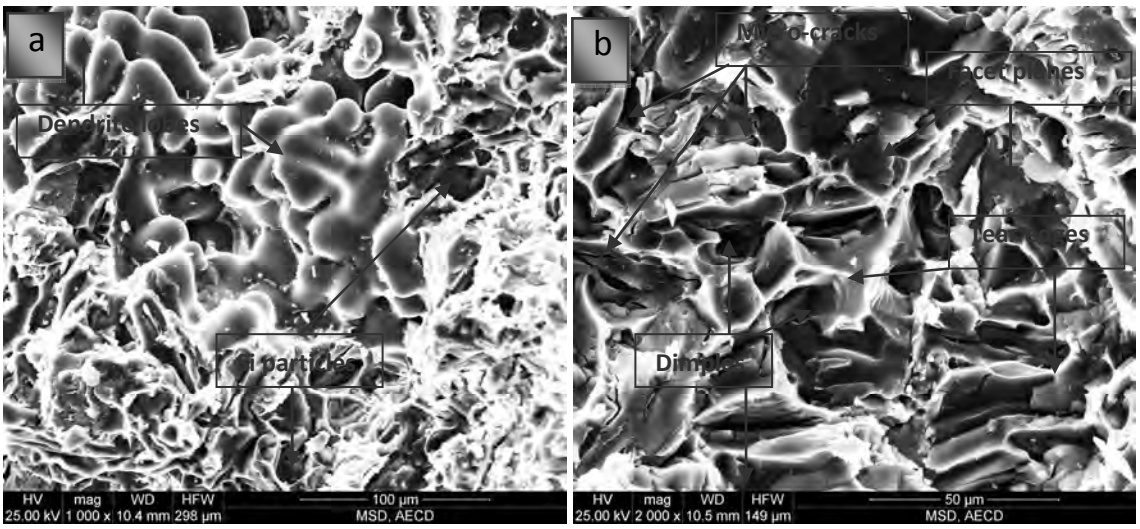

Figure 4.5.15: Fracture surface morphology of the peakaged Alloy-6 at a uniaxial tensile strain rate of $10^{-3}s^{-1}$

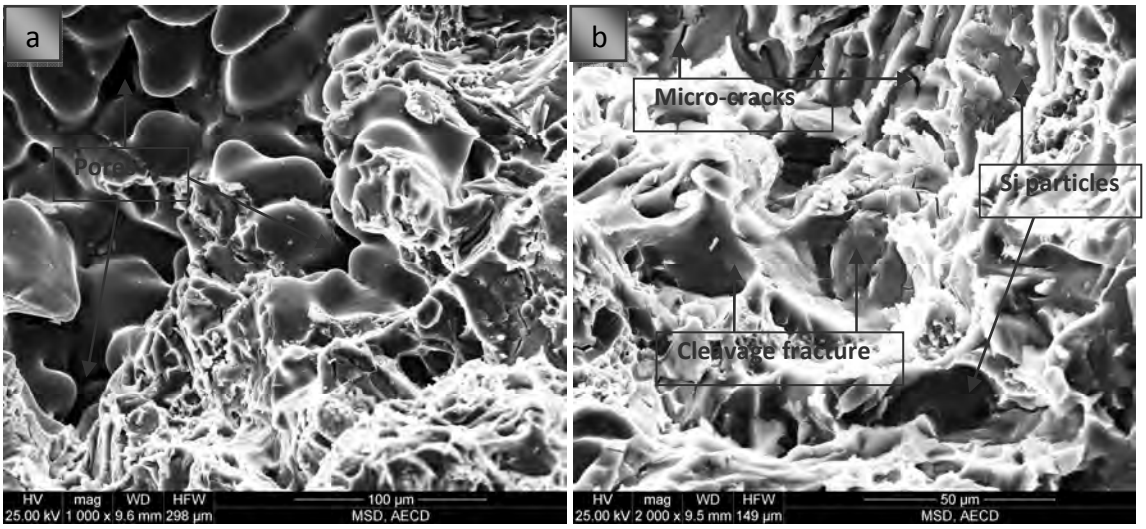

Figure 4.5.16: Fracture surface morphology of the peakaged Alloy-6 at a uniaxial tensile strain rate of $10^{-2}s^{-1}$

Compared with the fracture surface at solution treated condition, the fracture surface has more dimples indicate that the ductility increase obviously at peakaged condition. The fracture surface has many large and quasi-cleavage planes, tearing ridges and dimples. Figure 4.5.14 shows that the fracture surface at a lower strain rate ($10^{-4}s^{-1}$) and investigated higher number of dimples in the fracture surface at T6 heat treatment. So the number of dimples on the T6 state fracture surface increase obviously and there are also many bright tearing ridges exist which indicate that T6 state alloy has good ductility. As strain rate increases the number and shallowness of dimples decreases (Figure 4.5.16), as a results the materials behave less ductile in nature but has good tensile strength.

4.5.9 Tensile Fracture Behavior of Solutionized Alloy-7

Figure 4.5.17 shows the appearance of the fractured surface of the samples in the solution treated condition. The figure shows large and small dimple structure and broken or cracked primary Si particles and intermetallic particles. This indicates that the fracture was ductile fracture in the α-Al matrix and brittle in the thermal modified Si and intermetallic particles. It may thus be assumed that the fracture of the Si phases and intermetallics particles is responsible for the relatively low ductility of the T6 treated specimens. The crack front crosses the cleavage planes in the Si particles. The deformed micro necks of the α-aluminum solid solution are situated among them. Some dimples are present in these micro necks; as a result mixed

mechanism of fracture is present in this region. In the Si particle, the numerous cleavage cracks are visible in the Si particles and most of the Si particles the cleavage facets are situated. In the micro-region the oval and open shear dimples are revealed.

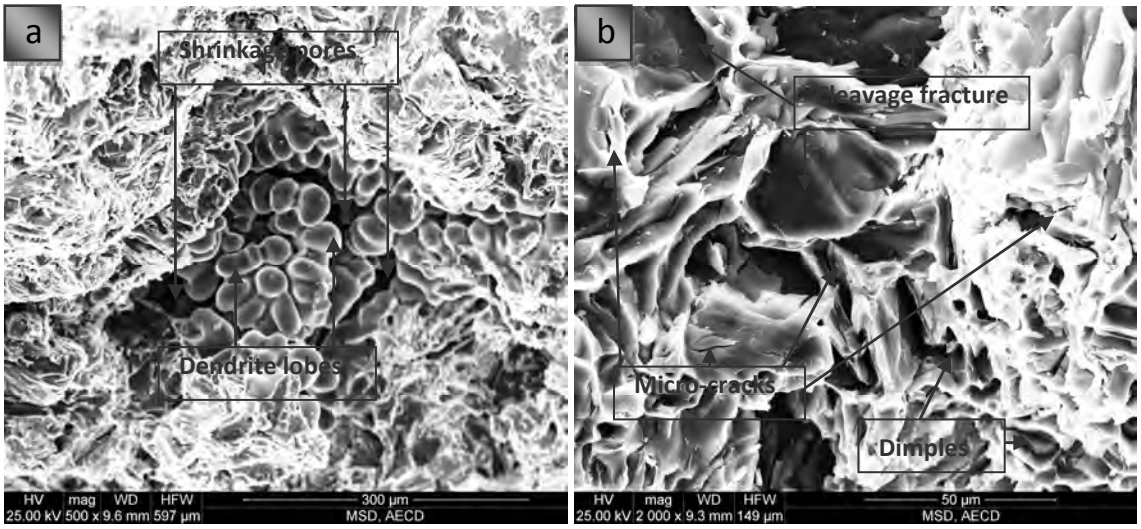

Figure 4.5.17: Fracture surface morphology of the solutionized Alloy-7 at a uniaxial tensile strain rate of $10^{-3}s^{-1}$

4.5.10 Tensile Fracture Behavior of Peakaged Alloy-7 at Various Strain Rates

Figures 4.5.18, 4.5.19 and 4.5.20 show fracture surfaces of Alloy-7 at three different strain rates $10^{-4}s^{-1}$, $10^{-3}s^{-1}$ & $10^{-2}s^{-1}$ respectively.

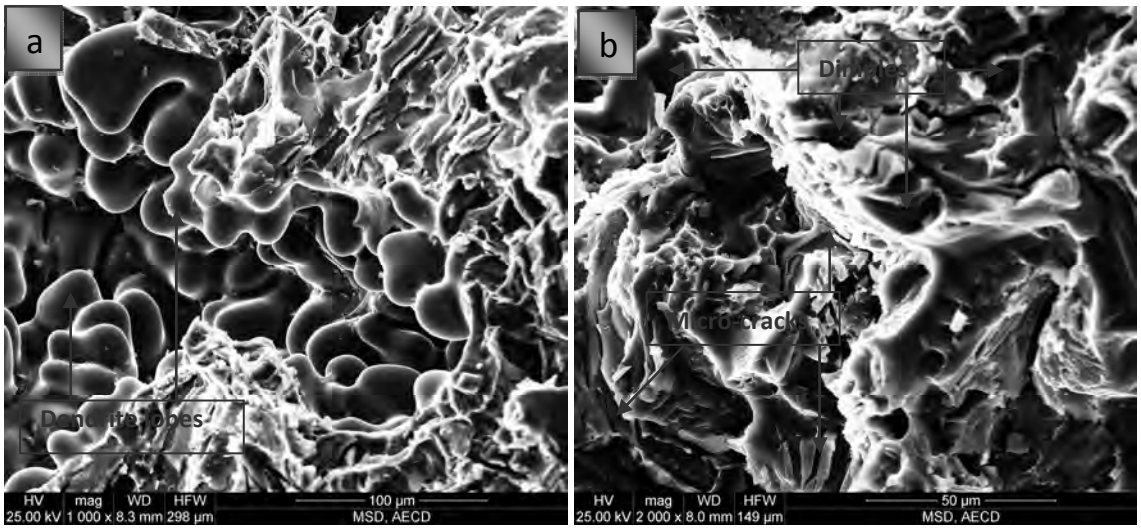

Figure 4.5.18: Fracture surface morphology of the peakaged Alloy-7 at a uniaxial tensile strain rate of $10^{-4}s^{-1}$

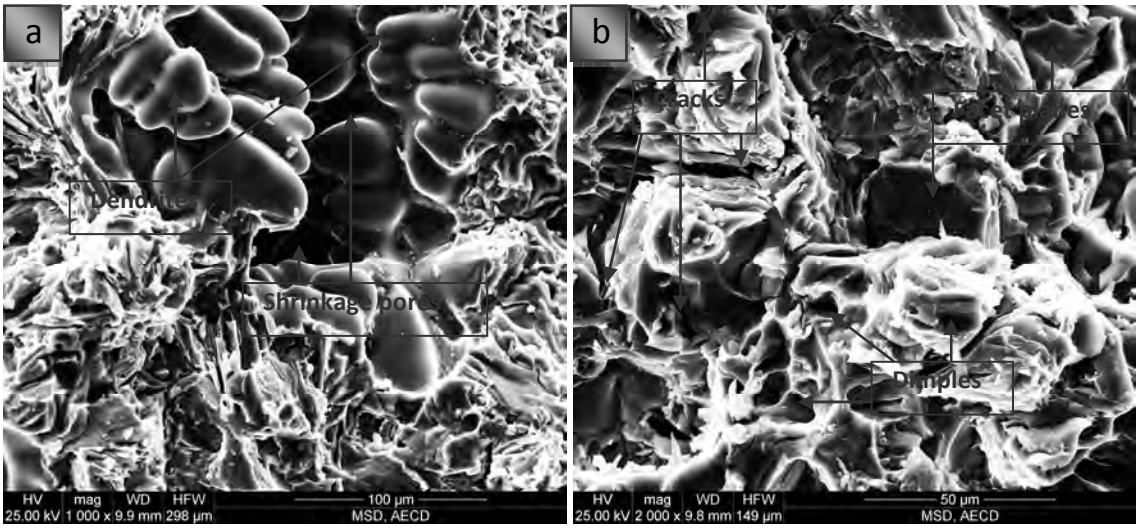

Figure 4.5.19: Fracture surface morphology of the peakaged Alloy-7 at a uniaxial tensile strain rate of $10^{-3}s^{-1}$

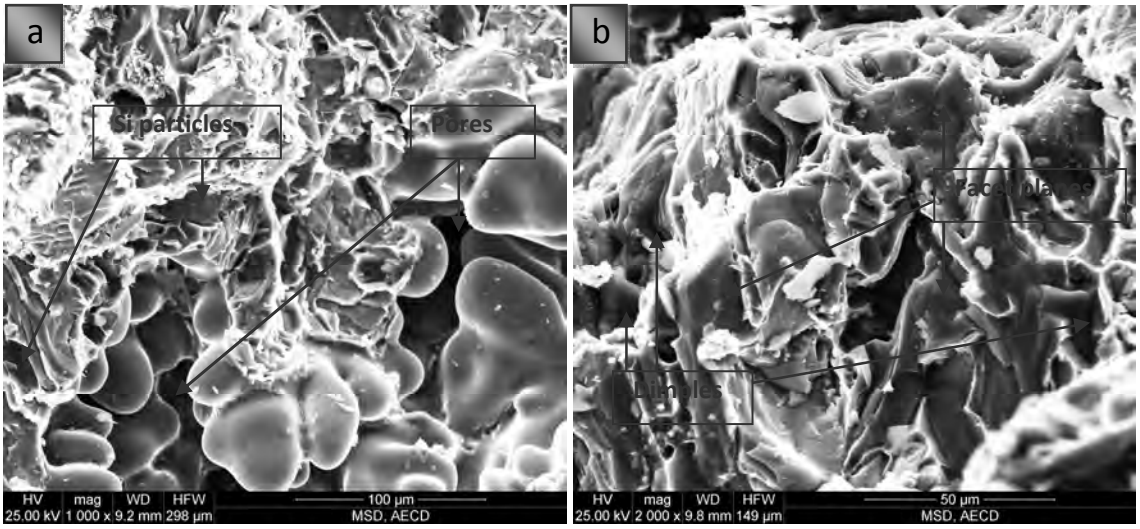

Figure 4.5.20: Fracture surface morphology of the peakaged Alloy-7 at a uniaxial tensile strain rate of $10^{-2}s^{-1}$

The fracture surfaces are perpendicular to tensile direction and show broken primary Si particles. As the strain rate increased to $10^{-2}s^{-1}$ the void coalescence occurred rapidly and the material shows gradually decreasing ductility. So the fracture behavior is greatly affected by strain rates. On a microscopic scale, the fractures appear to contain many microvoids, dimples and cracked Si particles in the α-Al matrix. The void coalescence occurs when the void elongates to the initial intervoid spacing. This leads to the dimple appearance of the fractured surfaces. There are fewer dimples at higher strain rate in the fracture surfaces (Figure 4.5.20).

Brittle fracture of these alloys indicates that void growth and coalescence occurred rapidly and at higher strain rates, the load could not be transferred from the matrix to the precipitates particles or second phases.

4.5.11 Charpy Impact Fracture Behavior of Peakaged Alloys

Figure 4.5.21 shows the SEM Fractographs of samples, tested under impact loading; of Alloy-1. Charpy impact specimen's exhibits shear induced fracture. Due to high strain rate involved in the impact specimens, the fracture surface shows complete dimple fracture. Transcrystalline fracture with the greatly developed surface and the main crack crossed the Si phases and intermetallic particles in the cleavage planes. There are seen some shallow dimples in the surfaces.

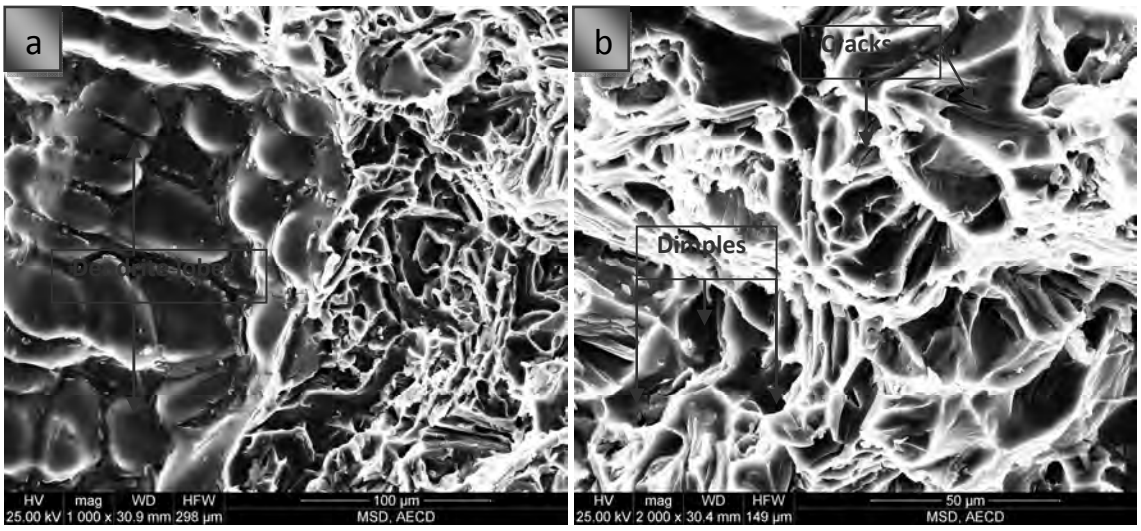

Figure 4.5.21: Fracture surface morphology of the peakaged Alloy-1 after impact test

Figure 4.5.22 shows the fracture appearance of an impact specimen of 4 wt% Cu content alloy (Alloy-5). There are very small and shallow dimples during deformation. The eutectic Si particle is surrounded with tear ridge of the micro-neck of the α-aluminium solid solution. The morphology of the dimples in the matrix is characteristic of the shear process. There are seen many brittle cracks in the Si particles.

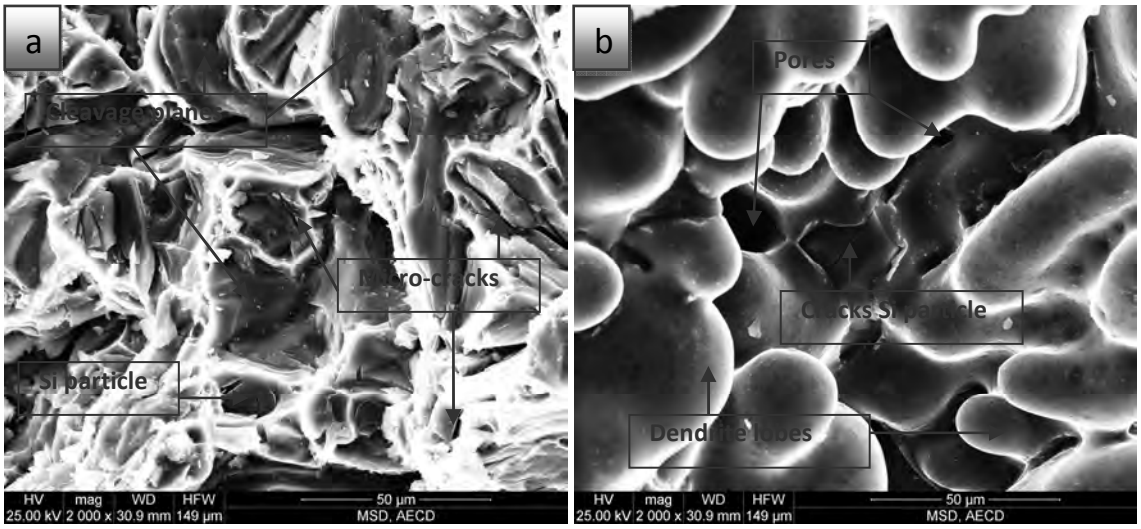

Figure 4.5.22: Fracture surface morphology of the peakaged Alloy-5 after impact test

The typical fracture characteristics in the impact fracture surface (Figure 4.5.23) show a cleavage pattern with flat facets representing Al-Si eutectic zone. These facets were more probably formed as a result of fracture of brittle Si phase crystals. On the other hand, some broken intermetallics might be found in this micrograph. There are seen some severe breakup occurred at the intermetallics, which presented a flower-like morphology with no obvious cleavage facets. This means that the stress field of the main crack broke up the intermetallics due to their poor deformation properties. The SEM image shows the transcrystalline fracture in the impact fracture surface. The cracks are presents in the Si particles and intermetallic particles. Some cleavage steps on the facets can be observed. Shear decohesion took place in the matrix.

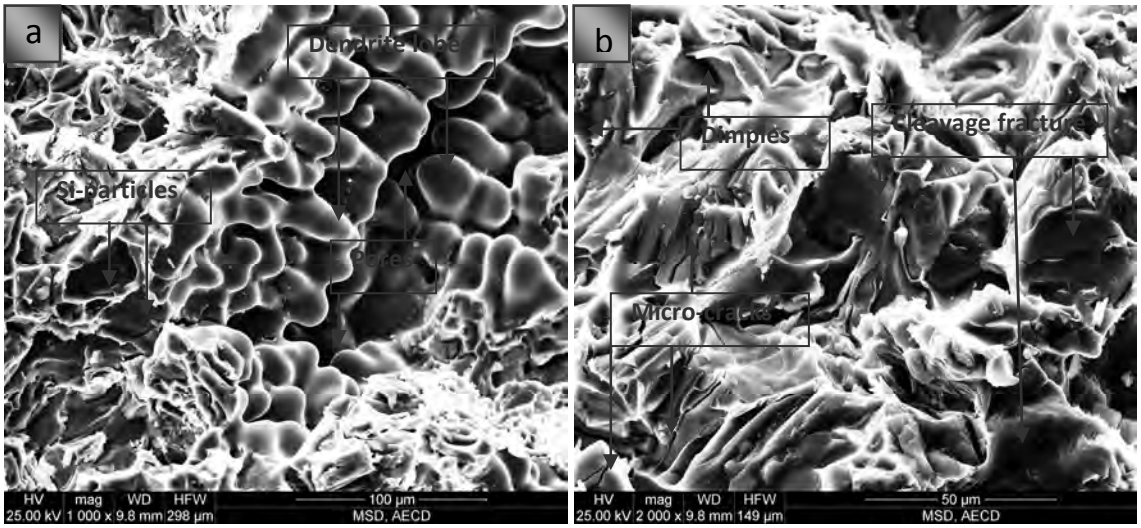

Figure 4.5.23: Fracture surface morphology of the peakaged Alloy-6 after impact test

The SEM micrograph (Figure 4.5.24) shows the Charpy impact fracture surface of Alloy-7 in the peakaged condition. There are some cracks in the Si phases and intermetallics. The facets are created only fracture at Si phases and sometimes in the intermetallic particles. There are severe decohesion present in the second phases and the α-aluminium matrix. The results of decohesion is the important cause of low impact absorbed energy. Some shear decohesion took place in the matrix and the fracture mode is transcrystalline brittle fracture.

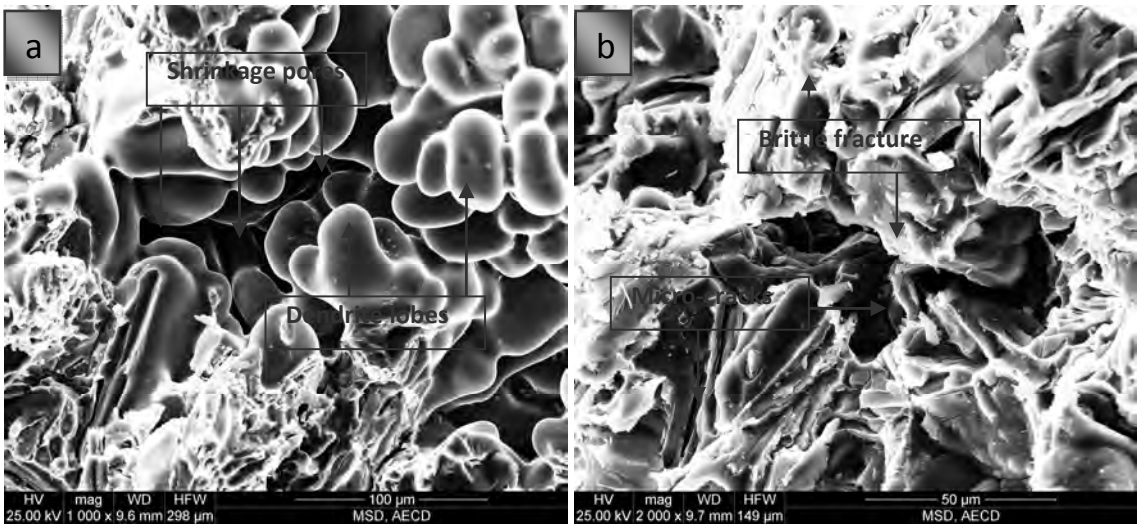

Figure 4.5.24: Fracture surface morphology of the peakaged Alloy-7 after impact test

There is a clear difference between the fracture surfaces. Fracture surface associated with the lowest toughness condition has an appearance consisting of dimples; small and shallow voids formed round the larger inclusions. The decrease in impact energy, in contrary to hardness, can be related to the formation of metastable precipitates. Increasing the hardness and the yield strength by precipitation makes the alloy more brittle and decreases the impact fracture energy since less plastic work can be done before the strain in the plastic zone is sufficient to fracture the test specimen.

4.6 Electrochemical Behaviors of the Alloys

The Electrochemical measurements were done to assess the corrosion behaviour of the peakaged (1hr at 225^{o}C) alloys only. Electrochemical Impedance Spectroscopy (EIS) test data were analysed by *Gamry Echem Analysis* software. The electrochemical impedance spectroscopy test results are shown in Table 4.6.1.

Table 4.6.1: EIS test results

Alloy Code	**Rs(Ω)**	**Rct(kΩ)**	**Cp(μF)**	**OCP(V/SCE)**
Alloy-1	40.37	15.57	1.259	-0.8454
Alloy-2	43.93	25.75	1.793	-0.7037
Alloy-3	44.08	27.13	3.219	-0.6534
Alloy-4	50.93	28.33	2.012	-0.6574
Alloy-5	47.97	6.435	2.942	-0.6263
Alloy-6	40.53	14.44	1.645	-0.6814
Alloy-7	44.40	27.95	1.773	-0.6445

The results of potentiodynamic polarization test are shown in Table 4.6.2.

Table 4.6.2: Potentiodynamic polarization test results

Alloy Code	Icorr(μA)	Ecorr(mV)	Epit (mV)	Corrosion rate(mpy)
Alloy-1	6.300	-764	-480	5.287
Alloy-2	5.640	-657	-408	4.732
Alloy-3	2.950	-697	-370	2.474
Alloy-4	20.30	-586	-353	17.050
Alloy-5	16.30	-583	-340	13.650
Alloy-6	2.540	-720	-426	2.132
Alloy-7	2.710	-644	-360	2.278

4.6.1 Corrosion Characteristics of Alloy-1

4.6.1.1 EIS Behavior of Alloy-1

OCP versus Times

Open circuit potential (OCP) versus time curves at neutral pH corrosive solution with Cl^- ions is presented in Figure 4.6.1. Initially the OCP decreased rapidly, showing minimum potential value at approximately -853mV to -855 mV in the solution. The OCP gradually increased to more noble potential values and finally achieved a steady state potential value at approximately -845 mV for Alloy-1 at pH=7. The OCP value measured with respect to saturated calomel electrode (SCE) as reference electrode and recorded for Alloy-1 in 0.1M NaCl solution at room temperature is -0.8454V, SCE. The OCP value of Alloy-1 is more negative than the other experimental alloys (Table 4.6.1).The more negative OCP indicates of corrosion being lower arrested in presence of chloride (Cl^-) ions and the strong lowering of the OCP values for Alloy-1 toward negative values is due to the fact that the chloride ions interact with the passive film which starts to dissolve slowly.

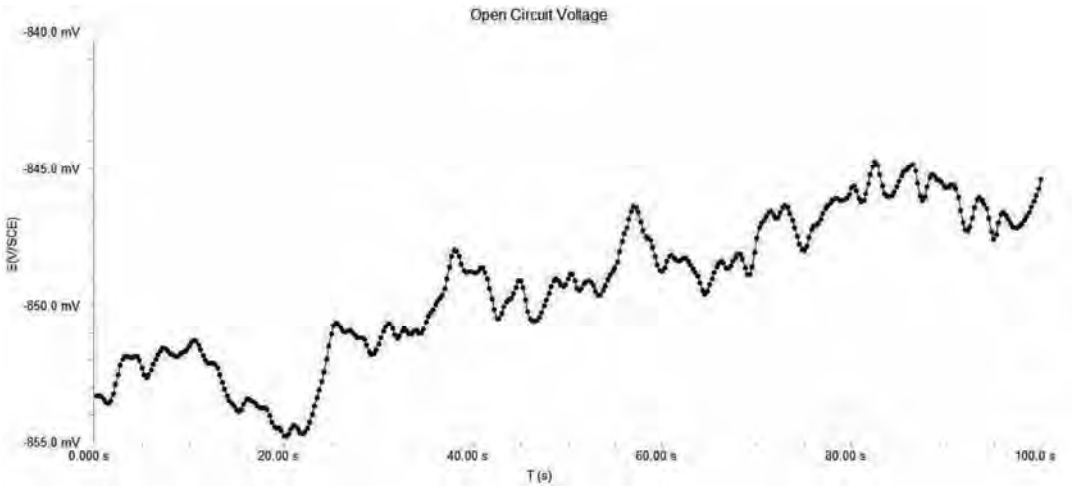

Figure 4.6.1: OCP variation with time for the peakaged Alloy-1 in 0.1M NaCl solution

Nyquist Plot

The data obtained (Table 4.6.1) were modeled and the equivalent circuit that best fitted to the results is shown in Figure 4.6.2. In Figure 4.6.2, Rs represents the ohmic resistance of the electrolyte, Rct and Cp are the charge transfer resistance and electrical double layer capacitance

respectively, which correspond to the Faradaic process at the alloy/media interface. Figure 4.6.3 shows the Nyquist diagrams of the Alloy-1 (Al-6Si-0.5Mg) in 0.1M NaCl in de-mineralized (DM) water. The impedance result shown in Table 4.6.1.

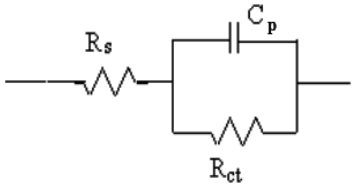

Figure 4.6.2: Electrical equivalent circuit used for fitting of the impedance data of the experimental alloys in 0.1M NaCl solution at neutral P^H

Figure 4.6.3 shows the results of the electrochemical impedance (EIS) tests on Al-6Si-0.5Mg alloy in 0.1M NaCl solution. The impedance plot, in Figure 4.6.3 shows the Nyquist representation of complex impedance. The charge transfer resistance (Rct) is 15.57kΩ and double layer capacitance (Cp) is 1.259μF, which clearly shows slightly higher corrosion resistance than Alloy-6. The low frequency impedance indicates the corrosion resistance of the surface. It is observed that the top has higher impedance than that of the bottom, because the semicircle radius of Nyquist plots. The solution resistance, Rs is 40.37Ω (very low with respect to Rct) i.e. the surface barrier is very high ion conductive.

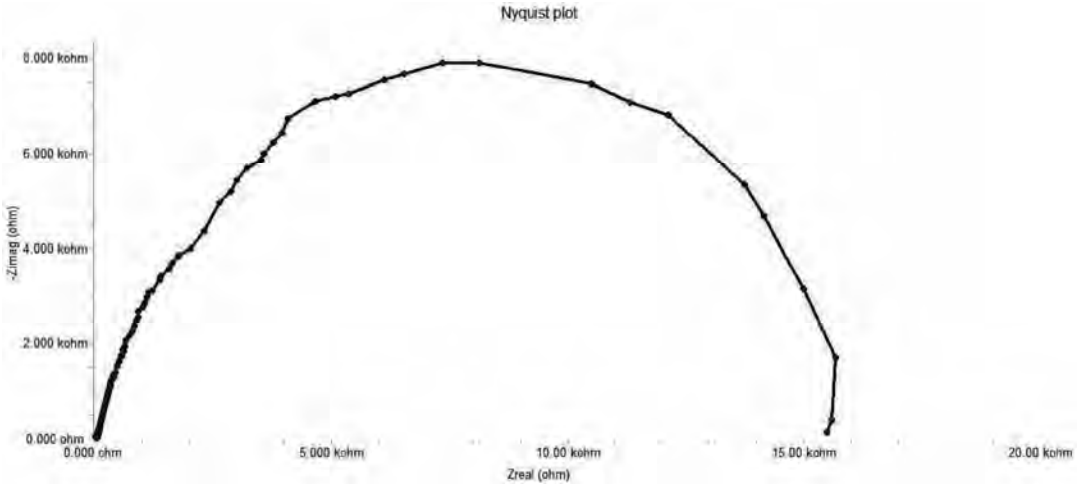

Figure 4.6.3: Nyquist plot for the peakaged Alloy-1 in 0.1M NaCl solution

Bode Plot

Figure 4.6.4 shows the experimental EIS results in Bode magnitude diagram for Alloy-1 in NaCl solution. Bode plots show the total impedance behaviour against applied frequency. At high frequencies, only the very mobile ions in solution are excited so that the solution resistance (Rs) can be assessed. At lower intermediate frequencies, capacitive charging of the solid-liquid interface occurs. The capacitive value Cp can provide very important information about oxide properties when passivation or thicker oxides are formed on the surface. Finally, at low frequency, the capacitive charging disappears because the charge transfer of electrochemical reaction can occur and this measured value of the resistance corresponds directly to the corrosion rate. For this reason, this low frequency impedance value is referred to polarization or charge transfer resistance (Rct).

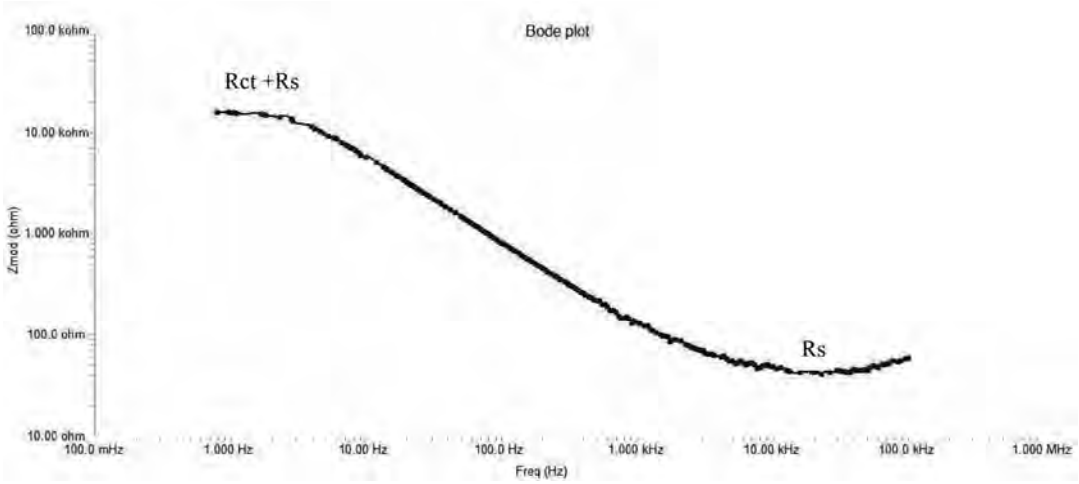

Figure 4.6.4: Bode plot for the peakaged Alloy-1 in 0·1M NaCl solution

4.6.1.2 Potentiodynamic Polarization Behavior of Alloy-1

Tafel plot

The potentiodynamic polarization curves of the alloys in 0.1M NaCl electrolyte solution of pH=7 were studied. The experiments were carried out in stagnant condition potential sweep of 0.5mV/SCE, in the range -1 to 1 V. The electrochemical parameters of the polarization curves of the alloys in aggressive solution are presented in Table 4.6.2. Tafel polarization test was carried out to find the pitting corrosion resistance. Anodic polarization curve was obtained by exposing the nugget area alone to 0.1M NaCl solution. Figure 4.6.5 shows the potentiodynamic polarization curve of Alloy-1 in NaCl solution. It is found that the corrosion potential Ecorr and Icorr values were - 0.764V and 6.30µA.The corrosion rate at this condition is 5.287mpy.

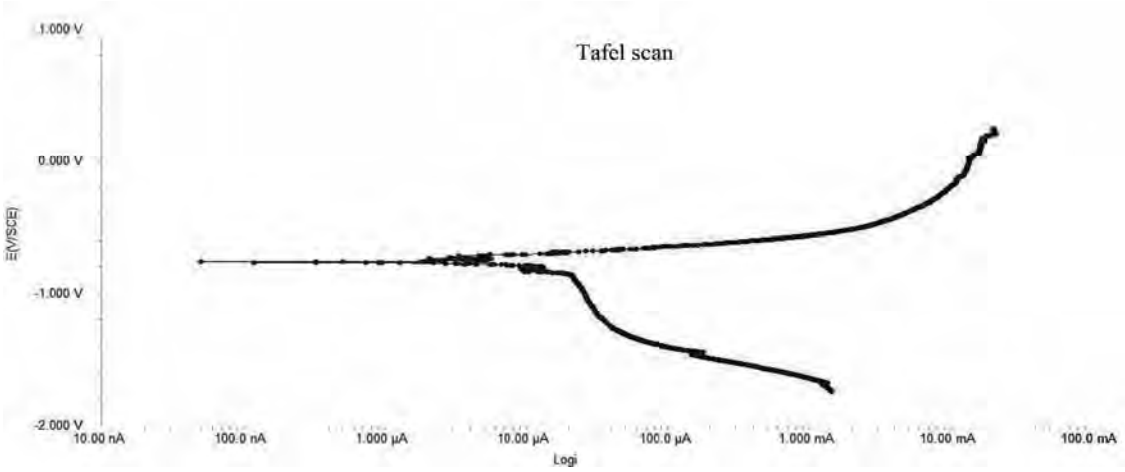

Figure 4.6.5: Potentiodynamic polarization curve of the peakaged Alloy-1 in 0.1M NaCl solution

Microstructures and Degradation Behavior

Figure 4.6.6 shows the microstructure of Alloy-1 after electrochemical corrosion study. The figure shows that the sample has suffered pitting corrosion. The exposed surface shows evidence of localized attack at the location of the intermetallic caused by the dissolution of the matrix. There was evidence of corrosion products of intermetallic compounds in all the samples examined. Greater degree of surface deterioration in Alloy-1 as observed from SEM images indicates the higher corrosion rate for the alloy. Besides, severe pits are visible in Alloy-1 examined at different magnifications. In Alloy-1 there seems to be uniform surface pits formations which are less deep as compared to those in Alloy-2, Alloy-3, Alloy-6 and Alloy-7. More pronounced deeper pits were seen in T6 225^{o}C/1hr Al-6Si-0.5Mg alloy.

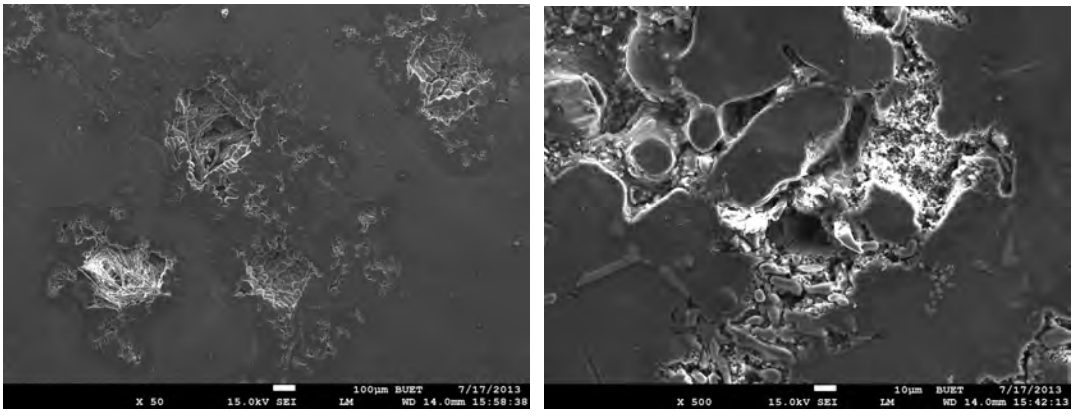

Figure 4.6.6: SEM Secondary Electron Image at different magnifications of the peakaged Alloy-1 as- corroded in 0.1M NaCl Solution

4.6.2 Corrosion Characteristics of Alloy-2

4.6.2.1 EIS Behavior of Alloy-2

OCP versus Time Behavior

Figure 4.6.7 shows the trend of the variations of open circuit potential (OCP) with exposure time of Al-6Si-0.5Mg-0.5Cu alloy (Alloy-2) after peakaged heat treatment in 0.1M NaCl solution. A small fluctuations and increasing potential to more positive direction was seen during the initial 55 second of exposure. Afterwards the OCP fluctuation decreases and reached about a steady state after 60 second of exposure. The steady state OCP is -0.7037V and it is more positive than the OCP value of Alloy-1.The occurrence of a positive shift in the OCP of 0.5wt% Cu added to Al-6Si-0.5Mg alloy indicates the existence anodically controlled reaction.

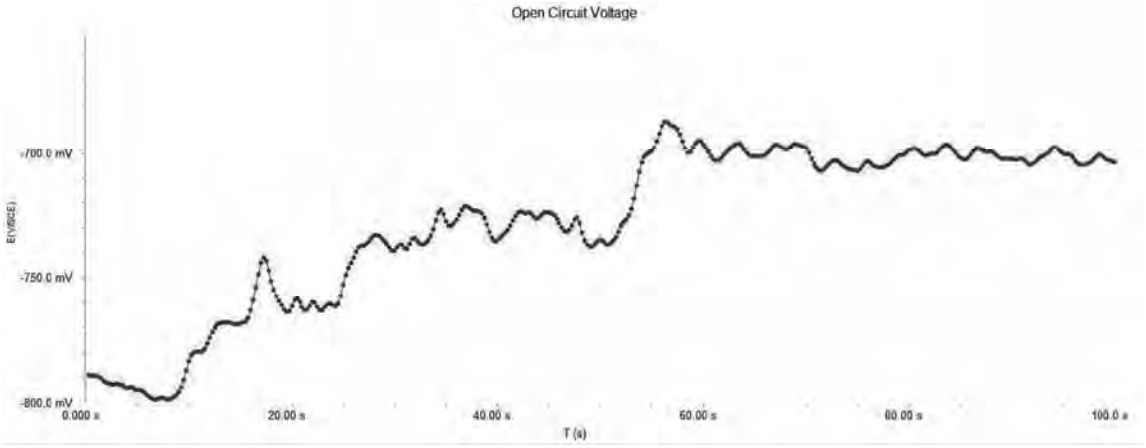

Figure 4.6.7: OCP variation with time for peakaged Alloy-2 in 0.1M NaCl solution

Nyquist Plot

EIS analysis of 0.5wt% Cu content Al-6Si-0.5Mg alloy (Alloy-2) was carried out at the same condition maintained for EIS analysis of Alloy-1. From the impedance plots (Figure 4.6.8), the charge transfer resistance (Rct) and the double layer capacitance (Cp) values were calculated using Gamry Echem software with an equivalent circuit where Rs is the solution resistance. The Charge transfer resistance (Rct) of Alloy-2 is 25.75kΩ, which is remarkably higher than the Cu free alloy (Alloy-1).The double layer capacitance, Cp=1.793µF is also slightly higher than the Alloy-1. So after 0.5wt% Cu addition to Al-6Si-0.5Mg alloy, the charge transfer resistance increases remarkably. Measurement of high charge transfer resistance and moderate double layer capacitance for Alloy-2 indicates less corrosion tendency in NaCl solution. The solution

resistance (Rct=43.93Ω) observed for Alloy-2 is very low and similar to Alloy-1.The low solution resistance indicates the existence of more ion conducting surface film. A porous oxide film of having a higher double layer capacitance increases the diffusion of chloride ions through metal/solution interfaces. An oxide film which possesses the above properties makes fast diffusion reaction.

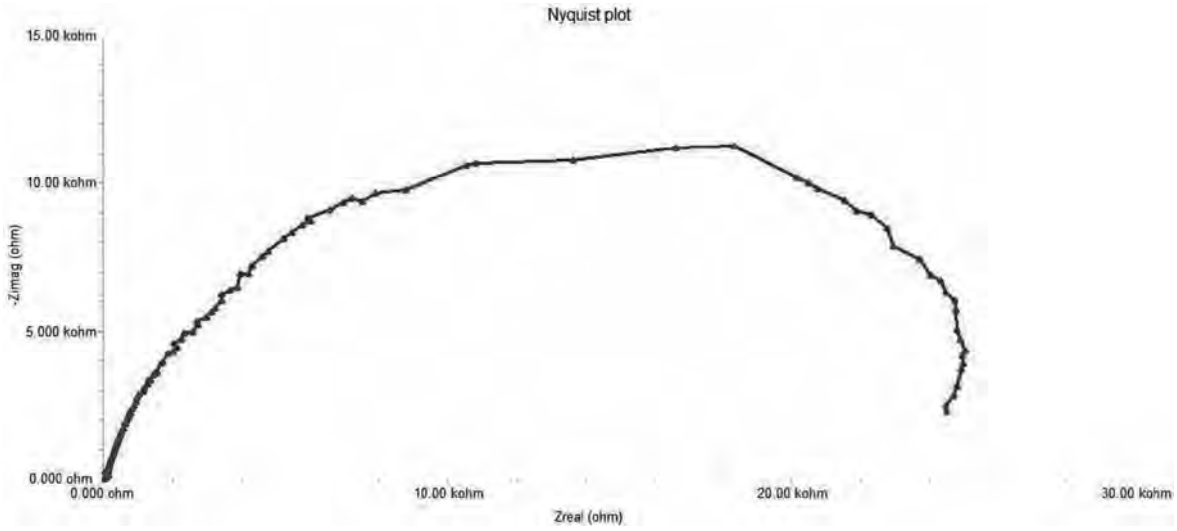

Figure 4.6.8: Nyquist plot for the peakaged Alloy-2 in 0.1M NaCl solution

Bode Plot

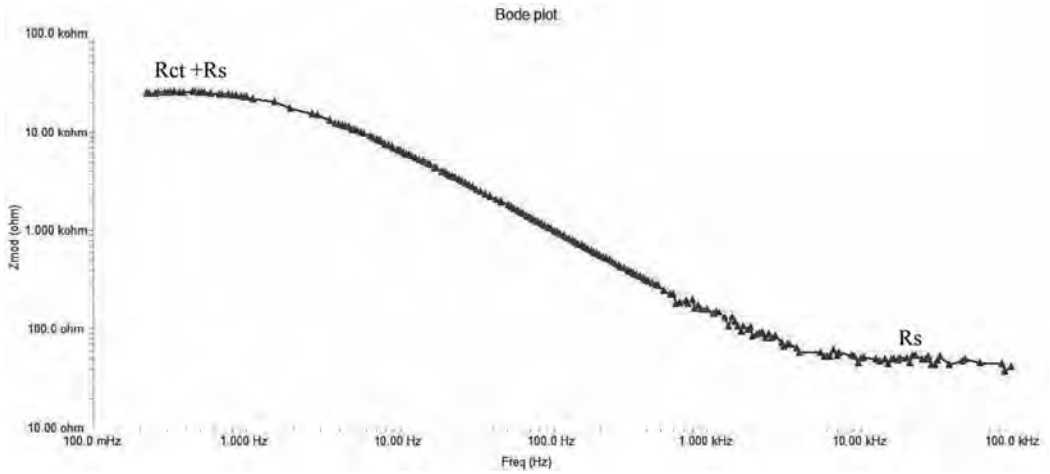

Figure 4.6.9: Bode plot for the peakaged Alloy-2 in 0·1M NaCl solution

Figure 4.6.9 gave the Bode plot of EIS spectra of Alloy-2. The impedance behaviour is very similar to the Alloy-1. At high frequency (10-100 kHz) the double layer capacitance act as a

short circuit and only the motion of charged ions in solution can be characterized as Rs. At lower intermediate frequencies (5-300 Hz), capacitive charging of the solid-liquid interface occurs. At lower frequencies (< 1Hz), the double layered capacitance disappears so that the current passing through the solid-liquid interface is revealed as a charge transfer resistance (Rct=25.7kΩ).

4.6.2.2 Potentiodynamic Polarization Behavior of Alloy-2

Tafel Plot

Figure 4.6.10 shows the polarization curves of the samples immersed in 0.1M NaCl solution at room temperature. From the potentiodynamic polarization curve, cathodic and anodic current density decreased due to 0.5wt% Cu addition to Al-6Si-0.5Mg alloy. This means the anodic and cathodic corrosion rates are reduced. The Ecorr value of Alloy-2 is -657mV which was nobler than the Cu free Alloy-1.The Icorr value (5.64µA) is also less than the Icorr value of Cu free Alloy-1.So the nobler potential and less current density indicates the lower corrosion rate (4.732mpy) of the Al-6Si-0.5Mg-0.5Cu alloy (Alloy-2).

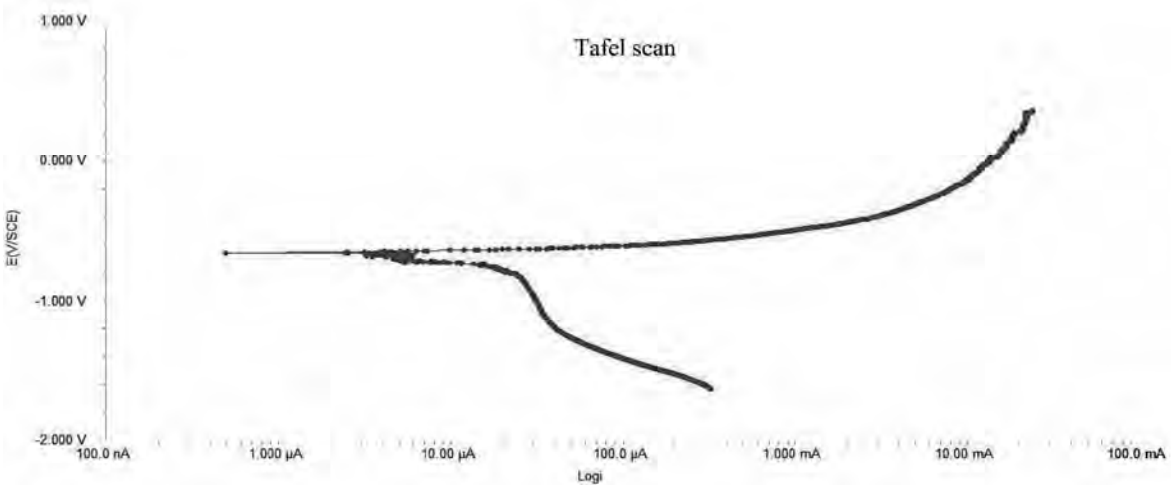

Figure 4.6.10: Potentiodynamic polarization curve of peakaged Alloy-2 in 0.1M NaCl solution

Microstructures and Degradation Behavior

Figure 4.6.11 shows a typical corroded microstructure of Al-6Si-0.5Mg-0.5Cu alloy (Alloy-2) after polarization tests. The Al_2Cu particles in α-solid solution and the solute element copper form micro galvanic cells with surrounding matrix and are responsible for the corrosion of alloy.

The observed pits in the Alloy-2 exposed surface are in less number and shallow compared to the reference alloy (Alloy-1), Alloy-6 and Alloy-7.

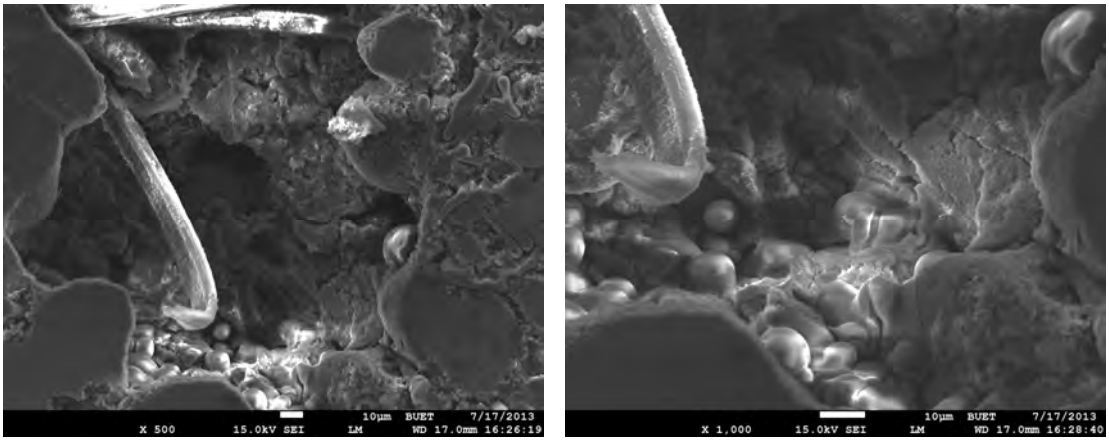

Figure 4.6.11: SEM Secondary Electron Image at different magnification of the peakaged Alloy-2 as- corroded in 0.1M NaCl Solution.

4.6.3 Corrosion Characteristics of Alloy-3

4.6.3.1 EIS Behavior of Alloy-3

OCP versus Time Behavior

The OCP values measured with respect to SCE reference electrode and recorded for the Alloy-3 in 0.1M NaCl solution at room temperature. The fluctuation of the OCP value is not so changes during the time of exposure. The steady state OCP value of Alloy-3 is -6534mV, which is the most positive value except Alloy-7. Due to addition of 1wt% Cu to Al-6Si-0.5Mg alloy, a considerable shift of OCP in noble direction is observed positive shift in OCP indicates the existence of anodically controlled reaction.

Figure 4.6.12: OCP variation with time for peakaged Alloy-3 in 0.1M NaCl solution

Nyquist Plot

The corrosion behavior is most explicit in the Nyquist plot (Figure 4.6.13) of impedance spectroscopy recorded at open circuit conditions after a steady state potential was attained with the 0.1M NaCl electrolyte in aerated conditions. The measured impedance data were analyzed based upon the Levenberg-Marquardt equivalent circuit (EC). The circuit includes a solution resistance (Rs), charge transfer or polarization resistance (Rct) of the surface oxide film, capacitance of the constant phase element (CPE) which substitutes the double layer capacitance (Cp) of the solid solution interface. The evaluated charge transfer resistance (Rct =27.13kΩ) by the increased value of Rct compared to the other alloys (except Alloy-4 & Alloy-7).The higher value of Rct means that the material corrosion resistance is high. The solution resistance (Rs=44.08Ω) of Alloy-3 in 0.1M NaCl solution is very similar to the investigated alloys.

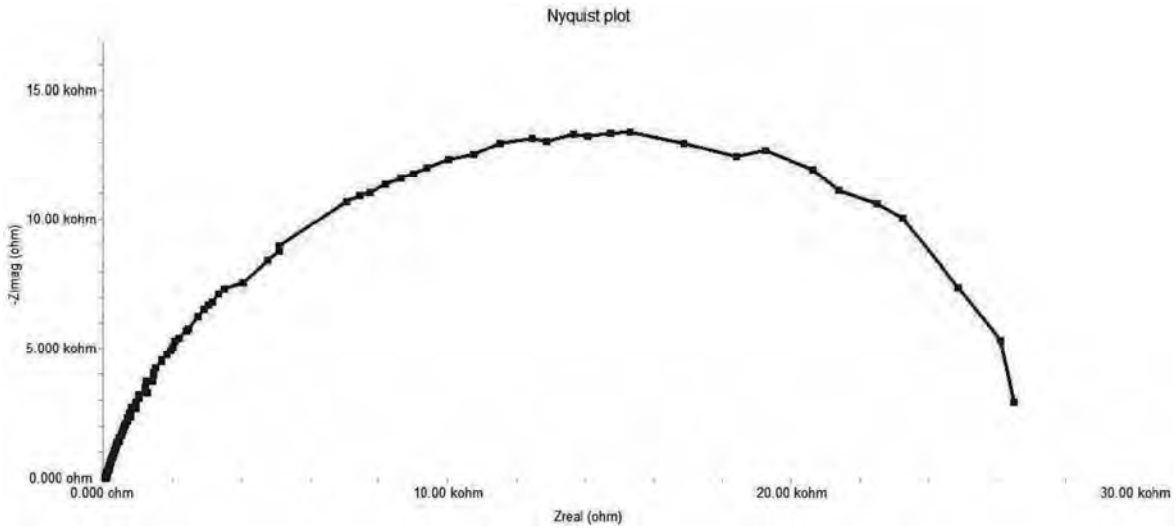

Figure4.6.13: Nyquist plot for the peakaged Alloy-3 in 0.1M NaCl solution

Bode Plot

At higher frequencies (Figure 4.6.14), the impedance is only the electrolytes resistance (Rs=44Ω) which is very small with respect to charge transfer resistance (Rct = 27.13kΩ). The impedance is very high at lower frequencies and the impedance is a measure of total corrosion resistance of the material.

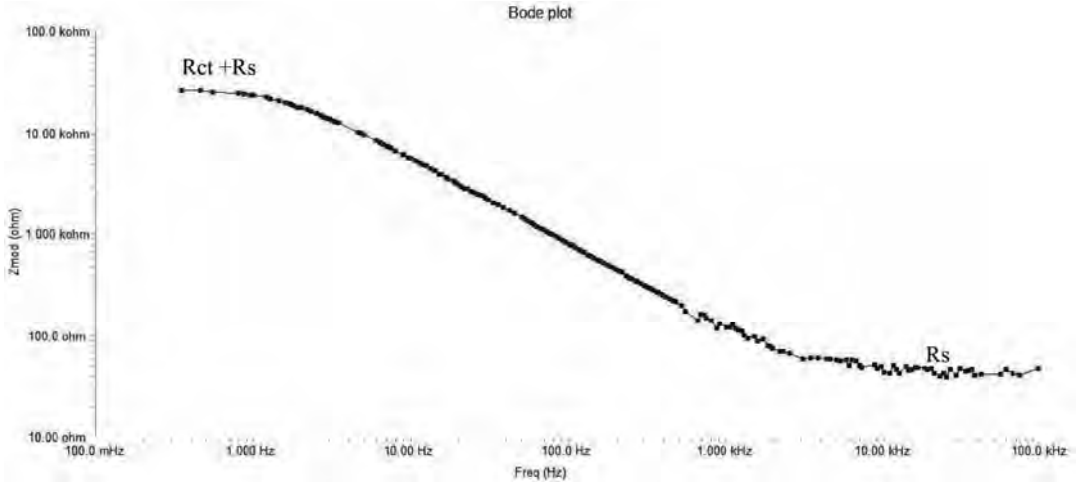

Figure 4.6.14: Bode plot for the peakaged Alloy-3 in 0·1M NaCl solution

4.6.3.2 Potentiodynamic Polarization Behavior of Alloy-3

Tafel Plot

The Ecorr value of Alloy-3 in 0.1M NaCl solution (Figure 4.6.15) is -697mV which is shifted to positive potential. The corrosion current density (Icorr) value is 2.950µA, which is lower than the Icorr value of Alloys 1 and 2. 1wt% Cu addition to Al-6Si-0.5Mg alloy decreases the corrosion current density. Al_2Cu intermetallic phase in Al-6Si-0.5Mg-Cu alloys reduces the electron transportation rate. The corrosion potential value of Alloy-3 move to more negative values and corrosion current density is reduced. The reduced corrosion current density decreases the corrosion rate (2.474mpy) of Alloy-3.

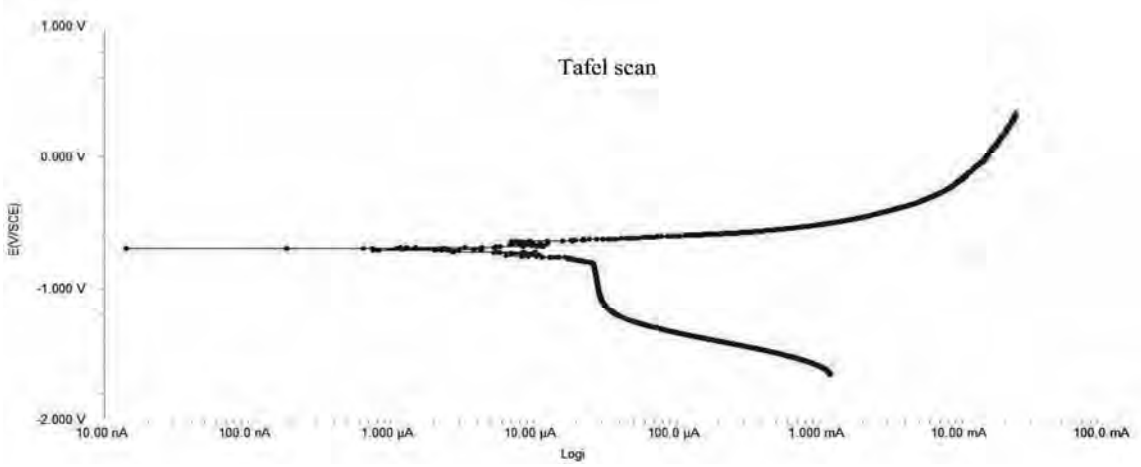

Figure 4.6.15: Potentiodynamic polarization curve of peakaged Alloy-3 in 0.1M NaCl solution

Microstructures and Degradation Behavior

The microstructure of as-corroded Alloy-3 using SEM indicates many pronounced pits; showing that the samples have suffered pitting corrosion attach (Figure 4.6.16). In the exposed surfaces there seems to be many surface pits formations which are less deep as compared to those in Alloys 2, 6 and 7. Less pronounced shallow pit were seen in T6 225^{o}C/1hr in the Alloy-3 corroded surface.

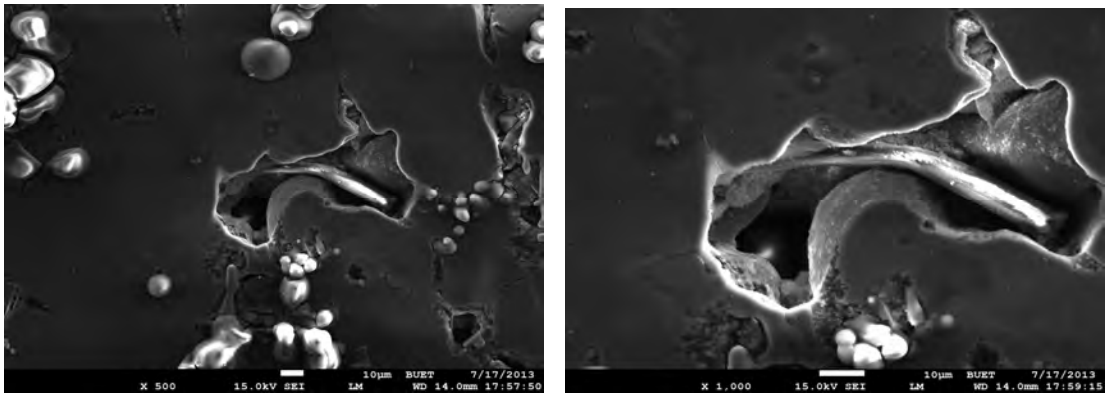

Figure 4.6.16: SEM Secondary Electron Image at different magnifications of the peakaged Alloy-3 as- corroded in 0.1M NaCl Solution

4.6.4 Corrosion Characteristics of Alloy-4

4.6.4.1 EIS Behavior of Alloy-4

OCP versus Time Behavior

A marked fluctuation in OCP for the Alloy-4 was recorded (Figure 4.6.17) during initial 20 second of exposure. After 40 seconds of exposure, its OCP attained a steady state. Alloy-4 showed a more positive OCP value (0.657V) than the other alloys. The occurrence of a positive shift in the OCP of Alloy-4 indicates the existence of anodically controlled reaction.

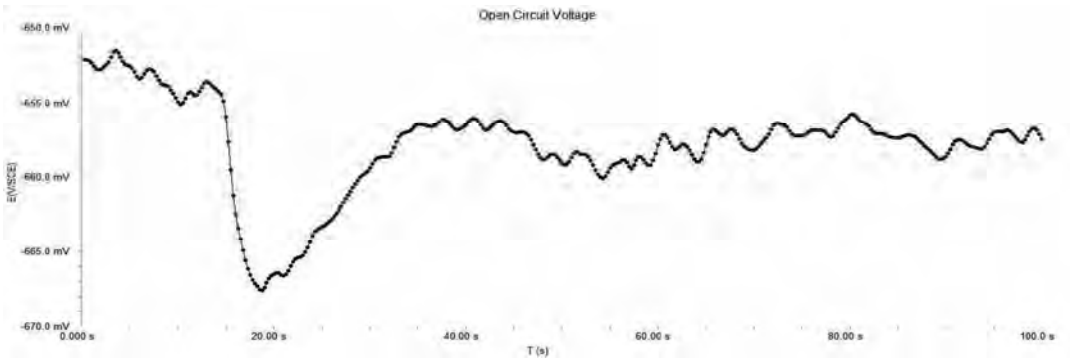

Figure 4.6.17: OCP variation with time for the peakaged Alloy-4 in 0.1M NaCl solution

Nyquist Plot

Impedance measurements showed that increasing Cu in the alloy increases charge transfer resistance, Rct. For Alloy-1 (no Cu) the Rct value is 15.57kΩ, and this value increases to 28.33kΩ in Alloy-4 (2wt% Cu) (Figure 4.6.18). This increase in polarization resistance (Rct) indicates increase in corrosion resistance of the alloys (Alloy-1 to Alloy-4). It can also be observed that Alloy-4 exhibited better corrosion resistance than did the other alloys. It seems that the more noble electrochemical behavior of this alloy essentially could be explained by the higher volume fraction of Cu containing intermetallic phases. Observation of less solution resistance, Rs=50.93Ω indicates the existence of highly conducting surface film.Alloy-4 has a moderate double layer capacitance (Cp) value than the other Cu containing Al-6Si-0.5Mg alloys. But this capacitance value 2.012µF is higher than the Cu free Alloy-1. The increase in charge transfer resistance with a moderate double layer capacitance was indicative of the reduction in the active corrosion area with 2 wt% Cu addition to Al-6si-0.5Mg alloy.

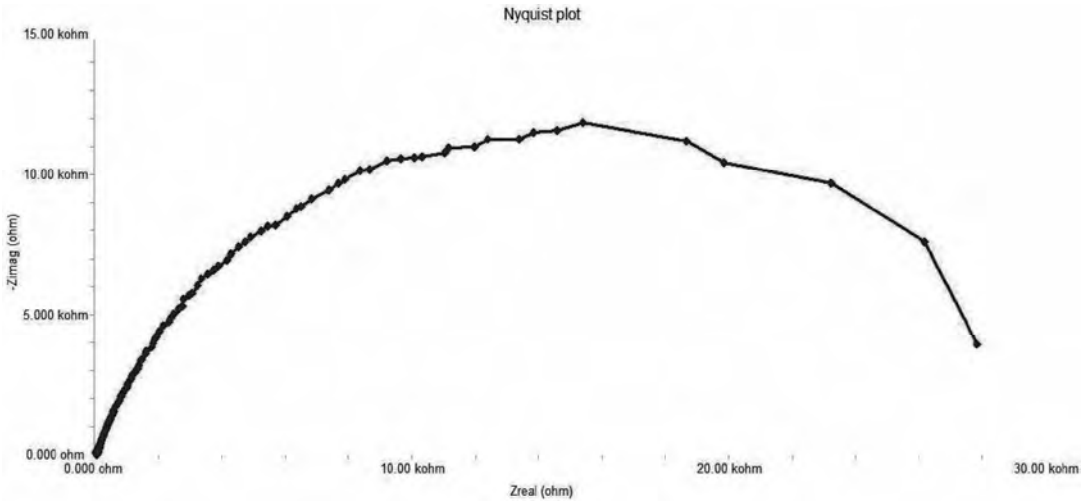

Figure 4.6.18: Nyquist plot for the peakaged Alloy-4 in 0.1M NaCl solution

Bode Plot

The Bode plot is shown in Figure 4.6.19. At higher frequencies, the impedance is revealed the electrolytes resistance (Rs=50.93Ω).

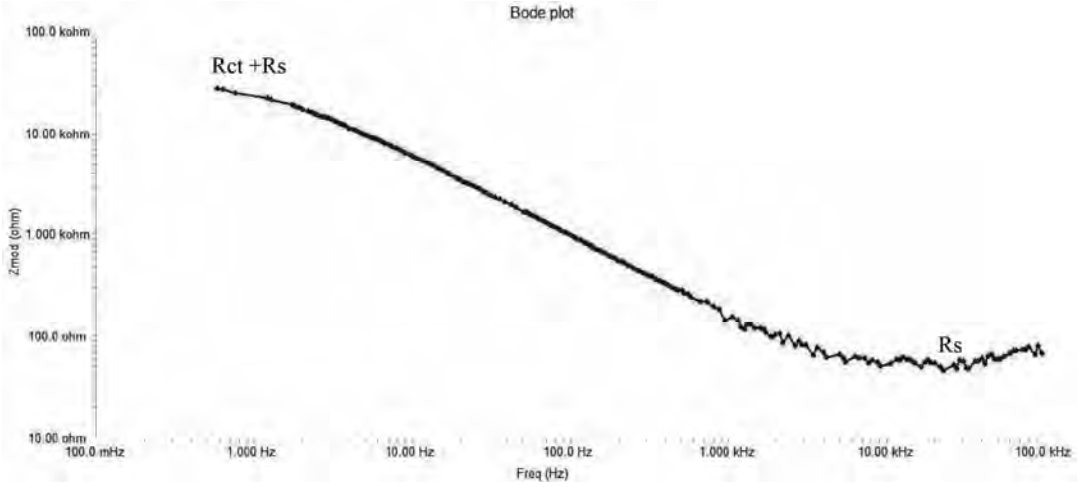

Figure 4.6.19: Bode plot for the peakaged Alloy-4 in 0·1M NaCl solution

4.6.4.2 Potentiodynamic Polarization Behavior of Alloy-4

Tafel Plot

Figure 4.6.20 shows that Ecorr value of Alloy-4 is -0.586V and Icorr is 20.30µA. The Ecorr value is more positive than the other alloys (except Alloy-5) and the higher current density indicates the higher corrosion rate (17.05 mpy).

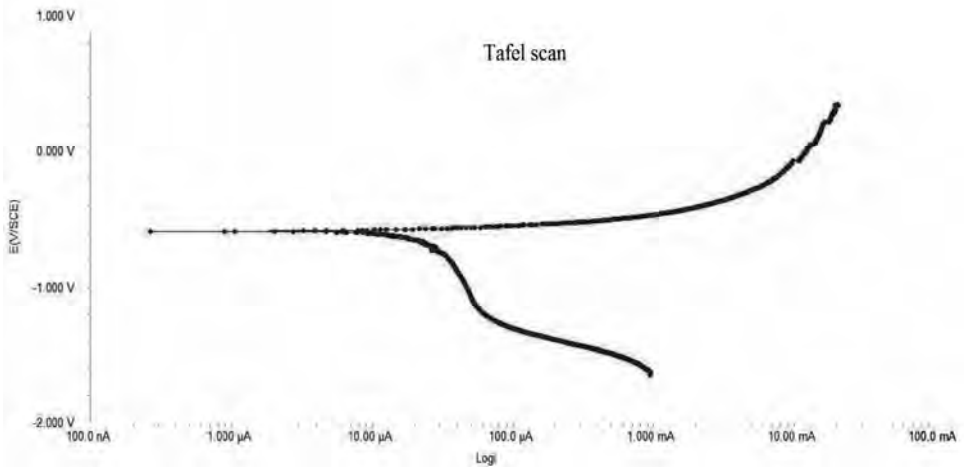

Figure 4.6.20: Potentiodynamic polarization curve of peakaged Alloy-4 in 0.1M NaCl solution

Microstructures and Degradation Behavior

The exposed surface (Figure 4.6.21) shows evidence of localized attach at the location of the intermetallic caused by the dissolution of the matrix. There was evidence of corrosion products

in all the samples examined. Besides, several pits are visible in all samples examined at different magnifications. It is provable that the pits are formed by intermetallic dropping out from the surface due to the dissolution of the surrounding matrix. However, it is also possible that the pits are caused by selective dissolution of the intermetallic/or particles of the second phase precipitates. Consequently, the forms of corrosion in the alloy are slightly uniform and predominantly pitting corrosion as obtained by the SEM. The pits are less deep than the other Cu content and reference alloy (Alloy-1) corroded surfaces existing.

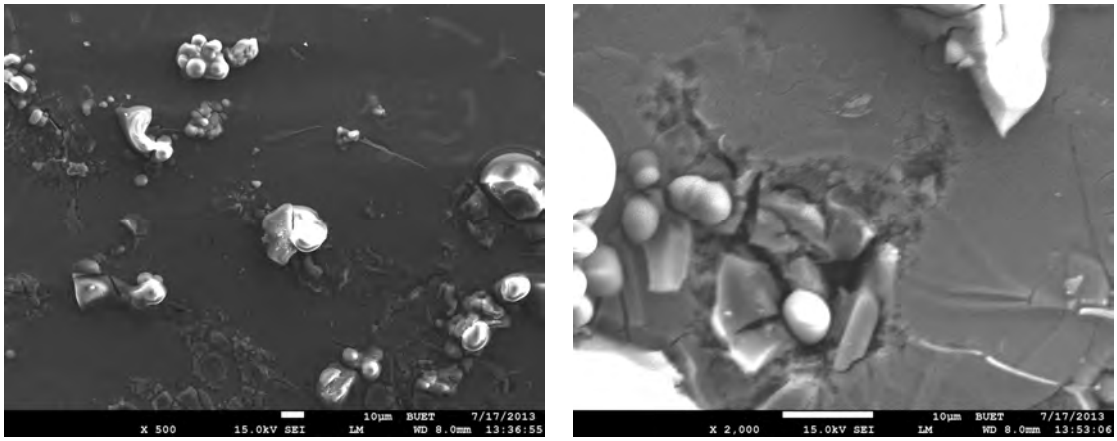

Figure 4.6.21: SEM Secondary Electron Image at different magnifications of the peakaged Alloy-4 as- corroded in 0.1M NaCl Solution

4.6.5 Corrosion Characteristics of Alloy-5

4.6.5.1 EIS Behavior of Alloy-5

OCP versus Time Behavior

The OCP value fluctuates with times (Figure 4.6.22) and the OCP of the peakaged sample became more positive with time, the rise in potential being largest during the first 25 seconds. After 25 seconds, continuous and very rapid changes in OCP with time were observed. The OCP gradually increased to more noble potential values and finally achieved about a steady state potential value at approximately -6263mV at pH=7. At this potential Alloy-5 present oscillations phenomena (passivation/depassivation of the film) due to the presence of Al, Si, Cu and Mg precipitation compounds which dissolves faster than others constituents. When the compound is dissolved the potential is decreased and the potential starts to rise again; The OCP stability of the reaction film allows us to determine the formation rate of the passive film of the alloys. The

strong increasing of the OCP values for Alloy-5 toward positive values (Figure 4.6.22) is due to the fact that the chloride ions interact with the passive film which starts to dissolve quickly.

Figure 4.6.22: OCP variation with time for the peakaged Alloy-5 in 0.1M NaCl solution

Nyquist Plot

Figure 4.6.23 illustrates the Nyquist plot obtained for 4 wt% Cu containing alloy. The corrosion parameters obtained from the Nyquist plot are given in Table 4.6.1.

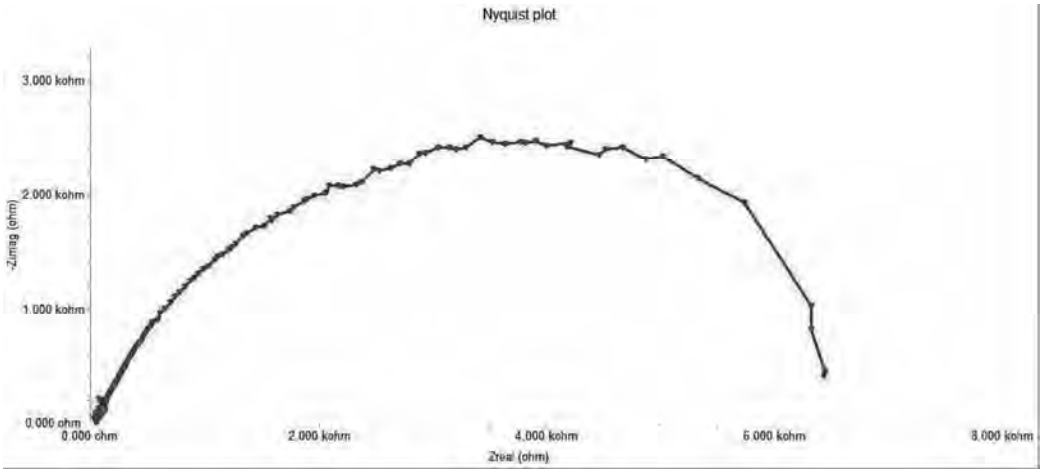

Figure 4.6.23: Nyquist plot for the peakaged Alloy-5 in 0.1M NaCl solution

Alloy-5 showed the lowest charge transfer resistance (6.435kΩ) among the investigated alloys. This lower corrosion resistance is due to the excess addition Cu (4wt %) and over distribution of Al_2Cu intermetallic phases in α-solid solution. The capacitance connected in parallel to the charge transfer resistance corresponds to interfacial double capacitance (Cp) and therefore may

approximately indicate the expanded surface area of the corroding electrode. The double layer capacitance is 2.942µF, which is higher than all other alloys (except Alloy-3).The relatively lower Rct and increased capacitance confirmed the lower corrosion resistance of Alloy-5. Presence of shrinkage pores and higher Cu rich phases in Alloy-5 is perhaps responsible for lower Rct. The solution resistance is 47.97Ω, which is very similar to the other alloys and its effect is negligible compared to the Rct.

Bode Plot

The solution resistance of the electrolyte reveals from the Bode plot (Figure 4.6.24) of the Alloy-5 at higher frequencies (>10 kHz). At higher frequencies the mobile ions are short circuited and only the electrolyte resistance is assessed as impedance. At lower intermediate frequencies (10Hz-10 kHz) there is only occurred the solid-liquid interface capacitive charging. The total impedance is observed from the Bode plots at very lower frequencies (< 1Hz).

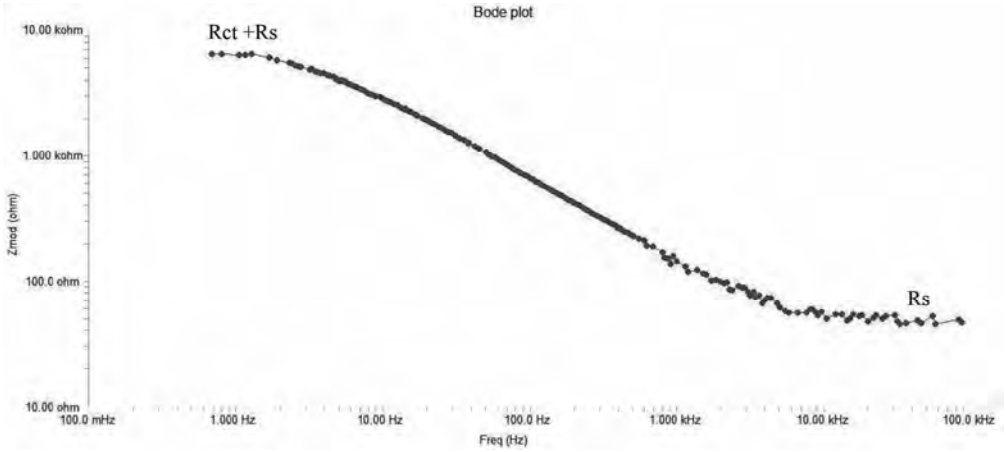

Figure 4.6.24: Bode plot for the peakaged Alloy-5 in 0.1M NaCl solution

4.6.5.2 Potentiodynamic Polarization Behavior of Alloy-5

Tafel Plot

Figure 4.6.25 shows the potentiodynamic curve for Alloy-5 in 0.1M NaCl solution at room temperature. Table 4.6.2 summarizes the various corrosion parameters obtained from Tafel plots. The value of corrosion potential (Ecorr) is -0.583V, which is most positive potential among the investigated alloys. The corrosion current (Icorr) density is 16.30µA which is higher than the other experimental alloys (except Alloy-4).This higher corrosion density confirms

higher corrosion rate (13.610mpy). It is clear from the polarization curve that all regions showed cathodic control reaction since it has higher cathodic Tafel slopes than anodic Tafel slopes.

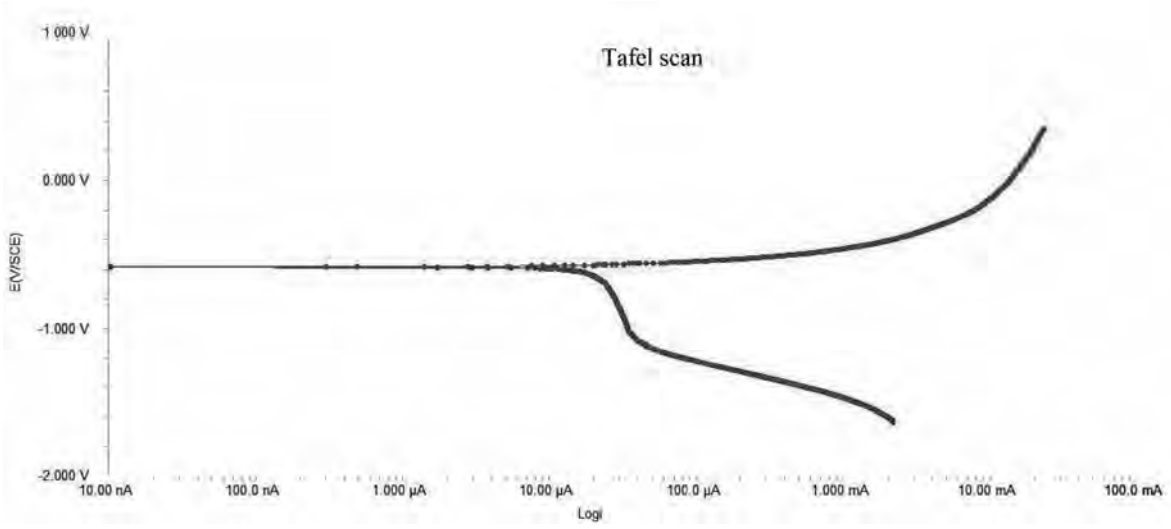

Figure 4.6.25: Potentiodynamic polarization curve of peakaged Alloy-5 in 0.1M NaCl solution

Microstructures and Degradation Behavior

Scanning electron micrographs of Alloy-5 (4wt% Cu) after corrosion in 0.1 N NaCl reveal most severe pitting in the peakaged condition (Figure 4.6.26).

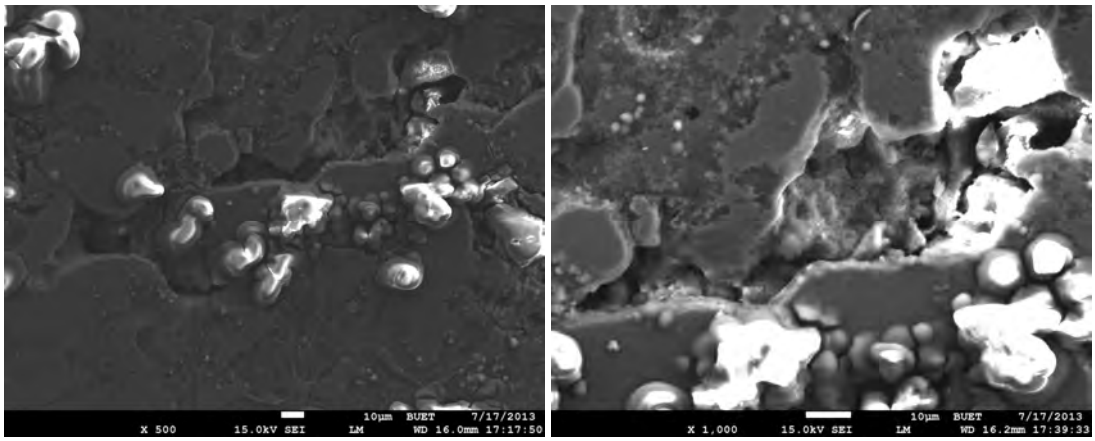

Figure 4.6.26: SEM Secondary Electron Image at different magnifications of the peakaged Alloy-5 as-corroded in 0.1M NaCl solution

Greater degree of surface deterioration in Alloy-5 as observed from SEM images indicates the higher corrosion rates for Alloy-5 than other alloys. The increased fraction of Al_2Cu particles into the matrix and grain boundaries increases the susceptibility to corrosion. The increased rate

of corrosion of Alloy-5 is due to the dissolution of higher Cu rich intermetallic particles in electrolytes. The 4 wt% Cu content peakaged Alloy-5 is more susceptible to pitting corrosion than that of the other alloys (Except Alloy-4). Figure 4.6.26 reveals clearly that pits density of Alloy-5 is much more than those of Cu free alloy Cu content alloys and surface pits are deeper as compared to the other alloys.

4.6.6 Corrosion Characteristics of Alloy-6

4.6.6.1 EIS Behavior of Alloy-6

OCP versus Time Behavior

The open circuit potential OCP value measured with respect to saturated calomel electrode (SCE) for Alloy-6 in 0.1M NaCl solution at room temperature is -0.6814V. The open circuit potential fluctuates with time and it is remarkable with the exposure time of 75 seconds (Figure 4.6.27). Afterward the OCP value is reached to nearly in steady state. The OCP value of Alloy-6 is more positive than the Alloy-1 and Alloy-2, but more negative than the other experimental alloys (Table 4.6.1).

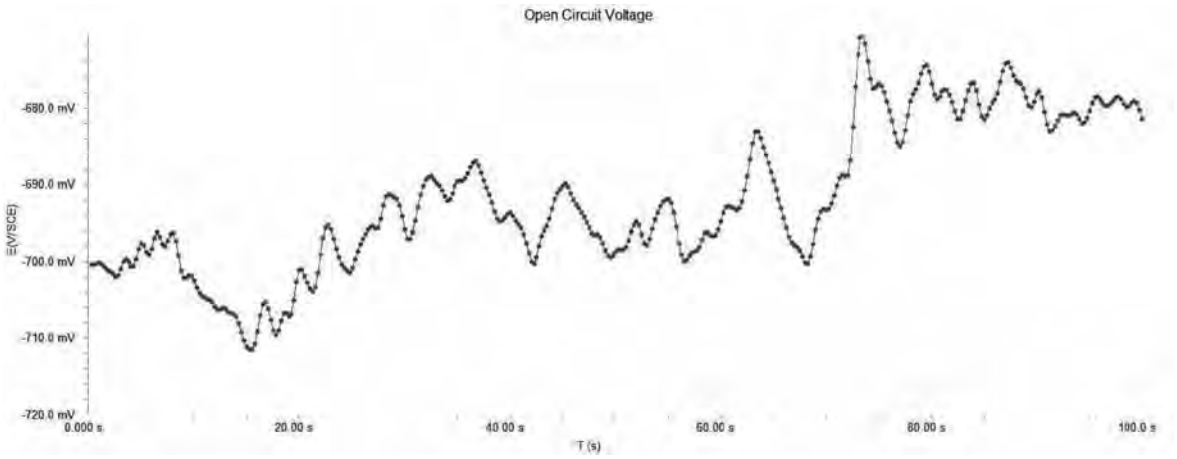

Figure 4.6.27: OCP variation with time for peakaged Alloy-6 in 0.1M NaCl solution

Nyquist Plot

The Nyquist plot for Alloy-6 is presented in Figure 4.6.28. The solution resistance, Rs=40.53Ω is very negligible with respect to the charge transfer resistance, Rct=14.44kΩ. The charge transfer resistance of Alloy-6 is lower than the other alloys but very close to Alloy-1.The lower

charge transfer resistance indicates the lower corrosion resistance. The double layer capacitance, Cp=1.645µF is also slightly higher than the base Alloy-1 but lower than rest of the alloys.

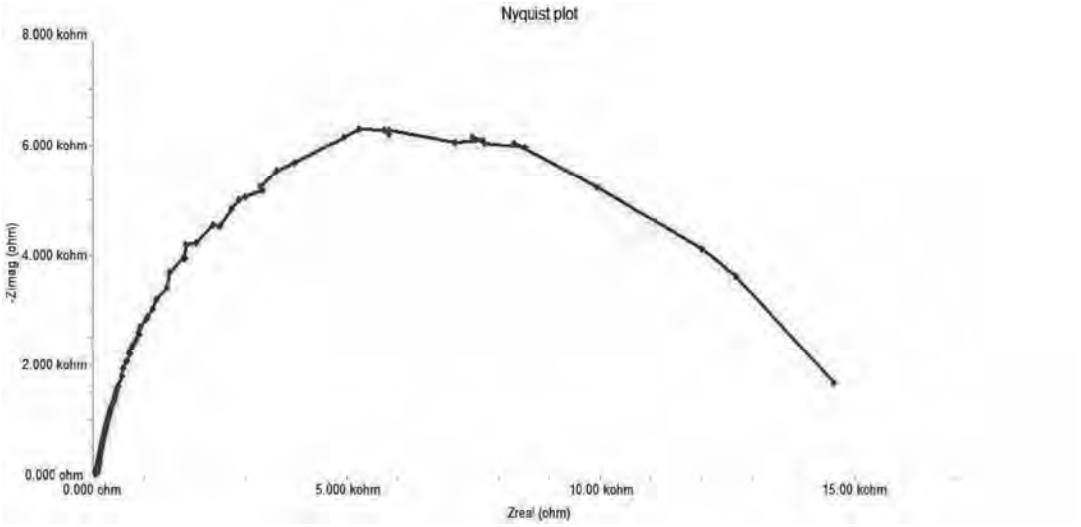

Figure 4.6.28: Nyquist plot for the peakaged Alloy-6 in 0.1M NaCl solution

Bode Plot

The Bode plot of EIS spectra of Alloy-6 shows that the impedance behaviour is similar to the other alloys (Figure 4.6.29).

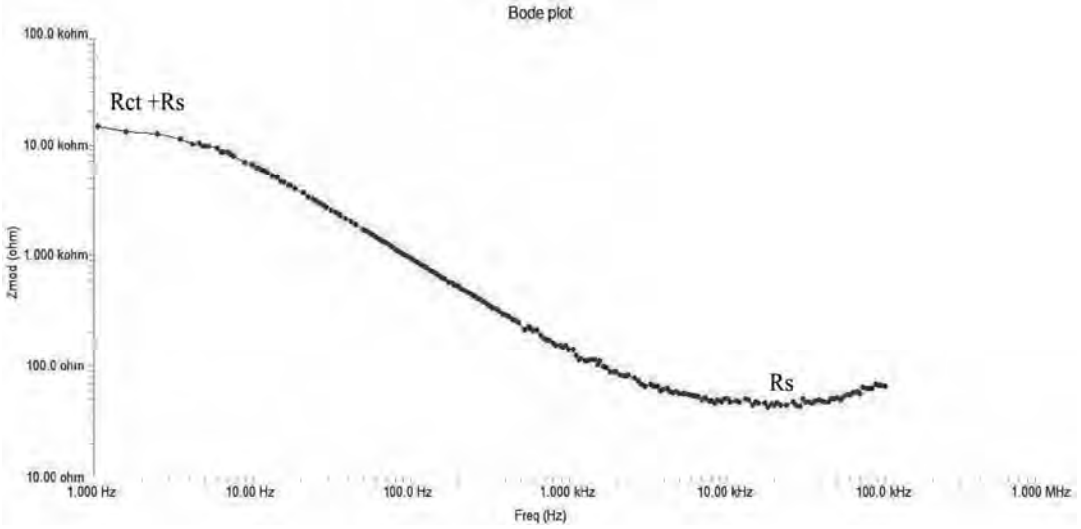

Figure 4.6.29: Bode plot for the peakaged Alloy-6 in 0.1M NaCl solution

4.6.6.2 Potentiodynamic Polarization Behavior of Alloy-6

Tafel Plot

Figure 4.6.30 shows the polarization curve of the Alloy-6 immersed in0.1M NaCl solution at room temperature. It is found that the corrosion potential Ecorr and Icorr values were - 0.720V and 2.54µA.The corrosion rate at this condition is 2.132mpy. The current density is lowest among the alloys investigated but pitting corrosion potential is more negative among the alloys (except Alloy-1). The lowest current density means the lower corrosion rate. So 2wt% Ni addition to Al-6Si-0.5Mg alloy decreases the pitting corrosion rate compared to the Cu content alloys.

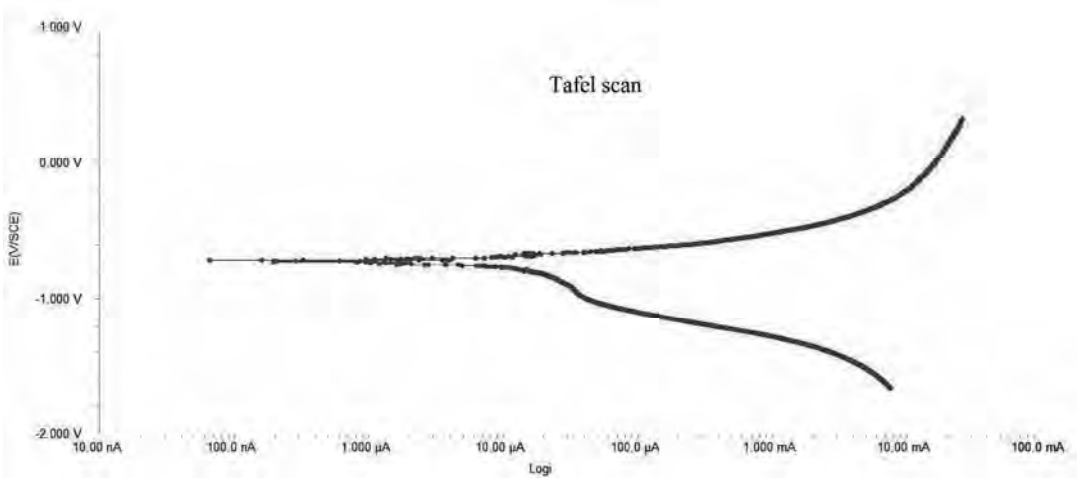

Figure 4.6.30: Potentiodynamic polarization curve of peakaged Alloy-6 in 0.1M NaCl solution

Microstructures and Degradation Behavior

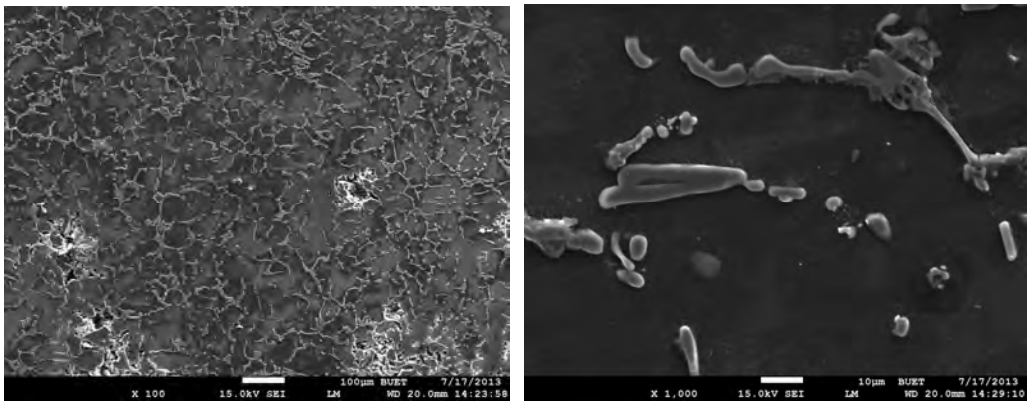

Figure 4.6.31: SEM Secondary Electron Image of the peakaged Alloy-6 as- corroded in 0.1M NaCl solution

Least pits are visible in the sample. Alloy-6 (2 wt% Ni) is least susceptible to pitting corrosion than that of the other alloys. Figure 4.6.31 reveals clearly that pit density of Alloy-6 is less than all the other alloys. In figure 4.6.31, there seems to be some surface pits formations which are lower and shallower as compared to those in other alloys. The pitting corrosion potential (Epit= - 426mV) of Alloy-6 is more positive than the other alloys.

4.6.7 Corrosion Characteristics of Alloy-7

4.6.7.1 EIS Behavior of Alloy-7

OCP versus Time Behavior

Figure 4.6.32 shows the open circuit potential (OCP) changes with time of Alloy-7 in 0.1M NaCl solution. The fluctuation of the OCP value is very negligible during the time of exposure but the OCP value increases with time. The steady state OCP value of Alloy-7 is -644.5mV, is more positive than the other alloys (except Alloy-5). So the more positive OCP is attained due to combined addition of 2wt% Cu and 2wt% Ni to Al-6Si-0.5Mg alloy. The occurrence of a positive shift in the OCP of the 2wt% Cu and 2wt% Ni content Al-6Si-0.5Mg alloy (Alloy-7) indicates the existence of anodically controlled reaction.

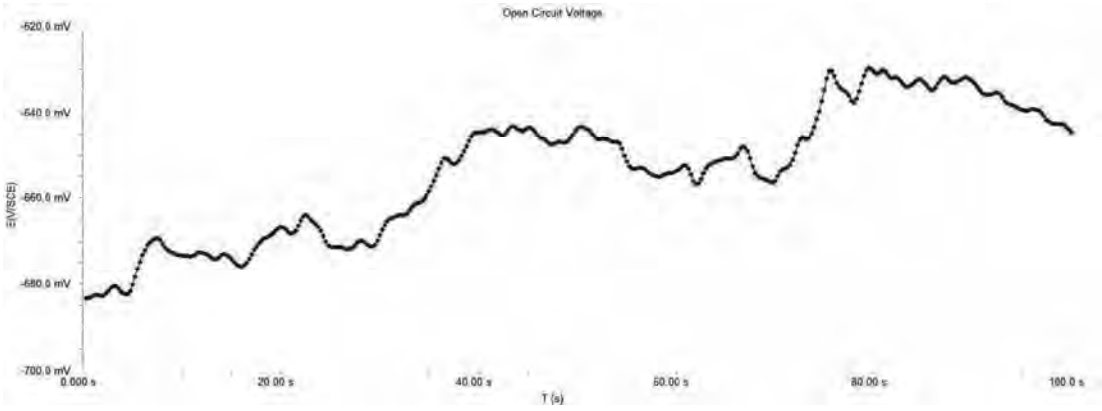

Figure 4.6.32: OCP variation with time for the peakaged Alloy-7 in 0.1M NaCl solution

Nyquist Plot

The shape of the Nyquist plot shows (Figure 4.6.33) single capacitive semicircle, showing that the corrosion process was mainly charge transfer controlled. The general shape of the curves is very similar for all the samples and this is maintained throughout the whole test period, indicating that almost no change in the corrosion mechanism. The charge transfer resistance (Rct) of Alloy-7 is 27.95kΩ, which is remarkably higher than the other alloys (except Alloy-4).

But the Rct value of Ally-7 is very close to Alloy-4. The double layer capacitance, Cp=1.773µF is also slightly higher than the base Alloy-1 and Alloy-6 but close to Alloy-2. So after 2wt% Cu and 2wt% Ni addition to Al-6Si-0.5Mg alloy, the charge transfer resistance increases significantly. Measurement of high charge transfer resistance and lower double layer capacitance for Alloy-7 indicates less corrosion tendency in NaCl solution. The solution resistance (Rct=44.40Ω) observed for Alloy-7 is very low and similar to the other alloys. The low solution resistance indicates the existence of more ion conducting surface film.

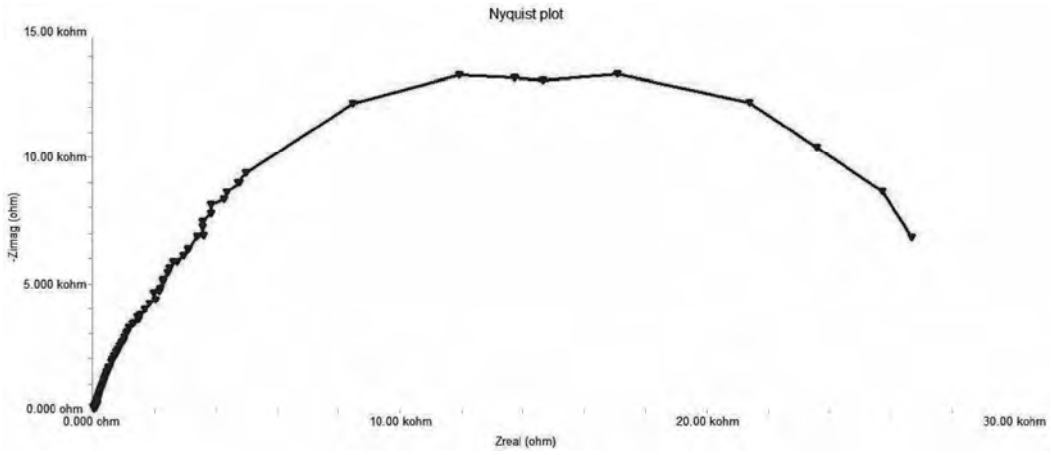

Figure 4.6.33: Nyquist plot for the peakaged Alloy-7 in 0.1M NaCl solution

Bode Plot

Figure 4.6.34 shows the experimental results of electrochemical impedance spectroscopy (EIS) carried out in a 0.1M NaCl solution at 25^{o}C in Bode plot for the Alloy-7.

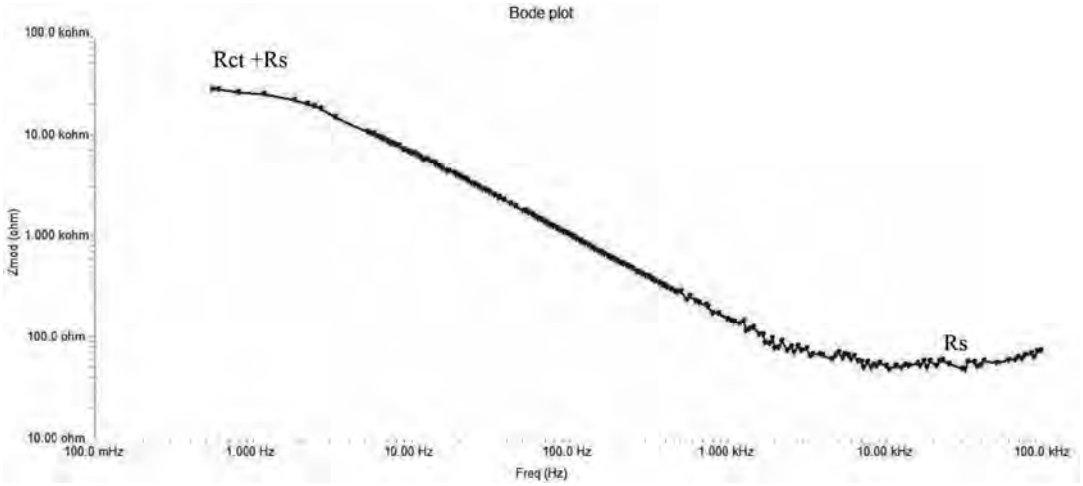

Figure 4.6.34: Bode plot for the peakaged Alloy-7 in 0.1M NaCl solution

4.6.7.2 Potentiodynamic Polarization Behavior of Alloy-7

Tafel Plot

Typical polarization curves in 0.1M solution of NaCl, Figure 4.6.35 shows that the polarization behaviour of Alloy-7 is similar to Alloy-6. The evaluated electrochemical corrosion parameters (Table 4.6.2) show that the corrosion current (Icorr=2.710µA) and the corrosion rate (2.278mpy) increased with the addition of 2wt% Ni (Alloy-6). The Ecorr value (-644mV) of Alloy-7 is more positive than the Alloy-1, Alloy-2, Alloy-3 and Alloy-6. These results point out to the fact that Alloy-7 has lower corrosion rate as compared to those alloys in chloride medium.

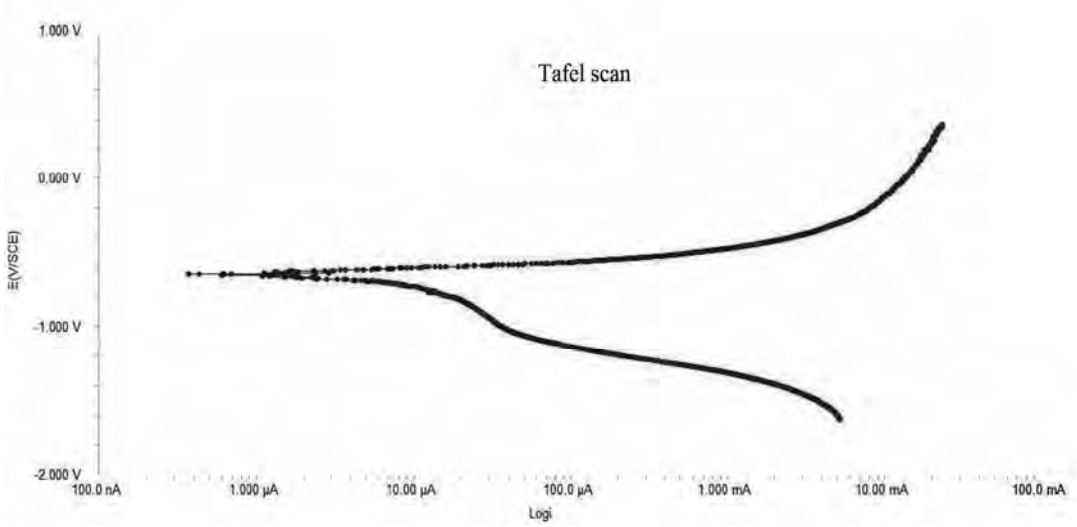

Figure4.6.35: Potentiodynamic polarization curve of peakaged Alloy-7 in 0.1M NaCl solution

Microstructures and Degradation Behavior

Figure 4.6.36 SEM Secondary Electron Image of the damage surface morphology of as-corroded T6 peakaged Alloy-7 (2Ni+2Cu) in 0.1M NaCl solution. Microstructures at different magnifications show some shallow and thin pits observed in Alloy-7 corroded surface. The 2 wt% Cu and 2 wt% Ni content peakaged Al-6Si-0.5Mg alloy (Alloy-7) is less susceptible to pitting corrosion than that of the other alloys (Except Alloy-6). The SEM micrographs reveal clearly that pits density of Alloy-7 is less than that of Cu free alloy (Alloy-1) and the Cu content alloys (Alloy-2 to Alloy-5).

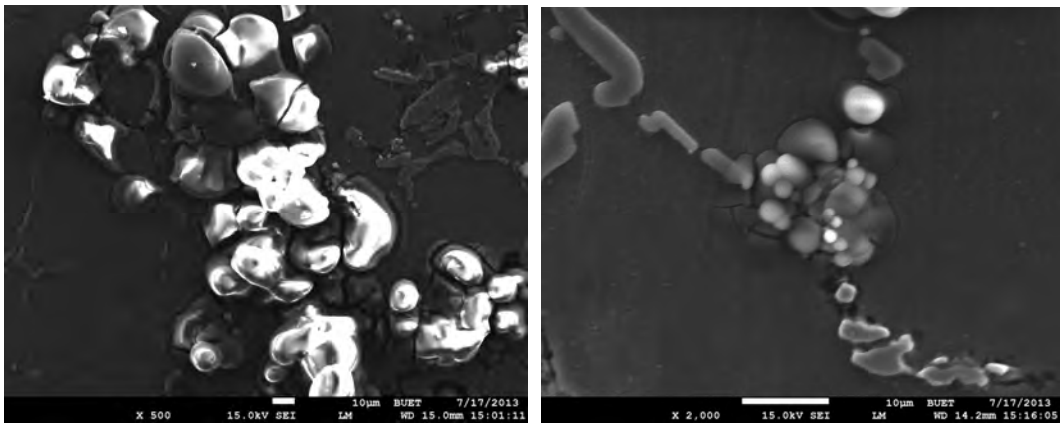

Figure 4.6.36: SEM Secondary Electron Image at different magnifications of the peakaged Alloy-7 as- corroded in 0.1M NaCl Solution

4.7 Wear Behaviour of the Alloys

A pin-on-disc test apparatus was used to investigate the dry sliding wear characteristics of the alloys. Wear specimen, 5 mm in diameter approximately 10 mm long were used for wear studies. Tests were conducted for the following two settings.

- 10 minutes with a load of 0.550 kg (5.4N)
- 5 minutes with a load of 1.150 kg (11.28N).

In all tests the Disc rpm was constant (~900 rpm). All tests were conducted at room temperature and wear loss was calculated by measuring weight before and after test. During the test, the pin was pressed against the counterpart rotating against a steel disc (hardness ~30 HRC) by applying the load.

4.7.1 Wear Behaviour of Cu Content Alloys (Load 5.4 N)

Figure 4.7.1 shows the wear test results i.e. weight loss (mass loss) vs. ageing temperature of alloys containing various amounts of Cu. Dry sliding wear behavior of Al-6Si-0.5Mg-xCu (x = 0, 0.5, 1, 2 and 4) alloys depends on size and shape of the silicon particles, size distribution of α-Al grains, Mg_2Si, $CuAl_2$, Al_2CuMg and other intermetallic and precipitate particles in the interdendritic region. Thermal modification converts large α-Al grains into fine equiaxed α-Al grains and forms fine fibrous silicon particles and fine Mg_2Si, $CuAl_2$, Al_2CuMg precipitate particles in the interdendritic region. These $CuAl_2$, Al_2CuMg precipitates are fully coherent but Mg_2Si precipitates are semi-coherent with the α-aluminium matrix. These affect the hardness and wear properties of the alloys.

Increasing amount of Cu increases the hardness. This is due to the formation of new hard intermetallics or precipitates during thermal treatment in the presence of Cu atoms. During solution treatment the Cu atoms go to solution and the Si particles are modified. After thermal modification, the Cu free alloy (Alloy-1) shows the highest wear loss among the Cu content alloys in solution treated, aged at 150^{o}C and 200^{o}C. During ageing precipitates form and increase the hardness and wear resistance. At peakaged condition (1hr at 225^{o}C), the wear loss of the Cu content alloys are slightly higher than when aged at 200^{o}C and 250^{o}C but lower than all other ageing conditions. The Cu containing alloys show maximum hardness when aged at 200^{o}C-250^{o}C and also show lower wear loss i.e. higher wear resistance. After excessive ageing, an increase was observed in wear loss of various Cu content Al-6Si-0.5Mg alloys. The higher

mass loss was obtained in the alloys which were aged at 300^{o}C. There was an increase in the mass loss with increasing the ageing temperature. This is due to the effect of overageing.

In solution treated condition (2hr at 540^{o}C) Cu free alloy, Alloy-1 shows the highest mass loss and Alloy-5 shows lower mass loss i.e. higher wear resistance. Addition of Cu to Al-6Si-0.5Mg alloy increases the wear resistance. After Ageing at 200^{o}C, Alloy-4 shows the higher wear resistance than other alloys. But in the peakaged condition (ageing at 225^{o}C), Alloy-4 shows better wear resistance among the investigated alloys.

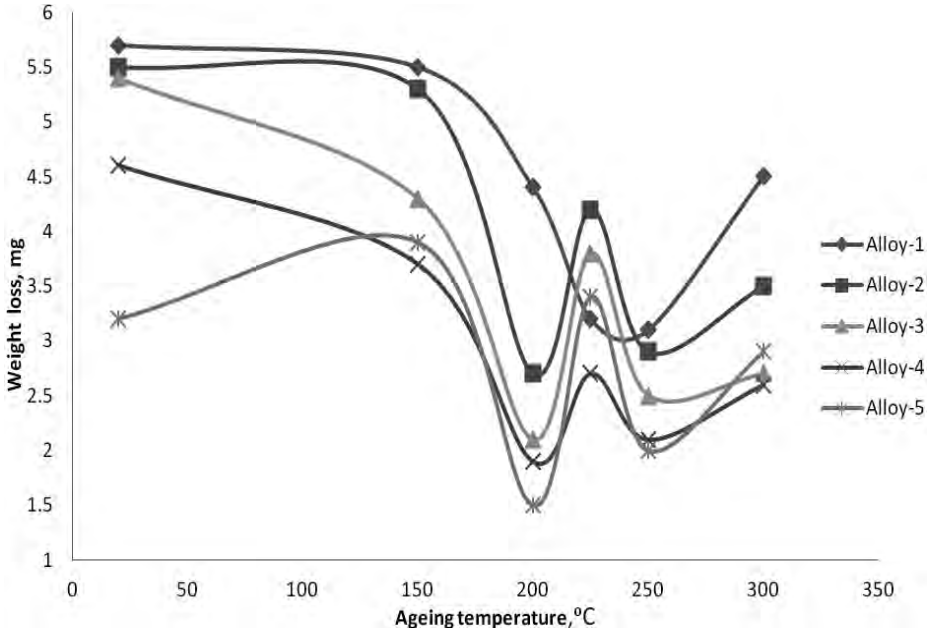

Figure 4.7.1: Wear behaviour of Alloys 1 – 5 at different ageing conditions

4.7.2 Wear Behaviour of Cu or/and Ni Content Alloys (Load 5.4 N)

The effect of Cu and/or Ni content on the wear behaviour of the Al-6Si-0.5Mg alloys is given in Figure 4.7.2. Addition of Ni (Alloy-6) increases the wear loss. This is due to the formation of new hard intermetallics in the presence of Ni atoms. Although the addition of Ni increases hardness of the alloy, wear resistance of the alloys (Alloys 6 and 7) decrease. Hardness increase caused by the Ni bearing intermetallics improves the wear resistance of the Al-6Si-0.5Mg alloy at peakaged condition. Alloy-4 (2wt% Cu) shows lower wear loss than Alloys 1 and 6.

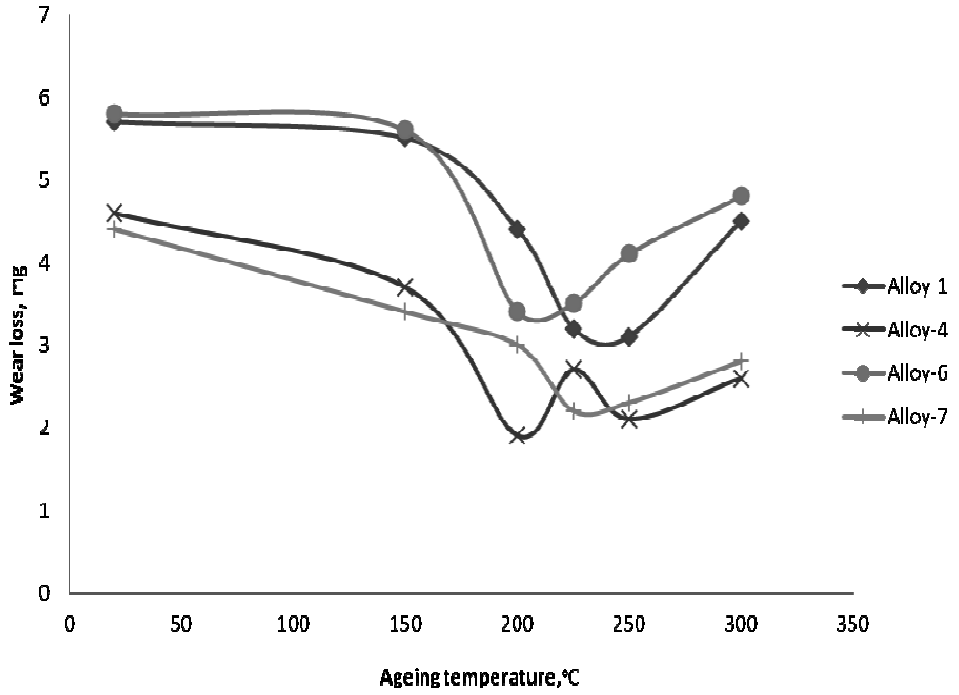

Figure 4.7.2: Wear behaviour of Alloys 1, 4, 6 and 7 at different ageing conditions and at a load of 5.4 N

Alloy-6 shows higher wear loss i.e. lower wear resistance among the alloys investigated at all ageing conditions (except 1hr at 200^{o}C). Addition of Ni causes an increment in the size of the intermetallics (Al_3Ni, Al_7Cu_4Ni etc.) along the grain boundaries. These hard intermetallic phases enhance crack formation and increase wear loss of the alloy. The drop in the wear resistance of the Al-6Si-0.5Mg-2Ni alloy may be attributed to the brittleness of these intermetallics.

In the as-quenched condition, Alloy 7 (2 wt% Cu and 2 wt% Ni) has better wear resistance than Alloy 4 (2 Wt% Cu) and Alloy 6 (2 wt% Ni). The wear resistance increases with increasing ageing temperature. Alloy-7 shows the maximum wear resistance when aged at 225^{o}C whereas Alloy-4 shows maximum wear resistance at 200^{o}C. Alloy-4 shows slightly lower wear resistance at 225^{o}C but Alloys 4 and 7 show better wear resistance at all ageing conditions. Cu in α-aluminium matrix produces $CuAl_2$, Al_2MgCu or other Cu containing precipitates which have a great effect on wear resistance and Ni bearing intermetallics drops the wear resistance of the alloys because of embrittlement of the intermetallic phases.

4.7.3 Wear Behaviour of Cu Content Peakaged Alloys (Load 11.28 N)

During the test, when the applied load on the pin is increased, the actual contact area would increase towards the nominal area which increases the frictional force between two sliding surfaces. The increased frictional force gives high wear. The wear losses (mass loss) vs. Cu content in Al-6Si-0.5Mg alloys at 225^{o}C are plotted in Figure 4.7.3. Cu has a significant effect on wear loss. Strong age hardening happens during peak ageing. Enhancing applied load results in an obvious increase in weight loss. At the peakaged condition, Cu free Alloy-1 shows the maximum weight loss. Mg_2Si is semi-coherent with the α-aluminium matrix. The thermal modified Si during solution treatment and Mg_2Si precipitate form during ageing. Cu was introduced into the Al-6Si-0.5Mg alloys and the precipitates containing Cu are fully coherent with the α-aluminum matrix. These coherent precipitates reduces the wear loss i.e. increases the wear resistance. The increase in wear resistance is more pronounced with increase of Cu contents.

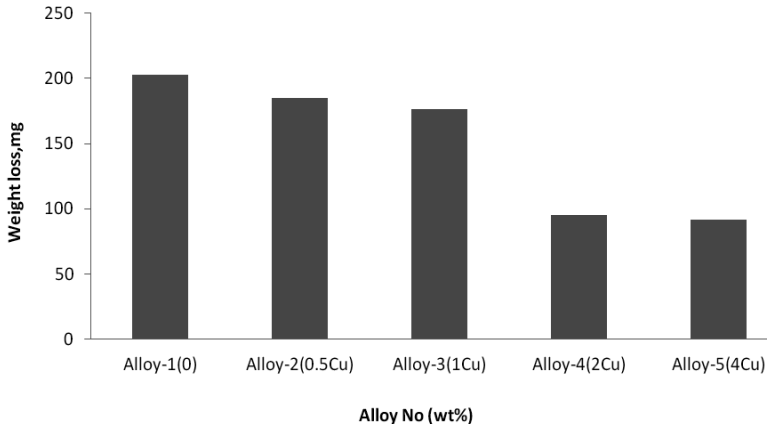

Figure 4.7.3: Wear behaviour of alloys containing Cu at peakaged condition and at a load of 11.28N

4.7.4 Wear Behaviour of Cu and/or Ni Containing Peakaged Alloys (Load 11.28 N)

The results of wear tests of the Cu and/or Ni containing alloys (Alloys 4, 6 and 7) aged at 225^{o}C for 1 hour is plotted in Figure 4.7.4. Enhancing load from 5.4N to 11.28N results in an obvious increase in wear loss. In Alloy-6, Ni containing intermetallics form along grain boundaries. These hard intermetallic phases are crack prone. As a result the wear loss increases in Alloy-6 (2 wt% Ni). In Alloy-7 (2Cu-2Ni), Cu goes to solution during solution treatment and there are no

Cu containing intermetallics in the interdendritic regions. But Ni and Cu-Ni containing intermetallics (as Al_3Ni, Al_3CuNi, and Al_7Cu_4Ni etc) stay along the interdendritic spaces. These brittle particles reduces the wear resistance but precipitates containing Mg and Cu are formed into the α-aluminium matrix during ageing and these increase the hardness and wear resistance. The wear loss is significantly reduced with Ni addition and lowest wear resistance was observed in the peakaged specimen. In Alloy-4 (2 wt% Cu), the Cu containing precipitates are fully coherent with the α-aluminium matrix and these precipitates increase the wear resistance of the matrix. Thus the increase in wear resistance of Al-6Si-0.5Mg alloys is more pronounced with the individual addition of Cu. Alloy-4 shows the highest wear resistance among the investigated alloys. But Alloy-7 (2 wt% Cu and 2wt% Ni) shows moderate wear resistance compared to Alloy-1 and Alloy-6.

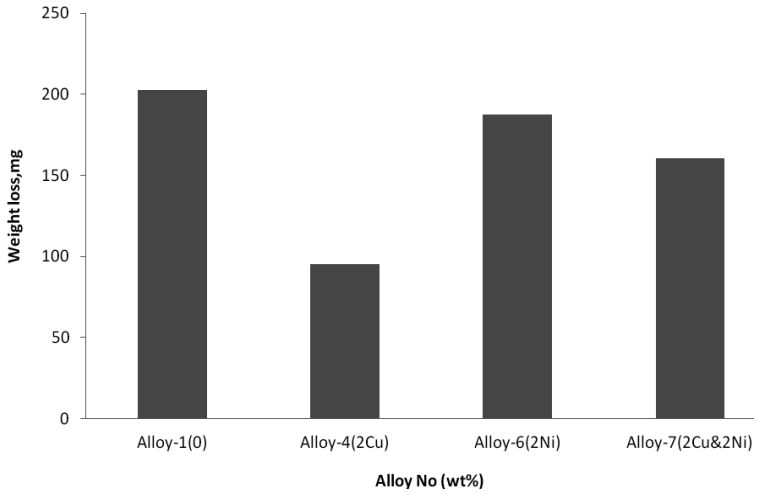

Figure 4.7.4: Wear behaviour of alloys containing Cu and/or Ni at a load of 11.28N

4.7.5 Wear Debris Analysis

The wear debris generated during dry sliding in an air atmosphere was collected and examined using an X-ray diffraction technique. An increase in the applied normal load formed wear debris of various shapes and sizes. The debris size ranged from a few microns, to a few millimeters. Visually, the debris produced at 5.4N load appeared very fine, equiaxed particles and smaller in amounts, but at 11.28N the worn particles were coarse and higher in amounts. The XRD analyses of the wear debris are presented in Appendix C. The X-ray Diffraction techniques revealed the Al and Si content debris worn out from the samples.

Chapter 5
Summary and Conclusions

Based on the results presented in the previous chapter, the following conclusions were derived.

- The as-cast Al-Si eutectics are fragmented and are modified after solution treatment. The addition of Cu and/or Ni into the Al-6Si-0.5Mg alloys result in the formation of Mg, Cu and Ni containing intermetallic phases during solidification. The Mg and Cu containing intermetallics (Mg_2Si, Al_2Cu etc.) completely dissolve but Ni containing intermetallics (Al_3Ni, Al_3CuNi etc.) dissolve partially during the solutionizing treatment.

- The addition of Cu and/or Ni increases the hardness of as quenched Al-6Si-0.5Mg alloy. Addition of 4wt% Cu to Al-6Si-0.5Mg alloy gives the highest hardness (89.8HRF), followed by hardness of alloy containing 2wt% Cu and 2wt% Ni (82.5HRF) .The hardness of 2wt% Cu containing alloy was (78HRF).

- Significant natural ageing occur upto 15 days. The natural ageing hardness of the alloy containing 4wt% Cu was the highest over all the ageing conditions investigated. The maximum hardness was obtained after isochronal ageing at 225^{o}C for 1 hour. The highest hardness was achieved after isothermal ageing for 60 minutes.

- The addition of Cu and/or Ni to the Al-6Si-0.5Mg alloy increases the ageing hardness and resistivity in the solution treated and also in the aged condition.

- 1 hour ageing at 225^{o}C resulted in the highest tensile strengths of the alloys. Addition of 2wt% Cu resulted in the highest UTS of 212 MPa and YS of 190 MPa at peakaged condition. Ageing for 1 hour at temperatures beyond 225^{o}C, caused significant decrease in strength.

- The ductility (%elongation) of the alloys decreased with ageing temperatures and maximum reduction occurred at peakaged condition. Addition of 2wt% Cu to Al-6Si-0.5Mg alloy significantly increase ductility. Alloy with 4wt. % showed the lowest ductility among the

alloys investigated over all the ageing conditions. The ductility of all the alloys increased in the overaged conditions.

- Evaluation of tensile properties at three different strain rates (10^{-4}, 10^{-3} and 10^{-2} s^{-1}) showed that strain rates affected the tensile properties significantly. At higher strain rates the strength was better but ductility was poor.

- The alloys showed better impact strength in the solution treated and in the overaged conditions; impact strength was very poor in the peakaged condition. The addition of 2wt% Ni to Al-6Si-0.5Mg alloy gave the lowest impact strength in the peakaged condition.

- Thermal treatments have a refining effect on the eutectic phases in the microstructures. The fracture morphology was found to be ductile or ductile-brittle mixed mode depending on the shape, size and distribution of the phases in the α-aluminum matrix.

- The Electrochemical measurements showed that addition of Cu and/or Ni causes a positive shift in the Open Circuit Potential (OCP). The charge transfer resistance (Rct=28.33kΩ) of Alloy containing 2wt% Cu was found to be the maximum amongst the alloys investigated. In potentiodynamic polarization test (severe perturbation), alloy containing 2 wt% Cu has the highest corrosion rate (17.05 mpy).

- The study on wear behavior was only exploratory in nature. The alloying additions were found to increase the wear resistance of the alloys over all the ageing conditions under investigation.

Recommendation for Future Works

Based on the results and conclusions presented previously, the following recommendations for future work are made.

- The relationship between the solidification conditions (solidification rate, modifiers, impurities etc.), as-cast microstructure (secondary dendrite arm spacing, eutectics morphology, segregations etc.) and the heat treatment behaviour of the alloys should be studied in details.

- Effect of variation in solutionization temperature and time on the dissolution of Ni containing intermetallics may be undertaken.

- The isochronal ageing at short temperature intervals after 200^{o}C would help determine the optimal range of peakaged condition.

- A detailed transmission electron microscopy (TEM) study may be undertaken to better understand the effect of alloying elements on the precipitation sequence and on the nature of the precipitates in the alloys studied.

- Tensile tests should be performed at elevated temperatures (ageing temperatures).

- Wear and corrosion tests at all ageing conditions may be performed to determine the optimum ageing conditions.

- Thermal analysis (DTA/DSC) may be done to identify the precipitation temperatures of the precipitates. This could also be supported with the TEM and ageing studies.

References

[1] Kaufman, J. G., and Rooy, E. L., “Aluminum Alloy Castings: Properties, Processes and Applications”, American Foundrymens Society, Schaumberg IL, 2005.

[2] Paz, J. F. H., Heat Treatment and Precipitation in A356 Aluminum Alloy, PhD Thesis, Department of Mining, Metals and Materials Engineering, McGill University, Montreal, Canada, 2003.

[3] Paray, F., Kulunk, B., and Gruzleski, J.E., “Impact Properties of Al-Si Foundry Alloys", *International Journal of Cast Metals Research*, vol. 13, pp. 17-37, 2000.

[4] Lumley, R. N., Polmear, I. J., and Morton, A. J., “International Patent Application PCT/AU00/01601”, 2000.

[5] Polmear, I., “Light alloys,” Fourth edition

[6] Seifeddine, S., *Characteristics of Cast Aluminium-silicon Alloys: Microstructures and Mechanical Properties*, Doctoral Thesis, Department of Management and Engineering, Engineering Materials, Linköping Studies in Science and Technology, Linköping University, The Institute of Technology, 2006.

[7] Edwards, G.A., Sigworth, G.K., Caceres, C.H., ST John, D.H., and Barresi, J., “Microporosity formation in Al-Si-Cu-Mg casting alloy”, *AFS Trans.*, vol.105, pp.809-818,1997.

[8] Shabestari, S.G. and Moemeni, H., “Effect of copper and solidification conditions on the microstructure and mechanical properties of Al-Si-Mg alloys”, *Journal of Materials Processing Technology*, vol.153-154, pp. 193-198, 2004.

[9] Wang, L., Makhlouf, M., and Apelian, D., “Aluminium die casting alloys: alloy composition, microstructure, and properties-performance relationships”, *International Materials Reviews*, vol. 40(6), pp. 221-238, 1995.

[10] Zhang, D.L. and StJohn, D. H., “The effect of composition and heat treatment on the microstructure and mechanical properties of cast Al-7wt%Si-Mg alloys”, *Casting and Solidification of Light Alloys*, IMMA, 30-31 Aug 1995, Gold Coast, pp. 21-25, 1995.

[11] Tash, M., Samuel, F.H., Mucciardi, F., and Doty, H.W., “Effect of metallurgical parameters on the hardness and microstructural characteristic of as-cast and heat treated 356 and 319 alloys”, *Material Science and Engineering A*, vol. 443, pp. 185-201, 2007.

[12] The Aluminum Association, Inc.900 19th Street, N.W. Washington, D.C. 20006 (202) 862-5100, www.aluminum.org.

[13] Mondolfo, L. E., “Aluminium Alloys: Structure and Properties,” Butterworths, London, 306, 1976.

[14] http://www.precisionenginetech.com

[15] http://www.dealernews.com

[16] http://www.delkron-mfg.com

[17] Dighe, M. D., Gokhale, A. M., and Horstemeyer, M. F., "Effect of Loading Condition and Stress State on Damage Evolution of Silicon Particles in an Al-Si-Mg-Base Cast Alloy", *Metallurgical and Materials Transactions A*, vol. 33(3), pp. 555-565, 2002.

[18] Stefanescu, D., "ASM Handbook", vol.15: Casting, ASM, pp. 1622-1696, 1988.

[19] Xu, H., Jian, X., Meek, T. T., and Han, Q., "Degassing of Molten Aluminum A356 Alloy using Ultrasonic Vibration", *Materials Letter*, vol. 58, pp. 3669-3673, 2004.

[20] Wang, J., He, S., Sun, B., Guo, Q., and Nishio, M., "Grain Refinement of Al-Si Alloy (A356) by Melt Thermal Treatment", *Journal of Materials Processing Technology*, vol. 141, pp. 29-34, 2003.

[21] Gruzleski, J. E., and Closset, B., "Structure and Properties of Hypoeutectic Al-Si-Mg Alloys Modified with Pure Strontium", *Metall Trans A*, vol.13, pp.945-951, 1982.

[22] Ozbakir, E., "Microstructural Modification of an A356 Alloy with Strontium and Its Effect on As-Cast Mechanical Properties", MIME 559, Physical Metallurgy of Aluminum, Lab Project, McGill University, Quebec, Canada, 2006.

[23] Ransley, C.E., and Neufeld, H., "The Solubility of Hydrogen in Liquid and Solid Aluminium", *Journal of Institute of Metals*, vol.74, pp. 599-620, 1947-48.

[24] Chamberlin, B., and Zabek, V. J., "Reappraisal of the tensile properties of Aluminum-Silicon-Magnesium Casting Alloys," *AFS Trans.*, vol.81, pp.322-327, 1973.

[25] Closset, B. M., and Khan, S., *In Proc. Conf. "Light Metals 1990*", 869, Warrendale, PA, TMS, 1990.

[26] Wang, H., Davidson, C. J., Taylor, J. A., and StJohn, D. H., "Semisolid Casting of AlSi7Mg0.35 Alloy Produced by Low-Temperature Pouring", *Material Science Forum*, vol.396-402, pp. 143-148, 2002.

[27] Wang, H., Davidson, C. J., StJohn, D. H., "Semisolid Microstructural Evolution of AlSi7Mg Alloy during Partial Remelting", *Material Science and Engineering A*, vol. 368, pp. 159-167, 2004.

[28] Wang, H., StJohn, D. H., Davidson, C. J., and Couper, M. J., "Characterization and Shear Behavior of Semisolid Al-7Si-0.35Mg Alloy Microstructures", *Aluminum Transactions*, vol.2, pp.56-66, 2000.

[29] Gruzleski, J. E., and Closset, B. M., "The Treatment of Liquid Aluminum-Silicon Alloys," American Foundry men's Society, Inc. Des Plaines, Illinois, vol.18, pp.25-91, 1990.

[30] Sjölander, E., and Seifeddine, S., "The heat treatment of Al-Si-Cu-Mg casting alloys", *Journal of Materials Processing Technology*, vol. 210(10), pp.1249-1259, 2010,

[31] Ma, Z., Samuel, F. H., Samuel, A. M., Doty, H. W., and Valtierra, S., "Effect of Fe Content and Cooling Rate on the Impact Toughness of Cast 319 and 356 Aluminum Alloys", *American Foundry Society*, vol.111, p.255, 2003.

[32] Wang, Q. G., Apelian, D., and Lados, D. A., "Fatigue Behavior of A356/357Aluminum Cast Alloys. Part II - Effect of Microstructural Constituents", *Journal of Light Metals*, vol. 1(1), pp. 85-97, 2001.

[33] Gruzleski, J. E. and Closset, B. M., "The Treatment of Liquid Aluminum-Silicon Alloys", American Foundrymen's Society, Inc. Des Plaines, Illinois 60016-8399, ISBN 0-87433-121-8, 1990.

[34] Murty, B. S., Kori, S. A., & Chakraborty, M., "Grain refinement of aluminium and its alloys by heterogeneous nucleation and alloying", *Int. Mater. Rev.*, vol.47, pp.3-29, 2002.

[35] Greer, A. L., Cooper, P. S., Meredith, M.W., Schneider, W., Schumacher, P., Spittle, J.A., and Tronche, A., "Grain Refinement of Aluminium Alloys by Inoculation", *Advanced Engineering Materials*, vol.5, pp.81-91, 2003.

[36] McCartney, D.G., "Grain Refining of Aluminium and its Alloys using Inoculants", *Int. Mater. Rev.*, vol.34, pp.247-260, 1989.

[37] Polmear, I. J., "Light Alloys, Metallurgy of the light metals", (third ed.) ISBN 0 340 63207 0, Publisher: Butterworth-Heinemann, Melbourne, 1995.

[38] Sundman B., Jansson B., and Andersson, J.O., "The Thermo-Calc databank system," CALPHAD, vol. 9, pp. 153-190, 1985.

[39] Yalamanchili, R., Quenching cooling rate influences on mechanical properties of cast aluminium alloys, Master Thesis, 2004.

[40] Zhang, D. L, and StJohn, D. H., "The effect of composition and heat treatment on the microstructure and mechanical properties of cast Al-7wt%Si-Mg alloys", 1995.

[41] Tash, M., Samuel, F.H., Mucciardi, F., and Doty, H.W., "Effect of metallurgical parameters on the hardness and microstructural characteristic of as-cast and heat treated 356 and 319 alloys", *Material Science and Engineering*, vol. 443(A), pp.185-201, 2007.

[42] Paray, F., "Heat treatment and mechanical properties of aluminium-silicon modified alloys" 1992.

[43] Shivkumar, S., Keller, C., and Apelian, D., "Ageing behavior Cast Al-Si-Mg Alloys", *AFS Transactions*, pp. 905-911, 1999.

[44] Seifeddine, S., "On the microstructure formation and mechanical properties of aluminium-silicon cast alloys", 2005

[44] Closset, B., Drew, R. A. L., and Gruzleski, J. E., "Eutectic Silicon Shape Control by in Situ Measurement of Electrical Resistivity", *Transactions of the American Foundrymens Society*, vol. 94, pp. 9-16, 1986.

[46] Shivkumar, S., Ricci, S., Steenhoff, B., Apelian, D., and Sigworth, G., "An Experimental Study to Optimize the Heat Treatment of A356 Alloy," *Transactions of the American Foundrymens Society*, vol. 97, pp. 791-810, 1989.

[47] Zhang, D. L., Zheng, L. H., and StJohn, D. H., "Effect of a short solution treatment time on microstructure and mechanical properties of modified Al-7wt.%Si-0.3wt.%Mg alloy", *Journal of Light Metals*, vol. 2 (1), pp. 27-36, 2002.

[48] Gustafsson, G., Thorvaldsson, T., and Dunlop, G. L., "The influence of Fe and Cr on the microstructure of cast Al-Si-Mg alloys", *Metallurgical and Materials Transactions A*, vol. 17 (1), pp. 45-52, 1986.

[49] Apelian, D., Shivkumar, S. and Sigworth, G., "Fundamental Aspects of Heat Treatment of Cast Al-Si-Mg Alloys", *Transactions of the American Foundrymens Society*, vol. 97, pp. 727-742, 1990.

[50] Chaudhury, S. K., and Apelian, D., "Effects of Rapid Heating on Solutionizing Characteristics of Al-Si-Mg Alloys Using a Fluidized Bed", *Metallurgical and Materials Transactions A*, vol. 37 (3), pp. 763-778, 2006.

[51] Ouellet, P., and Samuel, F. H., "Effect of Mg on the ageing behaviour of Al–Si–Cu 319 type aluminum casting alloys", *Journal of Materials Science*, vol. 34(19), pp. 4671-4497, 1999.

[52] Crowell, N., and Shivkumar, S., "Solution treatment effects in cast Al-Si-Cu alloys", *AFS Transactions*, vol. 103, pp. 721-726, 1995.

[53] Mondolfo, L.F., "Aluminum Alloys: Structure and Property (in Chinese)", Metallurgical Industry Press, Beijing, China, p.586, 1988,

[54] Gauthier, J., and. Samuel, F. H., "Tensile Properties and Fracture Behavior of Solution Heat Treated 319.2 Aluminum Automotive Alloy", *AFS Transactions*, vol. 103, pp. 849-858, 1995.

[55] Narayanan, L. A., Samuel, F. H., and Gruzleski, J. E., "Dissolution of iron intermetallics in Al-Si Alloys through nonequilibrium heat treatment", *Metallurgical and Materials Transactions A*, vol. 26(8), pp. 2161-2174, 1995.

[56] Sokolowski, J. H., Djurdjevic, M. B., Kierkus, C. A., and Northwood, D. O., "Improvement of 319 Aluminum Alloy Casting Durability by High Temperature Solution Treatment", *Journal of Advanced Materials Processing Technology*, vol. 109, pp. 174-180, 2001.

[57] Wang, G., Bian, X., Wang, W., and Zhang, J., "Influence of Cu and minor elements on solution treatment of Al–Si–Cu–Mg cast alloys", *Materials Letters*, vol. 57, pp. 4083-4087, 2003.

[58] Shivkumar, S., Ricci, S., Jr., Keller, C., and Apelian, D., "Effect of Solution Treatment Parameters on Tensile Properties of Cast Aluminum Alloys", *J. Heat Treating*, vol.8(1), pp.63-70, 1990.

[59] Samuel, F. H., "Incipient melting of Al5Mg8Si6Cu2 and Al2Cu intermetallics in unmodified and Sr-modified Al-Si-Cu-Mg alloys during solution heat treatment", *J. Mater. Sci.*, vol.33, pp. 2283-2297, 1998.

[60] Han, Y. M., Samuel, A. M., Samuel, F. H., and Doty, H. W., "Dissolution of Al2Cu phase in non-modified and Sr modified 319 type alloys", *International Journal of Cast Metals Research*, vol.21, pp. 387-393, 2008.

[61] Lasa, L., and Rodriguez-Ibabe, J.M., "Evolution of the main intermetallic phases in Al-Si-Cu-Mg casting alloys during solution treatment", *J. Mater. Sci.*, vol. 39, pp.1343-1355, 2004.

[62] Stadler, F., Antrekowitsch1, H., Fragner, W., Kaufmann, H., and Uggowitzer, P. J., "The effect of Ni on the high-temperature strength of Al-Si cast alloys", *Mater. Sci. Forum*, vol. 690, pp. 274-277, 2011.

[63] Stadler, F., Antrekowitsch1, H., Fragner, W., Kaufmann, H., and Uggowitzer, P. J., "Effect of main alloying elements on the strength of Al-Si cast alloys at elevated temperatures", *International Journal of Cast Metals Research*, vol. 25(4), pp. 215-224, 2012.

[64] Asghar, Z., Requena, G., and Kubel, F., "The role of Ni and Fe aluminides on the elevated temperature strength of an AlSi12 alloy", *Mater. Sci. and Eng. A*, vol. 527, pp. 5691-5698, 2010.

[65] Lasagni, F., Lasagni, A., Marks, E., Holzapfel, C., Mucklich, F., and Degischer, H. P., "Three-Dimensional Characterization of 'as-cast' and Solution-Treated AlSi12 (Sr) Alloys by High-Resolution FIB Tomography", *Acta Materialia*, vol. 55, No. 11, pp. 3875-3882, 2007.

[66] Stadler, F., Antrekowitsch, H., Fragner, W., Kaufmann, H., and Uggowitzer, P. J., "The influence of solution treatment on the high temperature strength of Al-Si foundry alloys with Ni", Light Metals, 2012 Edited by: Carlos E. Suarez TMS (The Minerals, Metals & Materials Society), 2012

[67] Belov, N.A., Eskin, D.G., and Avxentieva, N.N., "Constituent phase diagrams of the Al-Cu-Fe-Mg-Ni-Si system and their application to the analysis of aluminum piston alloys", *Acta Mater* , vol.53, pp.4709–4722, 2005.

[68] Zeren, M., "The effect of heat-treatment on aluminum-based piston alloys", *Mater Des*, vol. 28, pp. 2511–2517, 2007.

[69] Liu, X.F., Qiao, J.G., Wu, Y.Y., Liu, X.J., Bian, X.F., "EPMA analysis of calcium-rich compounds in near eutectic Al–Si alloys", *J. Alloys Compd* , vol.388, pp. 83-90, 2005.

[70] Song, X. G., Bian, X. F., Zhag, J. X., and Zhang, J., "Temperature-dependent viscosities of eutectic Al–Si alloys modified with Sr and P", *J. Alloys Compd*, vol.479 pp. 670–673. 2009.

[71] Yu, L. N., Liu, X. F., and Ding, H. M., "A new nucleation mechanism of primary Si by peritectic-like coupling of AlP and TiB2in near eutectic Al–Si alloy",. *J. Alloys Compd*, vol. 432, pp. 156–162, 2007.

[72] Liao, H., Sun, Y., and Sun, G., "Correlation between mechanical properties, amount of dendritic α-Al phase in as-cast near-eutectic Al–11.6% Si alloys modified with strontium", *Mater Sci. Eng A*, vol. 335, pp.62–66, 2002.

[73] Wang, G. Q., Bian, X. F., Wang, W.M., and Zhang, J. Y., "Influence of Cu and minor elements on solution treatment of Al–Si–Cu–Mg cast alloys", *Mater Lett* , vol. 57, pp. 4083- 4087, 2003.

[74] Qian, Z., Liu, X. F., and Zhao, D. G., "Effects of trace Mn addition on the elevated temperature tensile strength and microstructure of a low-iron Al-Si piston alloy", *Mater Lett* , vol.62, pp. 2146–2149, 2008.

[75] Mohamed, A. M. A., Samuel, A. M., Samuel, F. H., and Doty, H. W., "Influence of additives on the microstructure and tensile properties of near-eutectic Al–10.8% Si cast alloy", *Mater Des*, vol.30, pp.3943–3957, 2009.

[76] Cho, Y. H., Joo, D. H., Kim, C. H., and Lee, H. C., "The effect of alloy addition on the high temperature properties of over aged AlSi(CuMgNi) cast alloy", *Mater Sci Forum*, vol. 519–521, pp. 461–466, 2006.

[77] Davis, J. R., ed. ASM Specially Handbook, "Aluminum and Aluminum Alloys", ASM. International Materials Park, Ohio, pp.3-4, 1993.

[78] Li, R. X., Li, R. D., Zhao, Y. H., He, L. Z., Li, C. X., Guan, H. R., and Hu, Z. Q., "Age hardening behaviour of cast Al-Si base alloy," *Mater. Letter*, vol.58, pp. 2096-2101, 2004.

[79] Zhang, D. L., Zheng, L. H., and StJohn, D. H., "Effect of a Short Solution Treatment Time on Microstructure and Mechanical Properties of Modified Al–7wt.%Si–0.3wt.%Mg Alloy", *Journal of Light Metals*, pp. 27-36, 2002.

[80] He, K., Yu F., Zhao, D., and Zuo, L., "Microstructural evolution of direct chill cast Al-15.5Si-4Cu-1Mg-1Ni-0.5Cr alloy during solution treatment", *China Foundry*, vol.8 No.3, pp.264-268, 2011.

[81] Ouellet, P., and Samuel F. H., "Effect of Mg on the ageing behaviour of Al-Si-Cu 319 type aluminium casting alloys", *J. Mater. Sci*, vol. 34(19), pp. 4671-4697, 1999.

[82] Gupta, A. K., Jena, A. K., and Chaturvedi, M. C., "Insoluble phase in Al-1.52Cu-0.75Mg alloys containing silicon", *Mater.Sci.Tech.*vol.3 (12), pp.1012-1018, 1987.

[83] Baker, H., "Metals Handbook: Properties and Selection: Nonferrous Alloys and Pure Metals", vol. 2, 9th edition, American Society for Metals, p.41, 1979.

[84] Paray, F., "Heat treatment and mechanical properties of aluminium-silicon modified alloys", 1992

[85] Budinski, K. G., and Budinski, M. K., "Engineering materials-properties and selection", sixth edition, pp.546-569, 1999.

[86] William, D., and Callister, Jr., "Material science and engineering - an introduction", sixth edition, 2003.

[87] Polmear, I.J., "Light Alloys, Metallurgy of the light metals" third ed. Melbourne", ISBN 0 340 63207 0, Publisher: Butterworth-Heinemann, 1995.

[88] Edwards, G.A., Stiller, K., Dunlop, G.L., and Couper, M.J., "The precipitation sequence in Al-Mg-Si alloys", *Acta Mater*, vol.46, pp. 3893-3904, 1998.

[89] Li, Y.J., Brusethaug, S., and Olsen, A., "Influence of Cu on the Mechanical Properties and Precipitation Behavior of AlSi7Mg0.5 Alloy during Aging Treatment", *Scripta Mater.*, vol.54, pp. 99-103, 2006.

[90] Wang, G., Sun, Q., Feng, L., Hui, L., and Jing, C., "Influence of Cu content on ageing behavior of AlSiMgCu cast alloys", *Materials and Design*, vol.28, pp.1001-1005, 2007.

[91] Eskin, D. G., "Decomposition of supersaturated solid solutions in Al-Cu-Mg-Si alloys", Journal of Materials Science, vol.38, pp. 279-290, 2003.

[92] Whelan, M. J., "On the kinetics of precipitate dissolution", *Metal Science*, vol. 3(1), pp. 95-97, 1969.

[93] Aaron, H. D., Fainstein, D., and Kotler, G. R., "Diffusion-limited phase transformations: a comparison and critical evaluation of the mathematical approximations", *Journal of Applied Physics*, vol.41 (11), pp. 4404-4410, 1970.

[94] Tanzilli, R.A., and Heckel, R.W., "Numerical solutions to the finite, diffusion-controlled, two- phase, moving interface problem (with planar, cylindrical and spherical interfaces)", *Transactions of the AIME*, vol. 242, pp.2313-2321, 1968.

[95] Nolfi F. V., Shewmon, P. G., and Foster, J. S., "Dissolution and growth of spherical precipitates", *Transactions of the Metallurgical Society of AIME*, vol. 245(7), pp. 1427-1433, 1969.

[96] Aaron, H. D., and Kotler, G. R., "Second phase dissolution", Metallurgical and Materials Transactions B, vol. 2(2), pp. 393-408, 1971.

[97] Myhr, O. R., and Grong, O., "Process modeling applied to 6082-T6 aluminium weldments– I. Reaction kinetics", *Acta Metallurgica et Materialia*, vol. 39(11), pp. 2693-2072, 1991.

[98] Tundal, U. H., and Ryum, N., "Dissolution of particles in binary alloys: part I. computer simulations", *Metallurgical and Materials Transactions A*, vol. 23(2), pp. 433-444, 1992.

[99] Vermolen, F. J., and van der Zwaag, S., "A numerical model for the dissolution of spherical particles in binary alloys under mixed mode control", *Materials Science and Engineering A*, vol. 220(1), pp.140-146, 1996.

[100] Vermolen, F. J., Vuik, K., and van der Zwaag, S., "The dissolution of stoichiometric second phase in ternary alloys: a numerical analysis", *Materials Science and Engineering A*, vol. 246 1-2), pp. 93-103, 1998.

[101] Rometsch, P. A., Arnberg, L. and Zhang, D. L., "Modeling dissolution of Mg_2Si and homogenisation in Al-Si-Mg casting alloys", *International Journal of Cast Metals Research*, vol. 12(1), pp.1-8, 1999.

[102] Zhang, D. L., Zheng, L. H., and StJohn, D. H., "Effect of a short solution treatment time on microstructure and mechanical properties of modified Al-7wt.%Si-0.3wt.%Mg alloy", *Journal of Light Metals*, vol. 2(1), pp. 27-36, 2002.

[103] Rometsch, P. A., Schaffer, G. B., and Taylor, J. A., "Mass balance characterisation of Al-7Si- Mg alloy microstructures as a function of solution treatment time", *International Journal of Cast Metals Research*, vol. 14 (1), pp.59-69, 2001.

[104] Parker, B. A., Saunders D. S., and Griffiths, J. R., "The quantitative evaluation of the microstructure of a strontium-modified Al-Si-Mg alloy following prolonged solution treatment", *Metals Forum*, vol. 5(1), pp. 48-53, 1982.

[105] Rhines, F. N., and Aballe, M., "Growth of silicon particles in an aluminum matrix", *Metallurgical and Materials Transactions A*, vol.17 (12), pp.2139-2152, 1986.

[106] Meyers, C. W., "Solution Heat Treatment Effects on Ultimate Tensile Strength and Uniform Elongation in A357 Aluminum Alloy", *Transactions of the American Foundrymens Society*, vol. 94, pp.511-518, 1986.

[107] Shivkumar, S., Ricci, S., Steenhoff, B., Apelian, D., and Sigworth, G., "An Experimental Study to Optimize the Heat Treatment of A356 Alloy", *Transactions of the American Foundrymens Society*, vol.97, pp.791-810,1989.

[108] Apelian, D., Shivkumar, S. and Sigworth, G., "Fundamental Aspects of Heat Treatment of Cast Al-Si-Mg Alloys", *Transactions of the American Foundrymens Society*, vol.97, pp. 727-742, 1990.

[109] Paray, F. and Gruzleski, J. E., "Microstructure - mechanical property relationships in a 356 alloy, Part I. Microstructure", *Cast Metals*, vol. 7(1), pp.29-40, 1994.

[110] Lasagni, F., Lasagni, A., Marks, E., Holzapfel, C., Mucklich, F., and Degischer, H. P., "Three-dimensional characterization of 'as-cast' and solution-treated Al-$Si1_2$ (Sr) alloys by high resolution FIB tomography", *Acta Materialia*, vol.55 (11), pp.3875-3882, 2007.

[111] Nakagawa, Y. G., and Weatherly G. C., "The thermal stability of the rod Al3Ni-Al eutectic", *Acta Metallurgica*, vol.20 (3), pp.345-350, 1972.

[112] Walter, J. L., and Cline, H. E., "Stability of the directionally solidified eutectics NiAl-Cr and Ni-Al-Mo", *Metallurgical and Materials Transactions B*, vol.4 (1), pp.33-38. 1973.

[113] Ogris, E., Wahlen, A., Luchinger, H. and Uggowitzer, P.J., "On the silicon spheroidization in Al-Si alloys", *Journal of Light Metals*, vol.2 (4), pp.263-269, 2002.

[114] Kovacevic, I., "Simulation of spheroidisation of elongated Si-particle in Al-Si alloys by the phase field model", *Materials Science and Engineering A*, vol.496 (1-2), pp.345-354, 2008.

[115] Parker, B. A., Saunders D. S., and Griffiths, J. R., "The quantitative evaluation of the microstructure of a strontium-modified Al-Si-Mg alloy following prolonged solution treatment", *Metals Forum*, vol. 5 (1), pp.48-53, 1982.

[116] Shivkumar, S., Ricci, S., Steenhoff, B., Apelian, D., and Sigworth, G., "An Experimental Study to Optimize the Heat Treatment of A356 Alloy", *Transactions of the American Foundrymens Society*, vol.97, pp.791-810, 1989.

[117] Andersen, S.J., Zandbergen, H.W., Jansen, J., Traeholt, C., Tundal, U., and Reiso, O., "The crystal structure if the β″ phase in Al-Mg-Si alloys", *Acta Materialia*, vol.46 (9), pp.3283-3298, 1998.

[118] Edwards, G.A., Stiller, K., Dunlop, G.L., and Couper, M.J., "The precipitation sequence in Al-Mg-Si alloys", *Acta Materialia*, vol.46 (11), pp. 3893-3904, 1998.

[119] Murayama, M., and Hono, K., "Pre-precipitate clusters and precipitation processes in Al-Mg-Si alloys", *Acta Materialia*, vol.47 (5), pp.1537-1548, 1999.

[120] Porter, D.A., and Easterling, K.E., "Phase Transformations in Metals and Alloys", London: Chapman & Hall, 1992.

[121] Standard Practice for Heat Treatment of Aluminum Alloys, Annual Standard Book of ASTM Standards, B597, vol.02.02, p.430-441, 1998.

[122] Massardier, V., and Epicier, T., "Study of the Influence of a Low Copper Addition and of an Excess Silicon on the Precipitation Kinetics and on the Precipitation Sequence of AlMg2Si Alloys", *Materials Science Forum*, vol.396-402, pp. 851-856, 2002.

[123] Li, R. X., Li, R. D., He, L. Z., Li, C. X., Gruan, H. R., and Hu, Z. Q., "Age-Hardening Behavior of Cast Al-Si Base Alloy", *Materials Letters*, vol.58(15): pp. 2096-2101, 2004.

[124] Hernandez-Paz, J. F., Paray, F., Gruzleski, J. E., and Emadi, D., "Natural Aging and Heat Treatment of A356 Aluminum Alloy", *American Foundry Society*, vol.112: p. 155, 2004.

[125] Zhang, D., "Precipitation of Excess Silicon During Heat Treatment of Cast Al-7wt.%Si-0.4wt.%Mg Alloy", *Materials Science Forum*, vol.217-222: pp.771-776, 1996.

[126] Garat, M., and Laslaz, G., "Improved Aluminum Alloys for Common Rail Diesel Cylinder Heads", *AFS Transactions*, Schaumburg, IL, USA. pp.1-8, 2007.

[127] Chamberlain, B., and Zabek, V., "Reappraisal of the Tensile Properties of Aluminum- Silicon-Magnesium Casting Alloys", *AFS Transactions*, vol. 81, pp. 322-327, 1973.

[128] Samuel, A. M., Gauthier, J., and Samuel, F. H., "Microstructural Aspects of the Dissolution and Melting of Al_2Cu Phase in Al-Si Alloys during Solution Heat Treatment", *Metallurgical and Materials Transactions A*, vol. 27A, pp.1785-1798, 1996.

[129] Gloria, D., Hernandez, F., and Valtierra, S., "Dimensional Changes During Heat Treating of an Automotive 319 Alloy", *20th ASM Heat Treating Society Conference Proceedings*, 9-12October 2000, St. Louis, MO, ASM International Materials Park, OH, pp. 674-679, 2000.

[130] Eskin, D. G., "Decomposition of supersaturated solid solutions in Al-Cu-Mg-Si alloys", *Journal of Materials Science*, vol.38, pp. 279-290, 2003.

[131] Han, S. W., "Effects of Solidification Structure and Aging Condition on Cyclic Stress-Strain Response in Al-7%Si-0.4%Mg Cast Alloys", *Materials Science and Engineering A*, vol. 337, pp. 170-178, 2002.

[132] Porter, A. D., and Easterling, K. E., “Phase Transformations in Metals and Alloys”, Van Nostrand Reinhold, Berkshire, England, 1981.

[133] Verhoeven, J. D., “Fundamentals of Physical Metallurgy”, J. Wiley and Sons, New York, N.Y., 1975.

[134] Smith, W. F., “Structure and Properties of Engineering Alloys”, McGraw-Hill, New York, N.Y., 1981.

[135] Hatch, J. E., “Aluminum: Properties and Physical Metallurgy, American Society for Metals”, Metals Park, OH, pp. 50-51, 1984,

[136] Samuel, F. H., Samuel, A. M., and Liu, H., “Effect of Magnesium Content on the Aging Behaviour of Water-Chilled Al-Si-Cu-Mg-Fe-Mn (380) Alloy Castings”, *Journal of Materials Science*, vol. 30, pp. 1-10, 1995.

[137] Li, R. X., Li, R. D., Zhao, Y. H., He, L. Z., Li, C. X.,. Guan, H. R., and Hu, Z. Q., “Age-Hardening Behavior of Cast Al-Si Base Alloy,” *Materials Letters*, vol. 58, pp. 2096-2101, 2004.

[138] Zhang, D. L., and Zheng, L., “The quench sensitivity of cast Al-7wt pct Si–0.4wt pct Mg alloy”, *Metall Mater Trans A*, vol. 27A (12), pp.3983-3991, 1996.

[139] Zafar, S., Ikram, N., Shaikh, M. A., and Shoaib, K. A., “Microstructure studies in Al-6%Si- 1.9%Cu- X%Mg alloys”, *Journal of Material Science*, vol.25, pp.2595-2597,1990.

[140] Kang, H. G., Kida, M., Miyahara, H., and Ogi, K., “Age-hardening characteristics of Al-Si-Cu-base cast alloys", *AFS Trans.*, vol. 27, p.507-515, 1999.

[141] Ouellet, P., and Samuel, F. H., “Effect of Mg on the Ageing Behavior of Al-Si-Cu 319 Type Aluminum Casting Alloys”, *J. Mater. Sci.*,vol.34 (19), pp.4671-97. 1999,

[142] Beumler, H., Hammerstad, A., Wieting, B., and Dasgupta, R., “Analysis of Modified 319 Aluminum Alloy”, *AFS Transactions*, vol. 96, pp. 1-12, 1988.

[143] Li, Z., Samuel, A. M., Samuel, F. H., Ravindran, C., Valtierra, S., and Doty, H. W., “Parameters controlling the performance of AA319-type alloys -Part I. Tensile properties”, *Mater. Sci. Eng. A*, vol. 367(1-2), pp.96-110, 2004,

[144] Osamura, K. , Hiraoka, Y., and Murakami, Y., “The resistivity maximum during Guinier-Preston zone formation in Al-Zn alloys”, *Philos .Mag* ., vol.28, pp.809-825, 1973.

[145] Mulazimoglu, M. H., Drew, R. A. L., and Gruzleski, J. E., “The Electrical conductivity of cast Al-Si alloys in the range of 2 to 12.6 wt% Si”, *Metallurgical Transaction A*, vol.20A, pp.383-389, 1989.

[146] Mulazimoglu, M. H., Drew, R. A. L., and Gruzleski, J. E., “The effect of Sr on the Electrical resistivity and conductivity of Al-Si alloys”, *Metallurgical Transaction A*, vol.18A, pp.941-947, 1987.

[147] Mulazimoglu, M. H., Drew, R. A. L., and Gruzleski, J. E., “Electrical conductivity of Al rich Al-Si-Mg alloys”, *J. of Mat. Sci. Letters*, vol.9, pp.297-300, 1989.

[148] Kim, J. H., Kobayashi, E., and Sato, T., "Effects of Cu Addition on Behavior of Nanoclusters during Multi-Step Aging in Al-Mg-Si Alloys", *Materials Transactions*, vol. 52(5), pp. 906-913, 2011.

[149] Panseri, C., and Federighi, T., "A Resistometric Study of Precipitation in an Aluminium-1.4 % Mg_2Si Alloy", *Journal of the Institute of Metals*, vol. 94(3), pp.99-107, 1966.

[150] Rossiter, P. L., "The Electrical Resistivity of Metals and Alloys", Cambridge University Press, Cambridge, United Kingdom, pp.1–73, 1987.

[151] Lodgaard, L., and Ryum, N., "Precipitation of dispersoids containing Mn and/or Cr in Al-Mg-Si alloys", *Mat. Sci. Eng. A*, vol. 283(1–2), pp.144–52, 2000.

[152] Edwards, J. T., and Hillel, A. J., "The electrical resistivity of G.P. zones," *Philos. Mag.*, vol. 35 (5), pp. 1221–1229, 1977.

[153] Thakur, A., Raman, R., and Malhorta, S. N., "Effect of natural aging on the resistivity evolution during artificial aging of the Al–Zn–Mg–Zr alloy", *J. Mater. Process. Technol.*, vol. 194, pp. 184-186, 2007.

[154] Esmaeili, S., Lloyd, D. J., and Poole, W. J., "Effect of Natural Ageing on the Resistivity Evolution during Artificial Ageing of the Aluminum Alloy AA6111", *Materials Letters*, vol.59(5), pp. 575-577, 2005.

[155] Eivani, A. R., Ahmed, H., Zhou, J., and Duszczyk, J., "Correlation between Electrical Resistivity, Particle Dissolution, Precipitation of Dispersoids, and Recrystallization Behavior of AA7020 Aluminum Alloy", *Metallurgical and Materials Transaction A*, vol. 40A, pp.2435-2446, 2009.

[156] Heusler, L., Feikus, F. J., and Otte, M. O., "Alloy and Casting Process Optimization for Engine Block Application', *Transactions of the American Foundrymen's Society*, vol.109, p.443, 2001.

[157] Garat, M. and Laslaz, G., "Improved Aluminum Alloys for Common Rail Diesel Cylinder Heads", *AFS Transactions*, Schaumburg, IL, USA, pp.1-8, 2007.

[158] Feikus, F. J., "Optimization of Al-Si Cast Alloys for Cylinder Head Applications", *Transactions of the American Foundrymen's Society*, vol.106, p.225-231, 1998.

[159] Feiskus, F. J. and W. Schneider, "Process and Material Developments in Aluminum Engine Castings", *Light Metals Technology Conference*, 2003. Brisbane, Australia

[160] Caceres, C. H., Djurdjevic, M. B., Stockwell, T. J., and Sokolowski, J. H., "The Effect of Cu Content on the Level of Microporosity in Al-Si-Cu-Mg Casting Alloys", *Scripta Materialia*, vol.40(5), pp. 631-637, 1999.

[161] Cho, J., Loper, J. C. R., and Yan, X., "Microsegregation Effect of Copper in Aluminum-Silicon Casting Alloys", American Foundry Society, vol.112, pp. 447-460, 2004.

[162] Li, Y. J., S. Brusethaug, and Olsen, A., "Influence of Cu on the Mechanical Properties and Precipitation Behavior of AlSi7Mg0.5 Alloy During Aging Treatment", *Scripta Materialia*, vol.54(1), pp. 99-103, 2006.

[163] Kang, H. K., Kida, M., and Miyahara, H., "Age-Hardening Characteristics of Al-Si-Cu Cast Alloys", *AFS Transactions*, vol.107, pp. 507-515, 1999.

[164] Chakrabarti, D. J., and Laughlin, D. E., "Phase Relations and Precipitation in Al-Mg-Si Alloys with Cu Additions", *Progress in Materials Science*, vol.49(3-4), pp. 389- 410, 2004.

[162] Li, Y. J., S. Brusethaug, and Olsen, A., "Influence of Cu on the Mechanical Properties and Precipitation Behavior of AlSi7Mg0.5 Alloy during Aging Treatment", *Scripta Materialia*, vol.54(1), pp. 99-103, 2006.

[160] Caceres, C. H., Djurdjevic, M. B., Stockwell, T. J., and Sokolowski, J. H., "The Effect of Cu Content on the Level of Microporosity in Al-Si-Cu-Mg Casting Alloys", *Scripta Materialia*, vol.40(5), pp. 631-637, 1999.

[165] Wang, X., Poole, W. J., Esmaeili, S., Lloyd, D. J., and Embury, J. D., "Precipitation Strengthening of the Aluminum Alloy AA6111", *Metallurgical and Materials Transactions A*, vol.34A, pp.2913-2924, 2003.

[36] Wang, G., Sun, Q., Feng, L., Hui, L. and Jing, C., "Influence of Cu content on ageing behavior of AlSiMgCu cast alloys", *Materials and Design*, vol.28, pp.1001-1005, 2007.

[166] Cáceres, C. H., "A Rationale for the Quality Index of Al-Si-Mg Casting Alloys", *Int. J. Cast Met. Res.*, vol. 10, pp.293-299, 1998.

[167] Kaczorowski, M., Grabski, M.W., Sawicki, J., and Murza-Mucha, P., "A study of precipitation hardening of commercial Al-9wt% Si alloy", *J. Mater. Sci.*,vol.14, pp.2781-2786, 1979.

[168] Zhang, D.L.& StJohn, D.H., "The effect of composition and heat treatment on the microstructure and mechanical properties of cast Al–7wt%Si–Mg alloys", Casting & Solidification of Light Alloys, Gold Coast, IMMA, pp.21-25, 1995.

[169] Sjölander, E., "*Heat treatment of Al-Si-Cu-Mg casting alloys*", PhD Thesis, Department of Mechanical Engineering, School of Engineering, Jönköping University, SE-551 11 Jönköping, Sweden, ISBN 978-91-7385-529-7, 2011

[170] Cho, Y.H., Joo, D.H., Kim, C.H., and Lee, H.C., "The Effect of Alloy Addition on the High Temperature Properties of Over-Aged Al-Si(CuNiMg) Cast Alloys", *Mater. Sci. Forum*, vol.519-521, pp.461-466, 2006.

[171] Zeren, M., "The effect of heat-treatment on aluminum-based piston alloys", *Materials and Design*, vol.28, pp. 2511-2517, 2007.

[172] Li, Y., Yang, Y., Wu, Y., Wang, L., and Liu, X ., "Quantitative comparison of three Ni-containing phases to the elevated-temperature properties of Al-Si piston alloys", *Mater. Sci. and Eng. A*, vol.527, pp. 7132-7137, 2010.

[173] Asghar, Z., Requena, G., and Kubel, F., "The role of Ni and Fe aluminides on the elevated temperature strength of an AlSi12 alloy", *Mater. Sci. and Eng. A*, vol. 527, pp. 5691-5698, 2010.

[174] Stadlerl, F., Antrekowitsch1, H., Fragner, W., Kaufmann, H., and Uggowitzer, P. J., "The effect of Ni on the high-temperature strength of Al-Si cast alloys", *Mater. Sci. Forum*, vol.690, pp. 274-277, 2011.

[175] Stadlerl, F., Antrekowitsch1, H., Fragner, W., Kaufmann, H., and Uggowitzer, P. J., "Effect of main alloying elements on the strength of Al-Si cast alloys at elevated temperatures", *International Journal of Cast Metals Research*, vol. 25(4), pp. 215-224, 2012.

[176] Flinn, R.A., "Fundamentals of metal casting", first ed., Addison-Wesley Publishing Company, Massachusetts, 1963.

[177] Sicha, W.E., "Properties of commercial casting alloys", In: Kent, R., Van Horn, Aluminum vol. I-Properties, Physical Metallurgy and Phase Diagram, fourth ed., American Society for Metals, Metals Park, OH, pp. 277-302, 1971.

[178] Li, Z., Samuel, A.M., Samuel, F.H., Ravindran, C., Doty, H.W., Valtierra, S., "Parameters controlling the performance of AA319-type alloys Part II. Impact properties and fractography", *Mater. Sci. Eng. A*, vol.367, pp.111-122, 2004.

[179] Paray, F., Kulunk, B., Gruzleski, J.E., "Impact properties of Al-Si foundry alloys", *Int. J. Cast Met. Res.*, vol.13, pp.17-37, 2000.

[180] Srivastava, M. C., Lohne, O., Arnberg, L., Laukli, H. I., Gjestland, H., "Energy absorption of HPDC aluminium and magnesium alloys," *In: Proc. High Tech Die Casting 2006*, Vicenza, Italy, paper 10, 2006.

[181] Murali, S., Raman, K. S., Murthy, K. S. S., "Effect of magnesium, iron (impurity) and solidification rates on the fracture toughness of Al-7Si-0.3Mg casting alloy", *Mater. Sci. Eng. A*, vol.151, pp.1-10, 1992.

[182] Shivkumar, S., Wang, L., Keller, C., "Impact properties of A356-T6 alloys", *J. Mater. Eng. Perform.*, vol.3, pp.83-90, 1994.

[183] Zhang, D. L., Zheng, L. H., StJohn, D. H., "Effect of a short solution treatment time on microstructure and mechanical properties of modified Al-7wt.%Si-0.3wt.%Mg alloy", *J. Light Met.*, vol.2, pp.27-36, 2002.

[184] Cáceres, C. H., Davidson, C. J., Griffiths, J. R., "The deformation and fracture behaviour of an Al-Si-Mg casting alloy", *Mater. Sci. Eng. A*, vol.197, pp.171-179, 1995.

[185] Wang, Q. G., Cáceres, C. H., "The fracture mode in Al-Si-Mg casting alloys", *Mater. Sci. Eng. A*, vol.241, pp.72-82, 1998.

[186] Brown, L.M. and Ham, R.K., "Strengthening Methods in Crystals", Applied Science Publishers Ltd, London, John Wiley & Sons., 1971.

[187] Gerold, V., "Dislocations in Solids" Amsterdam: North Holland, 1979.

[188] Ardell, A., "Precipitation hardening", *Metallurgical and Materials Transactions A*, 16 (12), pp.2131-2165, 1985.

[189] Martin, J. W., "Precipitation hardening", 2nd edition, Butterworth, Heinemann, Oxford, 1998.

[190] Nie, J. F., Muddle, B. C., and Polmear, I. J., "Effect of Precipitates Shape and Orientation on Dispersion strengthening in High Strength Al Alloys", *Mater. Sci. Forum*, 217-222, 1257, (1996).

[191] Orowan, E., "Symposium on Internal Stresses in Metals and Alloys", Inst. Metals, London, 451, (1948).

[192] Embury, J. D., Loyd, D. J., and Ramachandran, T. R, "Aluminium Alloys: Contemporary Research and Applications, Treatise on Materials Science and Technology", *Academic Press*, vol.31, pp.579-601, 1989.

[193] Ardell, A., "Precipitation hardening", *Metallurgical and Materials Transactions A*, vol.16 (12), pp.2131-2165, 1985.

[194] Clyne, T. W. and Withers, P. J., "An Introduction to Metal Matrix Composites", Cambridge: Cambridge University Press, 1993

[195] Hertzberg, R. W., "Deformation and Fracture Mechanics of Engineering Materials", New York: John Wiley & Sons, 1996.

[200] Yang, L., (ed.). "Techniques for corrosion monitoring," Press ISBN 978-1-4200-7089-7, Cambridge, England, 2008.

[201] Trzaska, M., and Trzaska, Z., "Electrochemical impedance spectroscopy in materials science," Publ. Office of the Warsaw Univ. Technol., ISBN 978-83-7207-873-5, Warsaw, Poland, 2010.

[202] Bard, A. J., and Faulkner, L. R., "Electrochemical Methods: Fundamentals and Applications," New York: John Wiley & Sons, 2nd Edition, 2000.

[203] Srinivasa, K., Rao and Prasad Rao, K., "Pitting corrosion of heat treatable Al Alloys and Welds: A review", *Trans. Indian Inst. Met*. vol. 57(6), pp. 593-610, 2004.

[204] Orazem, M. E., and Tribollet B., "Electrochemical Impedance Spectroscopy," J. Wiley, ISBN 9780470041406, New York, USA, 2008.

[205] Sword, J., Pashley, D. H., Foulger, S., Tay, F. R., and Rodgers, R., "Use of electrochemical impedance spectroscopy to evaluate resin-dentin bonds," Journal of Biomedical Materials Research, vol. 84B(2), pp.468-477, ISSN1552-4981, 2007.

[206] Vargel, Ch., "Corrosion of Aluminium," Elseevier, ISBN 0 08 044495 4, New York, USA, 2004.

[207] Huang, Y., Shih, H., Huang, H., Daugherty, J., Wu, S., Ramanathan, S., Chang, Ch. and Mansfeld, F., "Evaluation of the corrosion resistance of anodized aluminum 6061 using electrochemical impedance spectroscopy (EIS)," *Corrosion Science*, vol.50(12), pp.3569-3575, ISSN 0010-938X, 2008, 2008.

[208] Bavarian, B., Reiner, L., Vajo, J., Wei, R., and Herrera, G., "Mathematical Modeling of Crevice Corrosion of Aluminum Alloys Using Extreme Value Analysis," *International Corrosion Congress: Frontiers in Corrosion Science and Technology*, 15th, Granada, Spain, pp.22-27, 2002.

[209] Yuan, X., and Xia, W., "Effect of Microstructure on Corrosion Resistance of Electrolytic AlSi7Mg0.3 Alloys," *Fushi Kexue Yu Fanghu Jishu*, vol.14 (5), pp. 263-266, 2002.

[210] Takahashi, T., Saga, T., and Kojima, Y., "Effect of Zinc and Magnesium on the Properties of Aluminum-Silicon-Copper Die-Casting Alloys," *Keikinzoku*, vol.17(6), pp. 368-376, 1967.

[211] Scully, J. R., Knight, T. O., Buchheit, R. G., and Peebles, D. E., "Electrochemical Characterization of the Al2Cu, Al3Ta and Al3Zr Intermetallic Phases and Their Relevancy to the Localized Corrosion of Al Alloys," *Corrosion Science*, vol.35(1-4), pp. 185-195, 1993.

[212] Buchheit, R. G., Boger, R. K., Carroll, M. C., Leard, R. M., Paglia, C., and Searles, J. L., "The Electrochemistry of Intermetallic Particles and Localized Corrosion in Al Alloys," *Journal of Metals*, vol.53(7), pp. 29-33, 2001.

[213] Mondolfo, L. F., "Aluminum Alloys: Structure and Properties," London, Boston: Butterworths, 1976.

[214] Hatch, J. E., "Aluminum: Properties and Physical Metallurgy," Metals Park, Ohio: ASM. pp. 320-350, 1984.

[215] Schweitzer, P. A., and. Schweitzer, P. A., "Corrosion and Corrosion Protection Handbook," Marcel Dekker, Inc., 1983.

[216] Chawla, S. L., and Gupta, R. K., "Materials Selection for Corrosion Control," ASM International, 159-211, 1993.

[217] Scully, J. R., Peebles, D. E., Romig, A. D., Frear, D. R., and Hills, C. R., "Metallurgical Factors Influencing the Corrosion of Aluminum, Al-Cu, and Al-Si Alloy Thin Films in Dilute Hydrofluoric Solution," *Metallurgical and Materials Science Transactions A*," vol. 23A(9), pp. 2641-2655,1992.

[218] Griffin A. J., Jr., and Brotzen, F. R., "Impedance-Spectroscopy Response of Aluminum-Copper-Silicon Alloys," *Journal of the Electrochemical Society*, vol.141(12), pp. 3473-3479, 1994.

[219] Kowal, K., Deluccia, J., Josefowicz, J. Y., Laird, C., and Farrington, G. C., "In Situ Atomic Force Microscopy Observations of the Corrosion Behavior of Aluminum- Copper Alloys," *Journal of the Electrochemical Society*, vol.143(8), pp. 2471- 2481, 1996.

[211] Scully, J. R., Knight, T. O., Buchheit, R. G., and Peebles, D. E., "Electrochemical Characterization of the Al2Cu, Al3Ta and Al3Zr Intermetallic Phases and Their Relevancy to the Localized Corrosion of Al Alloys," *Corrosion Science*, vol.35(1-4), pp. 185-195, 1993.

[212] Buchheit, R. G., Boger, R. K., Carroll, M. C., Leard, R. M., Paglia, C., and Searles, J. L., "The Electrochemistry of Intermetallic Particles and Localized Corrosion in Al Alloys," *Journal of Metals*, vol.53(7), pp. 29-33, 2001.

[217] Scully, J. R., Peebles, D. E., Romig, A. D., Frear, D. R., and Hills, C. R., "Metallurgical Factors Influencing the Corrosion of Aluminum, Al-Cu, and Al-Si

Alloy Thin Films in Dilute Hydrofluoric Solution," *Metallurgical and Materials Science Transactions A*, vol.23A(9), pp. 2641-2655, 1992.

[219] Kowal, K., Deluccia, J., Josefowicz, J. Y., Laird, C., and Farrington, G. C., "In Situ Atomic Force Microscopy Observations of the Corrosion Behavior of Aluminum-Copper Alloys," *Journal of the Electrochemical Society*, vol.143(8), pp. 2471-2481,1996.

[220] Galvele, J. R., and Micheli, S. M. D. D., "Mechanism of Intergranular Corrosion of Al-Cu Alloys," *Corrosion Science*, 10(11): pp. 795-807, 1970.

[221] Buchheit, R. G., "The Electrochemistry of Al2Cu, Al2CuMg and T1 (Al2CuLi) and Localized Corrosion and Environmental Assisted Cracking in High Strength Al Alloys," *Materials Science Forum*, vol.331-337, pp. 1641-1646, 2000.

[222] Leard, R. R., and Buchheit, R. G., "Electrochemical Characterization of Copper-Bearing Intermetallic Compounds and Localized Corrosion of Al-Cu-Mg-Mn Alloy 2024," *Materials Science Forum*, vol.396-402, pp. 1491-1496, 2002.

[223] Buchheit, R. G., Martinez, M. A., and Montes, L.P., "Evidence for Cu Ion Formation by Dissolution and Dealloying the Al2cumg Intermetallic Compound in Rotating Ring-Disk Collection Experiment," *Journal of the Electrochemical Society*, vol.147(1), pp. 119-124, 2000.

[224] Hayasaka, N., Koya, Y., Shimomura, K., Yoshida, Y., and Okano, H., "Mechanism of Corrosion in Al-Si-Cu," *Japanese Journal of Applied Physics*, Part 1, vol.30(7), pp. 1571-1575, 1991.

[225] Blanc, C., Lavelle, B., and. Mankowski, G., "The Role of Precipitates Enriched with Copper on the Susceptibility to Pitting Corrosion of the 2024 Aluminum Alloy," *Corrosion Science*, vol.39 (3), pp. 495-510, 1997.

[226] Guillaumin, V., and Mankowski, G., "Localized Corrosion of 2024 T351 Aluminium Alloy in Chloride Media," *Corrosion Science*, vol.41, pp. 421-438, 1999.

[227] Buchheit, R. G., Grant, R. P., Hlava, P. F., Mckenzie, B., and Zender, G. L., "Local Dissolution Phenomena Associated with S Phase (Al2CuMg) Particles in Aluminum Alloy 2024-T3," *Journal of the Electrochemical Society*, vol.144(8), pp.2621-2628, 1997.

[228] Buchheit, R. G., "A Compilation of Corrosion Potentials Reported for Intermetallic Phases in Aluminum Alloys," *Journal of the Electrochemical Society*, vol. 142(11), pp. 3994-3996, 1995.

[229] Buchheit, R. G., Montes, L. P., Martinez, M. A., Michael, J., and Hlava, P. F., "The Electrochemical Characterization of Bulk-Synthesized Al2CuMg," *Journal of the Electrochemical Society*, vol.146(12), pp. 4424-4428, 1999.

[230] Bhattamishra, A. K., and Lal, K., "Microstructural studies on the Effect of Si and Cr on the Intergranular Corrosion in Al-Si-Mg Alloys," *Materials and Design*, vol.18(1), pp.25-28, 1997.

[231] Mizuno, K., Nylund, A., and Olefjord, I., "Surface Reaction during Picking of an Aluminum-Magnesium-Silicon Alloy in Phosphoric Acid," *Corrosion Science*, vol.43, pp. 381-396, 2001.

[232] Nisancioglu, K., and Nordlien, J. H., "Understanding Corrosion Mechanisms of Commercial Aluminum and Magnesium Materials," *Keikinzoku (Light Metals)*, vol.50 (9), pp. 417-429, 2000.

[233] Williams John Austin, "Engineering Tribology", New York, Cambridge University Press, p.165, 2005.

[234] Torabian, H., Pathak, J., & Tiwari, S., "Wear characteristics of Al-Si alloys", *Wear*, vol.172 (1), pp.49-58, 1994.

[235] Yasmin, T., Khalid Asad, A., Haque, M. M., "Tribological (wear) properties of aluminum–silicon eutectic base alloy under dry sliding condition", *Journal of Materials Processing Technology*, vol.153–154 pp.833-838, 2004.

[236] Kori, S. A., Chandrashekharaiah, T. M., "Studies on the dry sliding wear behaviour of hypoeutectic and eutectic Al–Si alloys", *Wear*, vol.263 pp.745-755, 2007.

[237] Torabian, H., Pathak, J. P., and Tiwari, S. N., "Wear characteristics of Al-Si alloys", *Wear*, vol.172, pp.49-58, 1994.

[238] Rajaram, G., Rao, T., Srinivas, "High temperature tensile and wear behaviour of aluminum silicon alloy", *Materials Science and Engineering A*, vol.528 pp.247-253, 2010.

[239] Chandrashekharaiah, T. M, *Studies on sliding wear behaviour of grain refined and modified hypoeutectic*, eutectic and hypereutectic Al-Si alloys", PhD Thesis, VTU Belgaum, 2007.

[240] Standard test method for wear testing with a pin-on-disc Apparatus, Designation: G 99-90 ASTM, Raco St. Philodolphia, PA 19103, 1916.

[241] Shivanath, R., Sengupta, P. K., and Eyre, T. S., "Wear of aluminum-silicon alloy", *British Foundrymen*, vol.79, pp.349-356, 1977.

[242] Antoniou, R., and Borland, D. W., "Mild wear of Al-Si binary alloys during unlubricated sliding", *Materials Science and Engineering*, vol.93, pp.57-72, 1987.

[243] Reddy, A. S., Pramila Bai, B. N., Murthy, K. S. S., and Biswas, S. K., "Wear and seizure of binary Al-Si alloys", *Wear*, vol.171, pp.115-127, 1994.

[243] Beesly, C., and Eyre, T. S., "Friction and Wear of Aluminum Alloys Containing Copper and Zinc," *Tribology International*, vol. 9, pp. 63-69, 1976.

[244] Subramanian, C., "Some Considerations towards the Design of a Wear Resistant Aluminum Alloy," *Wear*, vol.155, pp.193-205, 1992

[245] Davis J.R., "ASM Specialty Handbook, Aluminum and Aluminum Alloys," ASM International, Materials Park, OH, 1993.

[246] Gaber, A., Gaffar, M.A., Mostafa, M.S., and Zeid, E.F.A., "Precipitation kinetics of Al-1.12 Mg2Si-0.35 Si and Al-1.07 Mg2Si-0.33 Cu alloys", *Journal of Alloys and Compounds*, vol.429, pp.167-175, 2007.

[247] Maniara R., Dobrzański, L. A., Krupiński, M. and Sokołowski, J. H., "The effect of copper concentration on the microstructure of Al-Si-Cu alloys", *Archiwes of Foundry engineering*, vol. 7(2), pp.119-124, 2007.

[248] Miller W. S., Zhuang, L., Bottema, J., Wittebrood, A. J., De Smet, P., Haszler, A. Vieregge, A., "Recent development in aluminium alloys for the automotive industry", *Materials Science and Engineering A*, vol.280, pp. 37-49, 2000.

[249] Ji-hua, P., Xiao-long, T., Jian-ting, H., and De-ying, X., "Effect of heat treatment on microstructure and tensile properties of A356 alloys", *Trans. Nonferrous Met. Soc. China*, vol.21, pp.1950-1956, 2011.

[250] Ogris, E., Wahlen, A., Luchinger, H., Uggoowitzer, P. J., "On the silicon spheroidization in Al-Si alloys", *J. Light Metals*, vol.2(4), pp.263-269, 2002.

[251] Meyers C.W., Hinton K.H., and Chou J.S., "Towards the Optimization of Heat Treatment in Aluminum Alloys*", Materials Sci. Forum*, vol.72, pp.102-104, 1992.

[252] Morley, A., *Atom Probe study of the 'Paint Bake' response of Al-Mg-Si (Cu) alloys in naturally aged and pre-aged conditions*, M. Engg. Thesis, Oxford Materials, University of Oxford, pp.1-108, 2004.

[253] Nagai, Y., Murayama, M., Tang, Z., Nonaka, T., Hono, K., and Hasegawa, M., "Role of vacancy-solute complex in the initial rapid age hardening in an Al-Cu-Mg alloy", *Acta Mater.*, vol. 49, pp.913-920, 2001.

[254] Lasa, L., Rodrigues-Ibade, J. M., "Characterization of the dissolution of the Al2Cu phase in two Al-Si-Cu-Mg casting alloys using calorimetry", *J. Materials Characterization*, vol.48(5), pp.371−378, 2002.

[256] ASTM B557-06

[257] ASTM E23

[257A] ASTM G99

[258] Engler-Pinto, C.C., et al., "A Comparative Investigation on the High Temperature Fatigue of Three Cast Aluminum Alloys", SAE -Technical Publication, 2004-01-1029, 2004.

Appendix A

Suggestion: The summary of the results obtained to be summarised in the form of a Table.

Response: The results are summarised in Table below:

The overall summary experimental results are listed below

Sample No	Ageing	Hardness, HRF	Tensile		Electrochemical			Wear (mass) Loss, mg	Impact strength, Joule
			UTS, MPa	E, %	Corr. Rate, mpy	Rct, kΩ	CPE, µF		
Alloy-1	UA	59.5	110	5.2				5.7	5.5
	PA	88.3	143	3.6	5.287	15.57	1.26	3.2	2.38
	OA	59	106	5.2				4.5	4.25
Alloy-2	UA	61.5	114	6.4				5.5	3.25
	PA	92.8	179	4.2	4.732	25.75	1.79	4.2	2.1
	OA	77.9	150	4.3				3.5	3.25
Alloy-3	UA	70	157	4.6				5.4	2.5
	PA	96.8	188	4.3	2.474	27.13	3.22	3.8	1.5
	OA	83.9	155	4.3				2.7	2.25
Alloy-4	UA	78	175	4.9				4.6	2.15
	PA	100.1	212	4.8	17.05	28.33	2.01	2.7	1.5
	OA	89.2	169	4.7				2.6	3
Alloy-5	UA	89.8	96	2.2				3.2	2.45
	PA	101.5	129	1.6	13.65	6.44	2.94	3.4	2
	OA	89.5	88	2				2.9	4
Alloy-6	UA	73	148	4.8				5.8	2
	PA	92.6	179	3.2	2.132	14.44	1.65	3.5	1.37
	OA	73.1	103	3				4.8	4
Alloy-7	UA	82.5	160	3.3				4.4	1.5
	PA	102.3	205	4	2.278	27.95	1.77	2.2	1.5
	OA	90.7	157	4				2.8	3

Note: UA-Under aged (20^{o}C), PA-Peak aged (225 ^{o}C), OA-Over aged (300 ^{o}C)

Suggestion: Summary of results and discussion of each section to be given as Appendix.

Response: Summary of each section is given below with a new section number.

4.1 Precipitation Treatment

4.1.4 Concluding Remarks

The hardness and resistivity of Al-6Si-0.5Mg alloys are function of ageing conditions and alloying elements. The hardness of the alloys increases up to 12-15 days during natural ageing; hardness changes on further ageing are insignificant. All the alloys show maximum hardness on ageing at 225^{o}C for 1 hour. Alloy-5 shows the highest hardness at solution treated, quenched and also in peak aged condition. Then Alloy-7 and Alloy-4 show better hardness. The hardness of all alloys falls on ageing at temperatures above 225^{o}C due to softening effects. The resistivity of the alloys also changes significantly with ageing conditions.

4.2 Microstructural Analysis of the Alloys

4.2.8 Concluding Remarks

The heat treatment of Al-6Si-0.5Mg alloys containing Cu and/or Ni result in a wide range microstructure conditions such as dissolution of soluble particles and morphological changes of insoluble particles during solution treatment. The Al-Si eutectics are fragmented and modified after heat treatment. The intermetallics containing Cu are totally dissolved but intermetallics containing Ni dissolve only partially during heat treatment.

4.3 Tensile Properties of the Alloys

4.3.5 Concluding Remarks

The UTS and YS increase with ageing temperature, the maximum being attained at peakaged condition. On the other hand the percent elongation (%E) of alloys decreases. The strength of the alloys increases with the increase of Cu and/or Ni addition to Al-6Si-0.5Mg alloy and ageing temperature. Maximum strength was found for 2wt% Cu addition to Al-6Si-0.5Mg alloy (Alloy-4) and on ageing at 225^{o}C. At this condition the ductility passes through the minima. Strain rates also affected the tensile properties. At higher strain rates the UTS and YS are higher but the ductility was poor.

4.4 Impact Properties of the Alloys

4.4.4 Concluding Remarks

The impact strengths (absorbed energy) of the alloys are function of the artificial ageing temperature and alloying elements. The alloys maintain higher impact strength at solution treated and quenched condition. The absorbed energy decreases to a minimum on ageing for 1 hour at 225^{o}C. On ageing beyond 225^{o}C, the impact strength of the alloys increases with ageing temperature.

4.5 Fracture Behavior of the Alloys

4.5.12 Concluding Remarks

The fracture surface morphologies of the alloys show the ductile or ductile-brittle mixed mode fracture during failures. Al-6Si-0.5Mg alloy maintains improved fracture strength up to 2 wt% Cu content at a common strain rate of $10^{-3}s^{-1}$. At lower strain rate the alloys produces many dimples and the fracture surfaces are in ductile (dimples present) in nature. But at higher strain rate shiny and smooth fracture surfaces reveal the transcrystalline cleavage or brittle fracture.

4.6 Electrochemical Behaviors of the Alloys

4.6.8 Concluding Remarks

The electrochemical measurements of corrosion behaviour of the alloys aged at 225^{o}C for 1 hour shows that the open circuit potential (OCP), corrosion potential (Ecorr), pitting potential (Epit) move towards positive or noble direction. The potentiodynamic polarization results indicate that Cu addition up to 1 wt% into Al-6Si-0.5Mg alloy decreases the corrosion rate. Alloys containing 2wt% Ni or combined 2wt% Ni and 2wt% Cu also show better corrosion resistance. In impedance spectroscopic method, up to 4wt% Cu addition, the alloys show better polarization resistance. Combined 2wt% Ni and 2wt% Cu addition also shows better polarization / corrosion resistance.

4.7 Wear Behaviour of the Alloys

4.7.6 Concluding Remarks

The wear resistance of the alloys is a function of ageing temperature and alloying elements. The wear resistance is lower at solution treated and in as-quenched condition. The wear resistance increases with ageing temperatures and developed best wear properties on ageing at 225^{o}C for 1 hour.

Suggestion: Percentage of error to be indicated in figures.

Response: The results of the isochronal ageing tests up to 400^{o}C for Alloys 1-5 are presented in Figure 4.1.6 without error bars. Calculations showed a maximum error of 3 percent. This graph (Figure 4.1.6) with 3 percent error bar is shown below. Even though the curves look very clumsy, the trend remains the same. The error bars have been ignored in the main text.

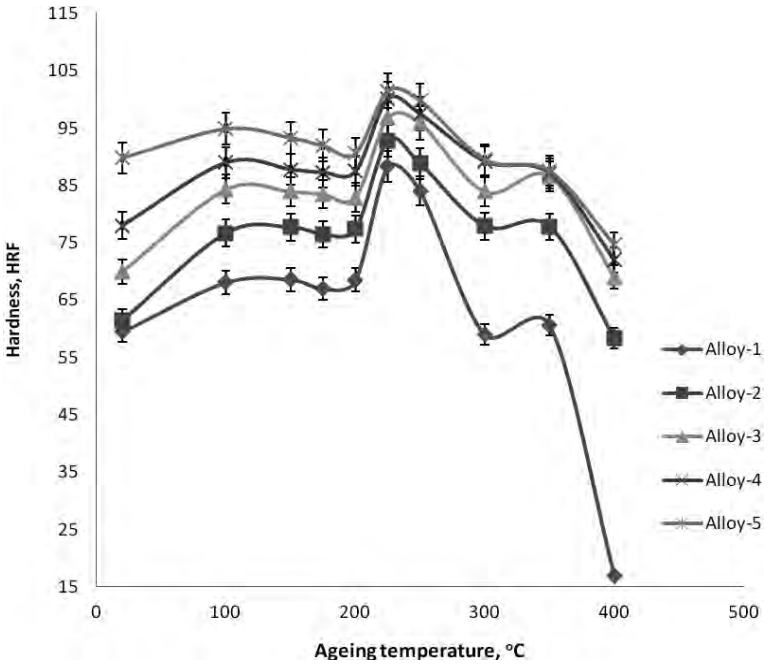

Figure 4.1.6: Variation in hardness during artificial ageing of Alloys 1 to 5 aged for 1 hour

Appendix B

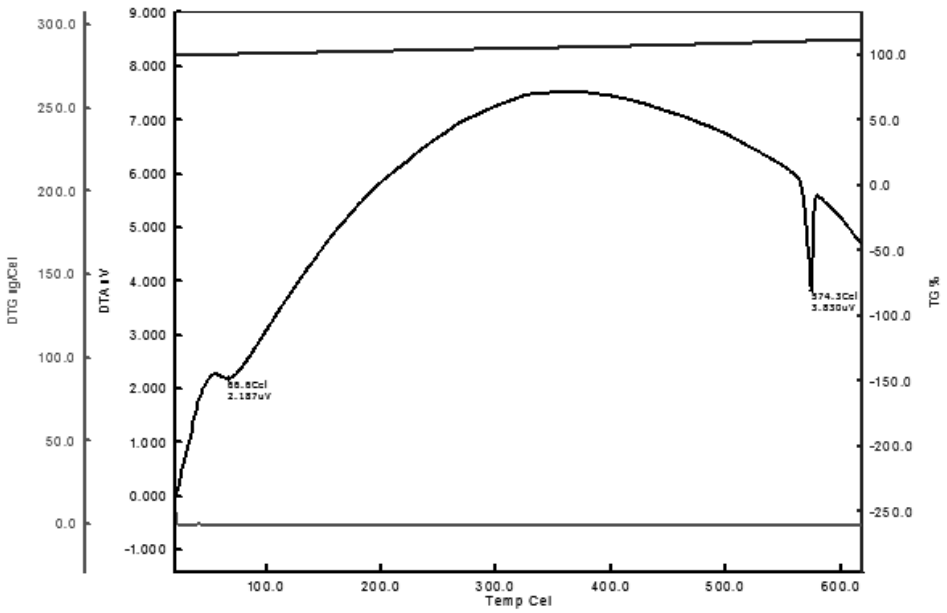

Differential Thermal Analysis (DTA) curve of solution treated Alloy-1

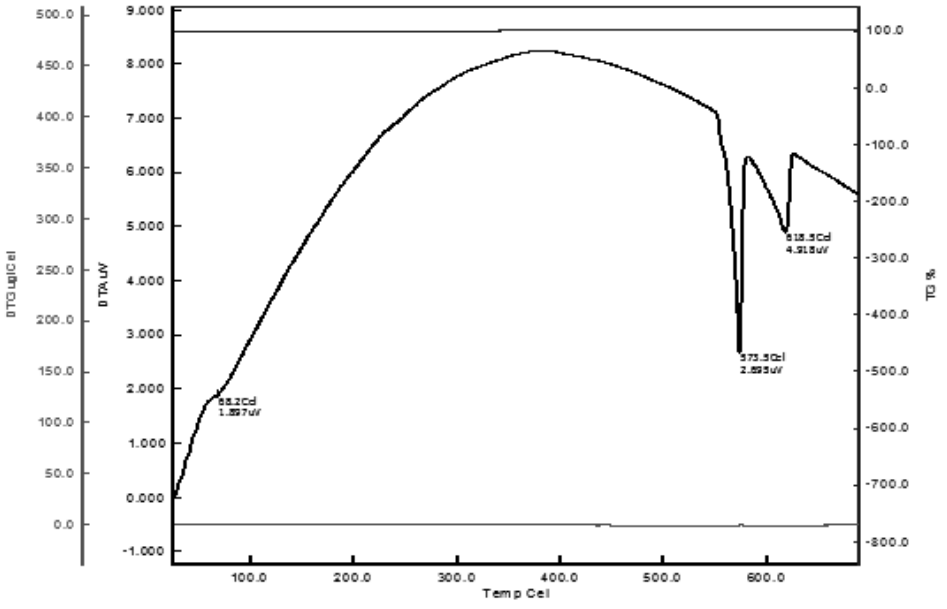

Differential Thermal Analysis (DTA) curve of solution treated Alloy-2

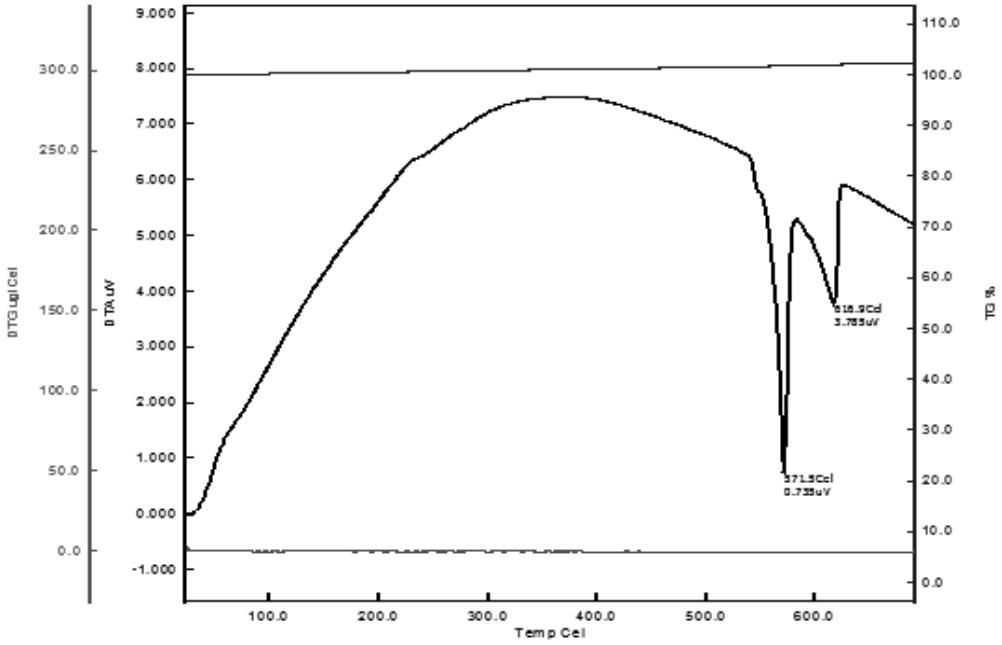

Differential Thermal Analysis (DTA) curve of solution treated Alloy-3

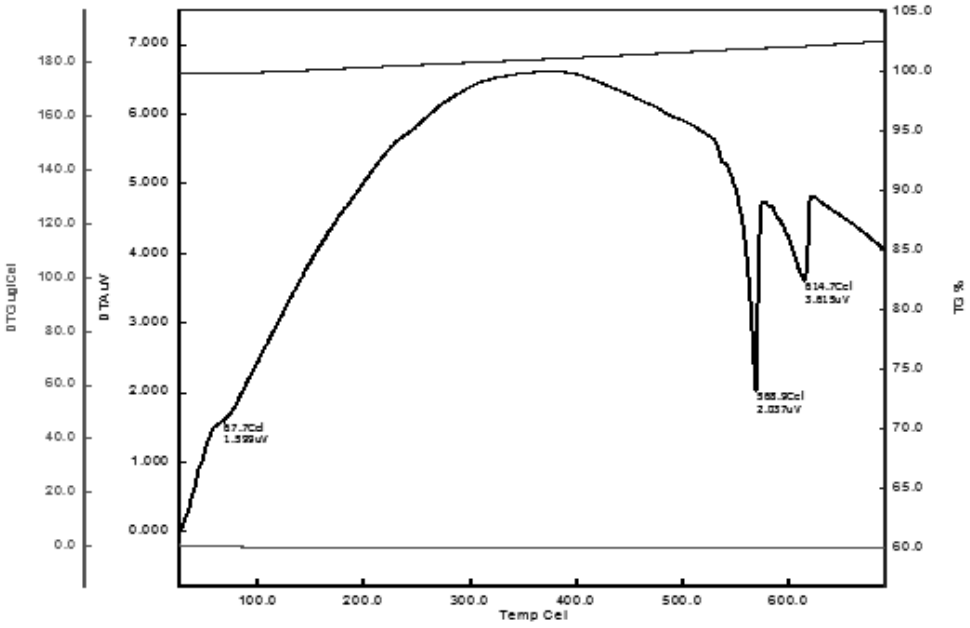

Differential Thermal Analysis (DTA) curve of solution treated Alloy-4

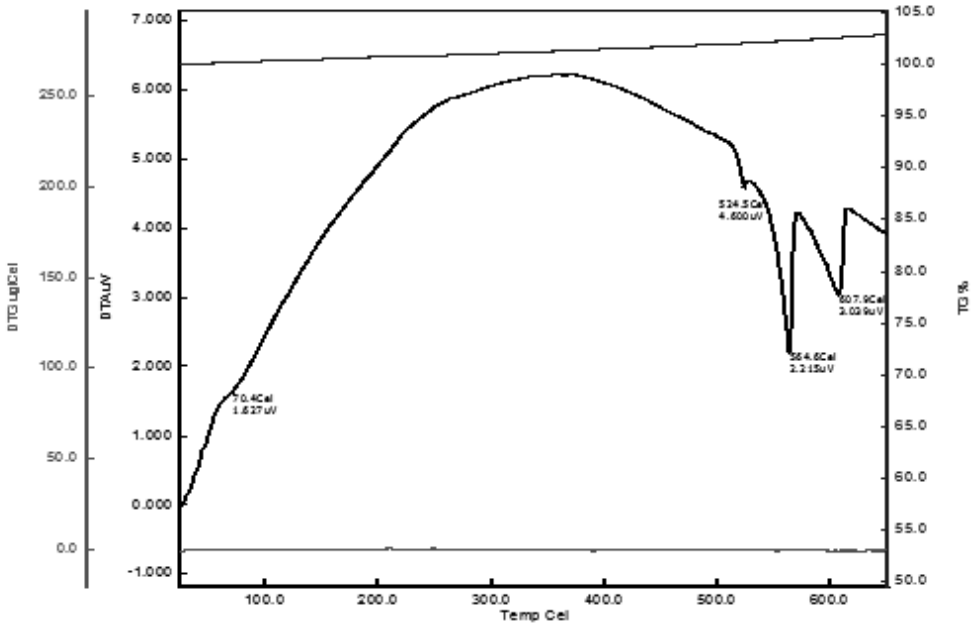

Differential Thermal Analysis (DTA) curve of solution treated Alloy-5

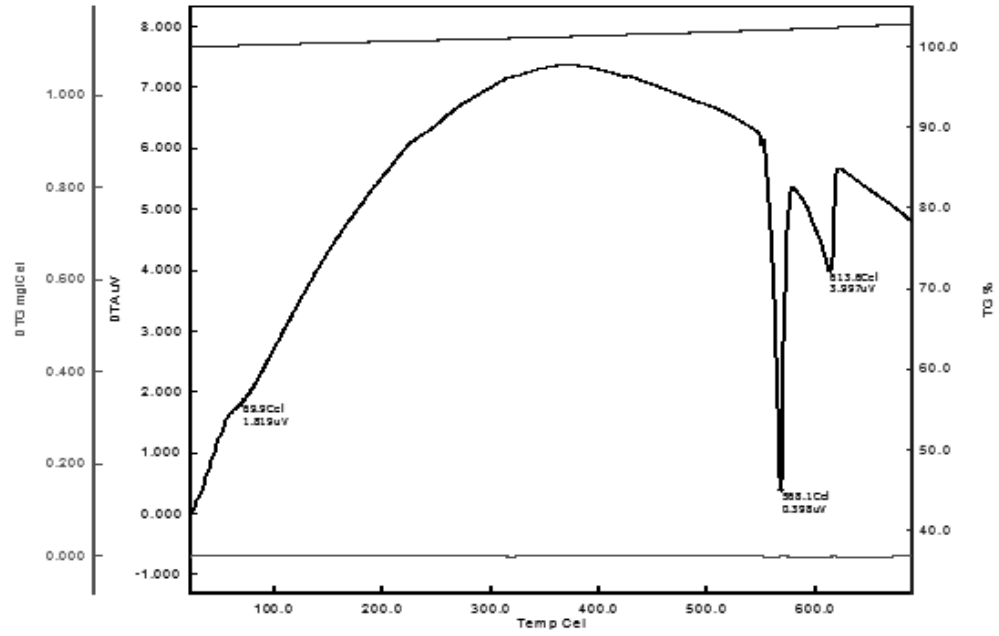

Differential Thermal Analysis (DTA) curve of solution treated Alloy-6

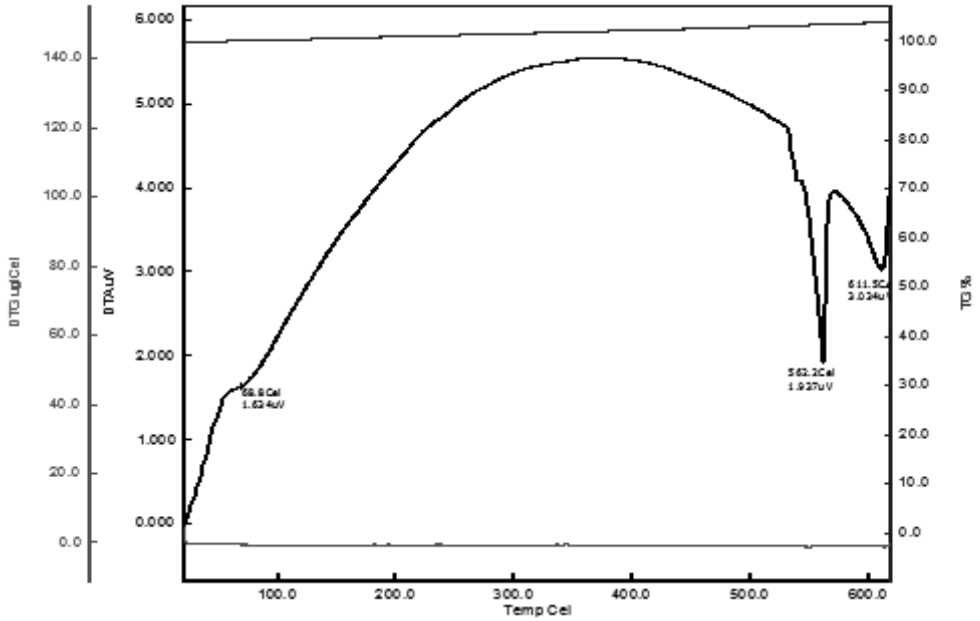

Differential Thermal Analysis (DTA) curve of solution treated Alloy-7

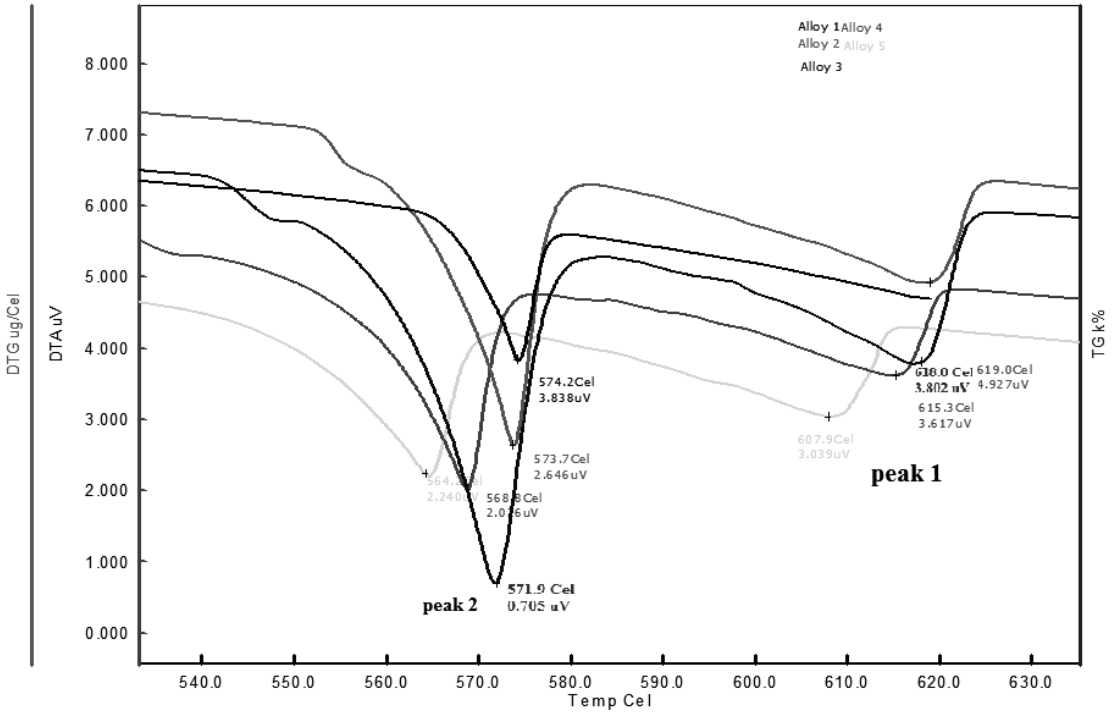

Differential Thermal Analysis (DTA) curves of solution treated Alloys 1-5

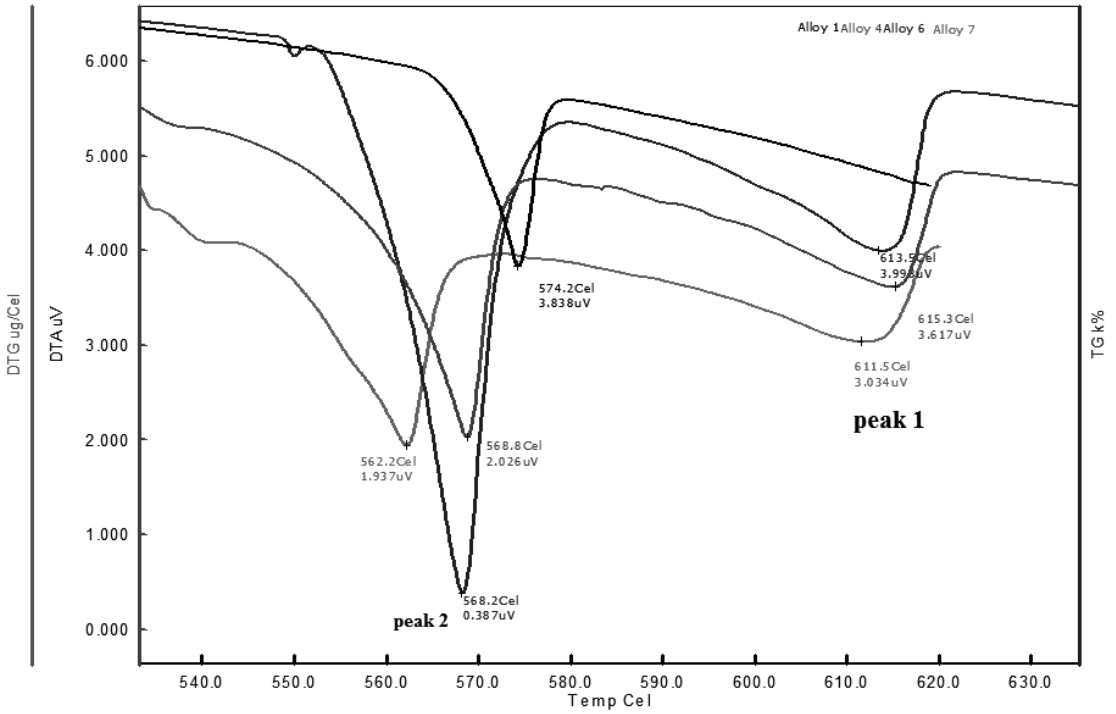

Differential Thermal Analysis (DTA) curves of solution treated Alloys 1, 4, 6 and 7

Appendix C

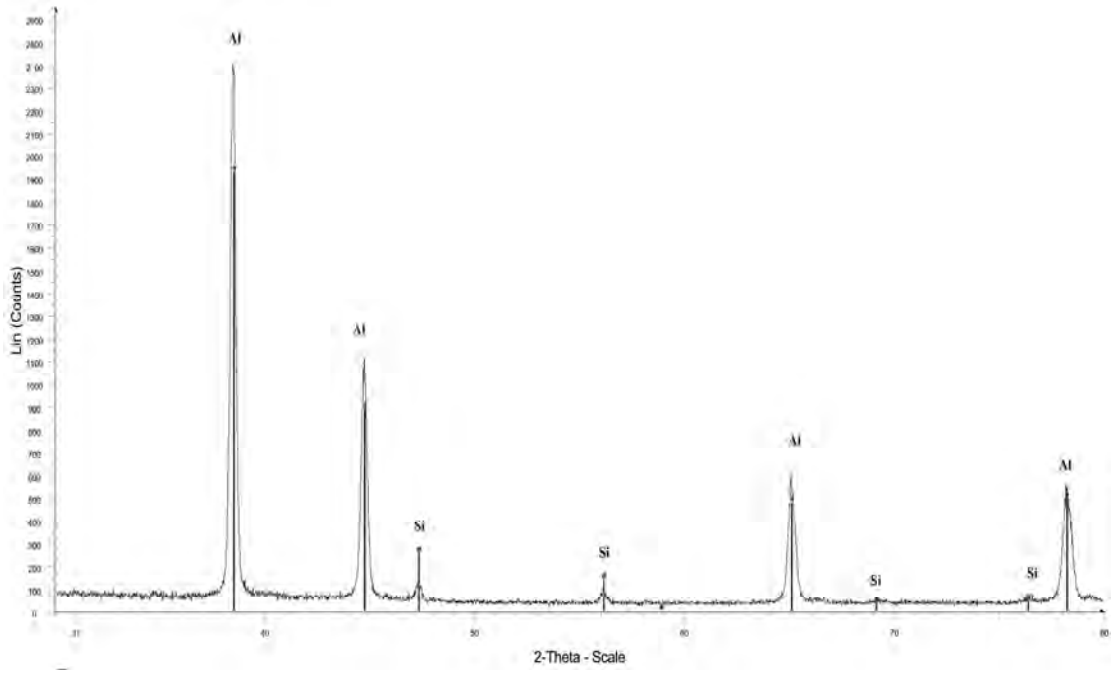

XRD pattern of wear debris of peakaged Alloy-1

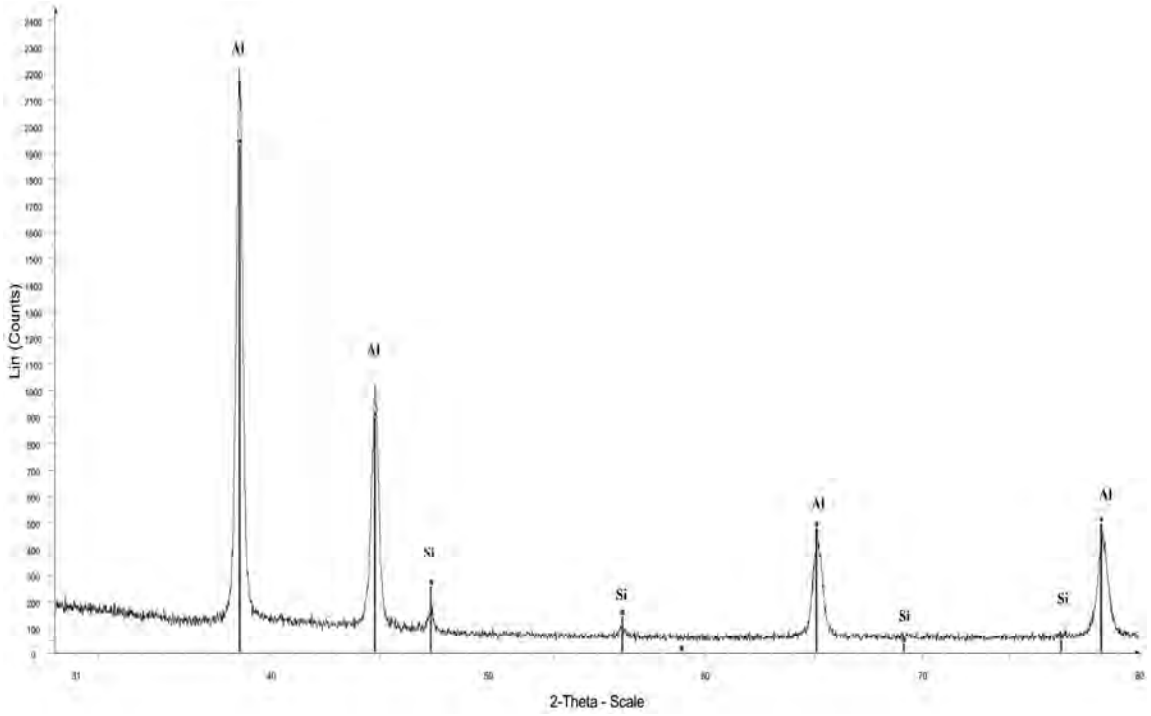

XRD pattern of wear debris of peakaged Alloy-4

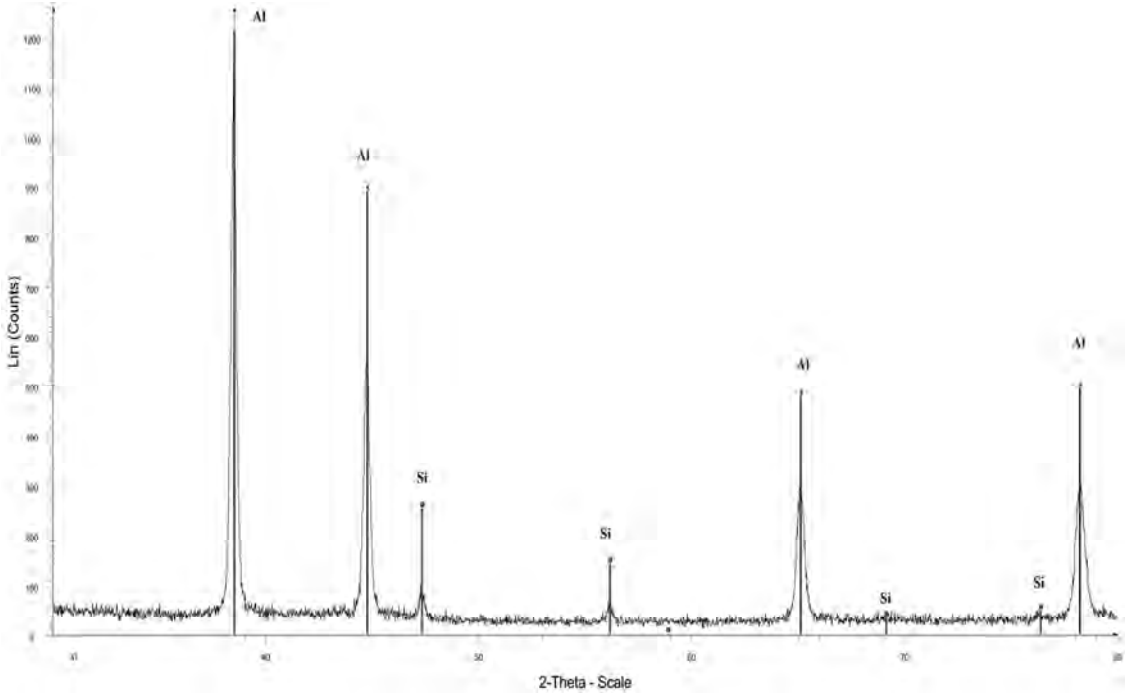

XRD pattern of wear debris of peakaged Alloy-6

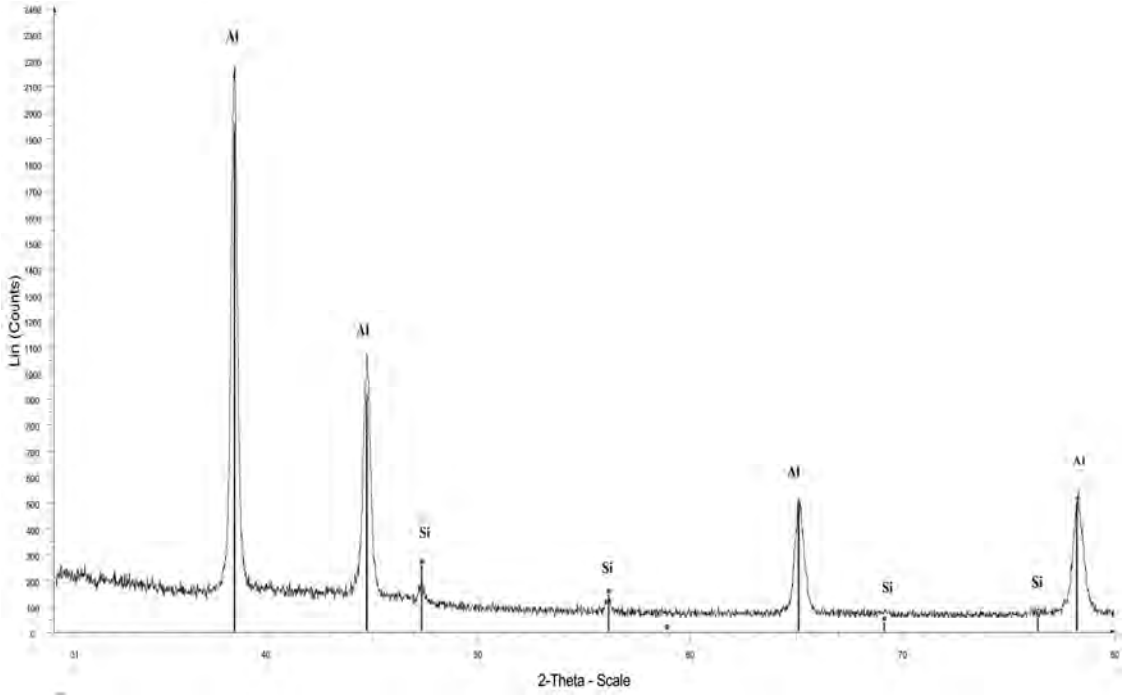

XRD pattern of wear debris of peakaged Alloy-7

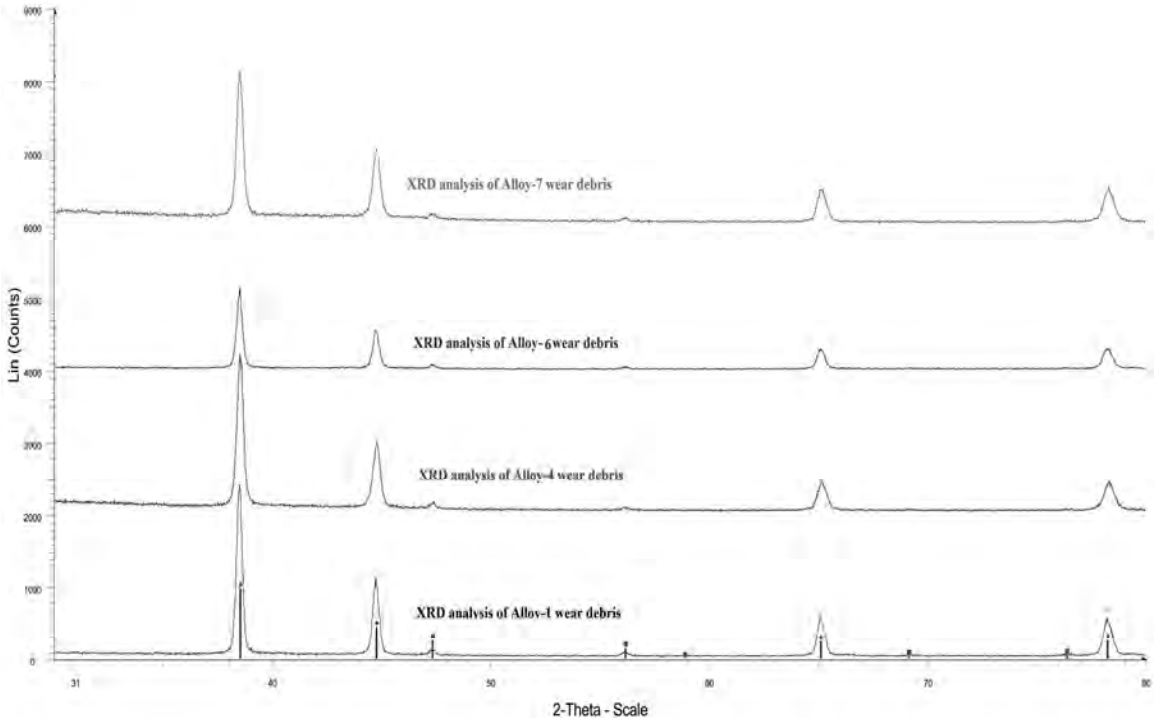

XRD pattern of wear debris of peakaged Alloys 1, 4, 6 and 7